Cover Page



Universiteit Leiden



The handle http://hdl.handle.net/1887/21861 holds various files of this Leiden University dissertation.

Author: Kant, Rik Henricus Nicolaas van der
Title: Cholesterol and multi-protein complexes in the control of late endosomal dynamics
Issue Date: 2013-09-26

Protein complexes and cholesterol in the control of late endosomal dynamics

Rik Henricus Nicolaas van der Kant

ISBN: 978-94-6182-318-2

Cover: the complex itinerary of endosomes

Photograph: **Highways 5, 10, 60 and 101 Looking West, L. A. River and Downtown Beyond** by Michael Light (http://www.michaellight.net). Copyright 2004 Michael Light.

Illustration by Rik van der Kant.

Layout and printing: Off Page, www.offpage.nl, with financial support from the Netherlands Cancer Institute

Copyright @ 2013 by R.H.N. van der Kant. All rights reserved. No part of this book may be reproduced, stored in retrieval system, or transmitted in any form or by any means, without prior permession of the author

The research described in this thesis was performed at the Division of Cell Biology II of the Netherlands Cancer Institute, Amsterdam, The Netherlands

Financial support was provided by Netherlands Organisation for Scientific Research (NWO) and the European Research Council (ERC)

Protein complexes and cholesterol in the control of late endosomal dynamics

PROEFSCHRIFT

Ter verkrijging van
de graad van Doctor aan de Universiteit Leiden,
op gezag van Rector Magnificus Prof.mr. C.J.J.M. Stolker,
volgens besluit van het College van Promoties
te verdedigen op donderdag 26 september 2013,
klokke 11.15 uur

door
Rik Henricus Nicolaas van der Kant
geboren te Deurne
in 1984

Promotiecomissie

Promotor:	Prof. Dr. J.J. Neefjes
Overige leden:	Prof. Dr. W.H. Molenaar
	Prof. Dr. F. Koning
	Prof. Dr. B. Koster
	Prof. Dr. J. Borst *Universiteit van Amsterdam*
	Prof. Dr. J. Klumperman *Universiteit Utrecht*
	Dr. A.Sonnenberg *Universiteit van Amsterdam*
	Dr. E.A.J. Reits *Universiteit van Amsterdam*

Table of Contents

Chapter 1	General introduction and scope of the thesis *Adapted from review in preparation, Trends in Neurosciences*	7
Chapter 2	The endoplasmic reticulum as a central organelle organizer *Adapted from review in preparation, Journal of Cell Science*	25
Chapter 3	Cholesterol sensor ORP1L contacts the ER protein VAP to control Rab7–RILP–p150Glued and late endosome positioning *Journal of Cell Biology, Volume 185, No.7. June 2009*	39
Chapter 4	Late endosomal transport and tethering are coupled processes controlled by RILP and the cholesterol sensor ORP1L *Journal of Cell Science, in press*	75
Chapter 5	Identification and characterization of the mammalian CORVET and HOPS tethering complexes and a VPS33b-SPE-39 complex mutated in ARC syndrome *In preparation*	117
Chapter 6	Cholesterol binding molecules MLN64 and ORP1L mark distinct late endosomes with transporters ABCA3 and NPC1 *Journal of Lipid Research, Volume 54, No.7. August 2013*	135
Chapter 7	Discussion	157
	Summary and discussion	159
	Nederlandse samenvatting	165
Appendices		171
	Curriculum Vitae	173
	Publications	175
	Acknowledgements	177

chapter ONE

General introduction and scope of the thesis

Adapted from review in preparation, Trends in Neurosciences

A scientific definition of "Cell"

"An autonomous self-replicating unit that may exist as functional independent unit of life (as in the case of unicellular organism), or as sub-unit in a multicellular organism (such as in plants and animals) that is specialized into carrying out particular functions towards the cause of the organism as a whole." Biology-online.org

A human cell is an organism in an organism; although capable of sustaining itself, it functions as a small unit in an organ. And together our organs function as a human being. Similar to this, cells contain organs (organelles) that cooperate to contribute to the cell's benefit. A primary cause for any cell is the intake of nutrients and the digestion of these to provide energy for other cellular processes. The digestive system of the cell is the endo-lysosomal system, which consists of numerous dynamic membrane-enclosed vesicles whose main task it is to process nutrients and protect against pathogens. This digestion pathway starts with endocytosis and endocytosed particles eventually end up in acidic lysosomes where they are degraded and nutrients become available for cellular use.

Early events in endocytosis

Endocytosis is the internalization of extracellular particles by cells via the invagination of the plasma membrane and subsequent pinching of a vesicle containing the endocytosed particles (Fig. 1). The initial event of pinching can take place in multiple ways (Mayor and Pagano, 2007) such as by clathrin-mediated, caveolin-mediated and dynamin-independent endocytosis. During this initial process, adapters bind to the plasma membrane and plasma membrane proteins to induce invagination of a patch of membrane (Mayor and Pagano, 2007). The cargo destined for degradation can also be very diverse, ranging from nutrients (amino-acids and lipo-protein particles) to receptor proteins on the plasma membrane, apoptotic bodies of other cells to viruses and bacteria (Mayor and Pagano, 2007; Stenmark, 2009; Ikonen, 2008). In the case of bacteria, viruses and other pathogens, the process is not called endocytosis, but phagocytosis (Fairn and Grinstein, 2012). Once a vesicle is pinched off from the plasma membrane it fuses with an early endosome (EE) (early phagosome if it concerns phagocytosis) (Bucci et al., 1992; Gorvel et al., 1991). A major determinant of an early endosome is the presence of the RAB5 GTPase, a member of the membrane-binding RAB GTPase family that specify organelle identity (Stenmark, 2009). RAB5 determines the dynamics of the early endosome by controlling transport, fusion and conversion events (Gorvel et al., 1991; Christoforidis et al., 1999; Bucci et al., 1992; Rink et al., 2005) leading to maturation of the EE to a late endosome (LE) (Fig. 1). A major regulator of early endosomal tethering and endo-lysosomal biogenesis in Yeast is the C core vacuole/endosome tethering (CORVET) complex that is recruited to membranes by vps21 (Yeast RAB5 homologue) (Peplowska et al., 2007). Whether the CORVET complex also exists and has a similar role in endosomal maturation in mammalian cells is unclear (Balderhaar and Ungermann, 2013).

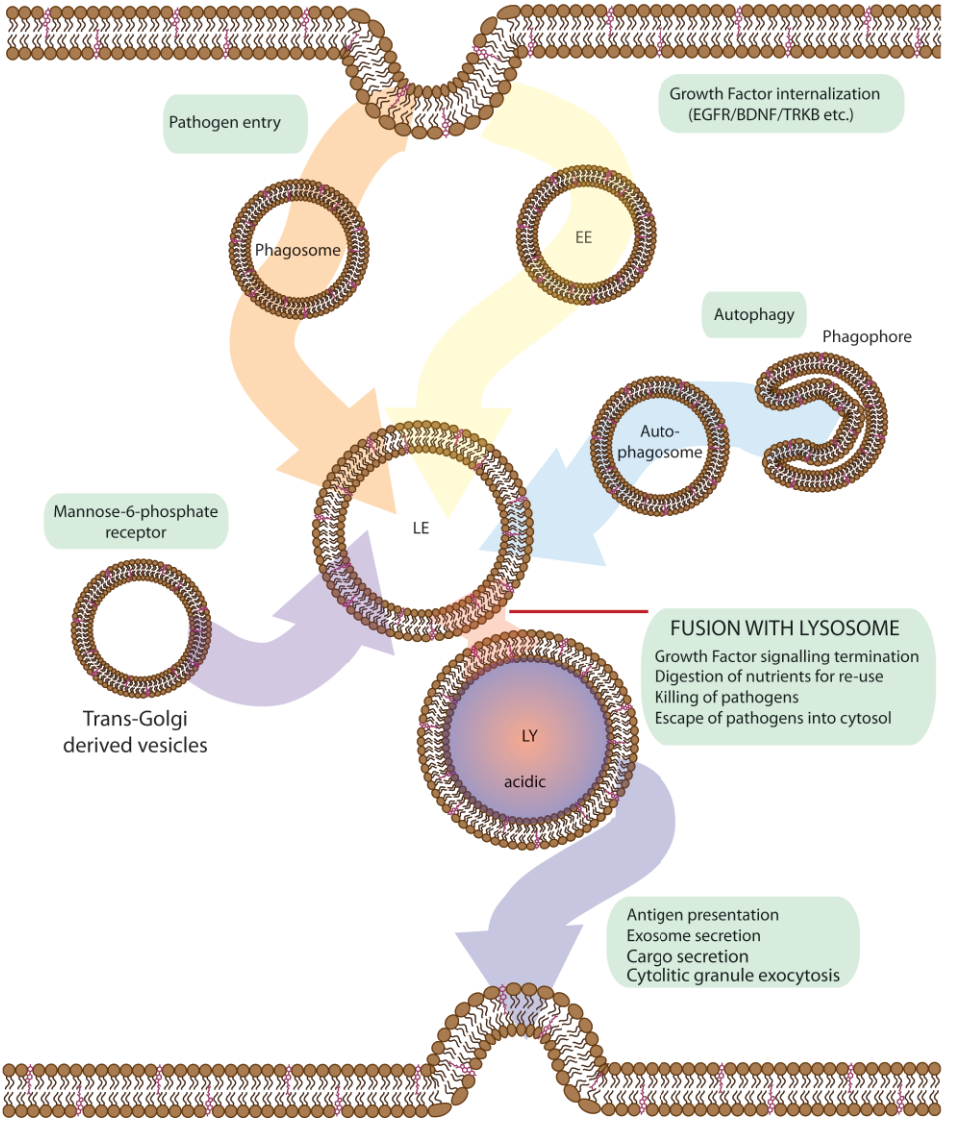


Figure 1. Pathways of late endosome/lysosome generation. Lysosomes are the end stage of endosomal maturation and can receive cargo from a range of preceding organelles. Nutrients, lipids and growth factors are internalized from the plasma-membrane via endocytosis to end up in an early endosome (EE), whereas pathogens such as viruses and bacteria enter via the homologous process of phagocytosis. Cytosolic proteins, defective organelles and other cytosolic components are engulfed by the Phagophore which closes to form the auto-phagosome. Due to maturation and/or fusion events, all these different endosomes mature into the late endosome (LE). Trans-Golgi-derived vesicles containing Mannose-6-Phosphate Receptor (M6PR) fuse to the LE to deliver acid hydrolases required for the degradation of LE cargo, or the LE fuses with a pre-existing lysosome containing these hydrolases. In the acidic environment, processes such as growth factor signalling is terminated, pathogens are killed and nutrients are recycled. Some pathogens such as Ebola-virus require the acidic environment of the lysosome and lysosomal proteins for their escape into the cytosol. Lysosomes, or lysosome related organelles (LRO) such as MIIC and melanosomes, can fuse with the plasma membrane to deliver their cargo in the extracellular environment.

An alternative way to generate LE is the autophagic pathway. In contrast to the endocytic pathway, where vesicles derived from the plasma membrane and engulf mostly extracellular cargo, autophagy is the process whereby cytosolic cargo is engulfed by membranes to recycle nutrients and degrade harmful agents such as protein aggregates or defective organelles. The membrane that engulfs and captures the cytosol is called a phagophore, and becomes an autophagosome after it has sealed to form a vesicle (Fig. 1) (Codogno et al., 2012). In order to degrade it's cargo the autophagosome fuses with, or matures into, a lysosome (Codogno et al., 2012).

Endosomal maturation

From the early endosome, cargo can be recycled back to the plasma membrane or sent for degradation to the acidic lysosomal compartment (Stenmark, 2009). In a series of not well defined transport-, fusion- and conversion steps, the early endosome can mature into a late endosome (LE), or transfer it's cargo to a late endosome. During maturation, the active GTP-bound RAB5 is inactivated, extracted from the membrane and replaced by the late endosomal GTPase RAB7 (Fig. 2) (Poteryaev et al., 2010; Rink et al., 2005).

In general, it is hard to distinguish autophagosomes, endosomes and phagosomes from each other later in their maturation processes apart from their cargo. During maturation of all these compartments their specific RAB GTPases are gradually replaced by RAB7 (Stenmark, 2009; Fairn and Grinstein, 2012). The resulting mature endosome derived from either of these pathways can therefore mechanistically be called a late endosome marked by RAB7 and the RAB7 machinery. At this stage, the late endosome has it's typical multivesicular appearance due to the pinching off of vesicles from the limiting membrane into the lumen of the endosome and is therefore often referred to as the Multi-Vesicular Body (MVB). The transition from a late endosome to a lysosome is not a strictly defined step either. Acidic hydrolases are delivered to early and late endosomes by Mannose-6-Phosphate Receptor (M6PR) positive trans-Golgi-derived vesicles in order to acidify the lumen (Saftig and Klumperman, 2009; Klumperman, 2011). In stages where the organelle becomes acidic enough the delivery stops. Therefore the RAB7 positive, but M6PR negative acidic organelle is often considered the lysosome. Late endosomes can however also fuse with pre-existing RAB7 positive lysosomes via the action of the Homotypic fusion and vacuole Protein Sorting complex (HOPS) complex (Luzio et al., 2000). In this hybrid compartment, M6PR is quickly sorted away by the retromer complex (Seaman, 2012). By definition it is very hard to discriminate a "late" late endosome and an "early" lysosome and in this thesis both lysosomes and late endosomes marked by RAB7 and the transmembrane protein CD63 are referred to as late endosomal compartments (LE). The process of endosomal maturation is considered to be uni-directional. Although cargo can be sorted away from late endosomal compartments, the current view is that a RAB7-positive endosome can not go back to being a RAB5-positive early endosome or any other preceding compartment. Lysosomes can continuously rejuvenate however by fusion with late endosomes and reformation of a hybrid organelle. RAB7 is a major regulator of these sorting, transport and fusion events.

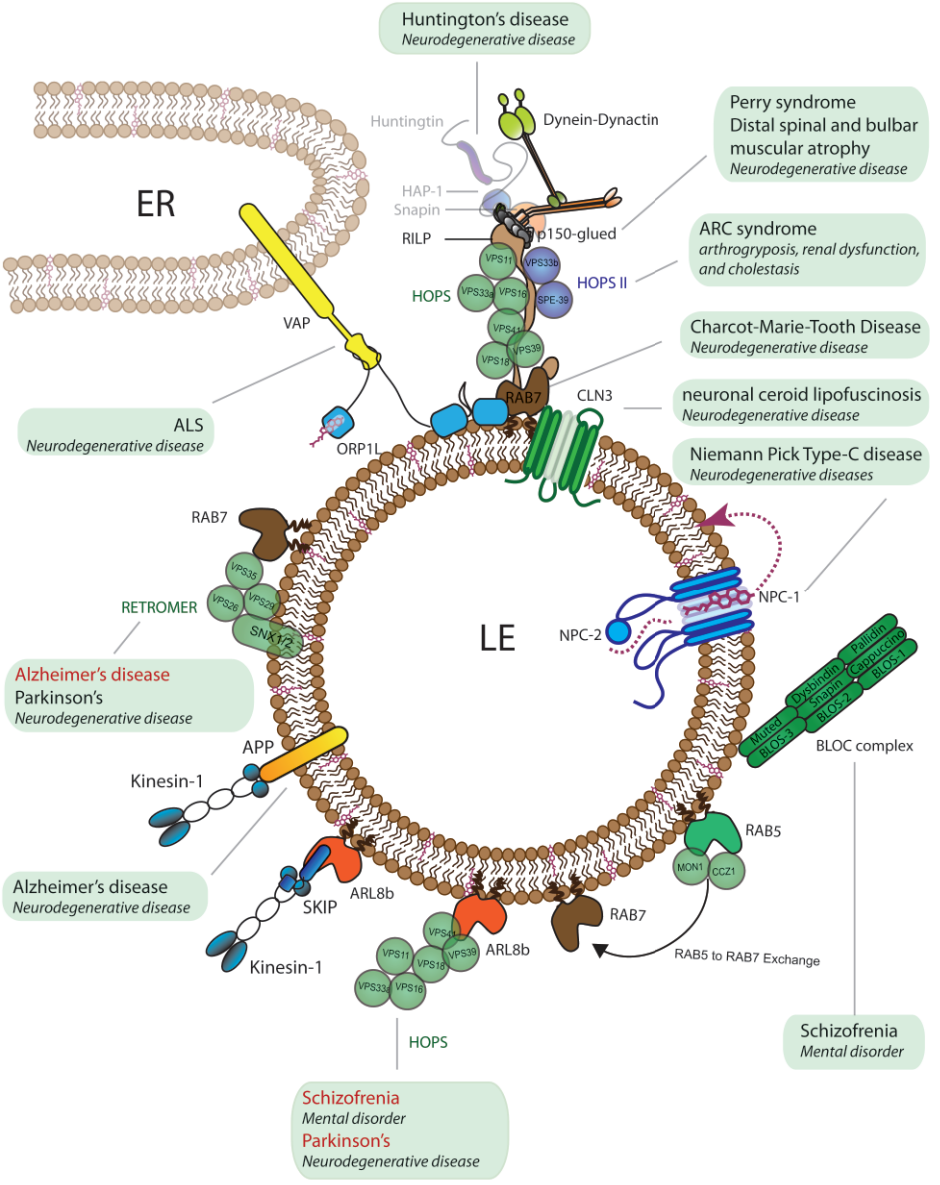


Figure 2. LE proteins discussed in this thesis related to disease. Overview of LE associated proteins whose functions have been linked to diseases by trafficking, sorting and fusion events. Proteins in red have been found by association studies and might act as risk factors.

RAB7, master regulator of endosomal dynamics

RAB7 can regulate the dynamics of LE in a number of ways. As a first step RAB7 can recruit the retromer complex to LE membranes in order to recycle cargo away from the late endosome.

Human retromer is an association of a cargo-selective trimer (VPS35, VPS26, VPS29) and Syntaxin (SNX) components (SNX1 or SNX2 with SNX5 or SNX60) (Swarbrick et al., 2011), yet the retromer complex is very dynamic and subcomplexes (reported for the SNX's) can function without requiring other subunits (Prosser et al., 2010; Nisar et al., 2010). The SNX proteins are recruited to membranes through binding to phosphatidylinositol (PtdIns) 3-phosphate [PtdIns(3)*P*] by the Phox homology (PX) domain, which is present in each SNX protein (Cozier et al., 2002) and the cargo-selective complex binds RAB7 (Seaman et al., 2009; Rojas et al., 2008). Ceroid-lipofusciosis neuronal 5 (CLN5) protein – a protein mutated in the lysosomal storage disorder Batten disease – has been also implicated as a regulator of RAB7 activity and retromer recruitment (Mamo et al., 2012). RAB7 is present on late endosomes and lysosomes, whereas retromer is absent from lysosomes, indicating that there are processes regulating the dissociation of retromer from RAB7. One of these processes might be the recruitment of RAB7 interacting lysosomal protein (RILP) and oxysterol-binding protein (OSBP)-related protein 1L (ORP1L) (Vihervaara et al., 2011; Jordens et al., 2001; Cantalupo et al., 2001; Johansson et al., 2007). Both these proteins have a function in the biogenesis of multi-vesicular bodies (Progida et al., 2007; Kobuna et al., 2010), indicating that they might function at the late endosomal to lysosomal transition.

RAB7 can associate into a big multi-protein complex of RAB7-RILP-ORP1L-dynein/dynactin-HOPS (Jordens et al., 2001; Johansson et al., 2007) that regulates endosomal minus-end transport and late endosomal tethering and fusion. RAB7 interacts simultaneously with the C-terminus of the RAB7 interacting lysosomal protein (RILP) (Cantalupo et al., 2001) and the ANK domain in ORP1L (Vihervaara et al., 2011; Johansson et al., 2007). Together, these two proteins function as the hardware (RILP) and the software (ORP1L) that regulate endosomal trafficking and tethering.

RILP directly binds the $p150^{glued}$ subunits of the dynein-dynactin and the HOPS complex. Dynein-dynactin is a large motor protein complex that associates with microtubules and transports cargo over these microtubules towards the minus-end of microtubules (towards the microtubule organizing center). In contrast, the kinesin-family of motors transport cargo toward the plus-end of microtubules (the end distant from the microtubule organization center). The HOPS complex is a 6-subunit complex (Nickerson et al., 2009; Nakamura et al., 1997; Wurmser et al., 2000; Huizing et al., 2001) conserved from yeast to mammals that interacts with RILP on the late endosomal membrane (this thesis) and can tether vesicles. Subsequently, the HOPS complex can interact with SNARE proteins to start actual fusion of two endosomes (Sato et al., 2000). In mammals there are two additional HOPS complex subunit homologues (SPE-39 and VPS33b) (Gissen et al., 2005; Zhu et al., 2009) that can form an alternative complex and also associate with RILP (this thesis). By recruiting both the dynein motor and the tethering machinery via RILP, vesicles that are moving towards each other by dynein motors can subsequently initiate contact via the HOPS complex and are prepared for subsequent fusion steps by SNARE proteins.

ORP1L is a cholesterol binding protein of the Oxysterol-binding protein Related Protein (ORP) family that controls the recruitment of HOPS/dynein-dynactin to RILP and thereby times LE transport and fusion (Rocha et al., 2009). The ORD domain of ORP1L senses cholesterol on the late endosomal membrane. When cholesterol is high, ORP1L allows binding of HOPS and dynein complexes to RILP. When cholesterol on the late endosome is low, ORP1L changes conformation exposing a small domain (FFAT motif) that interacts with the ER resident VAP-A. (Read more on cellular cholesterol metabolism in box 1). VAP-A subsequently removes both the HOPS complex and dynein from the vesicles allowing plus-end transport by kinesin motors (Rocha et al., 2009). In this way, RAB7 integrates the recruitment and regulation of transport and tethering events by the dynein-dynactin motor and the HOPS complex respectively.

How plus-end transport of the LE is controlled is less well understood. A GTPase of the ARF (like) family, ARL8b, has been shown to recruit the plus-end motor Kinesin-1 via SKIP (Rosa-Ferreira and Munro, 2011) facilitating plus-end transport of late endosomes. Interestingly ARL8b also recruits the HOPS complex (Garg et al., 2011), but it is not known whether Kinesin-1 and HOPS compete for ARL8b binding or whether they, similar to RAB7-RILP, combine binding of these two to allow plus-end directed late endosomal transport and tethering by kinesin and HOPS, respectively. Cross-talk between RILP and ARL8b might occur as these are both required for lysosomal tubulation upon lipopolysaccharide (LPS) stimulation of macrophages (Mrakovic et al., 2012). Amyloid precusor protein (APP) is another kinesin-interacting protein possibly present on LE is that has been suggested to recruit Kinesin-1 to membranes (Kamal et al., 2001). Both Kinesin-1 and KIF3 have been implicated in plus-end transport of lysosomes (Wubbolts et al., 1996; Hollenbeck and Swanson, 1990). Whether RAB7, ARL8b and APP are present on the same endosomes remains unclear. Other proteins can also associate to the RAB7-RILP-dynein-dynactin axis to control dynein activity. Examples of these are Huntingtin (Caviston et al., 2007; Colin et al., 2008; Caviston et al., 2011), Snapin (Cai et al., 2010; Yuzaki, 2010) (Falcon-Perez et al., 2002; Starcevic and Dell'Angelica, 2004; Ryder and Faundez, 2009; Lee et al., 2012) and Ceroid lipofuscin 3 (CLN3) (Uusi-Rauva et al., 2012) however the exact mechanism underlying their regulation with respect to late endosomal and lysosomal functioning is unknown.

Lysosome related organelles (LRO) and lysosome related organelle diseases

A number of specialized cells contain organelles called lysosome-related organelles (LRO). These organelles share characteristics of lysosomes, but have a specialized function in the cell and are often intended to transport LE cargo towards the plasma membrane or secrete material into the extra-cellular space (Dell'Angelica et al., 2000). Below is a summary of known LRO containing cells and the role of these LRO's in organismal homeostasis.

Neutrophils are the first line of defence against invading bacteria and contain lysosome-like organelles filled with anti-microbial polypeptides (Gullberg et al., 1997). When neutrophils are recruited to these sites of injury they release their LRO's to kill entering microbes. Similarly, basophils are cells involved in inflammatory reactions that use LRO's to release several effectors

of inflammation such as histamines and cytokines (Marone et al., 1997). Other cells of the immune system such as professional antigen presenting cells contain MHC class II positive lysosomes (MIIC) which are transported towards the plasma membrane during activation. At the membrane the MHC class II molecules aid in the activation of T-cells (Rocha and Neefjes, 2008). Activated Cytotoxic T-lymphocytes and natural killer cells kill virus-infected or tumorigenic cells by the release of lysosome-like cytotoxic granules that contain pore forming proteins and proteases (Griffiths and Argon, 1995). Blood plateles play a role in hemostasis (blood clotting) and thrombosis and contain secretory vesicles filled with factors to induce blood clotting (McNicol and Israels, 1999). In the bone cavity Osteoclasts release acidic LRO's at the osteoclast-bone interface to reabsorb minerals necessary for bone homeostasis. In lung tissue, exocytosis of LRO (lamellar bodies) containing pulmonary surfactant (a mix of lipids and proteins), is required for the formation of lipid surface lining layer of the alveolar epithelium of lungs (Cheong et al., 2007).

Skin, hair and eye color are some of the most obvious traits that are controlled by LRO's. Cells such as melanocytes and retinal pigment epithelial cells contain melanosomes, LRO's that contain melanins. These melanins form the pigment that provides protection from ultraviolet exposure. Melanosomes are LRO's that are generated in four maturation stages and mature melanosomes are secreted from melanocytes and transferred to skin keratinocytes (Orlow, 1995). Similar to this, eye colour is dependent on melanocyt-like cells that store pigment in membrane-bound compartments with lysosome like properties. Defects in many lysosomal-trafficking components such as the tethering HOPS complex and AP-complex proteins directly influence the eye-colour, and this trait is frequently used in genetic screens with Drosophila as a model system for lysosomal trafficking (Dell'Angelica et al., 2000).

Diseases affecting LRO in humans often result in pigmentation defects such as albinism. Chediak-Higashi syndrome, Griscelli syndrome (and related disorders) and Hermansky-Pudlak disease (Dell'Angelica et al., 2000) are all rare syndromes associated with lysosome-related organelle dysfunctions in which patients present with pigmentation defects such as albinism due to melanocyte dysfunction. Chediak-Higashi patients are also susceptible to bacterial and fungal infections, have bleeding problems (due to platelet-dense granule deficiency) and are prone to develop progressive neuropathy in their teenage years. Griscelli syndrome patients are also immuno-deficient, yet do not present with bleeding problems. Griscelli related syndromes such as partial albinism and immunodeficiency PAID syndrome or neuroectodermal melanolysosomal disease also display immuno-deficiency and pigmentation defects in addition to progressive dysfunction of the central nervous system. Hermansky-Pudlak patients do develop bleeding problems and store abnormal ceroid lipofuscin in lysosomes. This disease resembles lysosomal storage disorders of the neuronal ceroid lipofuscinoses (NCL) type.

Another disorder involving a bleeding phenotype and immuno-deficiency is arthrogryposis, renal dysfunction and cholestasis (ARC) syndrome that results from mutations in putative subunits of the HOPS complex (SPE-39 and VPS33b) (Gissen et al., 2005; Cullinane et al., 2010). Children with ARC syndrome grow poorly, display stiffened and contracted muscles, renal dysfunction and defects in bile production and very rarely live over more than 1 year. Whether

1

Box 1. Cellular cholesterol metabolism

The regulation of endosomal dynamics by cholesterol is a common theme in this Thesis. This box reviews (in short) how cells make and handle cholesterol (Ikonen, 2008). There are two sources for cells to acquire cholesterol; *de novo* cholesterol synthesis and dietary intake. All eukyarotes can synthesize cholesterol from acetyl CoA through the mevalonate pathway and this pathway is especially active in hepatocytes. In brief, acetyl CoA is converted to 3-hydroxy-3-methylglutaryl-CoA (HMG-CoA) and HMG-CoA reductase (the target of statins) reduces HMG-CoA to Mevalonic acid. In subsequent steps, the first sterol (lanosterol) is generated which is further converted into cholesterol. Dietary cholesterol is absorbed by enterocytes of the small intestine and transported to hepatocytes. Hepatocytes secrete lipids in very low density lipoprotein (VLDL) particles that are processed in the circulation into low density lipoprotein (LDL) particles, the main lipoprotein that delivers cholesterol to peripheral cells. In these peripheral cells, LDL particles are internalized by the LDL receptor (LDLR) present at the plasma membrane of most cells. These particles are then transported towards acidic endocytic LE where cholesteryl esters are hydrolysed by acid lipases to provide unesterified cholesterol for cellular needs (Fig. 3). NPC-1 and NPC-2 are LE proteins that contribute to the release of cholesterol from LE. How and to which initial receptor membrane cholesterol is transported has not been determined, but might involve ORP5 an ER membrane protein that might shuttle cholesterol from the LE to the ER (Du et al., 2011). Two proteins in late endosomes have been identified with sterol-binding domains that are exposed to the cytosol; MLN64 and ORP1L (Fig. 3). If and how these are involved in sterol trafficking out of the LE is not known. Alternatively cholesterol might be transported to recycling compartments from which it is further transported to other cellular compartments.

Cholesterol is heterogeneously distributed over cellular membranes (Ikonen, 2008). The plasma membrane, the Golgi, recycling and late-endosomes are relatively cholesterol rich, whereas the endoplasmic reticulum has a low cholesterol content. Excess unesterified cholesterol is stored in lipid droplets as cholesteryl esters. The cholesterol concentration of the ER serves as a regulator of ER to Golgi transport; by controlling the sterol-homoestatic machinery (SREBP-SCAP), transcription levels of sterol-regulated genes are controlled. Under low ER cholesterol levels the interaction between INSIG (ER retention protein) and the ER resident SCAP-SREBP is lost. Therefore SCAP-SREBP is transported to the Golgi where SREBP is prototypically processed. A cytosolic SREBP domain is released that translocates to the nucleus and acts as a transcription factor to activate sterol-regulated genes such as HMG-CoA reductase. This process is probably specific for SREBP-SCAP as low ER cholesterol inhibits the secretory pathway of other proteins (Ikonen, 2008).

Cholesterol can be effluxed from cells by ABC transporters that mediate the loading of cholesterol into lipoproteins. This efflux process involves plasma membrane and endocytic events, but how lipid release is compartmentalized in cells is yet unclear. There are indications that both lysosomes (cathepshin D and NPC1 dependent) and recycling endosomes (RAB8 dependent) have a role in this process.

Box 1. *Continued*

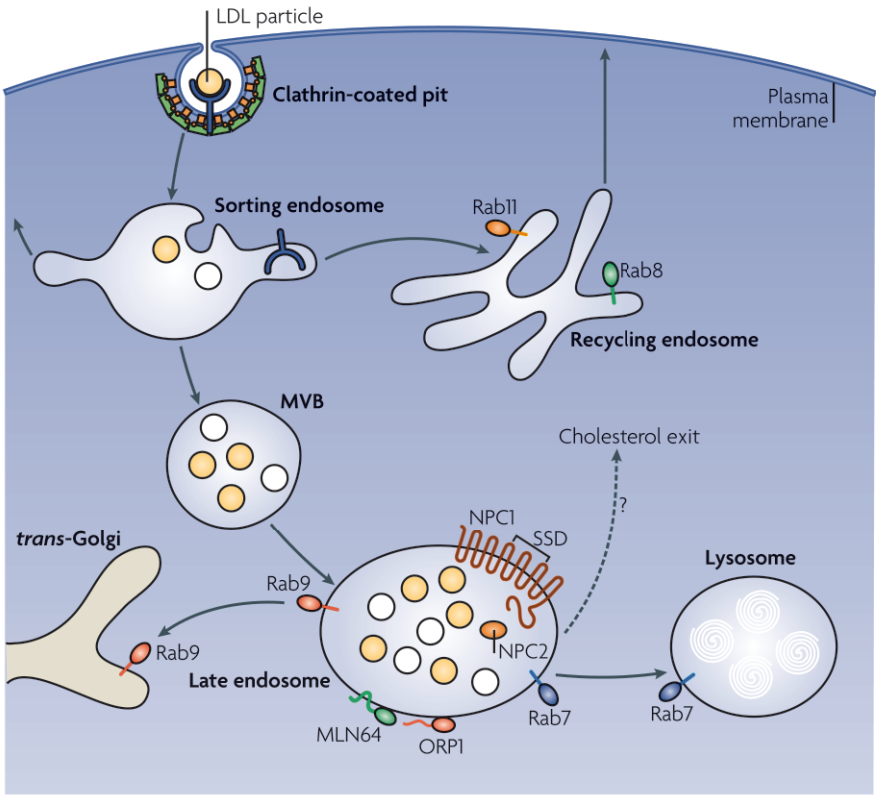


Figure 3. Endosomal cholesterol trafficking. Low density lipoprotein (LDL) receptors bind LDL particles (yellow) that are transported to acidic late endosomes where cholesterol is hydrolysed. Cholesterol efflux from LE is not well characterized but involves Niemann Pick C1 (NPC1) and NPC2 proteins and possibly MLN64 and ORP1L. Adapted from Ikonen, 2008. (MVB = Multi-vesicular body).

this disease should be classified as an LRO diseases or whether patients have general defects in lysosomal biogenesis, explaining the severity of symptoms, remains to be established.

Although some mutations are known for these syndromes, the underlying mechanisms for most of these diseases are not, and a better understanding of LRO biogenesis and its relationship to lysosomal functioning is urgently required. Although much of the immune-deficiency, bleeding problems and pigmentation problems can be explained by LRO dysfunction, how most of these diseases result in neuronal problems is not understood.

1

Lysosomal storage disorders and other lysosome-related diseases

Lysosomal storage disorders (LSD) form a group of rare diseases that often result from a deficiency in lysosomal enzymes or improper targeting of lysosomal enzymes and membrane pumps resulting in the accumulation of undigested material in the lysosome. Although the phenotypes of these diseases are very diverse and differ in the age of onset, many of these result in delayed development and/or neurological problems such as movement disorders, seizures and dementia. Sometimes patients also develop enlarged livers and spleen. For most LSD underlying mutations are known, yet the precise mechanism that causes the actual disease phenotype at the cellular level is not known. An example for this is Niemann Pick Type-C disease; a disease caused by mutations in NPC1 or NPC2 which are two proteins that transport cholesterol from the LE lumen to the limiting membrane and subsequently to a receptor membrane (probably ER). Deficiency leads to an accumulation of cholesterol in the LE (Chang et al., 2005; Ikonen, 2008). This accumulation is sensed by ORP1L, which subsequently results in upregulated minus-end transport and mis-localization of LE in cells. Whether the disease phenotype results directly from deficient cholesterol metabolism, a deficiency of late endosomal functioning (for example autophagosomes accumulate) or both is unclear. Another example of diseases on the cross-section of lysosomal storage and lysosomal trafficking are mutations in CLN3 and CLN5 that result in the neurodegenerative disorders of the neuronal ceroid lipofuscinosis group. Ceroid lipofuscin accumulates in lysosomes in these diseases and both CLN3 (dynein/RAB7/RILP) and CLN5 (BLOC complex) interact with lysosomal trafficking and sorting machineries (Mamo et al., 2012; Uusi-Rauva et al., 2012).

Malfunctioning of a large number of proteins involved in late endosomal transport and fusion also result in mainly neurodegenerative diseases (we propose the name lysosomal traffic disorders, LTD's) (Figure 2). Mutations in the retromer complex result in Parkinson's disease (Zimprich et al., 2011; Vilarino-Guell et al., 2011) and retromer malfunctioning has been implicated in Alzheimer's disease (Wen et al., 2011; Vardarajan et al., 2012). Also many proteins in the RAB7-RILP-dynein-HOPS complex are implicated in diseases. Mutations in RAB7 cause the neurodegenerative Charcot-Marie-Tooth disease and have been implied to be risk factors for Alzheimer's disease (Vardarajan et al., 2012). HOPS functioning is implicated in Schizofrenia (Xu et al., 2012) and Parkinson's (Harrington et al., 2012). Mutations in the dynein/dynactin motor subunit p150^{glued} cause Perry syndrome/Distal spinal and bulbary muscular atrophy (Chevalier-Larsen et al., 2008; Farrer et al., 2009) and proteins associated to p150glued such as Huntingtin (mutated in Huntington's disease) (Caviston et al., 2007; Colin et al., 2008; Zala et al., 2013; Caviston et al., 2011) and CLN3 (mutated in Neuronal Ceroid lipofuscinois) (Uusi-Rauva et al., 2012) also result in severe neurodegenerative diseases (Figure 2). Mutations in VAP-B cause *Amyotrophic lateral sclerosis* (ALS) (Nishimura et al., 2004), but whether VAP-B is involved in late endosomal traffic in similar ways to VAP-A is not clear. Mutations in APP, a possible kinesin-1 adapter cause early onset Alzheimer's disease (Bertram et al., 2010).

Scope of this thesis

Proteins that regulate lysosomal function are mutated in a large number of rare-genetic disorders, and many more mutations will likely be identified in the future. Also in sporadic diseases that affect many people, such as Alzheimer's disease, an increasing number of reports indicate that lysosomal malfunctioning is among the first observed disruptions. Yet, our understanding of the molecular processes that regulate lysosomal dynamics are limited, and do often not suffice to place the protein mutations in molecular pathways in order to explain disease development. The work described in this thesis aims at a better fundamental understanding of the molecular mechanisms that control lysosomal function. Understanding these processes is key to understanding the diseases that arise from disturbances in these systems and development of new therapeutic strategies.

Late endosomes and lysosomes are not functionally isolated organelles but play a major part in many aspects of cellular homeostasis. The dynamics of individual lysosomes need to be coordinated at a higher level. To ensure proper cellular homeostasis LE coordinate their functioning with other compartments such as the endoplasmic reticulum (ER). **Chapter 2** reviews the role of the ER in the control of late endosomal dynamics and the other organelles it contacts. **Chapter 3** describes the mechanism underlying ER and late endosomal cross-talk. We show that contacts between the ER and the late endosome are initiated when cholesterol levels on the late endosome are low. LE cholesterol levels are sensed by the cholesterol sensor Oxysterol Binding Protein Related Protein 1, ORP1L which can induce contact sites between the ER and the LE. Within these contacts the recruitment of dynein-dynactin to the RAB7/RILP/ORP1L complex is controlled thus regulating directionality of late endosomal transport. These consequences of these findings in regard to Niemann-Pick Type C (in which a late endosomal cholesterol exporter is mutated) are discussed. **Chapter 4** describes the finding that RAB7/RILP/ORP1L is not only the late endosomal receptor for the dynein/dynactin motor but also recruits the HOPS complex to endosomes. The HOPS complex serves as a tethering factor that is required to initiate fusion between endosomes. By combining recruitment of the tethering machinery (HOPS) and transport machinery (dynein/dynactin), RAB7/RILP efficiently integrates transport and fusion. Here we also show that ORP1L via the ER protein VAP-A can regulate both these processes, imposing a role for the ER in late endosomal fusion. In **Chapter 5** the molecular architecture of the mammalian endosomal tethering complexes is described. We map the mammalian CORVET and HOPS complexes and identify a third complex (SPE-39/VPS33b) that is mutated in ARC syndrome. We show that disease mutants of VPS33b and SPE-39 that cause ARC syndrome fail to interact with their partner proteins explaining the malfunctioning of these proteins at the molecular level. **Chapter 6** describes the cross-talk between the late endosomal lipid sensing proteins ORP1L and MLN64. LE are a major sorting station for cholesterol in cells and many diseases are associated to a failiure of cholesterol handling in these compartments. We show that the ORP1L and MLN64 localize to two subpopulations of late endosomes that differ in their cholesterol sensing and transporting proteins suggesting that they handle this important hydrophobic compound differently as well. Chapter 7 summarizes the findings in this thesis and discusses their implications.

1

Reference List

1. Balderhaar,H.J. and Ungermann,C. (2013). CORVET and HOPS tethering complexes - coordinators of endosome and lysosome fusion. J. Cell Sci. *126*, 1307-1316.
2. Bertram,L., Lill,C.M., and Tanzi,R.E. (2010). The genetics of Alzheimer disease: back to the future. Neuron *68*, 270-281.
3. Bucci,C., Parton,R.G., Mather,I.H., Stunnenberg,H., Simons,K., Hoflack,B., and Zerial,M. (1992). The small GTPase rab5 functions as a regulatory factor in the early endocytic pathway. Cell *70*, 715-728.
4. Cai,Q., Lu,L., Tian,J.H., Zhu,Y.B., Qiao,H., and Sheng,Z.H. (2010). Snapin-regulated late endosomal transport is critical for efficient autophagy-lysosomal function in neurons. Neuron *68*, 73-86.
5. Cantalupo,G., Alifano,P., Roberti,V., Bruni,C.B., and Bucci,C. (2001). Rab-interacting lysosomal protein (RILP): the Rab7 effector required for transport to lysosomes. EMBO J. *20*, 683-693.
6. Caviston,J.P., Ross,J.L., Antony,S.M., Tokito,M., and Holzbaur,E.L. (2007). Huntingtin facilitates dynein/dynactin-mediated vesicle transport. Proc. Natl. Acad. Sci. U S A *104*, 10045-10050.
7. Caviston,J.P., Zajac,A.L., Tokito,M., and Holzbaur,E.L. (2011). Huntingtin coordinates the dynein-mediated dynamic positioning of endosomes and lysosomes. Mol. Biol. Cell *22*, 478-492.
8. Chang,T.Y., Reid,P.C., Sugii,S., Ohgami,N., Cruz,J.C., and Chang,C.C. (2005). Niemann-Pick type C disease and intracellular cholesterol trafficking. J. Biol. Chem. *280*, 20917-20920.
9. Cheong,N., Zhang,H., Madesh,M., Zhao,M., Yu,K., Dodia,C., Fisher,A.B., Savani,R.C., and Shuman,H. (2007). ABCA3 is critical for lamellar body biogenesis in vivo. J. Biol. Chem. *282*, 23811-23817.
10. Chevalier-Larsen,E.S., Wallace,K.E., Pennise,C.R , and Holzbaur,E.L. (2008). Lysosomal proliferation and distal degeneration in motor neurons expressing the G59S mutation in the p150Glued subunit of dynactin. Hum. Mol. Genet. *17*, 1946-1955.
11. Christoforidis,S., McBride,H.M., Burgoyne,R.D., and Zerial,M. (1999). The Rab5 effector EEA1 is a core component of endosome docking. Nature *397*, 621-625.
12. Codogno,P., Mehrpour,M., and Proikas-Cezanne,T. (2012). Canonical and non-canonical autophagy: variations on a common theme of self-eating? Nat. Rev. Mol. Cell Biol. *13*, 7-12.
13. Colin,E., Zala,D., Liot,G., Rangone,H., Borrell-Pages,M., Li,X.J., Saudou,F., and Humbert,S. (2008). Huntingtin phosphorylation acts as a molecular switch for anterograde/retrograde transport in neurons. EMBO J. *27*, 2124-2134.
14. Cozier,G.E., Carlton,J., McGregor,A.H., Gleeson,P.A., Teasdale,R.D., Mellor,H., and Cullen,P.J. (2002). The phox homology (PX) domain-dependent, 3-phosphoinositide-mediated association of sorting nexin-1 with an early sorting endosomal compartment is required for its ability to regulate epidermal growth factor receptor degradation. J. Biol. Chem. *277*, 48730-48736.
15. Cullinane,A.R., Straatman-Iwanowska,A., Zaucker,A., Wakabayashi,Y., Bruce,C.K., Luo,G., Rahman,F., Gurakan,F., Utine,E., Ozkan,T.B., Denecke,J., Vukovic,J., Di Rocco,M., Mandel,H., Cangul,H., Matthews,R.P., Thomas,S.G., Rappoport,J.Z., Arias,I.M., Wolburg,H., Knisely,A.S., Kelly,D.A., Muller,F., Maher,E.R., and Gissen,P. (2010). Mutations in VIPAR cause an arthrogryposis, renal dysfunction and cholestasis syndrome phenotype with defects in epithelial polarization. Nat. Genet. *42*, 303-312.
16. Dell'Angelica,E.C., Mullins,C., Caplan,S., and Bonifacino,J.S. (2000). Lysosome-related organelles. FASEB J. *14*, 1265-1278.
17. Du,X., Kumar,J., Ferguson,C., Schulz,T.A., Ong,Y.S., Hong,W., Prinz,W.A., Parton,R.G., Brown,A.J., and Yang,H. (2011). A role for oxysterol-binding protein-related protein 5 in endosomal cholesterol trafficking. J. Cell Biol. *192*, 121-135.
18. Fairn,G.D. and Grinstein,S. (2012). How nascent phagosomes mature to become phagolysosomes. Trends Immunol. *33*, 397-405.
19. Falcon-Perez,J.M., Starcevic,M., Gautam,R., and Dell'Angelica,E.C. (2002). BLOC-1, a novel complex containing the pallidin and muted proteins involved in the biogenesis of melanosomes and platelet-dense granules. J. Biol. Chem. *277*, 28191-28199.
20. Farrer,M.J., Hulihan,M.M., Kachergus,J.M , Dachsel,J.C., Stoessl,A.J., Grantier,L.L., Calne,S , Calne,D.B., Lechevalier,B., Chapon,F., Tsuboi,Y , Yamada,T., Gutmann,L., Elibol,B., Bhatia,K.P., Wider,C., Vilarino-Guell,C., Ross,O.A., Brown,L.A., Castanedes-Casey,M., Dickson,D.W , and Wszolek,Z.K. (2009). DCTN1 mutations in Perry syndrome. Nat. Genet. *41*, 163-165.
21. Garg,S., Sharma,M., Ung,C., Tuli,A., Barral,D.C., Hava,D.L., Veerapen,N., Besra,G.S., Hacohen,N., and Brenner,M.B. (2011).

Lysosomal trafficking, antigen presentation, and microbial killing are controlled by the Arf-like GTPase Arl8b. Immunity *35*, 182-193.

22. Gissen,P., Johnson,C.A., Gentle,D., Hurst,L.D., Doherty,A.J., O'Kane,C.J., Kelly,D.A., and Maher,E.R. (2005). Comparative evolutionary analysis of VPS33 homologues: genetic and functional insights. Hum. Mol. Genet. *14*, 1261-1270.
23. Gorvel,J.P., Chavrier,P., Zerial,M., and Gruenberg,J. (1991). rab5 controls early endosome fusion in vitro. Cell *64*, 915-925.
24. Griffiths,G.M. and Argon,Y. (1995). Structure and biogenesis of lytic granules. Curr. Top. Microbiol. Immunol. *198*, 39-58.
25. Gullberg,U., Andersson,E., Garwicz,D., Lindmark,A., and Olsson,I. (1997). Biosynthesis, processing and sorting of neutrophil proteins: insight into neutrophil granule development. Eur. J. Haematol. *58*, 137-153.
26. Harrington,A.J., Yacoubian,T.A., Slone,S.R , Caldwell,K.A., and Caldwell,G.A. (2012). Functional analysis of VPS41-mediated neuroprotection in Caenorhabditis elegans and mammalian models of Parkinson's disease. J. Neurosci. *32*, 2142-2153.
27. Hollenbeck,P.J. and Swanson,J.A. (1990). Radial extension of macrophage tubular lysosomes supported by kinesin. Nature *346*, 864-866.
28. Huizing,M., Didier,A., Walenta,J., Anikster,Y., Gahl,W.A., and Kramer,H. (2001). Molecular cloning and characterization of human VPS18, VPS 11, VPS16, and VPS33. Gene *264*, 241-247.
29. Ikonen,E. (2008). Cellular cholesterol trafficking and compartmentalization. Nat. Rev. Mol. Cell Biol. *9*, 125-138.
30. Johansson,M., Rocha,N., Zwart,W., Jordens,I., Janssen,L., Kuijl,C., Olkkonen,V.M., and Neefjes,J. (2007). Activation of endosomal dynein motors by stepwise assembly of Rab7-RILP-p150Glued, ORP1L, and the receptor betalll spectrin. J. Cell Biol. *176*, 459-471.
31. Jordens,I., Fernandez-Borja,M., Marsman,M , Dusseljee,S., Janssen,L., Calafat,J., Janssen,H , Wubbolts,R., and Neefjes,J. (2001). The Rab7 effector protein RILP controls lysosomal transport by inducing the recruitment of dynein-dynactin motors. Curr. Biol. *11*, 1680-1685.
32. Kamal,A., Almenar-Queralt,A., LeBlanc,J.F., Roberts,E.A., and Goldstein,L.S. (2001). Kinesin-mediated axonal transport of a membrane compartment containing beta-secretase and presenilin-1 requires APP. Nature *414*, 643-648.
33. Klumperman,J. (2011). Architecture of the mammalian Golgi. Cold Spring Harb. Perspect. Biol. *3*.
34. Kobuna,H., Inoue,T., Shibata,M., Gengyo-Ando,K., Yamamoto,A., Mitani,S., and Arai,H. (2010). Multivesicular body formation requires OSBP-related proteins and cholesterol. PLoS Genet. *6*.
35. Lee,H.H., Nemecek,D., Schindler,C., Smith,W.J , Ghirlando,R , Steven,A.C., Bonifacino,J.S., and Hurley,J.H. (2012). Assembly and architecture of biogenesis of lysosome-related organelles complex-1 (BLOC-1). J. Biol. Chem. *287*, 5882-5890.
36. Luzio,J.P., Rous,B.A., Bright,N.A., Pryor,P.R., Mullock,B.M., and Piper,R.C. (2000). Lysosome-endosome fusion and lysosome biogenesis. J. Cell Sci. *113 (Pt 9)*, 1515-1524.
37. Mamo,A., Jules,F., Dumaresq-Doiron,K., Costantino,S., and Lefrancois,S. (2012). The role of ceroid lipofuscinosis neuronal protein 5 (CLN5) in endosomal sorting. Mol. Cell Biol. *32*, 1855-1866.
38. Marone,G., Casolaro,V., Patella,V., Florio,G., and Triggiani,M. (1997). Molecular and cellular biology of mast cells and basophils. Int Arch. Allergy Immunol. *114*, 207-217.
39. Mayor,S. and Pagano,R.E. (2007). Pathways of clathrin-independent endocytosis. Nat. Rev. Mol. Cell Biol. *8*, 603-612.
40. McNicol,A. and Israels,S.J. (1999). Platelet dense granules: structure, function and implications for haemostasis. Thromb. Res. *95*, 1-18.
41. Mrakovic,A., Kay,J.G., Furuya,W., Brumell,J.H., and Botelho,R.J. (2012). Rab7 and Arl8 GTPases are Necessary for Lysosome Tubulation in Macrophages. Traffic *13*, 1667-1679.
42. Nakamura,N., Hirata,A., Ohsumi,Y., and Wada,Y. (1997). Vam2/Vps41p and Vam6/Vps39p are components of a protein complex on the vacuolar membranes and involved in the vacuolar assembly in the yeast Saccharomyces cerevisiae. J. Biol. Chem. *272*, 11344-11349.
43. Nickerson,D.P., Brett,C.L., and Merz,A.J. (2009). Vps-C complexes: gatekeepers of endolysosomal traffic. Curr. Opin. Cell Biol. *21*, 543-551.
44. Nisar,S., Kelly,E., Cullen,P.J., and Mundell,S.J. (2010). Regulation of P2Y1 receptor traffic by sorting Nexin 1 is retromer independent. Traffic *11*, 508-519.
45. Nishimura,A.L., Mitne-Neto,M., Silva,H.C., Richieri-Costa,A., Middleton,S., Cascio,D., Kok,F., Oliveira,J.R., Gillingwater,T., Webb,J., Skehel,P., and Zatz,M. (2004). A mutation in the vesicle-trafficking protein VAPB causes late-onset spinal muscular atrophy and amyotrophic lateral sclerosis. Am. J. Hum. Genet. *75*, 822-831.
46. Orlow,S.J. (1995). Melanosomes are specialized members of the lysosomal lineage of organelles. J. Invest. Dermatol. *105*, 3-7.

47. Peplowska,K., Markgraf,D.F., Ostrowicz,C.W., Bange,G., and Ungermann,C. (2007). The CORVET tethering complex interacts with the yeast Rab5 homolog Vps21 and is involved in endo-lysosomal biogenesis. Dev. Cell *12*, 739-750.
48. Poteryaev,D., Datta,S., Ackema,K., Zerial,M., and Spang,A. (2010). Identification of the switch in early-to-late endosome transition. Cell *141*, 497-508.
49. Progida,C., Malerod,L., Stuffers,S., Brech,A., Bucci,C., and Stenmark,H. (2007). RILP is required for the proper morphology and function of late endosomes. J. Cell Sci. *120*, 3729-3737.
50. Prosser,D.C., Tran,D., Schooley,A., Wendland,B., and Ngsee,J.K. (2010). A novel, retromer-independent role for sorting nexins 1 and 2 in RhoG-dependent membrane remodeling. Traffic *11*, 1347-1362.
51. Rink,J., Ghigo,E., Kalaidzidis,Y., and Zerial,M. (2005). Rab conversion as a mechanism of progression from early to late endosomes. Cell *122*, 735-749.
52. Rocha,N., Kuijl,C., van der Kant,R., Janssen,L., Houben,D., Janssen,H., Zwart,W., and Neefjes,J. (2009). Cholesterol sensor ORP1L contacts the ER protein VAP to control Rab7-RILP-p150 Glued and late endosome positioning. J. Cell Biol. *185*, 1209-1225.
53. Rocha,N. and Neefjes,J. (2008). MHC class II molecules on the move for successful antigen presentation. EMBO J. *27*, 1-5.
54. Rojas,R., van Vlijmen,T., Mardones,G.A., Prabhu,Y., Rojas,A.L., Mohammed,S., Heck,A.J., Raposo,G., van der Sluijs,P., and Bonifacino,J.S. (2008). Regulation of retromer recruitment to endosomes by sequential action of Rab5 and Rab7. J. Cell Biol. *183*, 513-526.
55. Rosa-Ferreira,C. and Munro,S. (2011). Arl8 and SKIP act together to link lysosomes to kinesin-1. Dev. Cell *21*, 1171-1178.
56. Ryder,P.V. and Faundez,V. (2009). Schizophrenia: the "BLOC" may be in the endosomes. Sci. Signal *2*, e66.
57. Saftig,P. and Klumperman,J. (2009). Lysosome biogenesis and lysosomal membrane proteins: trafficking meets function. Nat. Rev. Mol. Cell Biol. *10*, 623-635.
58. Sato,T.K., Rehling,P., Peterson,M.R., and Emr,S.D. (2000). Class C Vps protein complex regulates vacuolar SNARE pairing and is required for vesicle docking/fusion. Mol. Cell *6*, 661-671.
59. Seaman,M.N. (2012). The retromer complex - endosomal protein recycling and beyond. J. Cell Sci. *125*, 4693-4702.
60. Seaman,M.N., Harbour,M.E., Tattersall,D., Read,E., and Bright,N. (2009). Membrane recruitment of the cargo-selective retromer subcomplex is catalysed by the small GTPase Rab7 and inhibited by the Rab-GAP TBC1D5. J. Cell Sci. *122*, 2371-2382.
61. Starcevic,M. and Dell'Angelica,E.C. (2004). Identification of snapin and three novel proteins (BLOS1, BLOS2, and BLOS3/reduced pigmentation) as subunits of biogenesis of lysosome-related organelles complex-1 (BLOC-1). J. Biol. Chem. *279*, 28393-28401.
62. Stenmark,H. (2009). Rab GTPases as coordinators of vesicle traffic. Nat. Rev. Mol. Cell Biol. *10*, 513-525.
63. Swarbrick,J.D., Shaw,D.J., Chhabra,S., Ghai,R., Valkov,E., Norwood,S.J., Seaman,M.N., and Collins,B.M. (2011). VPS29 is not an active metallo-phosphatase but is a rigid scaffold required for retromer interaction with accessory proteins. PLoS One *6*, e20420.
64. Uusi-Rauva,K., Kyttala,A., van der Kant,R., Vesa,J., Tanhuanpaa,K., Neefjes,J., Olkkonen,V.M., and Jalanko,A. (2012). Neuronal ceroid lipofuscinosis protein CLN3 interacts with motor proteins and modifies location of late endosomal compartments. Cell Mol. Life Sci. *69*, 2075-2089.
65. Vardarajan,B.N., Bruesegem,S.Y., Harbour,M.E., George-Hyslop,P., Seaman,M.N., and Farrer,L.A. (2012). Identification of Alzheimer disease-associated variants in genes that regulate retromer function. Neurobiol. Aging *33*, 2231.
66. Vihervaara,T., Uronen,R.L., Wohlfahrt,G., Bjorkhem,I., Ikonen,E., and Olkkonen,V.M. (2011). Sterol binding by OSBP-related protein 1L regulates late endosome motility and function. Cell Mol. Life Sci. *68*, 537-551.
67. Vilarino-Guell,C., Wider,C., Ross,O.A., Dachsel,J.C., Kachergus,J.M., Lincoln,S.J., Soto-Ortolaza,A.I., Cobb,S.A., Wilhoite,G.J., Bacon,J.A., Behrouz,B., Melrose,H.L., Hentati,E., Puschmann,A., Evans,D.M., Conibear,E., Wasserman,W.W., Aasly,J.O., Burkhard,P.R., Djaldetti,R., Ghika,J., Hentati,F., Krygowska-Wajs,A., Lynch,T., Melamed,E., Rajput,A., Rajput,A.H., Solida,A., Wu,R.M., Uitti,R.J., Wszolek,Z.K., Vingerhoets,F., and Farrer,M.J. (2011). VPS35 mutations in Parkinson disease. Am. J. Hum. Genet. *89*, 162-167.
68. Wen,L., Tang,F.L., Hong,Y., Luo,S.W., Wang,C.L., He,W., Shen,C., Jung,J.U., Xiong,F., Lee,D.H., Zhang,Q.G., Brann,D., Kim,T.W., Yan,R., Mei,L., and Xiong,W.C. (2011). VPS35 haploinsufficiency increases Alzheimer's disease neuropathology. J. Cell Biol. *195*, 765-779.

69. Wubbolts,R., Fernandez-Borja,M., Oomen,L., Verwoerd,D., Janssen,H., Calafat,J., Tulp,A., Dusseljee,S., and Neefjes,J. (1996). Direct vesicular transport of MHC class II molecules from lysosomal structures to the cell surface. J. Cell Biol. *135*, 611-622.

70. Wurmser,A.E., Sato,T.K., and Emr,S.D. (2000). New component of the vacuolar class C-Vps complex couples nucleotide exchange on the Ypt7 GTPase to SNARE-dependent docking and fusion. J. Cell Biol. *151*, 551-562.

71. Xu,B., Ionita-Laza,I., Roos,J.L., Boone,B., Woodrick,S., Sun,Y., Levy,S., Gogos,J.A., and Karayiorgou,M. (2012). De novo gene mutations highlight patterns of genetic and neural complexity in schizophrenia. Nat. Genet. *44*, 1365-1369.

72. Yuzaki,M. (2010). Snapin snaps into the dynein complex for late endosome-lysosome trafficking and autophagy. Neuron *68*, 4-6.

73. Zala,D., Hinckelmann,M.V., Yu,H., Lyra da Cunha,M.M., Liot,G., Cordelieres,F.P., Marco,S., and Saudou,F. (2013). Vesicular glycolysis provides on-board energy for fast axonal transport. Cell *152*, 479-491.

74. Zhu,G.D., Salazar,G., Zlatic,S.A., Fiza,B., Doucette,M.M., Heilman,C.J., Levey,A.I., Faundez,V., and L'hernault,S.W. (2009). SPE-39 family proteins interact with the HOPS complex and function in lysosomal delivery. Mol. Biol. Cell *20*, 1223-1240.

75. Zimprich,A , Benet-Pages,A., Struhal,W., Graf,E , Eck,S.H., Offman,M.N., Haubenberger,D., Spielberger,S., Schulte,E.C., Lichtner,P., Rossle,S.C., Klopp,N., Wolf,E., Seppi,K., Pirker,W , Presslauer,S., Mollenhauer,B., Katzenschlager,R , Foki,T., Hotzy,C., Reinthaler,E., Harutyunyan,A , Kralovics,R., Peters,A., Zimprich,F., Brucke,T , Poewe,W., Auff,E., Trenkwalder,C., Rost,B., Ransmayr,G., Winkelmann,J., Meitinger,T., and Strom,T.M. (2011). A mutation in VPS35, encoding a subunit of the retromer complex, causes late-onset Parkinson disease. Am. J. Hum. Genet. *89*, 168-175.

chapter **TWO**

The endoplasmic reticulum as a central organelle organizer

Rik van der Kant
Jacques Neefjes

Division of Cell Biology, the Netherlands Cancer Institute, Amsterdam NL

Correspondence: j.neefjes@nki.nl

Adapted from review in preparation, Journal of Cell Science

Abstract

The Endoplasmic Reticulum (ER) fills the cytosolic space and is by far the largest intracellular compartment. The ER is traditionally considered a site for protein synthesis, folding and export while other functions are usually ignored. This may be a limited view. Due to its size and omnipresence, the ER functions as a membrane source for organelles such as autophagosomes, peroxisomes and lipid droplets and is able to contact all intracellular organelles to control lipid transfer, signaling and intracellular transport. Here we postulate a more central role of the ER in distributing software between intracellular compartments to control their biochemistry, transport, signal transduction and without doubt many other processes yet to be uncovered. The ER is not large just for protein synthesis, but applies its intracellular corpulence for organelle contacts and control.

From its first description in 1945, the Endoplasmic Reticulum (ER) has been one of the most studied cellular organelles. In fact, it represents an interconnected network of tubules and cisternae that occupies the entire cytosolic space. Rough ER (ER lined by ribosomes) defines sites of protein translation, whereas the smooth ER is considered a site of lipid production and storage of lipids and ions. A third ER 'subdomain' recognized is the nuclear envelope. The ER is by far the largest intracellular organelle containing about 70% of cellular lipids and contributes to generation of other organelles such as the Golgi complex. By specific interactions between ER resident and organelle resident proteins, the ER can generate membrane contact sites (MCSs) with other compartments. MCS's resemble intracellular synapses where membrane proteins from two compartments can directly interact and regulate processes as diverse as lipid and ion transfer but also microtubule-motor binding. Given its omnipresence in the cytosol, the ER is the basic compartment to integrate and coordinate communication with and between different intracellular compartments. Here we will discuss how the ER guides the biogenesis and maintenance of other, apparently unrelated organelles and how information is exchanged between the ER and these organelles. We will elaborate on how the ER can integrate, rank and distribute information gathered from the different organelles and discuss the molecular mechanisms as understood at present. These uncover a new role for the ER in cellular homeostasis: distributing biochemical information from organelles to control life and location of other intracellular compartments.

The ER as an Organelle birth ground

Considering the origin of membranes for organelles touches the basis of cellular life. Membranes in the endocytic system are derived from the plasma membrane and the Golgi is derived from the ER. Yet, the origin of membranes for organelles such as peroxisomes, autophagosomes and lipid droplets (LD) has long been elusive. As the ER holds most cellular lipids, it may be the prime candidate for donating membranes to other organelles. The ER is indeed a major contributor to the formation of autophagosomes, peroxisomes and LD and the mechanisms are beginning to be elucidated, as illustrated below.

As a first step in LD biogenesis, neutral lipids accumulate between ER bilayer leaflets at defined sites[1]. Subsequently the hemi-membrane will bud into the cytosol to provide the phospholipid monolayer, while lipids accumulate in the interior before the mature LD releases itself from the ER. An alternative model suggest that the ER and LD are not continuous but that the ER membrane is tightly wrapped around the lipid droplet resembling an egg cup (the ER) holding an egg (the lipid droplet)[2]. Proteins involved in lipid metabolism such as the ER resident FATP1/acyl-CoA synthetase and the lipid droplet protein DGAT2/diacylglycerol acyltransferase interact at these ER-LD contact sites[3] (figure 1). Another ER protein, Seipin, also localizes to these inter-organellar contact sites and determines the morphology of lipid droplets and their metabolism[4]. The ER is thus involved in the control of various steps in the birth and life of lipid droplets.

Autophagosomes are compartments induced by starvation and require membranes to encapsulate cytosol before fusion to lysosomes for the degradation of cytosolic material. But what is the origin of the membranes for this compartment? PI3P is required to initiate autophagosome

formation[5] and is produced by Atg14. Atg14 localizes to the ER and the phagophore (the autophagosome precursor). The ER is critical in this process as a mutant of Atg14 unable to bind the ER impairs autophagosome formation[5,6]. The specialized regions of the ER that provide the autophagosomal membranes are termed "omegasomes" [7]. Omegasomes are continuous with the ER membrane and cradles between two ER membranes during early stages of growth [8] (figure 2). How scission of the omegasome from the ER occurs is -like for other ER derived compartments- unclear, as is the role of the ER in later stages of autophagosome maturation and fusion with lysosomes.

A third compartment originating from the ER is the peroxisome[9-11]. Two subpopulations of pre-peroxisomal vesicles (each containing half of the peroxisomal translocon machinery) bud from the ER[12]. These two populations fuse later to assemble a functional translocon allowing the peroxisome to import matrix proteins for its maturation.

The ER is the largest membrane-containing compartment in the cell and contributes to the early life of different compartments. As in normal adult-child interactions, the ER stays in close contact with these (and other) organelles long after their initial birth.

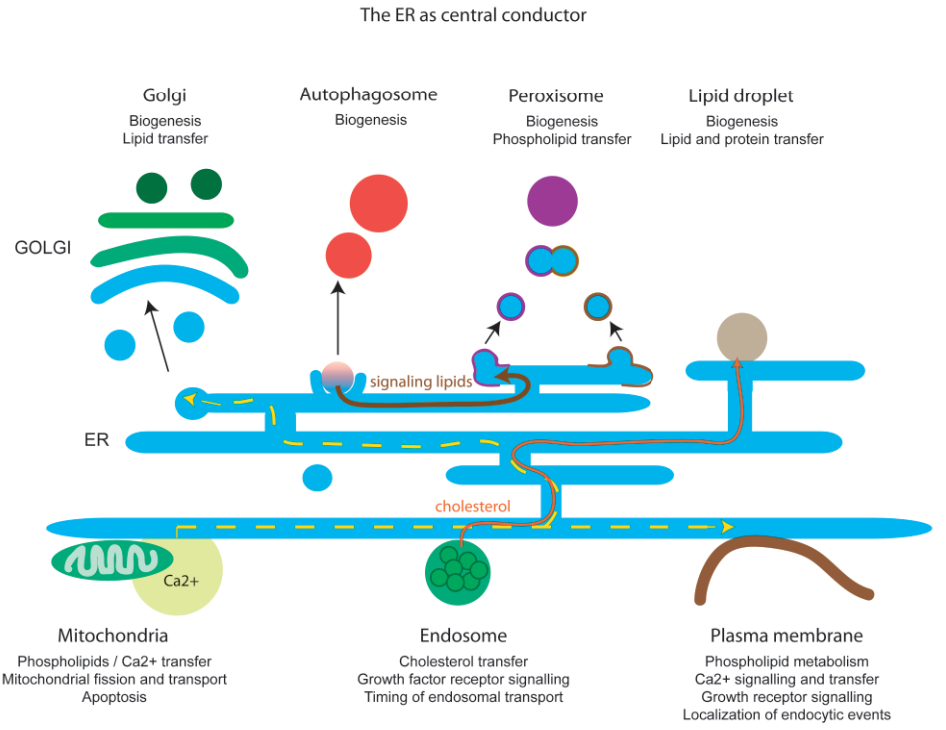


Figure 1. The ER as a central conductor. The ER is the largest intracellular compartment. Illustrated are new functions of the ER that relate to the birth of organelles (shown at top) and direct interactions in membrane contact sites- with organelles and the plasma membrane (bottom). The transfer of lipids and cholesterol by lateral diffusion in ER membranes is depicted. These and other molecules can use the ER to distribute to different compartments without exposure into the free cytosol. Some of the functions of organelles related to the ER is depicted in the figure.

Staying in touch

Membrane contact sites (MCS) are defined as sites where membranes of two organelles locate within 10-30 nm (for comparison, the thickness of a lipid bilayer is ~10 nm while a small protein like GFP is ~5 nm) (figure 3). Proteins of opposite compartments can interact to form functional inter-compartment interactions within this space[13,14]. MCS's are only recently recognized and their function (if only one) not fully specified. We asked leaders in this developing area on their opinion of the function of MCSs, and their quotes are summarized in Box 1. One dominant feeling is that information exchange between compartments occurs at MCS (as described below). In a way, the ER might be considered the cell's central nervous system, able to gather,

Box 1

Will Prinz National Institute of Diabetes and Digestive and Kidney diseases, NIH, Bethesda	"Membrane contact sites may be regions were signals and small molecules are effectively channeled between organelles, increasing the rate and efficiency of exchange."
Clare Futter UCL institute of Ophthalmology, London, UK	"The close apposition of the ER membrane with the membranes of other organelles generates a discrete micro-environment with the potential for lipid transfer and protein-protein interactions."
Scot Emr and Chris Stefan Cornell University, Ithaca, USA	"The endoplasmic reticulum is the foundation of the secretory pathway, as it serves essential roles in protein and lipid biosynthesis. Intracellular signaling at ER-organelle junctions provides an elegant system to coordinate protein and lipid synthesis in the ER, in response to cues from various compartments along the secretory and endocytic pathways."
Rik van der Kant and Jacques Neefjes, The Netherlands Cancer Institute, Amsterdam NL	"The ER controls the location of other compartments by affecting motor protein binding. This inter-organelle control is likely controlled by the transfer of lipids within the membrane contact sites.".
Tim Levine UCL institute of Ophthalmology, London, UK	"If lipids do not cross between organelles at contact sites by the action of lipid transfer proteins then I'll have been proved absolutely wrong."

integrate and distribute information between all organelles[13,15,16]. This information often comes in the form of (signaling) lipids and calcium that are exchanged at MCS between the ER and other organelles. The ER can subsequently distribute lipids via membrane diffusion and ions through the ER luminal space to other compartments thus acting as a passive, long-range pan-cellular distribution system[15]. MCS probably not only function as sites of substance transfer, but may also play a more active role in cellular homeostasis by sensing the need for ions, lipids (and other undefined substances) of individual organelles. The ER is thus a major distributor of molecules that are difficult to selectively distribute by other means. As a result, the ER senses the homeostasis of the different organelles in a cell. But what is transferred at MCS and how?

Information transfer at Membrane Contact Sites

Hydrophobic lipids can be distributed by vesicular transport or by lipid carriers[15]. Alternatively, lipids can use the ER for lateral diffusion to other compartments before actual transfer in MCS by lipid transfer proteins (summarized in figure 2). Examples of lipid transfer proteins are Golgi proteins such as CERT, Nir2, OSBP and possibly ORP9. These proteins possess an FFAT motif to contact the ER protein VAP (figure 2) for lipid transfer[17-19]. Cholesterol transport between endosomes and the ER also involves MCS containing ER protein ORP5 and endosomal proteins HRS and NPC-1[20,21]. Membrane contact sites between the ER and late endosome are established by another OSBP family member, ORP1L, that senses but may not transfer cholesterol[22]. Triglyceride synthesis in lipid droplets is controlled by the ER protein PATP1 [3]. In addition, the ER/Golgi resident PI/PC exchange protein Nir2 can appear on lipid droplets possibly to support lipid transfer at ER-lipid droplets contact sites [23]. Other lipid transfer proteins enriched in MCS between the ER and LD are Seipin (in yeast)[4], Adiphophilin[2] and possibly ORP2 [24]. The exchange of phospholipids between peroxisomes and the ER [25] likely also involves peroxisome-ER contacts sites[10,16]. In general, a theme emerges where the ER provides a distribution system for lipids and other compounds that cannot efficiently be delivered by simple diffusion in the hydrophilic milieu of the cytosol. The ER then dynamically contacts other compartments for specific exchange and delivery.

Data integration by membrane contact sites

While some lipids are membrane building blocks, other lipids can act as second messengers in signal transduction. If such lipids are transferred at MCS between compartments, signals are very specifically delivered in an undiluted manner. At present, there are two compartments defined for inter-compartmental signal control by the ER: the cell surface and mitochondria. Further studies may broaden this concept to other compartments.

How does the ER control signaling at the cell surface and mitochondria? Contact sites between ER and plasma membrane (PM) are particularly obvious in muscle where the sarcoplasmic reticulum (SR) (ER found in smooth and striated muscle) is positioned within 10-20 nm of the plasma membrane [26]. Upon ligand binding, many membrane receptors initiate the production of Inositol-1,4,5-trisphosphate (IP_3) at the PM. IP3 activates the IP3 receptor (IP3R) in the ER to release Ca^{2+} that acts as second messenger in signaling. After the depletion

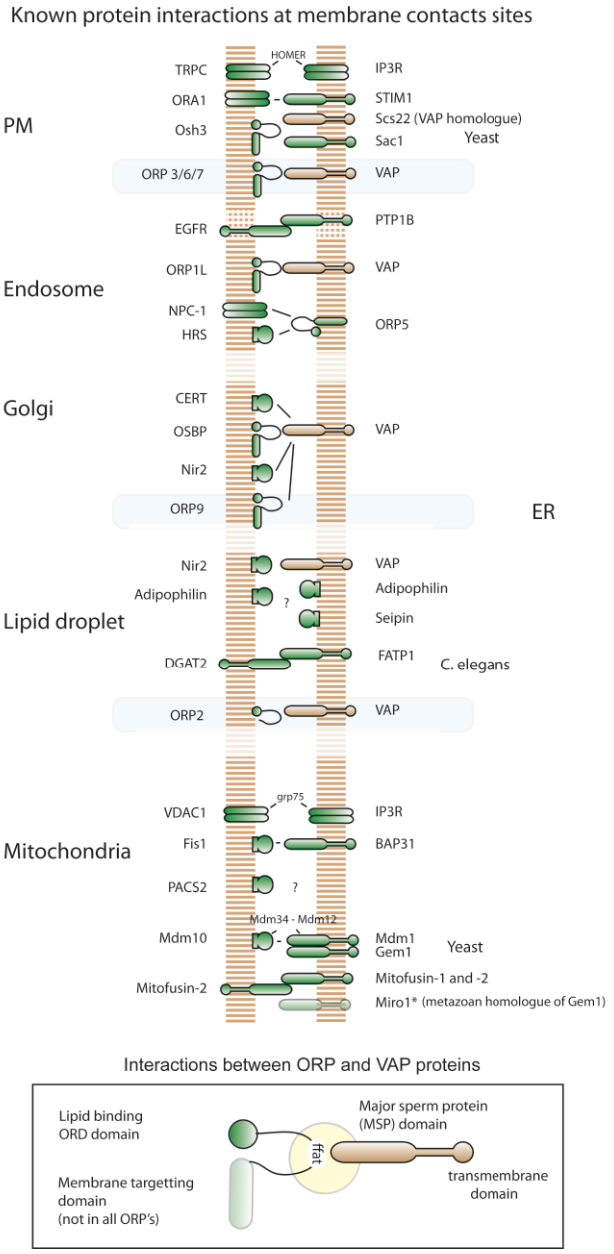


Figure 2. Protein-protein interactions in ER-organelle MCS's. ER protein interactions (Right) with proteins of other compartments as indicated (Left). These proteins meet in MCS's or MCS are formed as the result of these interactions. Proteins involved in these interactions are diverse. Bottom. Box illustrates a common interaction in MCS's where the integral ER protein VAP (**A** and **B**) (right) interacts with proteins containing a FFAT motif (meaning 'two phenylalanines in an acidic trail (Aspartate and Glutamate rich trail') (left). These proteins belong to from the ORP (oxysterol binding protein related protein, Osh in Yeast) family that are (often) lipid transfer proteins through the ORD domain. The FFAT motif is essential for interacting with the MSP domain of VAP (in yellow circle).

of Ca^{2+} from the ER lumen, Ca^{2+} channels in the PM open to allow entry of extra-cellular Ca^{2+} to fill the ER. Efficient directional transfer without long distance diffusion of Ca^{2+} in the cytosol is solved by MCS between plasma membrane and ER.

The molecular mechanisms are understood to some degree. The ER protein STIM1 is enriched at the PM-ER interface following depletion of Ca^{2+} from ER stores[27]. STIM1 then interacts with the ORA1 subunit of CRAC channels at the plasma membrane to open these for Ca^{2+} inflow[28]. IP3R in the ER also contacts other calcium (TRPC) channels in the plasma membrane via an adapter protein called Homer1[29]. Of note, Homer1 binds to a wide variety of receptors at the plasma membrane yielding probably a broader signaling response than currently anticipated[29]. As stated above, the first step in the response to calcium signaling is the generation of IP3. Also this may be cross-compartmentally controlled as studies in yeast suggest that ER-PM contact sites actually regulate plasma membrane PI metabolism[30], possibly controlling PI flux and calcium signaling at the plasma membrane via the ER. The plasma membrane controls Ca^{2+} release from the ER and the ER controls Ca^{2+} inflow via the plasma membrane to spatially control second messengers signaling.

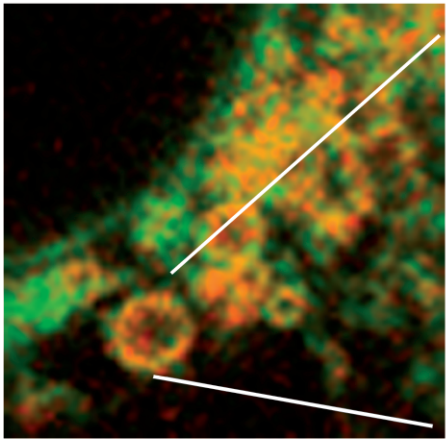
Is cross-talk between ER and plasma membrane the exception or does it exemplifies a broader concept? Other important mediators in Ca^{2+} signaling are mitochondria. Mitochondria store Ca^{2+} from the cytosol, participate in Ca^{2+} signaling and make frequent contacts with the ER to regulate Ca^{2+} transfer[31-35]. In addition, phospholipids (PS and PC) and probably cholesterol are also transported from the ER to mitochondria utilizing MCS[33,36]. How formation of these MCS is controlled is understood at some level of detail and involves the ERMES complex in yeast that includes Gem1[33,37]. Gem1 is a small GTPase with Ca^{2+} sensing abilities controlling phospholipid exchange between the ER and mitochondria[36]. The ERMES complex is absent in metazoans, but possibly replaced by another ER-mitochondria tethering complex of mitofusins that may interact with Miro1, the mammalian homologue of Gem1, to regulate ER-mitochondria MCS[37-39].

Local Ca^{2+} transfer between ER and other organelles has not yet been described. However, Ca^{2+} is involved in the dynamics of lysosomes[40], Golgi[41] and peroxisomes[42] and all of these organelles are also contacted by the ER. How the ER integrates lipid and Ca^{2+} signaling at MCS with these and other organelles, remains an intriguing question.

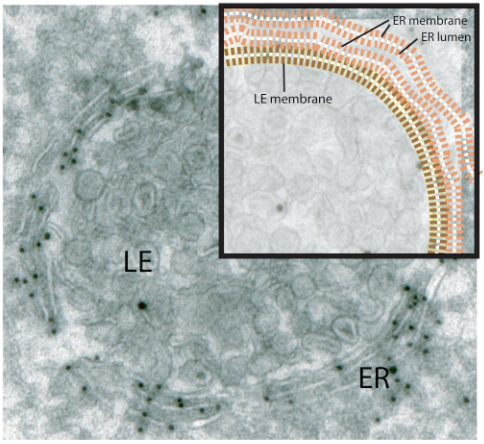
Textbook pictures suggest that a cell contains isolated organelles connected through vesicular transport. This view is now challenged by the concept of dynamic inter-organel interactions that serve to exchange lipid, ionic and other information between different compartments. The ER might serve as the central nervous system of the cell integrating signals acquired through the various MCS, acting as a middleman for different compartments to control intracellular dynamics and signaling.

The ER as terminator of extracellular signaling

The EGF-receptor (EGFR) is strongly phosphorylated following binding of EGF. Phosphorylation induces signal transduction that can be terminated by protein-tyrosine phosphatase 1B (PTP1B). A topological problem occurred when PTP1B was shown to reside on the cytosolic side of the ER implying the ER in control of EGFR signaling. Recent data indicate that the ER contacts



Confocal micropy
Green: VAP-A (ER protein)
Red: ORP1L (Late endosomal protein)



Immuno-EM
small gold: VAP-A (ER protein)
large gold: ORP1L (Late endosomal protein)

Figure 3. Contact site or fusion? Many organelles make transient - non-continuous - contacts with the ER. These can be easily observed by confocal microscopy (Left) when one compartment (late endosomes) is labeled differently than the ER. When ORP1L (a late endosomal protein) is expressed, the ER protein VAP perfectly colocalizes suggesting fusion of late endosomes with ER. The resolution of light microscopy is usually >240 nm leaving details below this unresolved. When the same cells are analyzed by electron microscopy, the formation of MCS between late endosomes and ER is observed with the two markers labeling exclusively their respective compartments. MCS appear as one membrane by light and as two by electron microscopy. No evidence for fusion of ER and late endosomes was observed at sufficient resolution (for details, see [22]).

endosomes carrying phosphorylated EGFR to induce contacts with PTP1B [43]. As PTP1B is involved in more signaling processes, the ER may have a broader involvement in the spatial and temporal control of these and other processes.

The ER as an organelle organizer

Is the ER only mediating inter-compartmental lipid and Ca^{2+} transfer at MCS or is the ER also actively controlling organelle behavior? Lipids and Ca^{2+} are known to affect the location of organelles, a system that might be co-regulated by the ER. The inter-compartmental control of these processes has only recently been realized and is illustrated by two examples that are understood in molecular detail: scission of mitochondria, and dynein motor-mediated transport of late endosomes and lysosomes.

One of the most spectacular examples of ER control of dynamics of other organelles is the fission of mitochondria[44]. The ER tightly wraps around mitochondria during fission events marking the site of mitochondrial division. The ER may further support fission by depositing Ca^{2+} at these (now scission) sites required for the recruitment of cytosolic Drp1 to mitochondrial membranes[45]. Drp1 is a dynamin-related protein that provides the mechanical force for fission[46].

Ca^{2+} also regulates mitochondrial transport via the calcium binding protein Miro1/Rhot1, a GTPase that interacts with motor proteins to regulate transport[47]. In yeast, Miro1 is found at the ER-mitochondrial interface, indicating a role for MCS in mitochondrial trafficking[39]. Of note, another protein enriched at the ER-mitochondrial interface is Fis1, a protein involved in apoptosis by controlling cytochrome C release. The ER-mitochondria MCS's may thus control apoptosis (figure 2)[48,49]. Since Fis1 and Drp1 are also involved in peroxisomal dynamics, a similar mechanism involving the ER may be at work there as well [50,51].

Endosomes move due to the activities of microtubule and actin-based motor proteins that determine their intracellular location[52]. The dynein motor transports vesicles such as late endosomes to the microtubule minus-end (where the microtubule organizing center (MTOC) resides). The dynein motor binds to late endosomes through the Rab7 effector RILP[53,54]. Rab7 also binds the FFAT motif containing cholesterol sensor ORP1L that changes conformation dependent on late endosomal cholesterol content [22]. Low LE cholesterol results in a conformation change of ORP1L allowing the FFAT motif in ORP1L to interact with ER-resident protein VAP-A. VAP-A then removes the dynein motor from late endosomes effectively allowing kinesin motors for transport to the cell periphery. Niemann-Pick and other lysosomal storage diseases such as Gaucher patients have lysosomes clustered around the MTOC and also high lysosomal cholesterol levels[55-57]. The cholesterol alters the conformation of ORP1L to not expose the FFAT motif thus preventing interactions with ER protein VAP-A. As a result, the dynein motor remains on the Rab7-RILP receptor and lysosomes cluster around the MTOC[22]. De-regulation of interactions within MCS's might also underlie other disease phenotypes such as Amyotrophic lateral sclerosis ALS[58], further illustrating the importance of inter-compartmental contacts in cellular homeostasis.

Concluding remarks

ER-organelle contact sites were first observed some 40 years ago [59]. Recent years have seen a burst of new observations and the beginning of a "molecular era of organelle contact sites" [60]. The ER is not only a site for protein synthesis and folding but is also a major organizer of other intracellular compartments, as a puppeteer controlling the marionettes. It is involved in the distribution of information in the form of Ca^{2+} and signaling lipids and the delivery of other lipids such as cholesterol between different compartments. In addition, the ER controls major cell biological events such as mitochondrial fission, organelle birth and transport of other compartments. As the ER fills the cytosolic space, it is probably the only compartment able to contact and connect every other organelle. The role of the ER as a master conductor that controls the nature of other intracellular compartments is only beginning to be appreciated and it is anticipated that many more processes involve this large and dynamic organelle. We are only at the beginning of understanding and appreciating the complexity of the ER as a central organizer of other intracellular compartments.

Reference List

1. Beller,M. *et al.* (2010) Lipid droplets: a dynamic organelle moves into focus. *FEBS Lett.* 584, 2176-2182
2. Robenek,H. *et al.* (2006) Adipophilin-enriched domains in the ER membrane are sites of lipid droplet biogenesis. *J. Cell Sci.* 119, 4215-4224
3. Xu,N. *et al.* (2012) The FATP1-DGAT2 complex facilitates lipid droplet expansion at the ER-lipid droplet interface. *J. Cell Biol.* 198, 895-911
4. Szymanski,K.M. *et al.* (2007) The lipodystrophy protein seipin is found at endoplasmic reticulum lipid droplet junctions and is important for droplet morphology. *Proc. Natl. Acad. Sci. U S A* 104, 20890-20895
5. Matsunaga,K. *et al.* (2010) Autophagy requires endoplasmic reticulum targeting of the PI3-kinase complex via Atg14L. *J. Cell Biol.* 190, 511-521
6. Axe,E.L. *et al.* (2008) Autophagosome formation from membrane compartments enriched in phosphatidylinositol 3-phosphate and dynamically connected to the endoplasmic reticulum. *J. Cell Biol.* 182, 685-701
7. Tooze,S.A. and Yoshimori,T. (2010) The origin of the autophagosomal membrane. *Nat. Cell Biol.* 12, 831-835
8. Hayashi-Nishino,M. *et al.* (2009) A subdomain of the endoplasmic reticulum forms a cradle for autophagosome formation. *Nat. Cell Biol.* 11, 1433-1437
9. Geuze,H.J. *et al.* (2003) Involvement of the endoplasmic reticulum in peroxisome formation. *Mol. Biol. Cell* 14, 2900-2907
10. Kim,P K. *et al.* (2006) The origin and maintenance of mammalian peroxisomes involves a de novo PEX16-dependent pathway from the ER. *J. Cell Biol.* 173, 521-532
11. Hoepfner,D. *et al.* (2005) Contribution of the endoplasmic reticulum to peroxisome formation. *Cell* 122, 85-95
12. van der Zand,A. *et al.* (2012) Biochemically distinct vesicles from the endoplasmic reticulum fuse to form peroxisomes. *Cell* 149, 397-409
13. Toulmay,A. and Prinz,W.A. (2011) Lipid transfer and signaling at organelle contact sites: the tip of the iceberg. *Curr. Opin. Cell Biol.* 23, 458-463
14. Toulmay,A. and Prinz,W.A. (2012) A conserved membrane-binding domain targets proteins to organelle contact sites. *J. Cell Sci.* 125, 49-58
15. Holthuis,J.C. and Levine,T.P. (2005) Lipid traffic: floppy drives and a superhighway. *Nat. Rev. Mol. Cell Biol.* 6, 209-220
16. Friedman,J.R. and Voeltz,G.K. (2011) The ER in 3D: a multifunctional dynamic membrane network. *Trends Cell Biol.* 21, 709-717
17. Peretti,D. *et al.* (2008) Coordinated lipid transfer between the endoplasmic reticulum and the Golgi complex requires the VAP proteins and is essential for Golgi-mediated transport. *Mol. Biol. Cell* 19, 3871-3884
18. Ngo,M. and Ridgway,N.D. (2009) Oxysterol binding protein-related Protein 9 (ORP9) is a cholesterol transfer protein that regulates Golgi structure and function. *Mol. Biol. Cell* 20, 1388-1399
19. Zhou,Y. *et al.* (2010) OSBP-related protein 11 (ORP11) dimerizes with ORP9 and localizes at the Golgi-late endosome interface. *Exp. Cell Res.* 316, 3304-3316
20. Du,X. *et al.* (2011) A role for oxysterol-binding protein-related protein 5 in endosomal cholesterol trafficking. *J. Cell Biol.* 192, 121-135
21. Du,X. *et al.* (2012) An essential role of hrs/vps27 in endosomal cholesterol trafficking. *Cell Rep.* 1, 29-35
22. Rocha,N. *et al.* (2009) Cholesterol sensor ORP1L contacts the ER protein VAP to control Rab7-RILP-p150 Glued and late endosome positioning. *J. Cell Biol.* 185, 1209-1225
23. Litvak,V. *et al.* (2002) Targeting of Nir2 to lipid droplets is regulated by a specific threonine residue within its PI-transfer domain. *Curr. Biol.* 12, 1513-1518
24. Hynynen,R. *et al.* (2009) OSBP-related protein 2 is a sterol receptor on lipid droplets that regulates the metabolism of neutral lipids. *J. Lipid Res.* 50, 1305-1315
25. Raychaudhuri,S. and Prinz,W.A. (2008) Nonvesicular phospholipid transfer between peroxisomes and the endoplasmic reticulum. *Proc. Natl. Acad. Sci. U S A* 105, 15785-15790
26. Shaw,L. *et al.* (2006) Caveolae and sarcoplasmic reticular coupling in smooth muscle cells of pressurised arteries: the relevance for Ca2+ oscillations and tone. *Cardiovasc. Res.* 69, 825-835
27. Wu,M.M. *et al.* (2006) Ca2+ store depletion causes STIM1 to accumulate in ER regions closely associated with the plasma membrane. *J. Cell Biol.* 174, 803-813
28. Mullins,F.M. *et al.* (2009) STIM1 and calmodulin interact with Orai1 to induce Ca2+-dependent inactivation of CRAC channels. *Proc. Natl. Acad. Sci. U S A* 106, 15495-15500

29. Yuan,J.P. *et al.* (2003) Homer binds TRPC family channels and is required for gating of TRPC1 by IP3 receptors. *Cell* 114, 777-789
30. Stefan,C.J. *et al.* (2011) Osh proteins regulate phosphoinositide metabolism at ER-plasma membrane contact sites. *Cell* 144, 389-401
31. Pizzo,P. and Pozzan,T. (2007) Mitochondria-endoplasmic reticulum choreography: structure and signaling dynamics. *Trends Cell Biol.* 17, 511-517
32. Csordas,G. *et al.* (2010) Imaging interorganelle contacts and local calcium dynamics at the ER-mitochondrial interface. *Mol. Cell* 39, 121-132
33. Kornmann,B. *et al.* (2009) An ER-mitochondria tethering complex revealed by a synthetic biology screen. *Science* 325, 477-481
34. Szabadkai,G. *et al.* (2006) Chaperone-mediated coupling of endoplasmic reticulum and mitochondrial Ca2+ channels. *J. Cell Biol.* 175, 901-911
35. Friedman,J.R. *et al.* (2010) ER sliding dynamics and ER-mitochondrial contacts occur on acetylated microtubules. *J. Cell Biol.* 190, 363-375
36. Osman,C. *et al.* (2011) Making heads or tails of phospholipids in mitochondria. *J. Cell Biol.* 192, 7-16
37. Kornmann,B. *et al.* (2011) The conserved GTPase Gem1 regulates endoplasmic reticulum-mitochondria connections. *Proc. Natl. Acad. Sci. U S A* 108, 14151-14156
38. Misko,A. *et al.* (2010) Mitofusin 2 is necessary for transport of axonal mitochondria and interacts with the Miro/Milton complex. *J. Neurosci.* 30, 4232-4240
39. Saotome,M. *et al.* (2008) Bidirectional Ca2+-dependent control of mitochondrial dynamics by the Miro GTPase. *Proc. Natl. Acad. Sci. U S A* 105, 20728-20733
40. Pryor,P.R. *et al.* (2000) The role of intraorganellar Ca(2+) in late endosome-lysosome heterotypic fusion and in the reformation of lysosomes from hybrid organelles. *J. Cell Biol.* 149, 1053-1062
41. Pizzo,P. *et al.* (2011) Ca(2+) signalling in the Golgi apparatus. *Cell Calcium* 50, 184-192
42. Lasorsa,F.M. *et al.* (2008) Peroxisomes as novel players in cell calcium homeostasis. *J. Biol. Chem.* 283, 15300-15308
43. Eden,E.R. *et al.* (2010) Membrane contacts between endosomes and ER provide sites for PTP1B-epidermal growth factor receptor interaction. *Nat. Cell Biol.* 12, 267-272
44. Friedman,J.R. *et al.* (2011) ER tubules mark sites of mitochondrial division. *Science* 334, 358-362
45. Han,X.J. *et al.* (2008) CaM kinase I alpha-induced phosphorylation of Drp1 regulates mitochondrial morphology. *J. Cell Biol.* 182, 573-585
46. Rambold,A.S. and Lippincott-Schwartz,J. (2011) Cell biology. SevERing mitochondria. *Science* 334, 186-187
47. de Brito,O.M. and Scorrano,L. (2008) Mitofusin 2 tethers endoplasmic reticulum to mitochondria. *Nature* 456, 605-610
48. Iwasawa,R. *et al.* (2011) Fis1 and Bap31 bridge the mitochondria-ER interface to establish a platform for apoptosis induction. *EMBO J.* 30, 556-568
49. Wang,B. *et al.* (2011) Fis1, Bap31 and the kiss of death between mitochondria and endoplasmic reticulum. *EMBO J.* 30, 451-452
50. Koch,A. *et al.* (2003) Dynamin-like protein 1 is involved in peroxisomal fission. *J. Biol. Chem.* 278, 8597-8605
51. Koch,A. *et al.* (2004) Peroxisome elongation and constriction but not fission can occur independently of dynamin-like protein 1. *J. Cell Sci.* 117, 3995-4006
52. Jordens,I. *et al.* (2005) Rab proteins, connecting transport and vesicle fusion. *Traffic* 6, 1070-1077
53. Jordens,I. *et al.* (2001) The Rab7 effector protein RILP controls lysosomal transport by inducing the recruitment of dynein-dynactin motors. *Curr. Biol.* 11, 1680-1685
54. Cantalupo,G. *et al.* (2001) Rab-interacting lysosomal protein (RILP): the Rab7 effector required for transport to lysosomes. *EMBO J.* 20, 683-693
55. Neufeld,E.B. *et al.* (2004) The ABCA1 transporter modulates late endocytic trafficking: insights from the correction of the genetic defect in Tangier disease. *J. Biol. Chem.* 279, 15571-15578
56. Mukherjee,S. and Maxfield,F.R. (2004) Lipid and cholesterol trafficking in NPC. *Biochim. Biophys. Acta* 1685, 28-37
57. Maxfield,F.R. and Tabas,I. (2005) Role of cholesterol and lipid organization in disease. *Nature* 438, 612-621
58. Lev,S. *et al.* (2008) The VAP protein family: from cellular functions to motor neuron disease. *Trends Cell Biol.* 18, 282-290
59. Novikoff,A.B. and Shin,W.Y. (1978) Endoplasmic reticulum and autophagy in rat hepatocytes. *Proc. Natl. Acad. Sci. U S A* 75, 5039-5042
60. Elbaz,Y. and Schuldiner,M. (2011) Staying in touch: the molecular era of organelle contact sites. *Trends Biochem. Sci.* 36, 616-623

chapter **THREE**

Cholesterol sensor ORP1L contacts the ER protein VAP to control Rab7–RILP–p150Glued and late endosome positioning

Nuno Rocha
Coenraad Kuijl*
Rik van der Kant*
Lennert Janssen
Diane Houben
Hans Janssen
Wilbert Zwart
Jacques Neefjes

Division of Cell Biology and 2Centre for Biomedical Genetics,
The Netherlands Cancer Institute, 1066CX Amsterdam, Netherlands

*C. Kuijl and R. van der Kant contributed equally to this paper

Correspondence to Wilbert Zwart: w.zwart@nki.nl; or Jacques Neefjes: j.neefjes@nki.nl

Journal of Cell Biology, Volume 185, No.7. June 2009

Abstract

Late endosomes (LEs) have characteristic intracellular distributions determined by their interactions with various motor proteins. Motor proteins associated to the dynactin subunit p150Glued bind to LEs via the Rab7 effector Rab7-interacting lysosomal protein (RILP) in association with the oxysterol-binding protein ORP1L. We found that cholesterol levels in LEs are sensed by ORP1L and are lower in peripheral vesicles. Under low cholesterol conditions, ORP1L conformation induces the formation of endoplasmic reticulum (ER)–LE membrane contact sites. At these sites, the ER protein VAP (VAMP [vesicle-associated membrane protein]-associated ER protein) can interact in trans with the Rab7–RILP complex to remove p150Glued and associated motors. LEs then move to the microtubule plus end. Under high cholesterol conditions, as in Niemann-Pick type C disease, this process is prevented, and LEs accumulate at the microtubule minus end as the result of dynein motor activity. These data explain how the ER and cholesterol control the association of LEs with motor proteins and their positioning in cells.

Abbreviations used in this paper

BP, band pass; CLSM, confocal laser-scanning microscopy; DIC, dynein intermediate chain; FLIM, fluorescence lifetime imaging microscopy; FRET, fluorescence resonance energy transfer; IMDM, Iscove's modified Dulbecco's medium; LE, late endosome; LUT, look up table; MBP, maltose-binding protein; MCS, membrane contact site; mRFP, monomeric RFP; MTOC, microtubule-organizing center; ORD, OSBP-related domain; OSBP, oxysterol-binding protein; PH, pleckstrin homology; qPCR, quantitative PCR; RILP, Rab7-interacting lysosomal protein; VAP, VAMP-associated ER protein.

Introduction

Late endosomes (LEs), lysosomes, and lysosome-related organelles are characteristically positioned by motor protein interactions with cytoskeletal elements. The typical steady-state perinuclear positioning of LEs is dictated by the net balance of vectorial movements toward opposite ends of microtubules. The dynein–dynactin motor drives minus end (centripetal) transport, and at least two kinesin motors (KIF5 and KIF3) have been implicated in plus end (centrifugal) transport (Haimo and Rozdzial, 1989; Hollenbeck and Swanson, 1990; Vale et al., 1992; Wubbolts et al., 1999; Brown et al., 2005). Other factors are also involved in maintaining the typical distribution of LEs, including small GTPases, kinases (Pelkmans et al., 2005), motor-associated factors like huntingtin (Colin et al., 2008), and cholesterol (Lebrand et al., 2002; Sugii et al., 2006).

Rab GTPases specify organelle identity (Pfeffer, 2001; Zerial and McBride, 2001) and control selective motor activity on defined compartments (Echard et al., 1998; Jordens et al., 2001, 2005; Hoepfner et al., 2005). The small GTPase Rab7 associates with the LE (Zerial and McBride, 2001), and its effector Rab7-interacting lysosomal protein (RILP) binds the p150Glued subunit of the dynactin protein complex (Jordens et al., 2001; Johansson et al., 2007). The p150Glued protein can bind to dynein heavy chain via the dynein intermediate chain (DIC), but it can also bind to the oppositely directed kinesin II (KIF3A) motor via KAP3 (Wubbolts et al., 1999; Deacon et al., 2003; Brown et al., 2005). Kinesin I (KIF5) also drives plus end transport of LEs (Hollenbeck and Swanson, 1990; Nakata and Hirokawa, 1995) via interactions with other receptors. When p150Glued binding to LEs is inhibited, the kinesin I motor remains active, resulting in net plus end transport (Wubbolts et al., 1999). Although Rab7 and RILP are sufficient for the recruitment of p150Glued-associated motor proteins, the actual translocation of LEs toward the microtubule-organizing center (MTOC) further requires βIII spectrin and the oxysterol-binding protein (OSBP)–related protein 1L (ORP1L; Johansson et al., 2007). ORP1L contains a pleckstrin homology (PH) domain that binds phosphoinositides (Johansson et al., 2005), a protein-interacting FFAT (two phenylalanines [FF] in an acidic tract) motif (Loewen et al., 2003; Loewen and Levine, 2005), and a C-terminal OSBP-related domain (ORD) able to bind 25-hydroxycholesterol (Im et al., 2005; Suchanek et al., 2007). The ER protein OSBP is related to ORP1L and also contains a FFAT motif that interacts with VAMP (vesicle-associated membrane protein)-associated ER protein (VAP) A and VAP-B (Loewen and Levine, 2005). VAP-A and VAP-B are homo- or heterodimeric integral ER proteins (Nishimura et al., 1999; Hamamoto et al., 2005) and participate in ER export of proteins and lipids (Wyles et al., 2002).

Cholesterol has been implicated in LE positioning. Cholesterol-laden LEs in Niemann-Pick type C patients cluster around the MTOC (Mukherjee and Maxfield, 2004). This phenotype is shared with other lysosomal storage diseases like Tangier, Fabry, and Gaucher (Neufeld et al., 2004; Maxfield and Tabas, 2005). Increasing endosomal cholesterol levels with the chemical compound U-18666A causes a similar phenotype (Roff et al., 1991; Koh and Cheung, 2006; Sobo et al., 2007). The LE clustering requires Rab7 and Rab9 (Lebrand et al., 2002; Narita et al., 2005; Chen et al., 2008). Conversely, cholesterol depletion results in LE positioning at the plus end of microtubules (Sugii et al., 2006). This suggests that motor protein activities controlling LE positioning involve Rab GTPases and cholesterol, but the mechanism is unclear.

We show that cholesterol in LEs is sensed by ORP1L, which transmits this information to the Rab7–RILP–p150Glued complex through the formation of ER–LE membrane contact sites (MCSs). At these sites, the ER protein VAP enters the Rab7–RILP complex to control p150Glued binding and positioning of LEs. The characteristic clustering of LEs at the microtubule minus end in Niemann-Pick type C and other lysosomal storage diseases is a result of this process.

Results

Chemical and genetic cholesterol manipulations in LEs and their positioning

Cholesterol is an essential component of cellular membranes and contributes to a host of different processes. To visualize the effects of intracellular cholesterol levels on LE positioning, MelJuSo cells were cultured under control or cholesterol-depleting or -increasing conditions. Cholesterol depletion required culturing cells in lipid-free medium supplemented with a statin to prevent the synthesis of endogenous cholesterol (Sugii et al., 2006). Chemical and genetic cholesterol accumulation in LEs were induced by exposure of MelJuSo cells to U-18666A (Liscum and Faust, 1989; Kobayashi et al., 1999) or by silencing NPC1 to mimic Niemann-Pick type C disease (Carstea et al., 1997).

To visualize the effect of these treatments, cells were fixed and stained with filipin (Sobo et al., 2007) to detect cholesterol (Fig. 1 A and Fig. S1 B) or stained for CD63 to label LEs (Fig. 1 B and Fig. S1 B). Images were made at identical microscope settings and show that these cholesterol-manipulating treatments decreased (statin) or increased (U-18666A or siNPC1) intracellular cholesterol levels (Fig. 1, A and C; and Fig. S1 B).

Does cholesterol affect the positioning of LEs? LysoTracker red–labeled LEs were followed by time-lapse fluorescence microscopy under the different cholesterol-manipulating conditions (Videos 1–3). A fraction of the LEs in cells exposed to low or high cholesterol conditions still moved in a bidirectional and stop and go manner, as in control cells. In response to high cholesterol, more vesicles accumulated near the nucleus and fewer in the cell periphery. This is reversed under low cholesterol conditions (Fig. 1 B). These data suggest that cholesterol influences LE positioning.

The effect of cholesterol on motor proteins was then investigated. The Rab7 effectors RILP and ORP1L control dynein motor-mediated transport of LEs. To test their involvement in cholesterol-dependent LE positioning, these proteins were silenced by means of siRNA (efficient silencing was confirmed by quantitative PCR [qPCR]). Cholesterol levels were then manipulated, and LEs were detected by staining for CD63 and ORP1L (Fig. 1 B). Endogenous ORP1L was bound to LEs under all cholesterol-manipulating settings. In addition, cholesterol manipulation did not affect the positioning of LEs when RILP or ORP1L was silenced.

Repositioning of LEs near the MTOC under high LE cholesterol concentrations may require the dynein–dynactin motor. To test this, dynactin's subunit p50dynamitin was overexpressed to physically disrupt the motor complex (Burkhardt et al., 1997) in NPC1-silenced cells, and LEs were detected by CD63 labeling. Overexpression of p50dynamitin abrogated clustering of LEs in NPC1-silenced MelJuSo cells, suggesting that functional dynein–dynactin complexes are involved in clustering NPC1-deficient, cholesterol-laden LEs (Fig. 1 C).

ORP1L controls p150Glued binding to Rab7–RILP

The N-terminal ankyrin repeats of ORP1L bind to Rab7 and are involved in dynein motor transport of LEs (Johansson et al., 2005, 2007). To resolve the ORP1L domains involved in the control of LE transport, a series of monomeric RFP (mRFP)–tagged C-terminal truncations of ORP1L constructs (Fig. 2 A and Fig. S2 A) were coexpressed with GFP-RILP in MelJuSo cells. qPCR data revealed that the ORP1L constructs and RILP were expressed 4- to 10-fold over endogenous expression levels (unpublished data). RILP expression was required to visualize recruitment of endogenous p150Glued and dynein motor binding, but the many motors present on a vesicle (Jordens et al., 2001) rendered localization insensitive to cholesterol manipulation (Fig. S1 C). Vesicles labeled by the mRFP-ORP1L constructs were characterized by immunostaining for LE labeling for CD63, LAMP-1, Rab7, and cholesterol, as detected by filipin (Fig. S2, B and C). Markers for the ER, Golgi, or early endosomes were absent on these vesicles (Fig. S2 D).

To assess the effect of ORP1L and ORP1L mutants on motor recruitment and LE positioning, cells were stained for the dynactin motor subunit p150Glued and DIC. Coexpression of ORP1L and RILP recruited p150Glued (Fig. 2 B) and DIC to LEs (Fig. 2 C) that were clustered near the MTOC. Removal of the C-terminal ORD (ΔORD) prevented p150Glued and DIC recruitment by RILP, resulting in the relocation of RILP-containing compartments to the cell periphery (Fig. 2, B and C).

ORP1L controls cholesterol-dependent LE positioning

OSBP/OSBP-related proteins are involved in nonvesicular transport of sterols, and their ORDs bind and possibly extract sterols from membranes (Ikonen, 2008). The ΔORD mutant of ORP1L should mimic a cholesterol-free conformation of ORP1L. To test whether p150Glued exclusion from Rab7–RILP requires ORD binding to membranes, ORD was exchanged for two ORP1L PH domains in tandem (ΔORDPHDPHD). Tandem PH domains will increase the avidity of binding to phosphoinositides (Lemmon and Ferguson, 2000) and mimic the ORD in a membrane-associated state. The ΔORDPHDPHD chimera allowed p150Glued and DIC recruitment by RILP, resulting in the clustering of RILP-positive compartments near the MTOC (Fig. 2, B and C). Silencing ORP1L with siRNA against ORD before ectopic expression of ΔORD or ΔORDPHDPHD showed no contribution of endogenous ORP1L on the phenotypes caused by the ORP1L mutants (unpublished data). The repositioning of LEs by the different ORP1L variants was confirmed in time-lapse experiments (Videos 4 and 5).

To test whether LE positioning requires cholesterol sensing by ORP1L, MelJuSo cells were transfected with mRFP-ORP1L before manipulating cholesterol levels. Cholesterol reduction by statin and lipid-free medium scattered the mRFP-ORP1L–positive vesicles, whereas U-18666A treatment positioned LEs around the MTOC (Fig. 3 A and Fig. S3). Removal of the cholesterol-binding ORD or its replacement by tandem PH domains rendered positioning of LEs insensitive to cholesterol levels. ΔORD induced scattering of LEs under all cholesterol-manipulated conditions, whereas ΔORDPHDPHD always induced dense clustering (Fig. 3 B and Fig. S3). Microscopy analyses revealed that the expression of the ORP1L constructs was increased by six- to 15-fold upon ectopic expression (unpublished data). We conclude that functional ORP1L is required for translating LE cholesterol content into LE positioning.

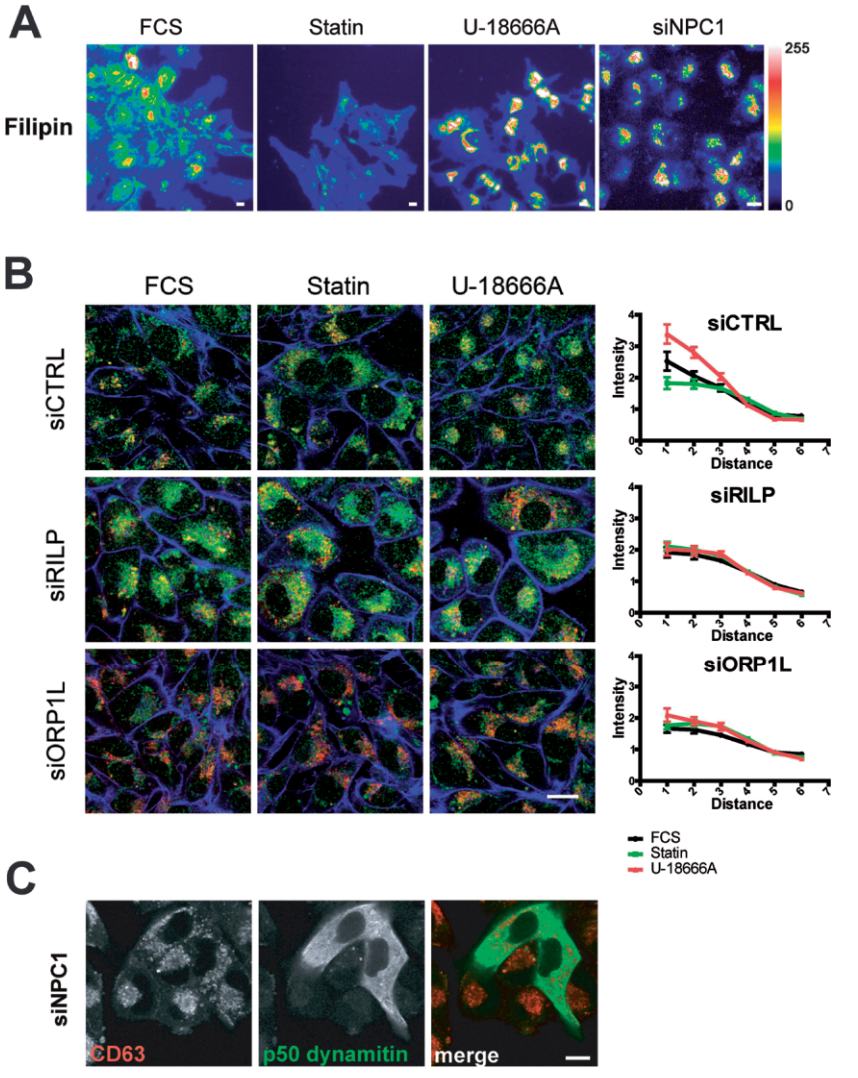


Figure 1. Chemical and genetic cholesterol manipulations and LEs. (**A**) Modulation of intracellular cholesterol levels. Mel JuSo cells were cultured in normal medium (FCS), cholesterol-depleted medium supplemented with lovastatin (statin), or normal medium supplemented with U-18666A, as indicated. Fixed cells were stained with filipin to detect cholesterol. A color look up table (LUT) shows fluorescence intensities. n > 100 for each condition. (**B**) Effects of intracellular cholesterol manipulation (control [CTRL], U-18666A, or statin treatment) on LE positioning in RILP- or ORP1L-silenced MelJuSo cells. Cells were stained for the LE marker CD63 (red), endogenous ORP1L (green), and actin (blue). The position of the CD63-positive vesicles relative to the nucleus (radial distribution) was determined for the various conditions (>50 cells per condition), binned, and plotted (right). The distributions were statistically different according to the Jonckheere-Terpstra test for control siRNA (P = 1.52 × 1025 and 7.76 × 1026 for CD63 and ORP1L, respectively) only. No difference was detected for siRILP (P = 0.20 and 0.54 for CD63 and ORP1L, respectively) and for siORP1L (P = 0.29 for CD63). (**C**) Dynein motor activity and clustering of LEs in NPC1-silenced cells. Mel JuSo cells were transfected with siRNA for NPC1 for 72 h and, after 48 h, transfected with an expression construct for p50dynamitin to disrupt the dynein–dynactin motor. Fixed cells were stained for CD63 and p50dynamitin to mark the overexpressing cells. n > 100. Bars: (**A** and **C**)10 µm; (**B**) 20 µm.

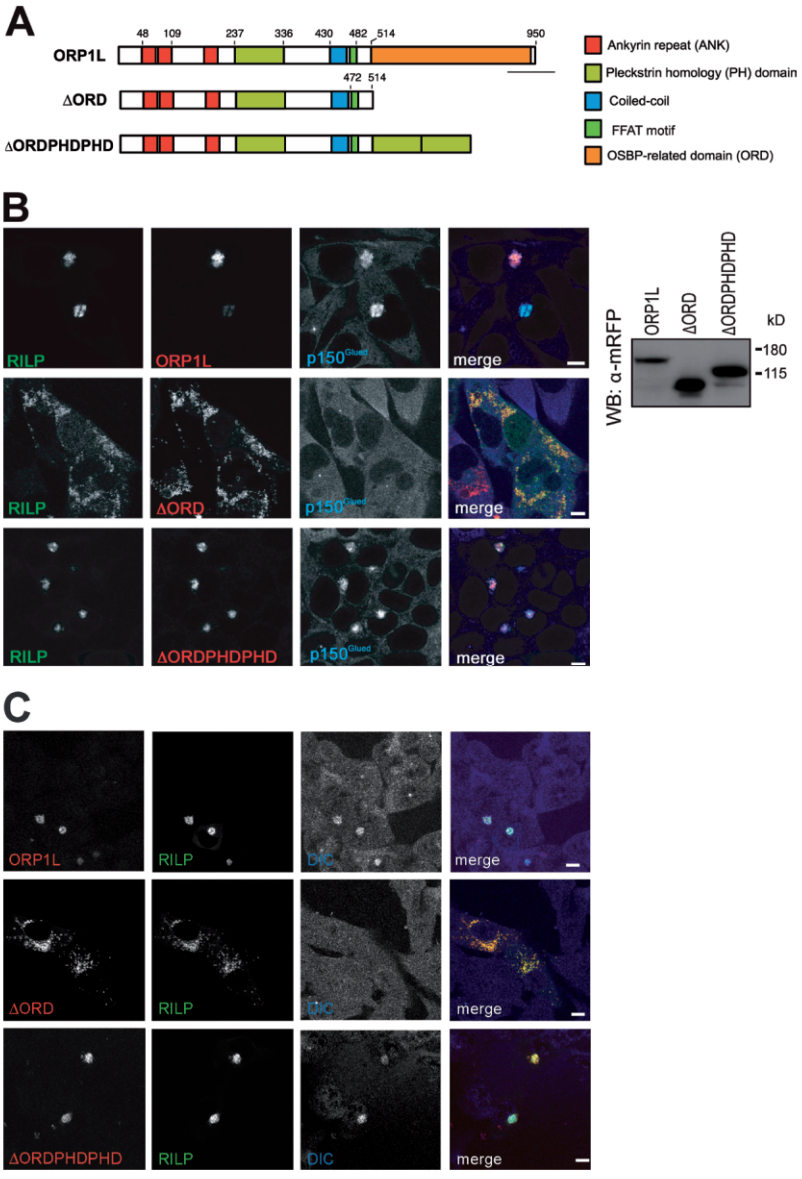


Figure 2. ORP1L controls recruitment of p150Glued to the Rab7–RILP receptor. (**A**) ORP1L domain structure and constructs. Five domains are predicted in ORP1L. Numbers indicate amino acid residue positions. Constructs were N-terminally tagged with mRFP. The ΔORDPHDPHD chimera had ORD exchanged for a tandem PH domain derived from ORP1L. (**B**) Effect of ORP1L deletion or chimeric constructs on RILP-mediated p150Glued recruitment. (left) Mel JuSo cells transfected with GFP-RILP and mRFP-ORP1L constructs and stained with anti-p150Glued antibodies before CLSM. For pixel analyses of the images, see Fig. S2 E. n > 200 for each condition. (right) Mel JuSo cells transfected with the indicated mRFP-ORP1L constructs and whole cell lysates analyzed by immunoblotting with anti-mRFP antibodies (WB: α-mRFP). Molecular standards are indicated. WB, Western blot. (**C**) Effect of ORP1L constructs on RILP recruitment of the p150Glued-associated dynein motor adapter DIC. MelJuSo cells were transfected with GFP-RILP and the mRFP-ORP1L constructs indicated and stained with anti-DIC antibodies. n > 100 for each condition. Bars, 10 µm.

LE cholesterol affects the conformation of ORP1L

To determine whether LE cholesterol content affects the conformation of ORP1L, an mRFP-ORP1L-GFP fusion protein was expressed to monitor intramolecular fluorescence resonance energy transfer (FRET). Energy transfer from a donor fluorophore to a suitable acceptor (Förster, 1948) is dependent on distance and orientation between the two fluorophores (Förster, 1948; Calleja et al., 2003) and was used in this study to reveal conformational changes within mRFP-ORP1L-GFP (Fig. 4 A).

FRET was determined by sensitized emission using confocal microscopy. GFP was excited with 488-nm light, and the donor mRFP signal was determined. mRFP-ORP1L-GFP–expressing MelJuSo cells were co-cultured with MelJuSo cells expressing only GFP or mRFP for imaging. These latter cells served as internal controls to calculate correction factors for bleed-through of GFP into the mRFP channel and for direct excitation of mRFP by the 488-nm laser (Zwart et al., 2005). FRET and donor FRET efficiency (ED; i.e., FRET normalized to donor fluorophore input) were determined under the various cholesterol-manipulating conditions (Fig. 4 B). Cholesterol depletion decreased FRET efficiency ED, and ED was increased after LE cholesterol accumulation (Fig. 4 B, right), implying that the ORP1L conformational changes were dependent on LE cholesterol content.

To exclude that these differences in ED were caused by the clustering of individual ORP1L molecules under the various conditions rather than conformational changes of each ORP1L molecule, the experiments were repeated with cells expressing both GFP-ORP1L and mRFP-ORP1L (Fig. S4 B). If changes in ED with mRFP-ORP1L-GFP were caused by intermolecular rather than intramolecular FRET, ED with GFP-ORP1L and mRFP-ORP1L would also change. However, ED values were not affected by cholesterol manipulation, implying that the FRET differences result from conformational changes within mRFP-ORP1L-GFP.

Two constructs, mRFP-ΔORD-GFP and mRFP-ΔORDPHDPHD-GFP, were used to test whether cholesterol-dependent conformational changes in ORP1L were mediated by the ORD. These constructs should not respond to variations in cholesterol levels because they lack ORD but may still respond to effects on the PH domain or other domains present in ORP1L. However, no effect of cholesterol manipulation on intramolecular donor FRET efficiency ED was detected, suggesting that cholesterol-induced conformational changes in mRFP-ORP1L-GFP were mediated by the cholesterol-sensing ORD (Fig. S4 A).

FRET efficiencies can also be calculated from differences in donor fluorophore lifetime (Bastiaens and Squire, 1999). The aforementioned FRET experiments were repeated with FRET determination by fluorescence lifetime imaging microscopy (FLIM). The lifetime of GFP is typically 2.7 ns (Pepperkok et al., 1999) but decreases in the case of FRET, when energy is transferred to the acceptor fluorophore mRFP. Cells expressing mRFP-ORP1L-GFP were imaged along with control cells expressing only GFP to determine GFP lifetime under non-FRET conditions. Again, FRET efficiency ED was decreased by cholesterol depletion and increased in response to enhanced cholesterol levels (Fig. S4 C). Cells grown under the various control conditions were also imaged by FLIM and showed no response to cholesterol manipulation, which is fully consistent with the results of FRET experiments measured by sensitized emission (Fig. S4, D and E). This shows that ORP1L senses cholesterol content in LEs through the C-terminal ORD.

ORP1L, cholesterol, and Niemann-Pick type C disease

Silencing NPC1 increases cholesterol in LEs and induces LE clustering. Cholesterol can distribute over the LE-limiting membrane and the internal vesicles by flip-flop mechanisms and/or specific transporters. ORP1L senses cholesterol in the cytosolic leaflet of the LE-limiting membrane before translating this into LE repositioning. To test whether cholesterol sensing by ORP1L is required for LE clustering in Niemann-Pick type C, NPC1-silenced MelJuSo cells (Fig. S1 B) were transfected with different mRFP-ORP1L constructs before analysis by confocal laser-scanning microscopy (CLSM; Fig. 4 C). Whereas ORP1L and ΔORDPHDPHD induced clustering of LEs, ΔORD induced scattering of LEs even when NPC1 is silenced (Fig. S4 F), suggesting that functional ORP1L is required to translate increased cholesterol levels into LE repositioning in NPC1-deficient cells.

To test whether NPC1 deficiency affects the cholesterol levels in the cytosolic leaflet of LEs, intramolecular FRET of mRFP-ORP1L-GFP was measured by sensitized emission in cells transfected with control or NPC1 siRNAs (Fig. 4 D). The FRET efficiency ED increased when NPC1 was silenced (Fig. 4 D). This result was confirmed in FLIM measurements (Fig. S4 G). The donor FRET efficiencies (ED) for mRFP-ORP1L-GFP in NPC1-silenced cells are similar to those observed in cells treated with U-18666A, which mimics NPC1 deficiency (Fig. 4 B; Koh and Cheung, 2006; Sobo et al., 2007).

Cholesterol accumulation in LEs of NPC1-silenced cells may be a cause or a consequence of the LE clustering observed in cells of Niemann-Pick type C patients (Kobayashi et al., 1999). To separate cholesterol accumulation from LE clustering, mRFP-ΔORD was expressed in NPC1-silenced cells. Fixed cells were stained for cholesterol with filipin (Fig. 4 E) and CD63 (Fig. S4 H). The CD63-positive LEs scattered by ΔORD expression still accumulated cholesterol when NPC1 was silenced. This suggests that the characteristic clustering of LEs near the MTOC, which is typical in Niemann-Pick type C, is a consequence of cholesterol accumulation, as sensed by ORP1L (and is abrogated by ΔORD). ORP1L transmits this information to the Rab7–RILP–p150Glued–dynein motor complex for microtubule minus end–driven transport and clustering of LEs.

ORP1L conformation differs between peripheral and perinuclear LEs

If cholesterol levels in LEs determine its intracellular positioning, these levels should be different between peripheral and perinuclear LEs. Cholesterol levels in the cytosolic leaflet of LEs cannot be detected by any currently available probe other than by the mRFP-ORP1L-GFP sensor (Fig. 4). We reanalyzed the images of cells expressing the mRFP-ORP1L-GFP FRET probe (Fig. 5 A) and, as a control, the mRFP-ΔORD-GFP FRET probe (Fig. 5 B). The latter construct lacks the cholesterol-sensing ORD. Donor FRET efficiency ED was determined in five concentric regions spanning the nucleus and cell surface, as indicated (Fig. 5). The results were binned and quantified (Fig. 5, A and B, bottom). ED, as determined with mRFP-ORP1L-GFP, was higher on perinuclear LEs than on peripheral LEs (Fig. 5 A). These differences were sensed by ORD because ED was unaffected with the mRFP-ΔORD-GFP construct (Fig. 5 B). This suggests that the positioning of LEs within one cell correlates with different conformations of ORP1L, as induced by different levels of cholesterol in the cytosolic leaflet of LEs.

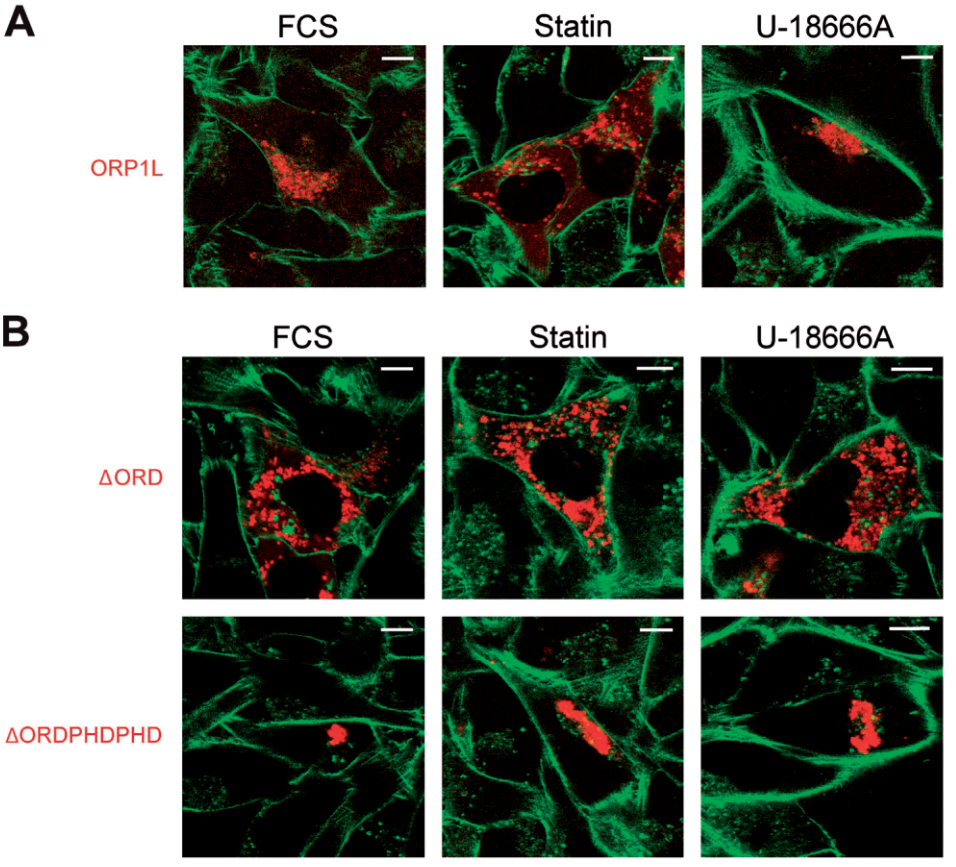
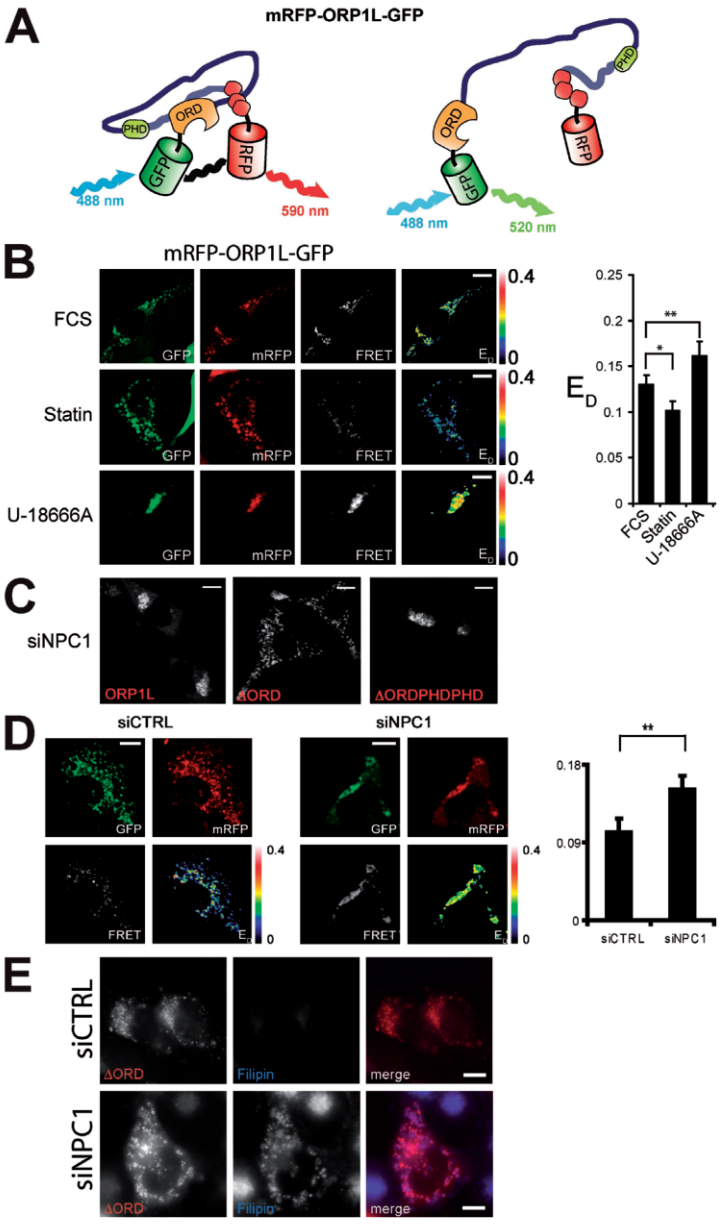


Figure 3. ORP1L controls cholesterol-dependent LE positioning. (**A**) Cholesterol-dependent ORP1L vesicle positioning. Mel JuSo cells expressing mRFPORP1L were cultured under control conditions (FCS) or conditions causing decreased (statin) or increased (U-18666A) cholesterol levels. Actin was stained with falloidin (green) to mark the cell boundaries before analyses by CLSM. n > 100. (**B**) ORP1L is dominant in vesicle repositioning as the result of cholesterol manipulations. MelJuSo cells expressing mRFP-ΔORDPHDPHD or mRFP-ΔORD were treated and imaged as described in A. n > 100. Bars, 10 µm.

Figure 4. LE cholesterol alters the conformation of ORP1L. (**A**) Intramolecular FRET for mRFP-ORP1L-GFP. GFP and mRFP are attached to the same molecule, allowing FRET from donor GFP to acceptor mRFP. FRET depends on distance and orientation and thus indicates conformational changes. FRET can be detected by sensitized emission. GFP is excited by 488-nm light, and then, after energy transfer 582–675-nm light emission by mRFP is detected. (**B**) Cholesterol effects on ORP1L conformation detected by sensitized emission. Mel JuSo cells expressing mRFP-ORP1L-GFP were cultured under control (FCS) or cholesterol-depleting (statin) or -enhancing (U-18666A) conditions before imaging by CLSM for FRET determination. Panels show the GFP signal, the mRFP signal, calculated FRET, and FRET related to donor fluorophore input: the donor FRET efficiency. (**ED**). The color LUT visualizes the differences in the ED panels. (right) quantification of the donor FRET efficiency detected ►



► (**Figure 4 continued**) for mRFPORP1L-GFP under the different conditions of cholesterol manipulation. The mean and SD from two experiments (>10 cells analyzed) are shown (*, P = 0.05; **, P = 0.03). (**C**) ORP1L controls LE positioning in NPC1-silenced cells. Mel JuSo cells were transfected with mRFPORP1L, -ΔORD, or -ΔORDPHDPHD and siRNA for NPC1 and analyzed by CLSM. n > 100. (**D**) Sensitized emission and ORP1L conformation in NPC1-deficient cells. mRFP-ORP1L-GFP–expressing MelJuSo cells were transfected with control (siCTRL) or NPC1 (siNPC1) siRNAs before imaging by confocal FRET. (right) Donor FRET efficiencies determined in >10 control siRNA– or NPC1 siRNA–transfected cells. The mean ± SD is shown (**, P = 5.1 × 1026). (**E**) NPC1, cholesterol, and LE clustering. Mel JuSo cells were transfected with control or NPC1 siRNA and then mRFP-ΔORD before staining with filipin for cholesterol. Pixel analyses are shown in Fig. S2 E. n > 50 for each condition. Bars, 10 µm.

ORP1L-dependent recruitment of VAP and removal of the p150Glued dynactin subunit

ORP1L allows RILP-induced clustering of LEs. ΔORD relocates LEs to the cell periphery, suggesting the exclusion of p150Glued from RILP (Fig. 2 B). Removal of the 20-kD region preceding the ORD restored RILP-induced clustering and p150Glued binding to RILP (Fig. 2 B). This region contains a predicted coiled-coil region (aa 430–463; Johansson et al., 2007) followed by a FFAT motif (aa 472–482; sequence, SEDEFYDALSD; Fig. 2 A; Loewen et al., 2003) and should contain the information for removal of p150Glued from RILP. To test whether the FFAT motif controlled p150Glued binding to RILP, an inactivating point mutation (D478A) in the FFAT motif (Loewen et al., 2003) was introduced in mRFP-ΔORD. This mutant was coexpressed with GFP-RILP before staining for p150Glued (Fig. 6 A). Whereas ΔORD excludes RILP-mediated recruitment of p150Glued (resulting in LE scattering), the ΔORDFFAT(D478A) point mutant permitted p150Glued binding to RILP, resulting in LE clustering around the MTOC.

The FFAT motif in the ER-located ORP1L homologue OSBP interacts with VAP-A and VAP-B, which are involved in protein and lipid export from the ER (Wyles et al., 2002; Loewen and Levine, 2005). VAP is an integral ER protein and not an obvious candidate for controlling p150Glued release from Rab7–RILP on LE membranes. To test whether VAP could be involved in this release, MelJuSo cells were transfected with mRFP-ΔORD and GFP-RILP in combination with siRNA against VAP-A and stained for p150Glued (Fig. 6 B). ΔORD expression again removed p150Glued from RILP in cells transfected with control siRNA, resulting in LE positioning in the cell periphery. When VAP-A was silenced, ΔORD remained associated with p150Glued-RILP, and the LEs clustered around the MTOC. Identical results were obtained when VAP-B was silenced (unpublished data). VAP-A silencing (with four independent siRNAs) reduced VAP-A mRNA levels by >99% and VAP-B levels by 70–80%, as determined by qPCR. Similarly, VAP-B silencing reduced VAP-A expression by 99% (unpublished data). Immunoblotting with VAP-A antibodies confirmed efficient silencing of VAP-A expression (Fig. 6 B).

Purified proteins were used to test whether VAP directly controls p150Glued binding to RILP. The p150Glued(C25) C-terminal domain interacts with the purified Rab7–RILP complex and was used for these experiments (Johansson et al., 2007). The ORP1L–Rab7–RILP–p150Glued complex was first assembled with purified proteins before VAP-A was added (Fig. 6 C). GTP-loaded, His-tagged Rab7 was bound to metal affinity beads before the addition of RILP and ORP1L. The complex was completed by p150Glued(C25), and nonbound proteins were removed by washing after every step during the construction of the complex. Subsequently, purified VAP-A was added to the complex followed again by washing of the beads. Its effect on the ORP1L–Rab7–RILP–p150Glued(C25) complex was determined by Western blotting (Fig. 6 C). Soluble VAP-A removed the C25 fragment of p150Glued from the preassembled Rab7–RILP–ORP1L complex.

To test whether VAP-A prevented binding of p150Glued to the Rab7–RILP complex or whether VAP-A induced the release of p150Glued and to determine the role of ORP1L in this process, various purified Rab7–RILP complexes were assembled in vitro (Fig. 6 D). When VAP-A was included during the assembly of the complex, the p150Glued(C25) fragment still entered the complex (Fig. 6 D, lanes 1 and 2). VAP-A was probably removed by washing during the assembly of the

Rab7–RILP complex, which explains why VAP-A only affected C25 binding when it was added to the preassembled Rab7–RILP–C25 complex. The presence or absence of ORP1L in the preassembled Rab7–RILP complex did not affect removal of the C25 fragment of p150Glued by VAP-A (Fig. 6 D, lanes 3 and 4). These data suggest that ORP1L is not directly involved in VAP-A–mediated removal of p150Glued from the Rab7–RILP complex but probably recruits VAP into this complex.

To test whether VAP-A directly interacts with the C25 fragment of p150Glued, GST–VAP-A or GST (as a control) was bound to GST beads, and purified p150Glued(C25) fragment was added. VAP-A interacted with the C-terminal p150Glued(C25) fragment (Fig. 6 E). These in vitro reconstitution experiments reveal a minimal set of proteins controlling dynein motor binding to LEs that includes Rab7, RILP, p150Glued, and the ER protein VAP.

ORP1L and VAP are involved in inducing ER–LE membrane contacts

If the integral ER protein VAP controls motor binding to LEs after recruitment by ORP1L, VAP should somehow contact these vesicles. To visualize this, MelJuSo cells were transfected with the various ORD variants of mRFP-ORP1L and stained for endogenous VAP (Fig. 7 A). Endogenous VAP accumulated on ΔORD- and, although to a lesser extent, on ORP1L-containing vesicles but was excluded from vesicles labeled by ΔORDPHDPHD, indicating that VAP recruitment is dependent on the conformation of ORP1L (Fig. 7 A). These results were confirmed in photoactivation experiments with MelJuSo cells expressing photoactivatable (PA)-GFP–tagged VAP-A and mRFP-ORP1L variants (Fig. S5 A and Videos 6–8) that also showed colocalization of VAP-A and ORP1L on moving vesicles. Accumulation of the ER protein VAP on LEs by ΔORD expression also coincided with the removal of p150Glued from RILP (Fig. S5 B). We then tested whether the ER–LE interactions could be observed by manipulating cholesterol levels in MelJuSo cells in which ORP1L and VAP were not ectopically expressed. TAP1-GFP labeled the ER (Reits et al., 2000). Decreasing cholesterol levels sufficed to induce the arrival of ER markers on LEs, as analyzed by CLSM and quantified by pixel analysis (Fig. 7 B).

The localization of VAP and ORP1L was subsequently visualized by EM in more detail. EM has a significantly higher spatial resolution than CLSM, which has a maximal resolution of ≈240 nm. MelJuSo cells were transfected with GFP-ΔORD, -ORP1L, or -ΔORDPHDPHD together with HA-tagged VAP-A. After expression of the ORP1L variants was observed (by GFP fluorescence), cells were processed for immuno-EM and stained with HA antibodies to detect VAP-A (Fig. 8 A). The frequency of ER contacts with LEs and the surface of the LEs covered by ER structures was quantified (Fig. 8 B). Note that HA-VAP was never detected at LE membranes, excluding fusion of the LE and ER under these conditions. The ER, as labeled by HA-tagged VAP-A, had to be within 40 nm of the LE-limiting membrane to be considered a contact. Most LEs (>95%) interacted, often over large surface areas, with the ER when ΔORD was expressed. Both the number of ER–LE interactions and the surface covered by the ER decreased when ORP1L was expressed. Additionally, contact sites were almost absent when the high cholesterol conformation of ORP1L (ΔORDPHDPHD) was expressed, suggesting that the cholesterol-dependent conformational state of ORP1L determines ER contact site formation with LEs. To test whether cholesterol levels determine the formation of these contact sites, cells expressing GFP-ORP1L were cultured under

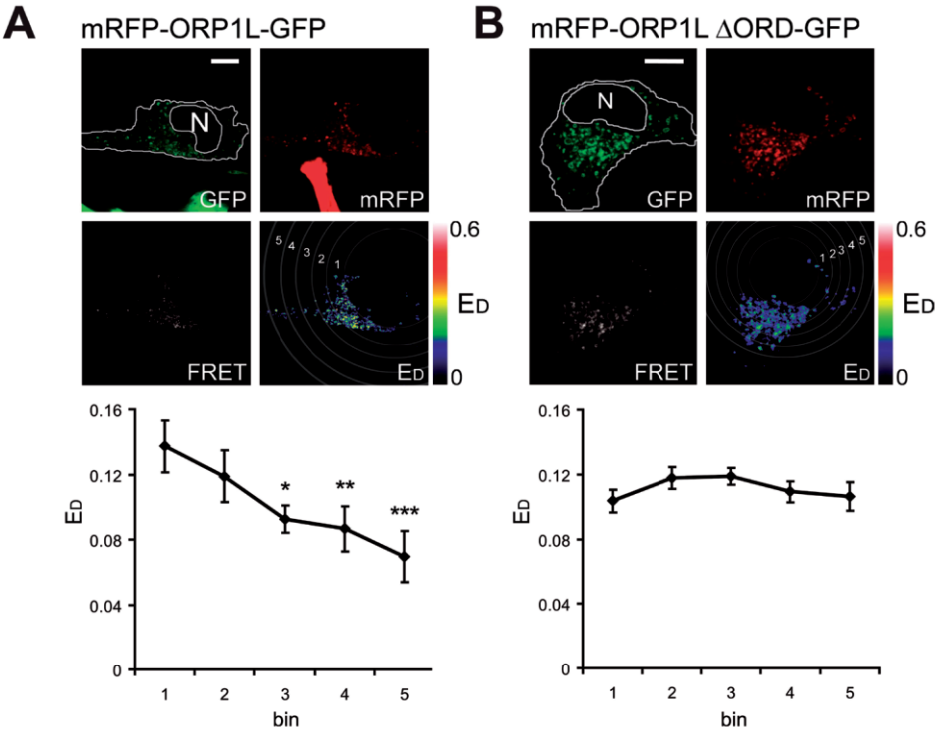


Figure 5. ORP1L conformation and LE positioning. (**A** and **B**, top) Mel JuSo cells expressing mRFP-ORP1L-GFP (**A**) or mRFP-ΔORD-GFP (**B**) were imaged for FRET by CLSM. The GFP image, mRFP image, calculated FRET, and donor FRET efficiency ED images are indicated. ED values are shown in false colors (the LUT shows the corresponding values). The position of the nucleus (N) and cell boundaries are drawn in the GFP channel. The cytosol is divided by five concentric rings, as indicated in the ED panel. (bottom) ED values for the constructs were collected and binned for the different rings. Values are shown for the different rings under the corresponding image. Mean ± SEM of ED values collected for >10 cells analyzed per construct are shown. The asterisks indicate a statistically significant difference in ED of that bin compared to bin 1 (the most internal ring; *, P = 0.024; **, P = 0.026; ***, P = 0.0063). Bars, 10 µm.

control (FCS) or cholesterol-increasing (U-18666A) or -depleting (statin) conditions, and sections were stained for HA-tagged VAP-A (Fig. 8 C). Under control conditions, some ER–LE interactions could be observed, usually over small LE surfaces. Whereas cholesterol accumulation in LEs (as the result of U-18666A) diminished these contacts, cholesterol depletion markedly induced formation of ER–LE contact sites (Fig. 8 D). These data suggest that the conformational state of ORP1L, as controlled by cholesterol levels, determines whether ER contacts the LE. This is required for the ER protein VAP to contact (and manipulate) the Rab7–RILP–p150Glued complex on LEs.

Discussion

Cholesterol is a hydrophobic molecule essential for fluidity and microdomain formation in biomembranes. The transfer of cholesterol to other organelles requires specific cholesterol-

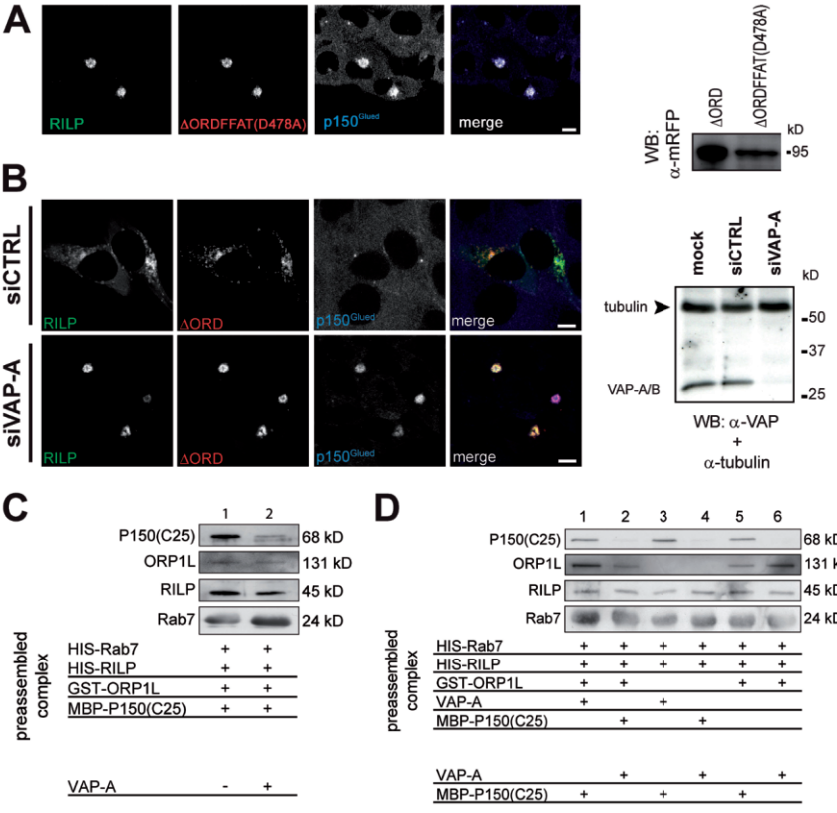


Figure 6. ORP1L requires VAP-A to remove p150Glued from Rab7–RILP. (**A**) Effect of the FFAT motif in ΔORD on RILP-mediated p150Glued recruitment. (left) Mel JuSo cells were transfected with GFP-RILP and mRFP-ΔORD containing a point mutation in its FFAT motif, ΔORDFFAT(D478A). Fixed cells were stained with anti-p150Glued antibodies. n > 200. (right) Mel JuSo cells were transfected with the mRFP-ΔORD or mRFP-ΔORDFFAT(D478A) constructs, and whole cell lysates were analyzed by immunoblotting with anti-mRFP antibodies (WB: α-mRFP). (**B**) p150Glued exclusion by ΔORD and VAP-A. VAP-A was silenced by siRNA (siVAP-A) in cells expressing GFP-RILP and mRFP-ΔORD. (left) Cells stained for p150Glued. Pixel analyses are shown in Fig. S2 E. n > 100 for each condition. (right) Western blot analysis of cells transfected with transfection reagent (mock), control (siCTRL), or VAP-A siRNA (siVAP-A) and probed for α-tubulin (as loading control) and anti–VAP-A antibodies. (**C**) VAP-A removes p150Glued from Rab7–RILP. GTP-locked His-Rab7(Q67L) was GTP loaded andcoupled to Talon beads before adding purified RILP, ORP1L, and p150Glued(C25) fragments in equimolar amounts to form a preassembled ORP1L–Rab7–RILP–p150Glued(C25) complex. Subsequently, the complex was incubated in the presence or absence of purified VAP-A. After washing, the bead-bound proteins were analyzed by SDS-PAGE and Western blotting. (**D**) ORP1L requirements for p150Glued removal by VAP-A. GTP-loaded His-Rab7(Q67L) was coupled to Talon Co2+ beads before adding the isolated proteins indicated in equimolar amounts to form a preassembled complex. After washing, these complexes were exposed to isolated VAP-A or the p150Glued(C25) fragment, as indicated, and the effects on the preformed complex were assessed by SDS-PAGE and Western blot analyses with antibodies, as indicated. (**E**) VAP-A interacts with p150Glued. GST or GST–VAP-A was coupled to beads before exposure to the p150Glued(C25) fragment. After washing, the complexes were analyzed by SDS PAGE and Western blotting. (**A**–**E**) Molecular masses are indicated. WB, Western blot. Bars, 10 µm.

binding chaperones. A series of proteins with cholesterol-binding domains like the steroidogenic acute regulatory protein–related lipid transfer domain and ORD have been identified in various compartments (Holthuis and Levine, 2005). Two such proteins, MLN64 and ORP1L, are located at LE membranes (Ikonen, 2008). The transfer of cholesterol over LE membranes requires transporters like ABCA1 and possibly NPC1 (Ikonen, 2008), but flip-flop of cholesterol may be another possibility (Hamilton, 2003). If so, high concentrations of cholesterol in the intraluminal vesicles of LEs should be reflected by high concentrations of cholesterol in their cytosolic leaflet.

High cholesterol content in LEs is typical for a series of lysosomal storage diseases with characteristic LE clustering at the minus end of microtubules. It has been suggested that cholesterol influences LE transport involving Rab GTPases (Holtta-Vuori et al., 2000; Lebrand et al., 2002). Minus end transport of LEs involves the dynein–dynactin motor complex and its receptor complex, Rab7–RILP–ORP1L. Because ORP1L binds both Rab7–RILP (Johansson et al., 2007) and cholesterol (Suchanek et al., 2007), we tested whether ORP1L could transfer information on LE cholesterol content to Rab7–RILP and then to p150Glued-associated motor proteins like the dynein motor. Using intramolecular FRET, we showed that the C-terminal ORD of ORP1L senses LE cholesterol. ORD can be in a membrane-bound state (when cholesterol levels are high) or in a cytosolic, membrane-free conformation (when cholesterol levels are low). Overexpression of ORP1L or one of its mutants did not change cholesterol levels in LEs (unpublished data), which suggests that ORP1L is merely a cholesterol sensor rather than an active contributor to extracting and redistributing cholesterol.

When ORD is in its cytosolic conformation or absent (as in the truncation mutant ΔORD), the FFAT motif of ORP1L prevents access of p150Glued to Rab7–RILP. This does not occur when ORD is in the membrane-associated state (as in the chimeric ΔORDPHDPHD). The ER protein VAP is directly involved in the removal of the dynein–dynactin subunit p150Glued from the Rab7–RILP complex because silencing VAP restores p150Glued binding to ΔORD–Rab7–RILP-containing vesicles. This was confirmed when purified VAP-A removed p150Glued from the RILP–Rab7–ORP1L complex (which also indicated that the minimal set of proteins involved in this process had been identified).

The ER protein VAP would not be an obvious candidate for regulating LE positioning. Light microscopy suggested that VAP localized to LEs when ΔORD was expressed (indicating ER–LE fusion). However, visualization of this process at a higher resolution by EM revealed that the ER (containing VAP) aligned to rather than fused with LEs, creating LE–ER contact sites. The formation of these contact sites is dependent on the conformation of ORP1L. ΔORD or low cholesterol levels in the LEs increased the number and area of contact sites, whereas ΔORDPHDPHD or high cholesterol decreased these interactions. ER–LE contact sites were proposed as sites where lipids like cholesterol could be transferred from LEs to the ER for further distribution (Underwood et al., 1998). However, the ER–LE contact sites are predominantly observed under conditions of low cholesterol and, to a lesser extent, under control conditions. It is possible that they are transiently formed when ORP1L changes conformation to expose the FFAT domain and released when ORP1L adopts the membrane-associated cholesterol-high state. Under low cholesterol conditions when the ER–LE MCSs form, the ER protein VAP can interact in trans with the Rab7–RILP receptor on LEs to release p150Glued. This then results

in microtubule plus end transport and scattering of LEs. The ER network is directly linked to the microtubule network that is also used by p150Glued-associated motors on LEs (Vedrenne and Hauri, 2006). The ER–LE contact sites are relatively stable between a dynamic ER and with moving vesicles, as can be appreciated in Videos 5–7. Whether other proteins contribute to stabilizing interactions between these organelles is unclear.

When NPC1 is depleted or mutated, as in Niemann-Pick type C disease (Carstea et al., 1997), or when chemical drugs raise cholesterol levels of LEs (Roff et al., 1991; Sobo et al., 2007), the ORD of ORP1L is membrane associated, preventing the formation of ER–LE MCSs. This allows enduring binding of p150Glued–DIC–dynein motor complexes to Rab7–RILP and transport to the microtubule minus end.

Why cholesterol is selected to dictate LE positioning is unclear. Cholesterol is present in the intraluminal vesicles as well as the cytosolic leaflet of LEs, allowing cytosolic exposure of intraluminal conditions. If cholesterol levels increase with maturation of the LE, the resulting ORP1L-controlled Rab7–RILP–p150Glued–DIC–dynein motor interactions would position the most matured compartments at the extreme minus end of microtubules with "shells" of less matured vesicles surrounding these at more plus end locations. Newly arriving LEs would then first encounter the youngest LE, resulting in spatial maturation before encountering lysosomes. Thus, cholesterol at the LE cytosolic leaflet would control the positioning of these organelles. We have tested this by analyzing the conformation of the cholesterol sensor ORP1L by FRET on LEs located in the perinuclear area versus the periphery. Donor FRET efficiency was lower in the cell periphery, indicating a lower cholesterol concentration.

We have visualized how the Rab7–RILP complex controls intracellular positioning of LEs. This process is controlled by cholesterol levels sensed by ORP1L to induce ER–LE contact sites via interaction with the ER protein VAP. In these contact sites, VAP interacts in trans with the Rab7–RILP receptor, promoting dissociation of p150Glued and its associated motor proteins (Fig. 9). This model explains how cholesterol depletion causes LE scattering and high cholesterol levels induce LE clustering, as observed in Niemann-Pick type C disease. We reveal an unexpected contribution of ER proteins in the control of LE intracellular positioning by motor proteins in a process controlled by cholesterol.

Materials and methods

Reagents

Rabbit anti-GFP and rabbit anti-mRFP antibodies were generated using purified His-mRFP or His-GFP recombinant proteins as immunogen, respectively. Cross-reactivity was excluded by Western blot analyses with various mRFP- or GFP-labeled fusion proteins. Other antibodies used were rabbit polyclonal anti-NPC1 (Novus Biologicals), rabbit anti-ORP1L (gift from V. Olkkonen [National Public Health Institute, Helsinki, Finland] and M. Johansson [Medical Research Council Centre for Developmental Neurobiology, London, England, UK]), rat monoclonal antitubulin antibody (Abcam), rabbit anti–human VAP antiserum (recognizing VAP-A; gift from N. Ridgway, Dalhousie University, Halifax, Nova Scotia, Canada; further analyses showed that this serum recognizes VAP-A

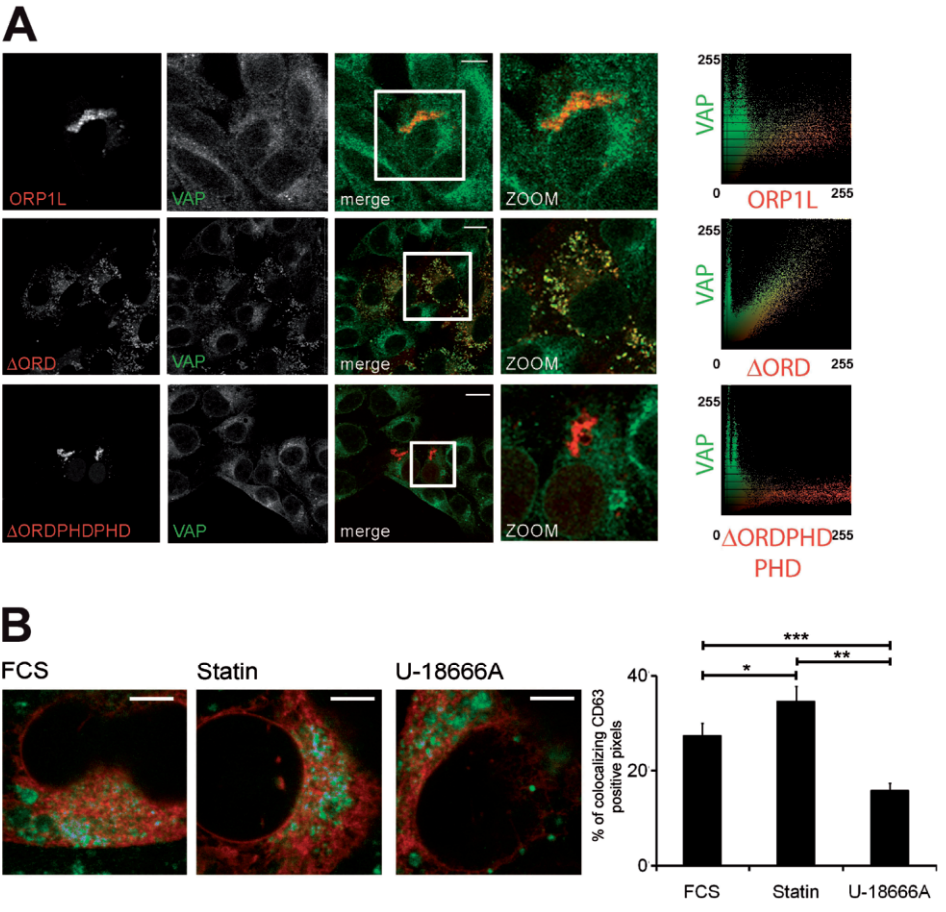
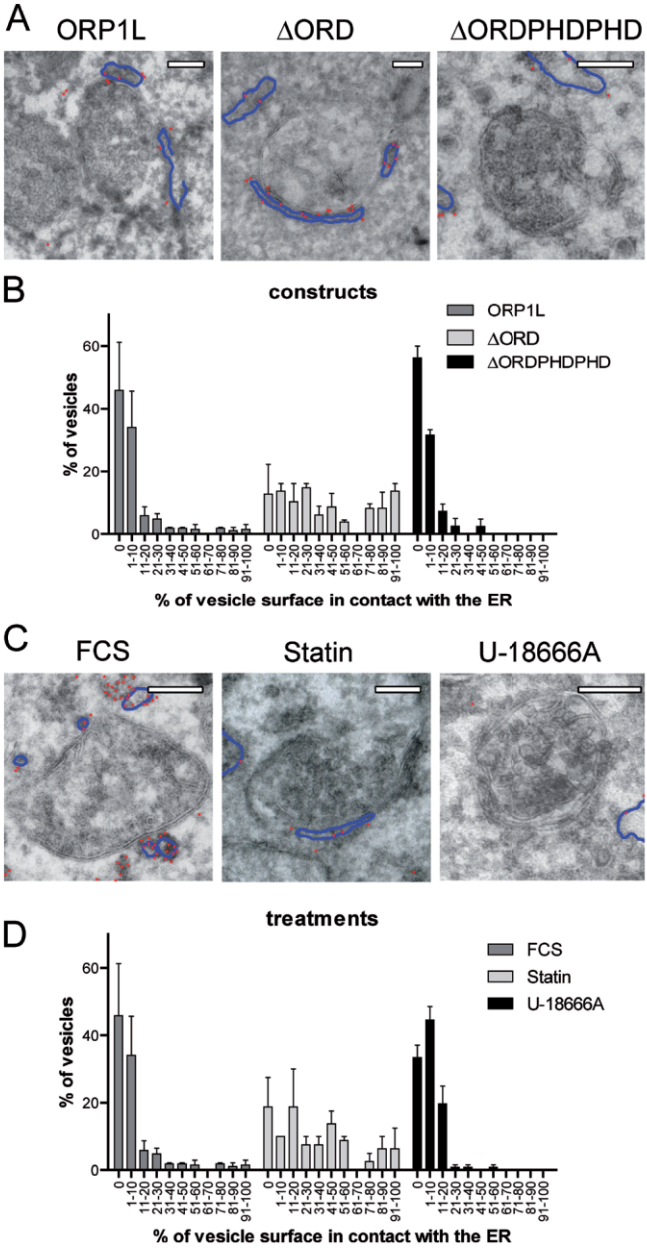


Figure 7. Cholesterol-dependent ORP1L-mediated contacts between LEs and the ER. (**A**) ΔORD recruits endogenous VAP-A. MelJuSo cells expressing mRFP-ΔORD, -ORP1L, or -ΔORDPHDPHD were stained for VAP-A. The merge panels show an overlay of the two channels, and the boxes indicate the zoomed-in areas. Pixel analyses of the zoomed-in areas for fluorescence distribution of the mRFP-ORP1L variants and VAP-A are shown. *n* > 100. (**B**) MelJuSo cells expressing TAP1-GFP (red) were exposed to different cholesterol manipulating conditions, as indicated. Cells were stained with antibodies for CD63 (green). Colocalization of the markers was determined by computational pixel analysis and visualized in blue. (right) Quantification of the colocalizing surface of the CD63-positive area. The mean ± SEM for >20 cells analyzed per condition is shown (*, P = 0.068; **, P = 1.55×10^{-6}; ***, P = 0.0003). Bars: (**A**) 10 µm; (**B**) 5 µm.

Figure 8. Cholesterol-dependent MCSs between Les and the ER allowing in trans VAP interactions with the Rab7–RILP complex. (**A**) Electron micrographs of multivesicular bodies in Mel JuSo cells expressing HA-VAP and different variants of GFP-ORP1L, as indicated. Sections were stained with anti-HA antibodies detected with 15-nm gold particles. The gold particles are highlighted by red dots, and the ER membrane (containing HA-VAP) is indicated by blue lines. The original images are shown in Fig. S5 C. (**B**) The percentage of multivesicular bodies contacting ER structures and the contact area between the ER and LE membranes was determined in Mel JuSo cells expressing the ORP1L variants as shown in A. Over 50 multivesicular bodies were considered per condition. The data on contact area from two independent quantifications were binned as indicated, and ►



► (**Figure 8 continued**) error bars show SEM. (**C**) Electron micrographs of multivesicular bodies in HA-VAP– and GFP-ORP1L–expressing MelJuSo cells exposed to different cholesterol-manipulating conditions, as indicated. Sections were stained with anti-HA antibodies marked by 15-nm gold particles. The gold particles are highlighted by red dots, and the ER membrane (containingHA-VAP) is indicated by blue lines. The original images are shown in Fig. S5 F. (**D**) The percentage of multivesicular bodies contacting ER structures and the contact area between the ER and LE membranes from MelJuSo cells expressing ORP1L under various conditions of cholesterol manipulation (as shown in **C**). Over 50 multivesicular bodies were considered per condition. The data on contact area from two independent quantifications were binned as indicated, and error bars show SEM. Bars, 200 nm.

only), mouse anti–calnexin AF8 (David et al., 1993), mouse anti-LAMP1 (BD), mouse anti-CD63 (Vennegoor et al., 1985), mouse monoclonal anti-EEA1 (BD), rabbit anti-Rab7 and rabbit anti-HA epitope tag (Santa Cruz Biotechnology, Inc.), rabbit anti–human protein disulfide-isomerase (gift from N. Bulleid, University of Manchester, Manchester, England, UK), mouse monoclonal Golgi-97 (Invitrogen), mouse monoclonal anti–HA epitope tag (12CA5; Roche), and mouse monoclonal anti-DIC (BD). Fluorescent secondary antibodies were obtained from Invitrogen.

Lovastatin (or mevinolin) was purchased from EMD and converted from its inactive prodrug form to its open acid form before use by first dissolving the prodrug in ethanol and heating to 50°C for 2 h in NaOH. Na-phosphate buffer was then added, and this solution was heated to 40°C for 30 min. Finally, the pH was adjusted to 7.3 with concentrated HCl. Mevalonate was prepared by dissolving mevalonolactone (Sigma-Aldrich) in a 0.05-M NaOH solution. The pH was adjusted to 7.0 with 0.1 M HCl. U-18666A (EMD) was dissolved in ethanol to a final concentration of 10 mg/ml. The lipoprotein-deficient serum was prepared as described previously (Goldstein et al., 1983) and was a gift from M. Jauhiainen (National Public Health Institute).

cDNA constructs and vectors

Rab7, RILP, VAP-A, VAP-B, TAP1-GFP, p150Glued(C25), and ORP1L cDNA constructs have been described previously (Reits et al., 2000; Jordens et al., 2001; Wyles et al., 2002; Marsman et al., 2004; Johansson et al., 2007). GST–VAP-A was a gift from M. Hardy and K. Ettayebi (Montana State University, Bozeman, MT), and HA–VAP-A and –VAP-B were gifts from C. Hoogenraad (Erasmus Medical Center, Rotterdam, Netherlands; Teuling et al., 2007). VAP-A was cut with BamHI–XhoI and cloned into both a pAGFP-C1 vector and a pYFP-C1 vector (in the BglII–SalI site). GFP-ANKPHD and mRFP-ANKPHD were generated by subcloning the ANKPHD fragment from pCDNA4-ANKPHD (Johansson et al., 2007) into a pEGFP-C1 vector (BD) or into a custom made pmRFP-C1 vector (Johansson et al., 2007), respectively, using the BamHI and XbaI sites.

ΔORD was generated by PCR using the primers 5′-ACTCGGATCCATGAACACAGAAGCG GAGCAACA-3′ and 5′-AAAGGATCCCTATCTGTGTTTTCTACTGCCCAAATGC-3′ and was inserted into the BamHI site of pcDNA4HisMax (Invitrogen) and the BglII site of pmRFP-C1 vectors (Johansson et al., 2007). To generate mRFP-ΔORDPHDPHD, mRFP-ΔORD was digested with XbaI and EcoRI. The remainder of ΔORD was amplified by PCR using the primers 5′-CTCAAAATGATTAAGGAGTGTGACATGGCTA-3′ and 5′-CCGGAATTCCATTCTGTGTTTTCTACT GCCCAAATGCTC-3′. The amplified fragment was inserted into the XbaI and EcoRI sites of the previously digested mRFP-ΔORD vector. The first PH domain was generated by PCR using the primers 5′-CCGGAATTCCGATATGAGGGCCCTCTCTGGAAGA-3′ and 5′-CGGGGTACCGCTGT AAGCAGAATGTTCTTCTATTGC-3′ and ligated into the EcoRI and KpnI sites. Subsequently, the second PH domain was also generated by PCR using the primers 5′-CGGGGTACCCGAT ATGAGGGCCCTCTCTGGAAGA-3′ and 5′-CGGGATCCATTCTAGCTGTAAGCAGAATGTTCTTCTATT GC-3′ and inserted using the KpnI and BamHI sites.

mRFP-ΔORDFFAT(D478A) was generated by PCR using mRFP-ΔORD as a template and 5′-CCCAGAATTCTATGCGGCGCTGTCAGATTCCGAGTC-3′ and 5′-AAGCAAGTAAAACCTCTACAA ATG-3′ as primers, followed by swapping of the wild-type FFAT motif in mRFP-ΔORD for the

mutated FFAT using the EcoRI and BamHI restriction sites. The ORP1L FRET construct (mRFP-ORP1L-GFP) was generated in two steps. First, mRFP-ORP1L was digested with NheI–SacI (internal site in ORP1L), which was subsequently cloned into pEGFP-N1 (Clontech Laboratories, Inc.) to obtain an N-terminal region of ORP1L, which was N-terminally tagged to mRFP and C-terminally tagged to GFP. In the second step, the C-terminal part of ORP1L was produced by PCR with a forward primer (5′-GGAGTGTGACATGGCTAA-3′) and a reverse primer (5′-CGG GATTCCATAAATGTCAGGCAAATTGAAG-3′), mutating the ORP1L stop codon. The PCR product was digested using SacI and BamHI and cloned into the aforementioned intermediate construct.

To obtain mRFP-ΔORDPHDPHD-GFP, mRFP-ΔORDPHD was subcloned into pEGFP-N3 (Clontech Laboratories, Inc.) using the restriction sites NheI and KpnI in mRFP-ΔORDPHDPHD (described above). The second PH domain in the tandem was generated by PCR using the primers 5′-CGGGGTACCCGATATGAGGGCCCTCTCTGGAAGA-3′ and 5′-CGGGGT ACCGCTGTAAGCAGAATGTTCTTCTATTGC-3′ and cloned into the KpnI restriction site. To obtain mRFP-ΔORD-GFP, mRFP-ΔORD was cloned into pEGFP-N2 (Clontech Laboratories, Inc.) using the restriction sites NheI and EcoRI in mRFP-ΔORDPHDPHD (described above).

For the generation of mRFP-ORP1L, ORP1L cDNA was cloned into mRFP-C1 using the BglII and BamHI restriction sites. Ectopic expression of RILP or ORP1L resulted in an approximately fourfold or sevenfold increase in mRNA levels (by qPCR), respectively. Expression (analyzed by qPCR) for RILP, ORP1L, and VAP related to actin (set at 100%) was 1.59% (SD, 0.01%), 2.16% (SD, 0.61%), and 1.78% (SD, 1.11%), respectively.

siRNAs for human NPC1 and ORP1L were obtained from Thermo Fisher Scientific (ON-TARGETplus SMARTpool for GenBank/EMBL/DDBJ accession nos. NM_000271 and NM_018030, respectively) and transfected using DharmaFECT 1 transfection reagent (Thermo Fisher Scientific). qPCR showed that RILP and ORP1L were expressed at <1% after siRNA silencing and VAP-A at 0.02%. All constructs were sequence verified. Expressed proteins had the expected molecular weight, as confirmed by SDS-PAGE and Western blot analyses.

Cell culture and drug treatment

Monolayers of MelJuSo cells were maintained in Iscove's modified Dulbecco's medium (IMDM; Invitrogen) supplemented with 8% FCS in 5% CO2 at 37°C. For cholesterol-depleting conditions, MelJuSo cells were washed with PBS and then cultured in IMDM supplemented with 5% lipoprotein-deficient serum, 50 µM lovastatin to inhibit HMG-CoA (3-hydroxy-3-methyl-glutaryl-CoA) reductase, and 230 µM mevalonate to supply essential nonsterol isoprenoids for cell growth and survival (Liscum et al., 1989; Sugii et al., 2006) for 4 h before analyses. For cholesterol enhancement, cells were washed with PBS and cultured in IMDM supplemented with 8% FCS and 3 µg/ml U-18666A for 15 h before analyses.

Microscopy

Transfected cells were fixed at 48 h (DNA or RNAi) or 72 h (RNAi and DNA) after transfection with 4% formaldehyde in PBS for 30 min and permeabilized for 5 min with 0.05% Triton X-100 in PBS at room temperature. Nonspecific binding of antibodies was blocked by 0.5% BSA/PBS for 40 min, after which cells were incubated with primary antibody in 0.5% BSA/PBS for 1 h at room temperature. Bound

primary antibodies were visualized with Alexa Fluor secondary antibody conjugates (Invitrogen). Cells were mounted in Vectashield mounting medium (Vector Laboratories). The specimens were analyzed with confocal laser-scanning microscopes (TCS-SP1, TCS-SP2, or AOBS; Leica) equipped with HCX Plan-Apochromat 63× NA 1.32 and HCX Plan-Apochromat lbd.bl 63× NA 1.4 oil-corrected objective lenses (Leica). The acquisition software used was LCS (Leica).

Colocalization analysis for TAP1 and CD63 was performed using Matlab (MathWorks), in which images were stretched to 255 Gy, and colocalization was performed on the pixels with intensities between100 and 255 Gy. The number of colocalizing pixels was related to total CD63 pixels for quantification. The colocalizing pixels were projected on the CD63/TAP1 overlay image for representation.

Photoactivation experiments were performed in MelJuSo cells transfected with PA-GFP tagged to VAP-A and cotransfected with mRFP-tagged ORP1L, ORP1LΔORD, or ORP1LΔORDPDHPDH. Cells were mounted in phenol red–free DME (Invitrogen), limiting autofluorescence of the medium. All measurements were performed on an AOBS system equipped with a 37°C culture chamber and an HCX Plan-Apochromat lbd.bl 63× NA 1.4 lens. Cells were imaged using a 488-nm and 561-nm laser to visualize the activated PA-GFP– and mRFP-tagged proteins, respectively. Point activation with full power from the 405-nm laser was performed for 3 s at the nuclear region, where the ER was activated at the sites below or under the nucleus. This location was devoid of LE structures. To confirm this, a z stack was made before activation.

Quantification of vesicle distribution

A mask was drawn for every cell to be quantified. Within each cell, the center of gravity of the stain to be quantified (e.g., CD63) was determined for each cell with the program CellProfiler (Broad Institute). The cell was divided into six fractions from the defined center to the edge of the cell. The mean fractional intensity at a given radius (fraction of total intensity normalized by fraction of pixels at a given radius) was determined and plotted for each fraction. For the modules and pipelines used, see http://cellprofiler.labstore.nl.

FLIM

FLIM experiments were performed with MelJuSo cells stably expressing mRFP-ORP1L-GFP cultured on Delta T dishes (Bioptechs). Before measurements, cells were mounted in bicarbonate-buffered saline medium (140 mM NaCl, 5 mM KCl, 2 mM MgCl2, 1 mM CaCl2, 23 mM NaHCO3, 10 mM d-glucose, and 10 mM Hepes, pH 7.3) and analyzed at 37°C in a 5% CO2 culture hood surrounding the objective stage of the microscope. Images were taken on an inverted microscope (DM-IRE2; Leica) with an HCX Plan-Apochromat 63× NA 1.35 glycerol-corrected objective lens equipped with a frequency domain lifetime attachment (Lambert Instruments) controlled by the manufacturer's FLIM software (Lambert Instruments). GFP was excited with ~4 mW of 488-nm light from a light-emitting diode modulated at 40 MHz, and emission was collected at 490–550 nm using an intensified charge-coupled device camera (CoolSNAP HQ; Roper Scientific). To calculate the GFP lifetime, the intensities from 12 phase-shifted images (modulation depth ~70%) were fitted with a sinus function, and lifetimes were derived from the phase shift between excitation and emission. For internal controls, cells were co-cultured

with MelJuSo cells expressing GFP only. Lifetimes were referenced to a 1-µM solution of rhodamine-G6 in saline that was set at a 4.11-ns lifetime. The donor FRET efficiency ED was calculated as ED = 1 − (measured lifetime/GFP lifetime in control cells) (Zwart et al., 2005).

Sensitized emission FRET by confocal microscopy

FRET between GFP and mRFP molecules was determined by calculating the sensitized emission (the mRFP emission after GFP excitation) from separately acquired donor and acceptor images (using an AOBS system equipped with a 37°C culture device at 5% CO2 and an HCX Plan-Apochromat 63× NA 1.32 oil-corrected objective lens). Three images were collected: GFP excited at 488 nm and detected between 500 and 549 nm, indirect mRFP excited at 488 nm and detected between 581 and 675 nm, and direct mRFP excited at 561 nm. Because of GFP-mRFP spectral overlap, indirect mRFP emission was corrected for bleed through of GFP in the 581–675-nm filter and for direct excitation of mRFP by 488-nm light. The correction factors were determined experimentally for each image by co-culturing cells expressing mRFP-ORP1L-GFP (or any of the ORP1L variants) with cells expressing only GFP (to detect the bleed through in the mRFP channel) or mRFP (to detect direct excitation with 488-nm light). FRET and donor FRET efficiency ED were calculated from these data as previously described in detail (van Rheenen et al., 2004; Zwart et al., 2005). For quantification of the intramolecular FRET gradient of mRFP-ORP1L-GFP and mRFP-ΔORD-GFP, ED was measured in five equally sized concentric rings covering the area between the nucleus and the cell surface at the most distant point. The ED in each circle was collected, binned, and expressed per cell analyzed. The mean ED and SEM of the different cells analyzed are calculated for the different rings.

Immuno-EM

Cells were fixed in 2% paraformaldehyde in 0.1 M PHEM buffer (60 mM Pipes, 25 mM Hepes, 2 mM MgCl2, and 10 mM EGTA, pH 6.9) and then processed for ultrathin cryosectioning as previously described (Calafat et al., 1997). 50-nm-thick cryosections were cut at −120°C using diamond knives in a cryoultramicrotome (Leica) and transferred with a mixture of sucrose and methylcellulose onto formvar-coated copper grids. The grids were placed on 35-mm Petri dishes containing 2% gelatin at 37°C. The grids were incubated with the various antibodies at room temperature and then incubated with 10-nm protein A–conjugated colloidal gold (EM Laboratory, Utrecht University) as previously described (Calafat et al., 1997). After immunolabeling, the sections were embedded in a mixture of methylcellulose and 0.4% uranyl acetate and examined with an electron microscope (CM10; Philips). The 40-nm spacing between the ER and LE membranes was derived from both digital and printed electron micrographs.

Filipin stainings

Formaldehyde-fixed cells were stained for 2 h at room temperature with 0.05 mg/ml filipin (Sigma-Aldrich) freshly dissolved in PBS supplemented with 0.5% BSA, and the staining was imaged with a microscope (AxioObserver Z1; Carl Zeiss, Inc.) equipped with a charge-coupled device camera (ORCA-ER; Hamamatsu Photonics) and a 63× NA 1.25 Plan-Neofluar oil-corrected objective lens. Filipin signal was recorded using a 390–415-nm band-pass (BP) excitation filter

and with a 450–470-nm BP emission filter. FITC signal was recorded with a 480–510-nm BP excitation filter and with a 515–550-nm BP emission filter. mRFP signal was recorded with a 555–590-nm BP excitation filter and with a 605–655-nm BP emission filter (Carl Zeiss, Inc.). For data acquisition, the manufacturers' software was used.

Protein purification

His-Rab7, His-RILP, and GST-ORP1L were produced as previously described (Johansson et al., 2007). Cells were lysed in 0.5% Triton X-100, 20 mM Hepes, pH 7.5, 200 mM NaCl, 8 mM β-mercaptoethanol, and complete EDTA-free protease inhibitors cocktail (Roche). The lysate was cleared by centrifugation, and the supernatant was incubated with pre-equilibrated Talon Co2+ resin (Clontech Laboratories, Inc.) for 30 min. The resin was then washed extensively with 20 mM Hepes, pH 7.5, 200 mM NaCl, and 8 mM β-mercaptoethanol. Proteins were stored in 8.7% glycerol at −80°C until use in protein reconstitution experiments. GST–VAP-A construct in pGEX was a gift from N. Ridgway (Wyles et al., 2002). GST was removed by cleavage with thrombin by incubation at 30°C for 2 h before inactivation and precipitation by 0.1 mM PMSF. The GST moiety was removed using a glutathione-Sepharose column (GE Healthcare), and the purity of GST-free VAP-A was confirmed by SDS-PAGE and Coomassie staining.

In vitro VAP-A induced p150Glued removal from the Rab7–RILP protein complex

The reconstitution assay was performed in a detergent/salt buffer (20 mM Hepes, pH 7.5, 200 mM NaCl, 4 mM β-mercaptoethanol, 5 mM MgCl2, 0.05% [vol/vol] Triton X-100, and 50 µM GTP). 15 µg His-Rab7(Q67L) was coupled to 3 µl of Talon Co2+ beads and preloaded with GTP. Beads were washed to remove unbound His-Rab7(Q67L), and recombinant purified proteins were added in equimolar concentrations. 3 µg His-RILP, 8.7 µg GST-ORP1L, 2.2 µg VAP-A, and 4.5 µg maltose-binding protein (MBP)–p150Glued(C25) were added to the beads as indicated and incubated in a total volume of 0.4 ml for 2 h at 4°C. Beads were washed extensively, and 4.5 µg MBP-p150Glued(C25) or 2.2 µg VAP-A was added to the beads as indicated. Proteins were subsequently incubated in a total volume of 0.4 ml of detergent/salt buffer for 30 min at 22°C. Beads were washed extensively, and proteins bound to His-Rab7(Q67L) were analyzed by SDS-PAGE and Western blotting. Proteins were detected with the following antibodies: α-His (GE Healthcare), α-MBP (New England Biolabs, Inc.), and α-GST (gift from W. Moolenaar, The Netherlands Cancer Institute, Amsterdam, Netherlands). Direct binding of p150Glued to VAP-A was assayed as follows. 30 µg GST–VAP-A or 15 µg GST was coupled to 15 µl of glutathione–Sepharose 4B beads (GE Healthcare). Beads were washed to remove unbound proteins, and 4.5 µg MBP-p150Glued(C25) was added to the beads in a total volume of 0.4 ml for 30 min at 22°C. Beads were washed extensively, and proteins bound to the glutathione–Sepharose 4B beads were analyzed by SDS-PAGE and Western blotting.

Supplemental material

Fig. S1 shows cholesterol, NPC1, the ORD, and vesicle distribution. Fig. S2 shows colocalization experiments of RILP and ORP1L variants with compartment markers and dynein motor subunits. Fig. S3 shows the chemical manipulation of cholesterol levels and location of ORP1L variants on LEs.

Fig. S4 shows control-sensitized emission FRET and FLIM experiments, the effect of NPC1 silencing on ORP1L conformation, and vesicle distribution of ORP1L mutants. Fig. S5 shows ORP1L-mediated recruitment of VAP-A from the ER and the release of p150Glued from RILP. Videos 1–3 show time-lapse experiments of LysoTracker red–labeled MelJuSo cells when cholesterol levels were manipulated. Videos 4 and 5 show time-lapse experiments of MelJuSo cells in which expression of mRFP-ΔORD and mRFP-ΔORDPHDPHD is induced and the distribution of LEs is followed. Videos 6–8 show time-lapse experiments in MelJuSo cells expressing mRFP-ORP1L, mRFP-ΔORD, and mRFP-ΔORDPHDPHD combined with photoactivation of PA-GFP–tagged VAP-A. Online supplemental material is available at http://www.jcb.org/cgi/content/full/jcb.200811005/DC1.

Acknowledgments

We thank K. Jalink for support with sensitized emission and FLIM measurements, P. Peters for support with EM, and V. Olkkonen and M. Johansson for ORP1L reagents and constructs. We also thank N. Ridgway, M. Hardy, K. Ettayebi, and C. Hoogenraad for VAP-A and VAP-B reagents, N. Ong for processing electron micrographs, and M. Hauptmann for help with statistics. We thank H. Pickersgill, R. Michalides, S. Godsave, J. Pierson, and V. Menendez-Benito for critically reading the manuscript and S. Krom for helping with experiments.

N. Rocha was supported by a Fundação para a Ciência ea Tecnologia Fundo Social Europeu PhD scholarship within the Third Framework Program. This work was supported by grants from the Dutch Cancer Society Koningin Wilhelmina Fonds and the Chemical Sciences Section of the Nederlandse Organisatie voor Wetenschappelijk Onderzoek (TOP grant).

Abbreviations used in this paper: BP, band pass; CLSM, confocal laser-scanning microscopy; DIC, dynein intermediate chain; FLIM, fluorescence lifetime imaging microscopy; FRET, fluorescence resonance energy transfer; IMDM, Iscove's modified Dulbecco's medium; LE, late endosome; LUT, look up table; MBP, maltose-binding protein; MCS, membrane contact site; mRFP, monomeric RFP; MTOC, microtubule-organizing center; ORD, OSBP-related domain; OSBP, oxysterol-binding protein; PH, pleckstrin homology; qPCR, quantitative PCR; RILP, Rab7-interacting lysosomal protein; VAP, VAMP-associated ER protein.

References

1. Bastiaens, P.I., and A. Squire. 1999. Fluorescence lifetime imaging microscopy: spatial resolution of biochemical processes in the cell. Trends Cell Biol. 9:48–52.
2. Brown, C.L., K.C. Maier, T. Stauber, L.M. Ginkel, L. Wordeman, I. Vernos, andT.A. Schroer. 2005. Kinesin-2 is a motor for late endosomes and lysosomes.Traffic. 6:1114–1124.
3. Burkhardt, J.K , C.J. Echeverri, T. Nilsson, and R B. Vallee. 1997. Overexpressionof the dynamitin (p50) subunit of the dynactin complex disrupts dyneindependent maintenance of membrane organelle distribution. J. Cell Biol.139:469–484.
4. Calafat, J., H. Janssen, M. Stahle-Backdahl, A.E. Zuurbier, E.F. Knol, and A. Egesten.1997. Human monocytes and neutrophils store transforming growth factoralpha in a subpopulation of cytoplasmic granules. Blood. 90:1255–1266.
5. Calleja, V., S.M. Ameer-Beg, B. Vojnovic, R. Woscholski, J. Downward, and B. Larijani. 2003. Monitoring conformational changes of proteins in cells by fluorescence lifetime imaging microscopy. Biochem. J. 372:33–40.
6. Carstea, E.D., J.A. Morris, K.G. Coleman, S.K. Loftus, D. Zhang, C. Cummings, J. Gu, M.A. Rosenfeld, W.J. Pavan, D.B. Krizman, et al. 1997.

Niemann- Pick C1 disease gene: homology to mediators of cholesterol homeostasis. Science. 277:228–231.

7. Chen, H., J. Yang, P.S. Low, and J.X. Cheng. 2008. Cholesterol level regulates endosome motility via Rab proteins. Biophys. J. 94:1508–1520.
8. Colin, E., D. Zala, G. Liot, H. Rangone, M. Borrell-Pages, X.J. Li, F. Saudou, and S. Humbert. 2008. Huntingtin phosphorylation acts as a molecular switch for anterograde/retrograde transport in neurons. EMBO J. 27:2124–2134.
9. David, V., F. Hochstenbach, S. Rajagopalan, and M.B. Brenner. 1993. Interaction with newly synthesized and retained proteins in the endoplasmic reticulum suggests a chaperone function for human integral membrane protein IP90 (calnexin). J. Biol. Chem. 268:9585–9592.
10. Deacon, S.W., A.S. Serpinskaya, P.S. Vaughan, M. Lopez Fanarraga, I. Vernos, K.T. Vaughan, and V.I. Gelfand. 2003. Dynactin is required for bidirectional organelle transport. J. Cell Biol. 160:297–301.
11. Echard, A., F. Jollivet, O. Martinez, J.J. Lacapere, A. Rousselet, I. Janoueix- Lerosey, and B. Goud. 1998. Interaction of a Golgi-associated kinesinlike protein with Rab6. Science. 279:580–585.
12. Förster, T. 1948. Zwischenmolekulare energiewandering und fluoreszenz. Annalen Physik. 437:55–75.
13. Goldstein, J.L., S.K. Basu, and M.S. Brown. 1983. Receptor-mediated endocytosis of low-density lipoprotein in cultured cells. Methods Enzymol. 98:241–260.
14. Haimo, L.T., and M.M. Rozdzial. 1989. Lysed chromatophores: a model system for the study of bidirectional organelle transport. Methods Cell Biol. 31:3–24.
15. Hamamoto, I., Y. Nishimura, T. Okamoto, H. Aizaki, M. Liu, Y. Mori, T. Abe, T. Suzuki, M.M. Lai, T. Miyamura, et al. 2005. Human VAP-B is involved in hepatitis C virus replication through interaction with NS5A and NS5B. J. Virol. 79:13473–13482.
16. Hamilton, J.A. 2003. Fast flip-flop of cholesterol and fatty acids in membranes: implications for membrane transport proteins. Curr. Opin. Lipidol. 14:263–271. Hoepfner, S., F. Severin, A. Cabezas, B. Habermann, A. Runge, D. Gillooly, H. Stenmark, and M. Zerial. 2005. Modulation of receptor recycling and degradation by the endosomal kinesin KIF16B. Cell. 121:437–450.
17. Hollenbeck, P.J., and J.A. Swanson. 1990. Radial extension of macrophage tubular lysosomes supported by kinesin. Nature. 346:864–866. Holthuis, J.C., and T.P. Levine. 2005. Lipid traffic: floppy drives and a superhighway. Nat. Rev. Mol. Cell Biol. 6:209–220.
18. Holtta-Vuori, M., J. Maatta, O. Ullrich, E. Kuismanen, and E. Ikonen. 2000. Mobilization of late-endosomal cholesterol is inhibited by Rab guanine nucleotide dissociation inhibitor. Curr. Biol. 10:95–98.
19. Ikonen, E. 2008. Cellular cholesterol trafficking and compartmentalization. Nat. Rev. Mol. Cell Biol. 9:125–138.
20. Im, Y.J., S. Raychaudhuri, W.A. Prinz, and J.H. Hurley. 2005. Structural mechanism for sterol sensing and transport by OSBP-related proteins. Nature. 437:154–158.
21. Johansson, M., M. Lehto, K. Tanhuanpää, T.L. Cover, and V.M. Olkkonen. 2005.The oxysterol-binding protein homologue ORP1L interacts with Rab7 and alters functional properties of late endocytic compartments. Mol. Biol. Cell. 16:5480–5492.
22. Johansson, M., N. Rocha, W. Zwart, I. Jordens, L. Janssen, C. Kuijl, V.M. Olkkonen, and J. Neefjes. 2007. Activation of endosomal dynein motors by stepwise assembly of Rab7–RILP–p150Glued, ORP1L, and the receptor bIII spectrin. J. Cell Biol. 176:459–471.
23. Jordens, I., M. Fernandez-Borja, M. Marsman, S. Dusseljee, L. Janssen, J. Calafat, H. Janssen, R. Wubbolts, and J. Neefjes. 2001. The Rab7 effector protein RILP controls lysosomal transport by inducing the recruitment ofdynein-dynactin motors. Curr. Biol. 11:1680–1685.
24. Jordens, I., M. Marsman, C. Kuijl, and J. Neefjes. 2005. Rab proteins, connecting transport and vesicle fusion. Traffic. 6:1070–1077.
25. Kobayashi, T., M.H. Beuchat, M. Lindsay, S. Frias, R.D. Palmiter, H. Sakuraba, R.G. Parton, and J. Gruenberg. 1999. Late endosomal membranes rich in lysobisphosphatidic acid regulate cholesterol transport. Nat. Cell Biol. 1:113–118.
26. Koh, C.H., and N.S. Cheung. 2006. Cellular mechanism of U18666A-mediated apoptosis in cultured murine cortical neurons: bridging Niemann-Pick disease type C and Alzheimer's disease. Cell. Signal. 18:1844–1853.
27. Lebrand, C., M. Corti, H. Goodson, P. Cosson, V. Cavalli, N. Mayran, J. Faure, and J. Gruenberg. 2002. Late endosome motility depends on lipids via the small GTPase Rab7. EMBO J. 21:1289–1300.
28. Lemmon, M.A., and K.M. Ferguson. 2000. Signal-dependent membrane targetingby pleckstrin homology (PH) domains. Biochem. J. 350:1–18.
29. Liscum, L , and J R. Faust. 1989. The intracellular transport of low density lipoprotein-derived cholesterol is inhibited in Chinese hamster ovary cells cultured with 3-beta-[2-(diethylamino)

ethoxy]androst-5-en-17-one. J. Biol. Chem. 264:11796–11806.

30. Liscum, L., R.M. Ruggiero, and J.R. Faust. 1989. The intracellular transport of low density lipoprotein-derived cholesterol is defective in Niemann-Pick type C fibroblasts. J. Cell Biol. 108:1625–1636.
31. Loewen, C.J., and T.P. Levine. 2005. A highly conserved binding site in vesicleassociated membrane protein-associated protein (VAP) for the FFAT motif of lipid-binding proteins. J. Biol. Chem. 280:14097–14104.
32. Loewen, C.J., A. Roy, and T.P. Levine. 2003. A conserved ER targeting motif in three families of lipid binding proteins and in Opi1p binds VAP. EMBO J. 22:2025–2035.
33. Marsman, M., I. Jordens, C. Kuijl, L. Janssen, and J. Neefjes. 2004. Dyneinmediated vesicle transport controls intracellular Salmonella replication. Mol. Biol. Cell. 15:2954–2964.
34. Maxfield, F.R., and I. Tabas. 2005. Role of cholesterol and lipid organization in disease. Nature. 438:612–621.
35. Mukherjee, S., and F.R. Maxfield. 2004. Lipid and cholesterol trafficking in NPC. Biochim. Biophys. Acta. 1685:28–37.
36. Nakata, T., and N. Hirokawa. 1995. Point mutation of adenosine triphosphatebinding motif generated rigor kinesin that selectively blocks anterograde lysosome membrane transport. J. Cell Biol. 131:1039–1053.
37. Narita, K., A. Choudhury, K. Dobrenis, D.K. Sharma, E.L. Holicky, D.L. Marks, S.U. Walkley, and R.E. Pagano. 2005. Protein transduction of Rab9 in Niemann- Pick C cells reduces cholesterol storage. FASEB J. 19:1558–1560.
38. Neufeld, E.B., J.A. Stonik, S.J. Demosky Jr., C.L. Knapper, C.A. Combs, A. Cooney, M. Comly, N. Dwyer, J. Blanchette-Mackie, A.T. Remaley, et al. 2004. The ABCA1 transporter modulates late endocytic trafficking: insights from the correction of the genetic defect in Tangier disease. J. Biol. Chem. 279:15571–15578.
39. Nishimura, Y., M. Hayashi, H. Inada, and T. Tanaka. 1999. Molecular cloning and characterization mammalian homologues of vesicle-associated membrane protein-associated (VAMP-associated) proteins. Biochem. Biophys. Res.
40. Commun. 254:21–26. Pelkmans, L., E. Fava, H. Grabner, M. Hannus, B. Habermann, E. Krausz, and M. Zerial. 2005. Genome-wide analysis of human kinases in clathrin- and caveolae/raft-mediated endocytosis. Nature. 436:78–86.
41. Pepperkok, R., A. Squire, S. Geley, and P.I. Bastiaens. 1999. Simultaneous detection of multiple green fluorescent proteins in live cells by fluorescence lifetime imaging microscopy. Curr. Biol. 9:269–272.
42. Pfeffer, S.R. 2001. Rab GTPases: specifying and deciphering organelle identity and function. Trends Cell Biol. 11:487–491.
43. Reits, E.A., J.C. Vos, M. Gromme, and J. Neefjes. 2000. The major substrates for TAP in vivo are derived from newly synthesized proteins. Nature. 404:774–778.
44. Roff, C.F., E. Goldin, M.E. Comly, A. Cooney, A. Brown, M.T. Vanier, S P. Miller, R.O. Brady, and P.G. Pentchev. 1991. Type C Niemann-Pick disease: use of hydrophobic amines to study defective cholesterol transport. Dev. Neurosci. 13:315–319.
45. Sobo, K., I. Le Blanc, P.P. Luyet, M. Fivaz, C. Ferguson, R.C. Parton, J. Gruenberg, and F.G. van der Goot. 2007. Late endosomal cholesterol accumulation leads to impaired intra-endosomal trafficking. PLoS ONE. 2:e851.
46. Suchanek, M., R. Hynynen, G. Wohlfahrt, M. Lehto, M. Johansson, H. Saarinen, A. Radzikowska, C. Thiele, and V.M. Olkkonen. 2007. The mammalian oxysterol-binding protein-related proteins (ORPs) bind 25-hydroxycholesterol in an evolutionarily conserved pocket. Biochem. J. 405:473–480.
47. Sugii, S., S. Lin, N. Ohgami, M. Ohashi, C.C. Chang, and T.Y. Chang. 2006. Roles of endogenously synthesized sterols in the endocytic pathway. J. Biol. Chem. 281:23191–23206.
48. Teuling, E., S. Ahmed, E. Haasdijk, J. Demmers, M.O. Steinmetz, A. Akhmanova, D. Jaarsma, and C.C. Hoogenraad. 2007. Motor neuron disease-associated mutant vesicle-associated membrane protein-associated protein (VAP) B recruits wild-type VAPs into endoplasmic reticulum-derived tubular aggregates. J. Neurosci. 27:9801–9815.
49. Underwood, K.W., N.L. Jacobs, A. Howley, and L. Liscum. 1998. Evidence for a cholesterol transport pathway from lysosomes to endoplasmic reticulum that is independent of the plasma membrane. J. Biol. Chem. 273:4266–4274.
50. Vale, R.D., F. Malik, and D. Brown. 1992. Directional instability of microtubule transport in the presence of kinesin and dynein, two opposite polarity motor proteins. J. Cell Biol. 119:1589–1596.
51. van Rheenen, J., M. Langeslag, and K. Jalink. 2004. Correcting confocal acquisition to optimize imaging of fluorescence resonance energy transfer by sensitized emission. Biophys. J. 86:2517–2529.
52. Vedrenne, C., and H.P. Hauri. 2006. Morphogenesis of the endoplasmic reticulum: beyond active membrane expansion. Traffic. 7:639–646.

53. Vennegoor, C., J. Calafat, P. Hageman, F. van Buitenen, H. Janssen, A. Kolk, and P. Rumke. 1985. Biochemical characterization and cellular localization of a formalin-resistant melanoma-associated antigen reacting with monoclonal antibody NKI/C-3. Int. J. Cancer. 35:287–295.

54. Wubbolts, R., M. Fernandez-Borja, I. Jordens, E. Reits, S. Dusseljee, C. Echeverri, R.B. Vallee, and J. Neefjes. 1999. Opposing motor activities of dynein and kinesin determine retention and transport of MHC class II-containing compartments. J. Cell Sci. 112:785–795.

55. Wyles, J.P., C.R. McMaster, and N.D. Ridgway. 2002. Vesicle-associated membrane protein-associated protein-A (VAP-A) interacts with the oxysterolbinding protein to modify export from the endoplasmic reticulum. J. Biol. Chem. 277:29908–29918.

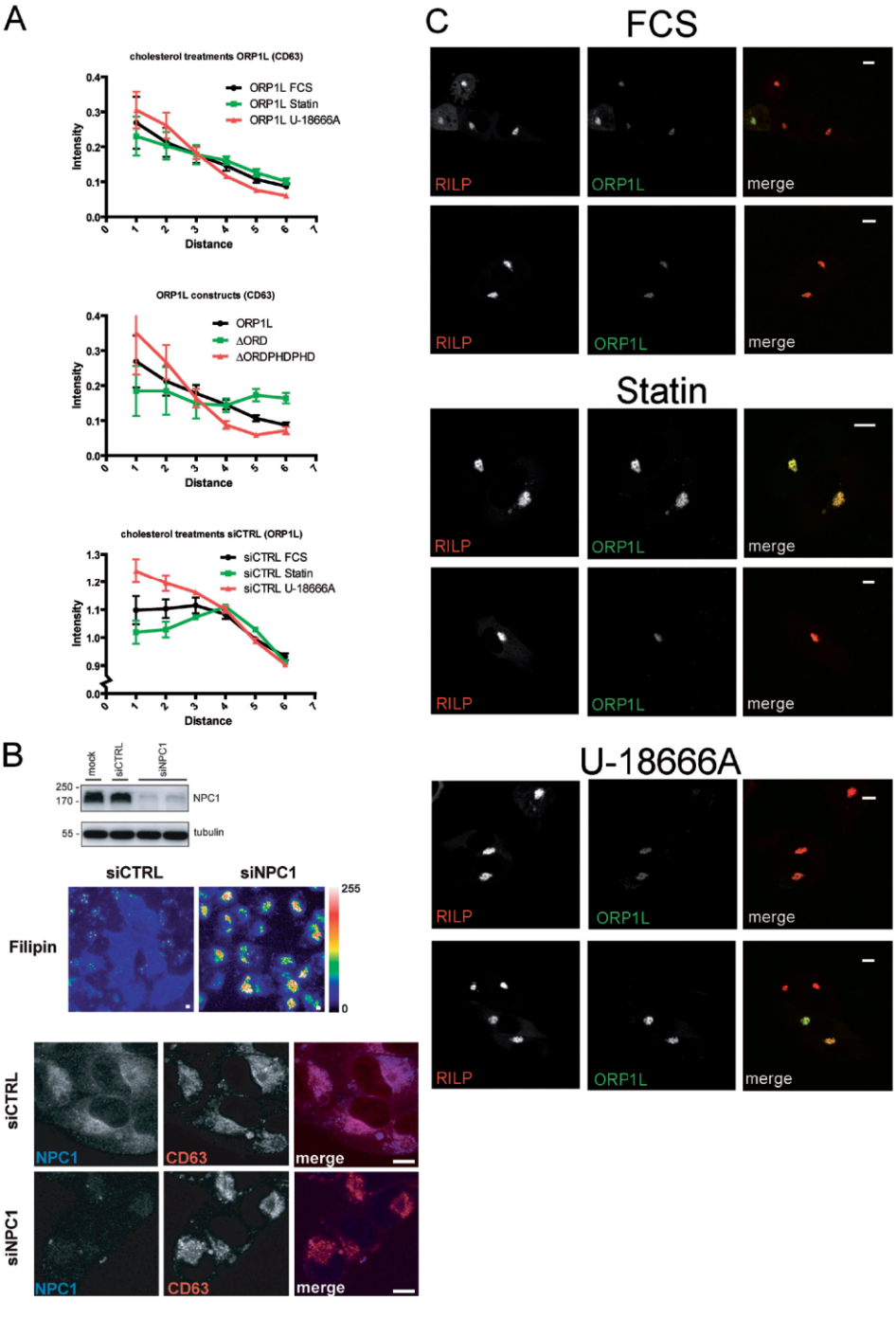
56. Zerial, M., and H. McBride. 2001. Rab proteins as membrane organizers. Nat. Rev. Mol. Cell Biol. 2:107–117.

57. Zwart, W., A. Griekspoor, C. Kuijl, M. Marsman, J. van Rheenen, H. Janssen, J. Calafat, M. van Ham, L. Janssen, M. van Lith, et al. 2005. Spatial separation of HLA-DM/HLA-DR interactions within MIIC and phagosomeinduced immune escape. Immunity. 22:221–233.

Supplementary material

Supplemental material available online at high resolution (http://jcb.rupress.org/content/185/7/1209/suppl/DC1)

Figure S1. Cholesterol, NPC1, the ORD, and vesicle distribution. (**A**) LE distribution under expression of ORP1L and mutants or cellular cholesterol content modifi cations. (top) Cells were transfected with ORP1L and treated with U-18666A to enhance cellular cholesterol content (red) or with statin and delipidated FCS to decrease cellular cholesterol content (green) or not treated (black). Endogenous CD63 was stained with anti-CD63 (NKI-C3), and the radial distribution of the fl uorescence was measured in six fractions with CellProfiler, in which fraction 1 starts in the center of gravity of the CD63 stain and subsequent fractions are progressively closer to the edge of the cell. (middle) Cells were transfected with ORP1L (black), ΔORD (green), and ΔORDPHDPHD (red). The distribution of the endogenous CD63 molecule was measured as described above. Vesicles cluster when the cholesterol content of cells is increased or when ΔORDPHDPHD is expressed. Scattering is observed when the cholesterol content of cells is decreased or when ΔORD is expressed. Mean and SEM values of >20 cells per condition are shown. The slopes of the curves were determined, and the dependence of vesicle distribution (based on mean intensity per fraction) on cholesterol content was tested (Jonckheere-Terpstra test) from enhanced (U-18666A) to control (FCS) to decreased cholesterol (statin) content ($P = 0.0002572$). In the case of the different ORP1L constructs (Fig. 2), vesicle distribution was tested from ΔORDPHDPHD (high cholesterol mimic) to ORP1L to ΔORD (low cholesterol mimic; $P = 5.122 \times 10^{5}$). (bottom) siRNA control (siCTRL) transfected cells were treated with U-18666A to enhance cellular cholesterol content (red) or with statin and delipidated FCS to decrease cellular cholesterol content (green) or not treated (black). Endogenous ORP1L was stained with a rabbit polyclonal antibody. The radial distribution of the fluorescence was measured in six fractions with CellProfiler, in which fraction 1 starts in the center of gravity of the ORP1L stain, and subsequent fractions are progressively closer to the edge of the cell. The slopes of the curves were determined, and the dependence of vesicle distribution (based on mean intensity per fraction) on cholesterol content was tested (Jonckheere-Terpstra test) from enhanced (U-18666A) to control (FCS) to decreased cholesterol (statin) content ($P = 7.76 \times 10^{6}$). (**B**) LE vesicle distribution and cholesterol levels in NPC1-silenced cells and siRNA-mediated silencing of NPC1 and intracellular cholesterol. (top) MelJuSo cells were mock transfected or transfected with a control siRNA or siRNA for NPC1. After 72 h, cell lysates were separated by SDS-PAGE and Western blotting, and fi lters were probed with anti-NPC1 antibodies or tubulin antibodies as a loading control. The positions of the molecular mass standards are indicated in kilodaltons. (middle) MelJuSo cells were transfected with control (siCTRL) or NPC1 siRNA (siNPC1) for 72 h before fi xation and staining with filipin. Images were made under identical settings, and a color LUT is applied to illustrate differences in intensities. $n > 200$ for each condition. (bottom) Effect of silencing NPC1 on LE positioning. MelJuSo cells were transfected with control of NPC1 siRNA before fixations and staining for NPC1 and the LE marker CD63, as indicated. $n > 100$. (**C**) RILP and ORLP1L binding under different cholesterol levels. MelJuSo cells were transfected with GFP-RILP and mRFP-ORP1L and exposed to control (FCS) or cholesterol- enhancing (U-18666A) or -decreasing (statin) conditions before fixation and analysis by CLSM. Representative images are shown. $n > 100$. No effect of cholesterol manipulation on GFP-RILP or mRFP-ORP1L binding to LEs is observed. Bars, 10 µm. ►


A
cholesterol treatments ORP1L (CD63)
ORP1L FCS
ORP1L Statin
ORP1L U-18666A
Intensity
Distance
ORP1L constructs (CD63)
ORP1L
ΔORD
ΔORDPHDPHD
cholesterol treatments siCTRL (ORP1L)
siCTRL FCS
siCTRL Statin
siCTRL U-18666A
B
mock
siCTRL
siNPC1
250
170
NPC1
55
tubulin
siCTRL
siNPC1
Filipin
255
0
NPC1
CD63
merge
C
FCS
Statin
U-18666A
RILP
ORP1L
merge

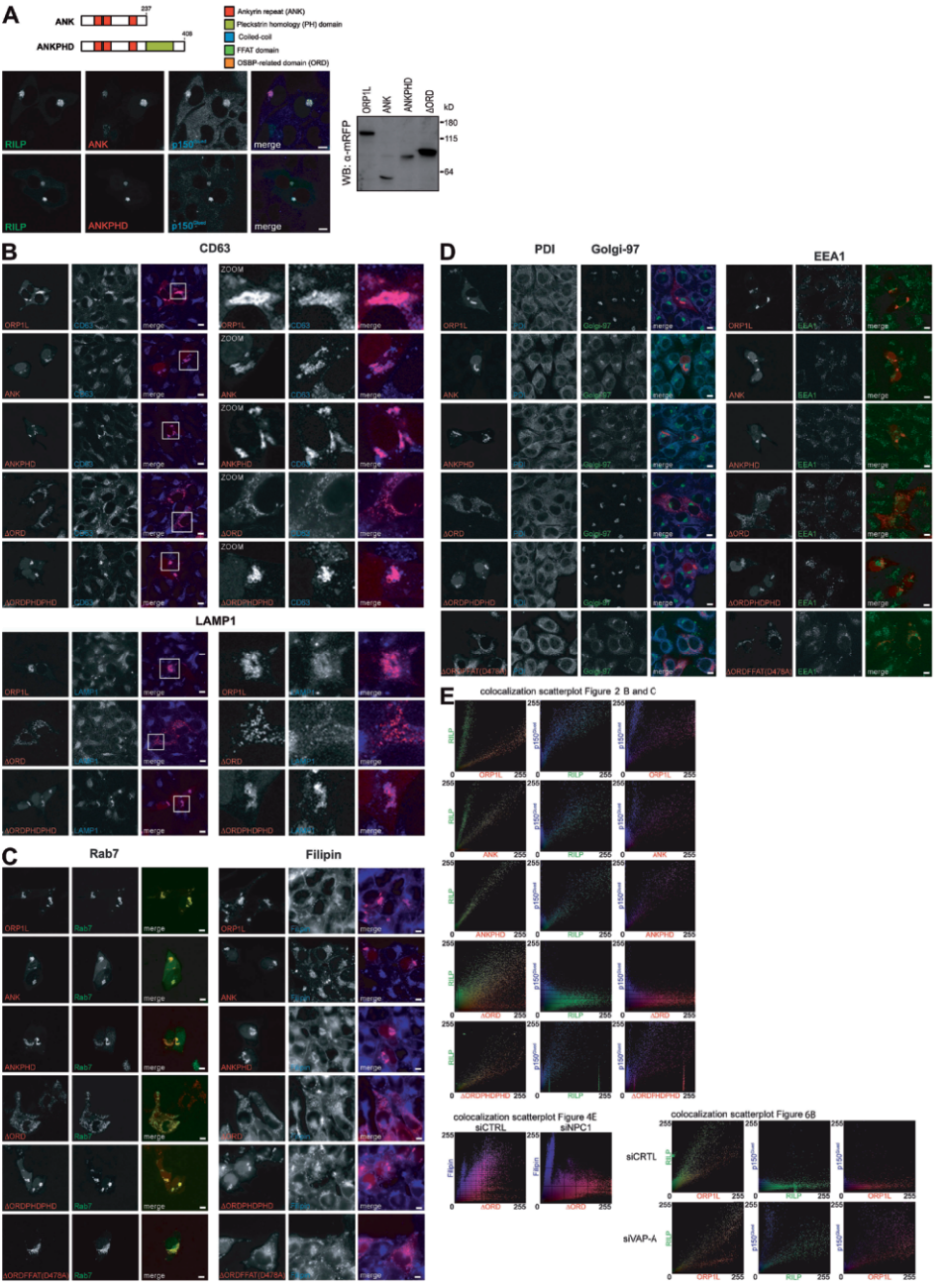


Figure S2. Colocalization experiments of RILP and ORP1L variants with compartment markers and dynein motor subunits. (**A**) ANK and ANKPHD enable recruitment of p150 Glued to the Rab7–RILP receptor. (top) ANK and ANKPHD domain structure and constructs. Numbers indicate amino acid residue positions. Both constructs were N-terminally tagged with mRFP. (bottom) Effect of ANK and ANKPHD chimeric constructs on RILP-mediated p150 Glued recruitment. (left) MelJuSo cells were transfected with GFP-RILP and mRFP- ►

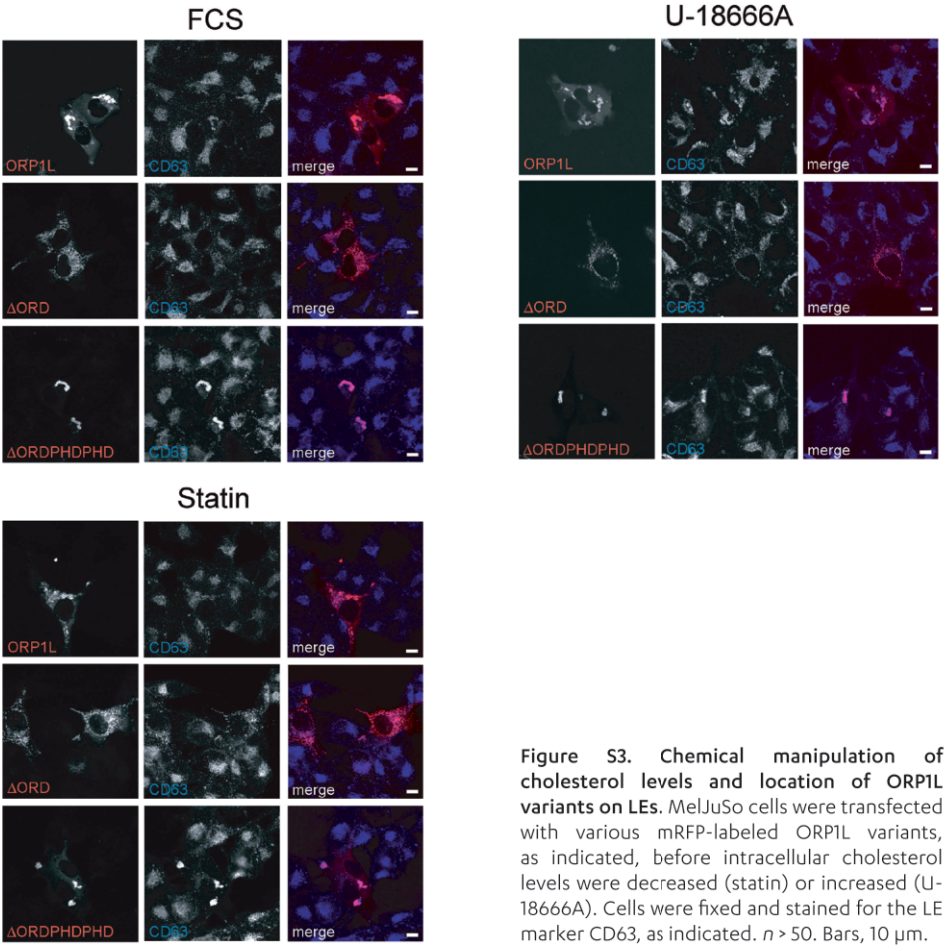
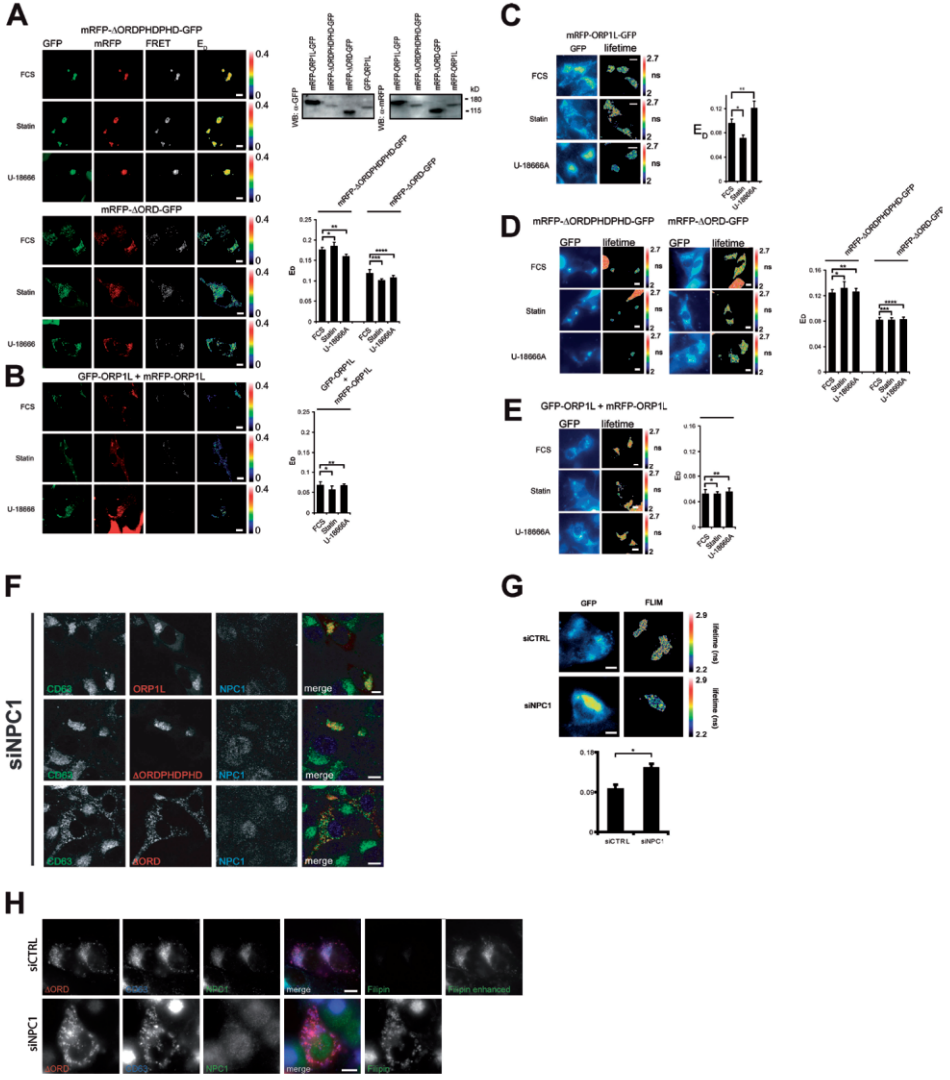


Figure S3. Chemical manipulation of cholesterol levels and location of ORP1L variants on LEs. MelJuSo cells were transfected with various mRFP-labeled ORP1L variants, as indicated, before intracellular cholesterol levels were decreased (statin) or increased (U-18666A). Cells were fixed and stained for the LE marker CD63, as indicated. *n* > 50. Bars, 10 µm.

► ORP1L constructs. Cells were fixed and stained with anti-p150 Glued antibodies before confocal microscopy. *n* > 200 for each condition. (right) MelJuSo cells were transfected with the indicated mRFP-ORP1L, -ANK, -ANKPHD, and - ΔORD constructs, and whole cell lysates were analyzed by SDS-PAGE and Western blotting with anti-mRFP antibodies (WB: α-mRFP). Positions of the molecular mass standards are indicated. WB, Western blot. (**B**) ORP1L and variants label CD63- and LAMP1-positive LEs. MelJuSo cells were transfected with various mRFP tagged ORP1L variants, as indicated. Cells were fixed and stained for CD63 or LAMP1. The right panel shows a zoom-in of the region where the vesicles locate. *n* > 100. (**C**) ORP1L and variants label Rab7- and cholesterol-positive vesicles. MelJuSo cells were transfected with various mRFP-tagged ORP1L variants, as indicated. Cells were fixed and stained for Rab7 or for cholesterol by filipin. *n* > 80. (**D**) ORP1L and variants do not label the ER, Golgi, or early endosomes. MelJuSo cells were transfected with various mRFP-tagged ORP1L variants, as indicated. Cells were stained and labeled for the ER marker protein disulfide-isomerase (PDI), the Golgi marker Golgi-97, or the early endosomal marker EEA1 (right). *n* > 100 for each panel. (E) 2D pixel analyses for colocalization of markers. The confocal microscopy images shown in Figs. 2 (**B** and **C**), 4 E, and 6 B were analyzed pixel by pixel for colocalization (intensity correlation analysis) of the markers indicated using ImageJ software (National Institutes of Health) with the WCIF plug-ins (http://www.uhnresearch.ca/facilities/wcif/imagej/). Proteins analyzed are shown along the x and y axes of the scatter plot in the color of analysis. Colocalization is indicated by a correlation in the x–y axis. Bars, 10 µm.

3

Figure S4. Control-sensitized emission FRET and FLIM experiments, the effect of NPC1 silencing on ORP1L conformation, and vesicle distribution of ORP1L mutants. (**A**) Sensitized emission confocal FRET for ORP1L variants and cholesterol level manipulations. MelJuSo cells were transfected with GFP-ΔORDPHDPHD- mRFP or GFP- ΔORD-mRFP, and sensitized emission was determined under control conditions (FCS) or conditions of cholesterol depletion (statin) or accumulation (U-18666A). Cells were co-cultured with control cells expressing GFP or mRFP only, which were used to control for bleed through and indirect excitation (not depicted). (left) For the different constructs (as indicated), the GFP channel (after excitation with 488-nm light), the mRFP signal (after excitation with 568-nm laser light), FRET (after correction for bleed through and indirect excitation), and donor FRET efficiency (ED) are shown. A color LUT directly reveals differences in donor FRET efficiency. (top right) The constructs tested in A–E and G were expressed, separated by SDS-PAGE and Western blotting, and probed with antibodies against GFP or mRFP, as indicated. The molecular mass standards are indicated. WB, Western blot. (bottom right) Donor FRET efficiency E D plotted from eight measurements per condition. Mean ± SEM is shown (*, P = 0.33; **, P = 0.11; ***, P = 0.10; ****, P = 0.29). (**B**) Sensitized emission confocal FRET to test clustering GFP-ORP1L and mRFP-ORP1L under different conditions of cholesterol manipulation. MelJuSo cells were transfected with the two constructs GFP-ORP1L and mRFP-ORP1L and co-cultured with control cells expressing GFP or mRFP only. (left) Two control cells expressing mRFP only are shown in the bottom panel. Cells were cultured under the various conditions of cholesterol manipulation before GFP, corrected mRFP, FRET, and donor FRET efficiency were measured, as described in A. (right) Quantification of donor FRET efficiency E D calculated from nine measurements per condition. Mean ± SEM is shown (*, P = 0.39; **, P = 0.98). (**C** and **D**) FLIM to detect conformational changes in ORP1L variants in response to cholesterol level manipulations. MelJuSo cells were transfected with GFP-ORP1L-mRFP (**C**) or GFP- ΔORDPHDPHD-mRFP or GFP- ΔORD-mRFP (**D**), and GFP fl uorescence lifetime was determined under control conditions (FCS) or conditions of cholesterol depletion (statin) or accumulation (U-18666A). (left) Cells were co-cultured with control cells expressing GFP only as an internal control for GFP lifetime not involved in a FRET pair. FLIM was measured by wide-field microscopy. The GFP panel shows the GFP signal, and the FLIM panel shows the fl uorescence lifetime in nanoseconds, which is visualized using a color LUT. (right) Quantification of donor FRET efficiency E D for the FRET constructs calculated from 20 measurements per condition. Mean ±SEM is shown (for C: *, P = 4.9×10^{-7} ; and **, P = 9.5×10^{-12} ; for D: *, P = 0.28; **, P = 0.74; ***, P = 0.98; and ****, P = 0.83). (**E**) FLIM measurements to test clustering of GFPORP1L and mRFP-ORP1L under different conditions of cholesterol manipulation. MelJuSo cells were transfected with the two constructs, GFP-ORP1L and mRFP-ORP1L, and co-cultured with control cells expressing GFP only before exposure to the conditions of cholesterol manipulation, as in C and D. (left) Wide-field image of GFP fl uorescence and lifetime detection, which is shown in false colors for lifetime differences, as shown by a color LUT. (right) Calculated donor FRET efficiency ED under the different conditions of cholesterol manipulation from 20 measurements. Mean ± SEM is shown (*, P = 0.94; **, P = 0.63). (**F**) Silencing NPC1 and location of ORP1L variants on CD63-containing endosomes. MelJuSo cells were transfected with siRNA for NPC1 and 48 h later with the various mRFP-labeled ORP1L constructs, as indicated. After another 24 h, cells were fixed and stained for the LE marker CD63 and NPC1 to control for actual silencing. $n > 100$. (**G**) ORP1L conformation in NPC1-deficient cells as detected by FLIM. mRFP-ORP1L-GFP–expressing MelJuSo cells were transfected with control (siCTRL) or NPC1 (siNPC1) siRNAs. (top) GFP fl uorescence detected the distribution of the ORP1L-containing vesicles by wide-field microscopy. GFP lifetime was detected by FLIM. The lifetime was determined (in nanoseconds) and plotted in a false color LUT. (bottom) donor FRET efficiencies (ED) as calculated from the FLIM data. The mean and SD from 75 cells analyzed in three independent experiments are shown (*, P = 3.1×10^{-16}). (**H**) LE scattering in NPC1-deficient cells. MelJuSo cells were transfected with control siRNA or siRNA for NPC1 and 48 h later with mRFP- ΔORD. 24 h later, cells were fixed and stained for the LE marker CD63, NPC1 (as control), and filipin to detect cholesterol. Microscopy images were made under identical settings. An additional image for filipin made after long exposure is shown (filipin enhanced) to show that control cells also contain cholesterol. *N*=50. Bars, 10 µm. ►


A
mRFP-ΔORDPHDPHD-GFP
GFP
mRFP
FRET
E_D
FCS
Statin
U-18666
mRFP-ΔORD-GFP
WB: α-GFP
WB: α-mRFP
kD
180
115
B
GFP-ORP1L + mRFP-ORP1L
C
mRFP-ORP1L-GFP
GFP
lifetime
ns
U-18666A
D
mRFP-ΔORDPHDPHD-GFP
mRFP-ΔORD-GFP
E
GFP-ORP1L + mRFP-ORP1L
F
siNPC1
CD63
ORP1L
NPC1
merge
ΔORDPHDPHD
ΔORD
G
siCTRL
siNPC1
FLIM
lifetime (ns)
H
siCTRL
siNPC1
ΔORD
CD63
NPC1
merge
Filipin
Filipin enhanced

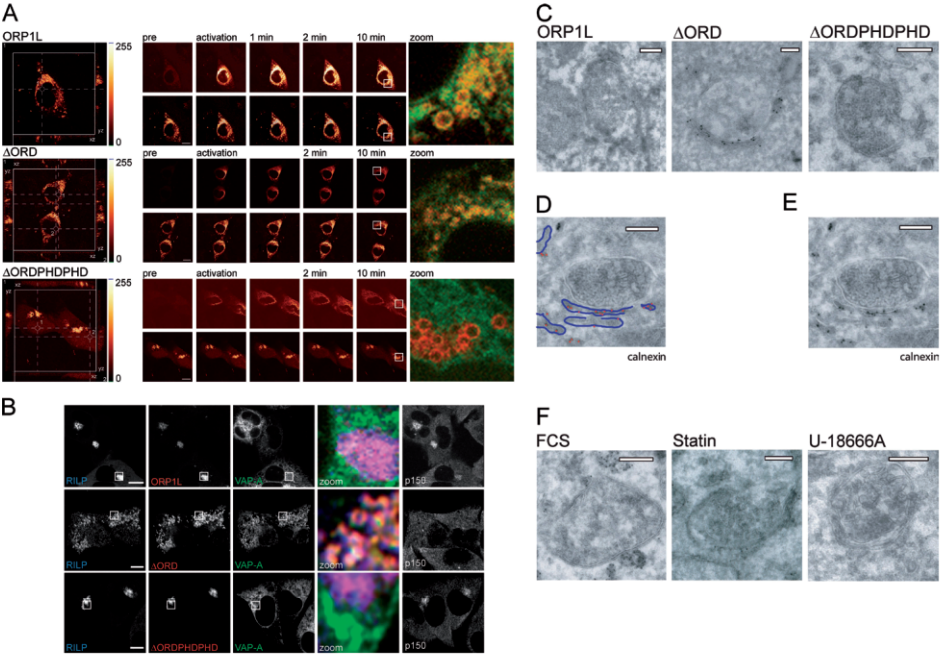


Figure S5. ORP1L-mediated recruitment VAP-A from the ER and the release of p150 Glued from RILP. (**A**) ORP1L recruits VAP-A from the ER. PA-GFP–tagged VAP-A in mRFP- ΔORDPHDPHD, - ΔORD, or -ORP1L–expressing MelJuSo cells was photoactivated with a 405-nm light to follow transport of ER-located PAGFP– VAP-A to LEs by time-lapse microscopy. First, a z stack of cells was made to identify a location for selective photoactivation of the ER pool of VAP-A. The left shows an x–y, x–z, and y–z projection through the site of photoactivation (the 405-nm laser spot position is shown as a circle). Cells were followed by time-lapse confocal microscopy, and various snapshots of the mRFP and GFP channels before and after photoactivation of PA-GFP–VAP-A are shown. Images are presented in glow-over/under mode to represent different fl uorescent intensities. The right panel shows a magnification of LEs (indicated by the boxed area) and a merge of the mRFP and GFP channel. $n > 10$ for each condition. See Videos 1–3. (**B**) VAP-A recruitment by ΔORD and release of p150 Glued from RILP. MelJuSo cells were transfected with GFP-RILP, mRFP-ORP1L constructs (as indicated), and HA-tagged VAP-A before fixation and staining with anti-HA and anti-p150 Glued antibodies before four-color confocal microscopy. The boxed area in the images indicates the zoomed-in region shown in overlay colors as the fourth panel. The right panel shows p150 Glued. ΔORD recruits VAP-A and excludes p150 Glued from RILP resulting in scattered vesicles. (**C**) Electron micrographs of multivesicular bodies in MelJuSo cells expressing HA-VAP and different variants of GFP-ORP1L, as indicated. Cells were fixed, and cryosections were stained with anti-HA antibodies detected with 15-nm gold particles. These images correspond to Fig. 8 A. (**D**) Electron micrographs of multivesicular bodies in MelJuSo cells expressing GFP- ΔORD. Cryosections were labeled with anticalnexin antibodies detected by 15-nm gold particles.The gold particles are highlighted by red dots, and the ER membrane is indicated by blue lines. (**E**) Original electron micrograph from multivesicular bodies in MelJuSo cells expressing GFP- ΔORD. Cryosections were labeled with anticalnexin antibodies detected by 15-nm gold particles. This image corresponds to D. (**F**) Electron micrographs of multivesicular bodies in HA-VAP– and GFP-ORP1L–expressing MelJuSo cells exposed to different cholesterol-manipulating conditions, as indicated. Cells were fixed and stained with anti-HA antibodies marked by 15-nm gold particles. These images correspond to Fig. 8C. Bars: (**A** and **B**) 10 µm; (**C**–**F**) 200 nm.

Video 1. Motility of LEs in untreated cells. LysoTracker red was used to label LEs in MelJuSo cells. Vesicle movement is visualized as a ratiometric glow LUT. Cells were imaged using a Leica SP2 system equipped with a heated chamber (37°C with 5% CO 2). Frames were taken every 1.6 s. The video is shown at 10 frames/s with 100 total frames.

Video 2. Motility of LEs in cholesterol-depleted cells. LysoTracker red was used to label LEs in MelJuSo cells, which were cultured and imaged in cholesterol-depleted medium containing statins overnight (as in Fig. 1, **A** and **B**). Vesicle movement is visualized as a ratiometric glow LUT. Cells were imaged using a Leica SP2 system equipped with a heated chamber (37°C with 5% CO_2). Frames were taken every 1.6 s. The video is shown at 10 frames/s with 100 total frames.

Video 3. Motility of LEs in cholesterol-enriched cells. LysoTracker red was used to label LEs in MelJuSo cells, which were cultured and imaged in medium containing U-18666A (as in Fig. 1, **A** and **B**). Vesicle movement is visualized as a ratiometric glow LUT. Cells were imaged using a Leica SP2 system equipped with a heated chamber (37°C with 5% CO 2). Frames were taken every 1.6 s. The video is shown at 10 frames/s with 100 total frames.

Video 4. Repositioning of LEs in cells expressing the ORP1L- ΔORD mutant. MelJuSo cells stably expressing CD63-GFP (green) to label LEs were microinjected with vectors encoding mRFP- ΔORD (red), H2B (histone-2B)-GFP (green; nuclear) as an expression control, and 70-kD Texas red dextran as an injection marker in the presence of cycloheximide. The cycloheximide block was washed away 2 h after microinjection. Cells were imaged using a Leica SP2 system equipped with a heated chamber (37°C with 5% CO_2). Frames were taken every 10 min. The video is shown at 5 frames/s with 30 total frames.

Video 5. Repositioning of LEs in cells expressing the ORP1L- ΔORDPHDPHD mutant. MelJuSo cells stably expressing CD63-GFP (green) to label LEs were microinjected with vectors encoding mRFP- ΔORDPHDPHD (red), H2B (histone-2B)-GFP (green; nuclear) as an expression control, and 70-kD Texas red dextran as an injection marker in the presence of cycloheximide. The cycloheximide block was washed away 2 h after microinjection, immediately before imaging. Cells were imaged using a Leica SP2 system equipped with a heated chamber (37°C with 5% CO_2). Frames were taken every 10 min. The video is shown at 5 frames/s with 30 total frames.

Video 6. VAP-A diffusion in cells expressing ORP1L. MelJuSo cells were transiently transfected with expression vectors for PAGFP–VAP-A (green) and mRFP-ORP1L (red). PA-GFP–VAP-A was activated by a 405-nm laser at a site where the ER is present but LEs are not. To exclude that the 405-nm laser beam would hit LEs, a z stack was made to locate ER pools of VAP-A away from the mRFP-labeled LEs. Cells were imaged using a Leica AOBS system equipped with a 37°C chamber culture hood with 5% CO_2. Frames were taken every 1 min. The video is shown at 3 frames/s with 30 total frames. The still images are presented in Fig. S5A.

Video 7. VAP-A diffusion in cells expressing the ORP1L- ΔORD mutant. MelJuSo cells were transiently transfected with expression vectors for PA-GFP–VAP-A (green) and mRFP- ΔORD (red). PA-GFP–VAP-A was activated by a 405-nm laser at a site where the ER is present but LEs are not. To exclude that the 405-nm laser beam would hit LEs, a z stack was made to locate ER pools of VAP-A away from the mRFP-labeled LEs. Cells were imaged using a Leica AOBS system equipped with a 37°C chamber culture hood with 5% CO_2. Frames were taken every 1 min. The video is shown at 3 frames/s with 30 total frames. The still images are presented in Fig. S5A.

Video 8. VAP-A diffusion in cells expressing the ORP1L- ΔORDPHDPHD mutant. MelJuSo cells were transiently transfected with expression vectors for PA-GFP–VAP-A (green) and mRFP- ΔORDPHDPHD (red). PA-GFP–VAP-A was activated by a 405-nm laser at a site where the ER is present but LEs are not. To exclude that the 405-nm laser beam would hit LEs, a z stack was made to locate ER pools of VAP-A away from the mRFP-labeled LEs. Cells were imaged using a Leica AOBS system equipped with a 37°C chamber culture hood with 5% CO_2 . Frames were taken every 1 min. The video is shown at 3 frames/s with 30 total frames. The still images are presented in Fig. S5A.

chapter **FOUR**

Late endosomal transport and tethering are coupled processes controlled by RILP and the cholesterol sensor ORP1L

Rik van der Kant[1]
Alexander Fish[2]
Lennert Janssen[1]
Hans Janssen[1]
Sabine Krom[1]
Nataschja Ho[1]
Thijn Brummelkamp[2]
Jan Carette[3]
Nuno Rocha[1]
Jacques Neefjes[*]

[1]Division of Cell Biology and [2]Division of Biochemistry,
the Netherlands Cancer Institute, Plesmanlaan 121, 1066CX Amsterdam NL
[3]Department of Microbiology and Immunology, Stanford University School of Medicine,
299 Campus Drive, Stanford CA 94305

[*]Correspondence; j.neefjes@nki.nl – Tel; +31-20-5122017 Fax; +31-20-5122029

Journal of Cell Science, in press

Abstract

Late endosomes and lysosomes are dynamic organelles that constantly move and fuse to acquire cargo from early endosomes, phagosomes and autophagosome. Defects in lysosomal dynamics cause severe neurodegenerative and developmental diseases such as Niemann-Pick Type C disease and ARC syndrome, yet little is know about regulation of late endosomal fusion in a mammalian system. Mammalian endosomes destined for fusion need to be transported over very long distances before they tether to initiate contact. Here we describe that lysosomal tethering and transport are combined processes co-regulated by one multi-protein complex; RAB7-RILP-ORP1L. We show that RILP directly and concomitantly binds the tethering HOPS complex and the p150^{glued} subunit of the dynein motor. ORP1L then functions as a cholesterol-sensing switch controlling RILP-HOPS-p150^{Glued} interactions. We show that RILP and ORP1L control Ebola virus infection, a process dependent on late endosomal fusion. By combining recruitment and regulation of both the dynein motor and HOPS complex into a single multiprotein complex, the RAB7-RILP-ORP1L complex efficiently couples and times microtubule minus-end transport and fusion, two major events in endosomal biology.

Keywords: endosomal fusion, Ebola virus, HOPS complex, RAB7, RILP,ORP1L

Abbreviations

HOPS complex, Homotypic fusion and vacuole Protein Sorting complex; LE, late endosome; LY, lysosome; NPC-1, Niemann Pick disease type C1; ORP1L, Oxysterol binding protein Related Protein 1L; RILP, RAB7-interacting lysosomal protein; SPR, Surface Plasmon Resonance.

Introduction

Intracellular organelles continuously move and fuse due to the activities of motor proteins and fusion complexes. Fusion of organelles occurs in a series of sequential steps starting with transport of organelles along the cytoskeleton towards each other. Subsequently, these organelles tether, dock and fuse to exchange cargo (Brocker et al., 2010). Early endosomes, autophagosomes and phagosomes fuse with acidic late endosomes and lysosomes (LE) in order to degrade endosomal cargo and recycle nutrients. Defects in the lysosomal transport and fusion machinery result in severe neurodegenerative and developmental diseases such as Niemann-Pick Type C disease (Sobo et al., 2007; Rocha et al., 2009), Charcot–Marie–Tooth disease (CMT) (Basuray et al., 2013; Spinosa et al., 2008), classical juvenile onset neuronal ceroid lipofuscinosis (Uusi-Rauva et al., 2012) and arthrogryposis-renal dysfunction-cholestasis (ARC) syndrome (Gissen et al., 2004; Cullinane et al., 2010).

Much of our understanding of LE fusion is derived from studies in yeast where vacuolar (lysosomal) tethering is orchestrated by the HOmotypic fusion and vacuole Protein Sorting (HOPS) complex that subsequently interacts with SNARE proteins to induce fusion (Ostrowicz et al., 2010). In contrast to yeast cells, LE in mammalian cells first need to be transported over long distances before they can meet, tether and fuse to exchange cargo. LE transport is well studied in mammalian cells, but tethering for fusion as well as the cross-talk between transport and tethering processes are poorly understood.

In the endo-lysosomal system, various small GTPases of the Rab and Arf family facilitate transport by recruitment of relevant motor proteins from the dynein, kinesin or myosin families (Hoepfner et al., 2005; Wu et al., 2002; Paul et al., 2011; Kuijl et al., 2007; Stenmark, 2009) that specify directionality. The RAB7 effector RILP interacts with the $p150^{Glued}$ subunit of the dynein/dynactin motor complex thus controlling microtubule minus-end transport of late endosomes, lysosomes and lysosome-related organelles such as early melanosomes and cytolytic granules (Johansson et al., 2007; Rocha et al., 2009; Jordens et al., 2001; Daniele et al., 2011; Jordens et al., 2006; Vallee et al., 2012). Silencing of RILP or ectopic expression of its dominant negative N-terminally truncated mutant (RILPΔ199) have been shown to impair endosomal maturation as well as phagosome fusion to lysosomes thereby facilitating intracellular *Salmonella* survival (Marsman et al., 2004; Harrison et al., 2004; Guignot et al., 2004). Dynein motor recruitment to RAB7-RILP is controlled by interactions between the cholesterol sensor ORP1L and the ER protein VAP-A and this mechanism is responsible for vesicle clustering observed in lysosomal storage diseases characterized by accumulation of cholesterol in the late endosomal compartments (Rocha et al., 2009; (Vihervaara et al., 2011).

While the spatial control of motor protein recruitment to vesicles is understood at some level of detail, this is not the case for tethering and subsequent fusion of vesicles. Tethering factors function to physically bridge two opposing membranes, establish quality control (i.e. prevent fusion between unrelated compartments) before recruiting SNARE proteins for actual membrane fusion. RAB GTPases are also involved in vesicle tethering and fusion (Brocker et al., 2010). The RAB5 effector EEA1 can promote docking and fusion of early endosomes (Christoforidis et al., 1999) and other RAB GTPases support multisubunit tethering complexes at the ER, Golgi and the plasma membrane (Brocker et al., 2010). Late endosomal tethering is

best understood in yeast where vacuolar (lysosomal) tethering is orchestrated by the HOPS complex comprised of six vacuolar protein-sorting (Vps) components: Vps18, Vps11, Vps16, Vps41, Vps39 and Vps33 (Wickner, 2010). Homologues of all these Vps subunits are found in mammalian systems with some expansion. Specifically two VPS33 proteins exist -VPS33A and VPS33B- and a new VPS33B interacting protein has evolved; SPE-39 (Huizing et al., 2001; Zhu et al., 2009; Gissen et al., 2005). The yeast RAB7 homologue Ypt7 recruits and assembles the HOPS complex by interacting with Vps39 and Vps41 on different sides of the HOPS complex, suggesting that HOPS bridges Ypt7 on two vesicles (Cabrera et al., 2009; Brocker et al., 2012).

In yeast, the HOPS complex is the only known Ypt7 effector and no RILP homologue is found. In contrast to mammals, the dynein motor appears to not be essential for late endosomal transport in yeast, indicating that interactions around Ypt7/RAB7 may be different between yeast and human with respect to vesicular transport and tethering functions. Despite significant evolutionary conservation of the actual tethering complex from yeast to human, the current understanding of the HOPS complex composition, recruitment and function in mammalian systems remains limited. Human HOPS has been implicated in EGFR routing (Chirivino et al., 2011) and autophagosome maturation (Liang et al., 2008), and is critical for efficient cytosolic entry of Ebola virus from NPC-1 containing late endosomes (Carette et al., 2011). Mutations in the additional HOPS subunits VPS33b and SPE-39 cause complex multiorgan failures such as arthrogryposis-renal dysfunction-cholestasis (ARC) syndrome characterized by impairments in granule secretion and membrane fusion (Gissen et al., 2004; Cullinane et al., 2010). Another HOPS interactor, the small GTPase ARL8b controls lipid loading of CD1 molecules in lysosomes through interactions with some subunits of the HOPS complex (Garg et al., 2011). How the mammalian HOPS complex is recruited to late endosomal membranes, is unclear.

Here, we demonstrate that RAB7 effector RILP recruits the mammalian HOPS complex to late endosomal membranes, and an ARC-syndrome disease mutant of VPS33b fails to be recruited to RILP. RILP simultaneously binds both the HOPS complex and dynein motor, thereby coupling transport and tethering for fusion in one protein complex. Uncoupling these processes has major effects on cargo delivery as illustrated for Ebola infectivity. The cholesterol sensor ORP1L controls RILP-HOPS-dynein motor interactions and times both transport and tethering. Collectively, our observations suggest that two main aspects of late endosomal life - transport and fusion - are integrated and regulated by a single RAB7-RILP-ORP1L protein complex to promote efficient transport and delivery of late endosomal cargo.

Results

RILP induces late endosomal tethering in the absence of functional dynein-motor

The RAB7 effector RILP recruits the $p150^{Glued}$ subunit of the dynein/dynactin motor complex to late endosomal membranes to induce microtubule minus-end transport (Cantalupo et al., 2001; Jordens et al., 2001). Expression of RILP in cells induces late endosomal clustering at the microtubule-organizing centre (MTOC) of cells (Rocha et al., 2009, Cantalupo et al., 2001; Jordens et al., 2001) (Fig. 1A) due to dynein motor activity. As active GTP-bound Ypt7 (the yeast

RAB7 homologue) is involved in late endosomal tethering (Cabrera et al., 2009) and RILP locks RAB7 in an active GTP-bound state, we wondered whether RILP present on LE might also induce its tethering. To test this, we expressed RILP in cells where dynein motor activity was abrogated by overexpressing p50^{dynamitin} (Fig. 1A) or silencing the dynein chain (DHC) (Fig. 1B). As DHC is 500kDa and difficult to assess by SDS-PAGE, protein expression was determined by its surrogate marker Dynein intermediate chain (DIC) that is stable only in presence of DHC. DIC was efficiently eliminated when DHC was silenced. Under these conditions RILP-labelled endosomes remained in one or two large clusters per cell. This data shows that RILP induces LE clustering even in the absence of functional dynein motor, and that RILP might be involved in tethering LEs. To visualize the clusters induced by RILP expression in higher resolution, MelJuSo cells were transfected with GFP-RILP, fixed and sections stained with anti-GFP (10 nm-gold) antibodies for analysis by electron microscopy. RILP was often observed at contact sites between LE (Fig. 1C), again suggesting a link between RILP and tethering. LE tethering in yeast is achieved by the HOPS complex which is recruited to LE membranes via the small RAB-GTPase Ypt7. To test the localization of the HOPS complex in mammalian cells, we reconstituted a VPS11 KO cell-line (Carette et al., 2011) with GFP-VPS11. GFP-tagged VPS11 could be successfully incorporated into high molecular weight complexes similar to their endogenous equivalents as assessed by gel filtration and western blotting (Fig 1D) and a cytosolic distribution was observed for VPS11 (Fig 1E). To test whether RILP promotes HOPS recruitment to late endosomes, we co-expressed RILP in the GFP-VPS11 expressing cells. In this case we observed a striking recruitment of VPS11 to RILP-labeled late endosomes (Fig 1E). While the C-terminus of RILP binds and locks RAB7 in a GTP-bound state, the N-terminus of RILP directly binds the dynein motor (Johansson et al., 2007). Expression of an N-terminally truncated RILP mutant (RILPΔ199) in GFP-VPS11 expressing cells failed to recruit VPS11 to LE (Fig 1E). These data suggest that the N-terminus of RILP, recruits the dynein motor and is also involved in recruitment of the HOPS complex to late endosomes for tethering.

Mammalian HOPS is recruited to membranes by RILP and regulated by ORP1L

To study localization of the other mammalian HOPS complex subunits, we co-expressed the eight (tagged)-HOPS complex subunits in the melanoma cell line MelJuSo (S1A, S1B). Expression levels were moderate (Fig S1C) and the epitope-tagged proteins were successfully incorporated into high molecular weight complexes similar to their endogenous equivalents as determined by gel filtration (Fig S1D). A cytosolic distribution for all of the HOPS complex subunits was observed upon ectopic expression. Additional expression of constitutively-active RAB7 did not suffice to induce recruitment of HOPS to LE (Fig. 2A, S1A and S1B). However, when co-expressed with RILP (Fig. S1A, S1B) 7 of 8 HOPS subunits were recruited to RILP-decorated late endosomes. Only VPS33a was not recruited to RILP unless its interaction partner VPS16 was co-expressed (Fig. S1B). Mutations in one of the HOPS complex subunits, VPS33b, causes ARC-syndrome and one disease mutant of VPS33b (L30P), has been reported to be deficient in membrane recruitment(Gissen et al., 2004). Indeed, the latter VPS33b mutant failed to be recruited by RILP to late endosomes (Fig 2B). To further confirm interactions between HOPS and RILP, we performed co-immunoprecipitation experiments. RILP could be co-isolated with VPS11, VPS18 as well as SPE-39 (Fig 2C).

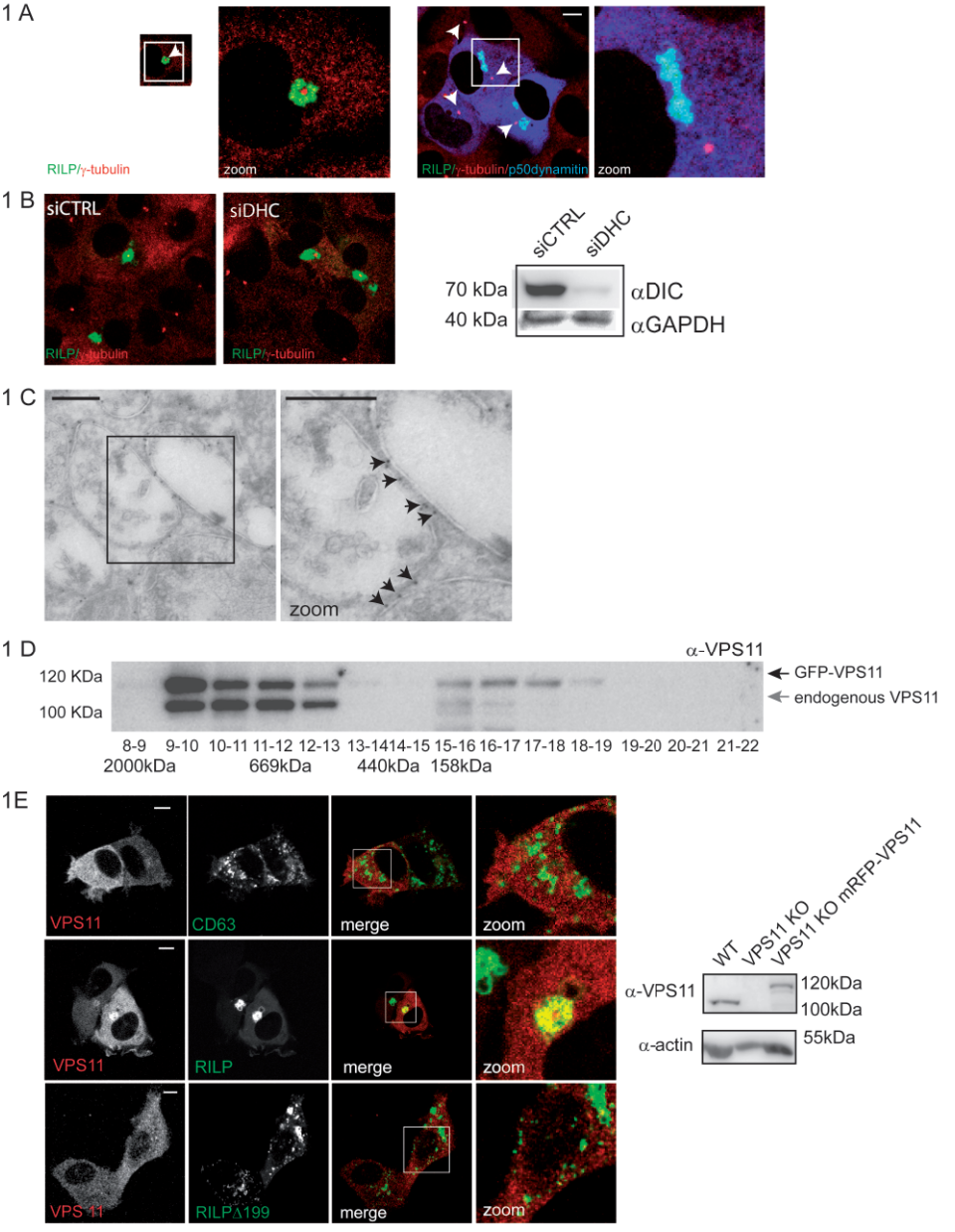


Figure 1. RILP induces late endosomal tethering independent of dynein-motor recruitment. (**A**) MelJuSo cells expressing HA-RILP and either or not co-expressing mRFP-p50^{dynamitin} (blue) were fixed, immunolabelled with HA-antibodies (green) and γ-tubulin (red) and imaged by CLSM. Scale bar: 10μm, n>100. Arrowheads indicate microtubule organizing centers. (**B**) MelJuSo cells silenced for Dynein heavy chain (DHC) and expressing HA-RILP were fixed, immunolabelled with HA-antibodies (green) and γ-tubulin (red) and imaged by CLSM. Scale bar: 10μm, representative of n>100. Western blot shows silencing for Dynein heavy chain by staining for co-depleted Dynein intermediate chain (Raaijmakers et al., 2012). (**C**) Electron micrographs of tethered late endosomal multivesicular bodies in MelJuSo cells expressing ▶

Binding of the dynein motor to RAB7-RILP is controlled by the cholesterol sensor ORP1L (Rocha et al., 2009). ORP1L also binds RAB7 and prevents binding of the dynein motor to RILP under low cholesterol conditions, as ORP1L then binds to ER protein VAP-A which removes p150^{Glued} from RILP (Rocha et al., 2009). To test if ORP1L also controls RILP-HOPS interactions, we co-expressed various subunits of the HOPS complex with RILP and wild-type ORP1L or a mutant of ORP1L mimicking low cholesterol conditions (ORP1LΔORD) that releases p150^{Glued} from the RAB7-RILP complex (Fig 2D, S1E, S1F). wtORP1L allowed binding of all subunits of the HOPS complex to RILP-labelled endosomes unlike ORP1LΔORD that effectively prevented HOPS subunit recruitment to endosomes (Rocha et al., 2009). Under low cholesterol conditions, ORP1L changes conformation to expose an FFAT motif that subsequently interacts with VAP-A to remove the dynein motor from RAB7-RILP (Rocha et al., 2009). To test whether VAP-A is involved in removing the HOPS complex from RILP under low cholesterol conditions, we repeated the experiments with an ORP1L mutant: ORP1LΔORDFFAT(D478A) that is similar to ORP1LΔORD with a single mutation in the FFAT domain to abolish interactions with ER protein VAP-A (Rocha et al., 2009) (Fig S1G). This ORP1L mutant again allowed recruitment of HOPS complex subunits to RILP labelled endosomes suggesting that HOPS binding to RILP is –like p150^{Glued} binding- controlled by cholesterol sensor ORP1L through ER protein VAP-A. Together our data indicate that the HOPS complex is recruited to membranes by the RAB7 effector RILP and that recruitment is further regulated by the cholesterol sensor ORP1L.

Fine-mapping of HOPS subunit recruitment to the N-terminus of RILP

In the yeast HOPS complex there are multiple Ypt7 (the yeast RAB7 homologue) binding sites (Brocker et al., 2012). To define whether the mammalian HOPS complex interacts with multiple sites on RILP, N-terminal RILP truncations were constructed and expressed with different HOPS complex subunits in MelJuSo cells (Fig. 3A, S2B, quantified in 3B). Expression levels of the various RILP constructs were similar and all RILP mutants localized properly to late endosomes (Fig S2A). All HOPS subunits (except for VPS33a (Fig. S2C)) were recruited to the N-terminal 199 amino acids of RILP that also binds the dynein motor-complex subunit p150^{Glued} (Johansson et al., 2007). We observed that different HOPS complex subunits where recruited to different regions of RILP (summarized in Fig. 3D). As HOPS subunits were overexpressed, these should be interactions of free HOPS subunits to the different RILP deletion mutants. Recruitment of the entire HOPS complex to RILP probably requires multiple binding sites as deletion of RILP aa

► GFP-RILP. Sections were stained with anti-GFP antibodies (15nm-gold particles). Right panels: zoom-in of boxed region in overview image (left). Scale bar: 250nm (**D**) Tagged VPS11 is incorporated into high molecular weight complexes. Lysates of MelJuSo cells expressing GFP-tagged VPS11 were size separated by gel filtration. The elution of control proteins (and their mass) is indicated. Fractions of different sizes were separated by SDS-PAGE and WB and probed for anti-VPS11 to detect complexes containing GFP-tagged (black arrow) and endogenous VPS11 (gray arrow). (**E**) VPS11 KO HAP1 cells expressing mRFP-VPS11 were transfected with GFP-RILP or GFP-RILPΔ199. Merge shows co-localization of VPS11 and RILP. Scale bar: 10μm. n>100. Right panel: expression levels of endogenous and ectopically expressed mRFP-VPS11. Lysates of the WT, VPS11 knock-out and the reconstituted HAP1 cells were separated by SDS-PAGE and WB with an anti-VPS11 antibody. Actin staining is used as a loading control.

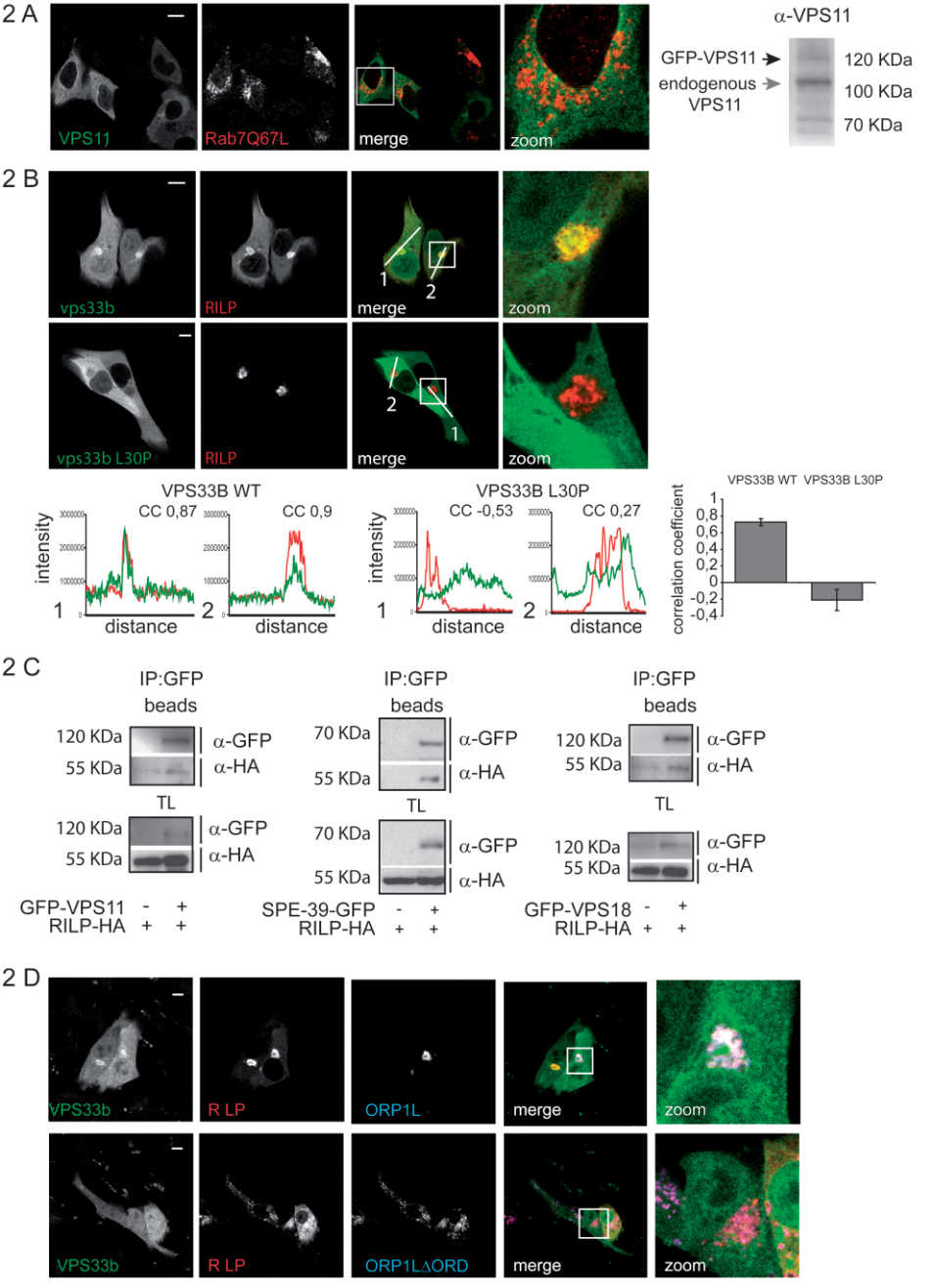


Figure 2. Mammalian HOPS is recruited to membranes by RILP and regulated by ORP1L. (**A**) MelJuSo cells expressing GFP-VPS11 in combination with myc-RAB7Q67L were stained with myc-antibodies and imaged by confocal microscopy. Zoom-ins of merged pictures indicated. Scale bar: 10μm. n>100. Right panel shows expression level of GFP-VPS11 (gray arrow) compared to endogenous VPS11 (black arrow) as assessed by WB and probing with an anti-VPS11 antibody. (**B**) MelJuSo cells expressing GFP-VPS33b or GFP-VPS33b ►

1-100 (disrupting recruitment of VPS11 and VPS16) also negatively affected recruitment of VPS18 (Fig. 3B). These experiments were further confirmed in biochemical experiments where VPS18 was co-isolated with different RILP truncation mutants (Fig. 3C, S2D). While RILPΔ199 failed to co-isolate VPS18, RILPΔ150 and smaller deletion mutants were successful, as also shown in Fig 3B. Together these data indicate that the mammalian HOPS complex is recruited to late endosomes by multiple interactions with the N-terminal half of the RAB7 effector RILP, the same region that accepts the p150^{Glued} subunit of the dynein motor.

RILP concomitantly binds the dynein motor and HOPS complex

The p150^{Glued} subunit of the dynein motor binds directly to RILP (Jordens et al., 2001). To test if the interactions between RILP and HOPS subunits are also direct, we assayed *in vitro* the binding of two HOPS subunits (VPS18 and VPS41) to Rab7 and/or RILP by SPR. The recombinant proteins used (Fig. 4A) were incorporated into higher molecular weight complexes running at similar complex-sizes as endogenous HOPS indicating that the proteins are well-folded and can interact with their endogenous partners (Fig. 4B). The N-terminus of VPS18 (as for the soluble isolated protein) was shown to be sufficient for recruitment to late endosomes by RILP(Fig S3A) and RAB7/RILP assembled into a stable complex for the SPR experiments (Fig S3B). The recombinant soluble HOPS subunits GST-VPS18 (aa 1-580) and GST-VPS41 were bound to a Surface Plasmon Resonance (SPR)-CHIP and responses were determined in the presence of GTP at different concentrations of RAB7, RILP, the RAB7-RILP complex or the C-terminus of p150^{Glued} (C25) (Fig. 4C). These values were corrected for a GST-only control and from the SPR response curves the equilibrium association constant KA (1/KD) was determined (Fig. 4C). GTP-loaded RAB7 associated to VPS18 and VPS41 with a low but detectable affinity ($4.12x10^4$ and $5.80x10^4$ M^{-1}. respectively). Binding affinities of RILP to the same HOPS subunits was approximately 10-fold higher ($3.41x10^5$ and $5.39x10^5M^{-1}$, respectively). The RAB7-RILP complex had a further 2-3 fold increase in affinity for VPS18 and VPS41 ($5.98x10^5$ and $1.13x10^6M^{-1}$, respectively). No productive binding was detected for VPS18 and VPS41 to C25 ($KA<1x10^4M^{-1}$). Together our data indicate that both HOPS complex subunits and the C-terminus of p150^{Glued} (Johansson et al., 2007) can associate to RILP in cells and *in vitro*.

This suggests that two general processes in late endosomal life – fusion and transport - are directly coupled through the RAB7-effector RILP. To test this, GFP-tagged VPS41 was co-expressed with RILP and cells were subsequently stained for the dynein motor subunit p150^{Glued}. RILP recruited both p150^{Glued} and VPS41 to clustered endosomes (Fig. 4D). Similar results were obtained with VPS18 (Fig. 4D). To further address whether HOPS and p150^{Glued} bind to RILP simultaneously or mutually

► L30P in combination with RILP-HA were stained with HA-antibodies and imaged by confocal microscopy. Zoom-ins of merged pictures indicated. Scale bar: 10µm. n>100. Plot profiles for cells indicated in lower panels. In Red: mRFP intensity and in Green: GFP intensity (VPS33b) over lines indicated in left panel. CC = correlation coefficient. Graph shows average correlation coefficient + sem. n>25. (**C**) Interaction of SPE39, VPS18 and VPS11 with RILP. Lysates of MelJuSo expressing GFP-tagged HOPS subunits and RILP-HA were immunoprecipitated (IP) with anti-GFP before separation by SDS-PAGE, WB and probed with anti-HA and anti-GFP antibodies. (**D**) MelJuSo cells expressing GFP-VPS33b, RILP-HA in combination with mRFP-ORP1L or mRFP-ORP1LΔORD (as indicated) were immunolabelled with HA-antibodies and imaged by confocal microscopy. Zoom-in of merged pictures indicated. Scale bar: 10µm. n>100.

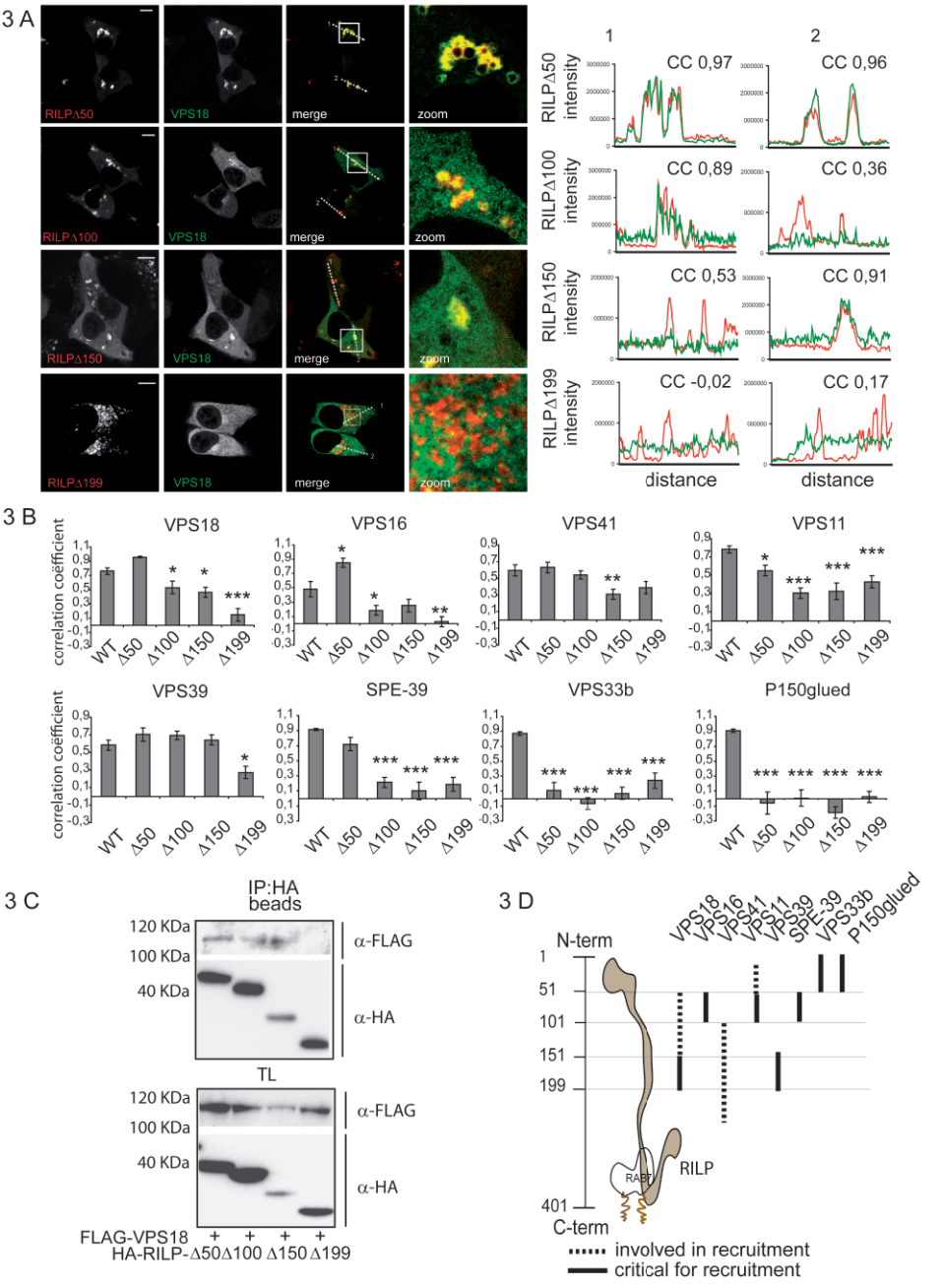


Figure 3. Recruitment of HOPS complex subunits to RILP. (**A**) Left panel: MelJuSo cells expressing GFP-VPS18 and HA-tagged truncation mutants of RILP (Δ50, Δ100, Δ150 and Δ199 respectively) were fixed and stained with HA-antibodies before imaging by confocal microscopy. Zoom-ins of merged pictures indicated. Scale bar: 10μm. n>100. Right panel: Plot profiles for cells indicated in left panels. In Red: mRFP intensity (RILP mutants) and in Green: GFP intensity (VPS) over lines indicated in left panel. CC = correlation coefficient. (**B**) Quantification of HOPS subunits recruited to RILP mutants. Mean correlation coefficients ▶

exclusive (compete for the same site on RILP), RAB7-RILP and RAB7-RILP-C25 complexes were reconstituted using purified recombinant Rab7, RILP and the C-terminus of p150^{Glued} (C25). Their binding to VPS18 (aa1-580) and VPS41 subunits of the HOPS complex was assessed by SPR (Fig. 4E). Whereas p150^{Glued}-C25 failed to interact with the HOPS subunits, RAB7-RILP-C25 associated with a higher binding affinity than RAB7-RILP only (KA VPS18 (aa1-580); 1.22x10^{6}M^{-1}, VPS41; 1.67x10^{6}M^{-1}). This suggests that the C-terminal part of p150^{Glued} supports, rather than competes for, the interaction of the RAB7-RILP complex to HOPS subunits and that p150^{Glued} and HOPS subunits can simultaneously bind to RILP, effectively integrating a motor protein for transport and a tethering complex for fusion on a single late endosomal receptor: RAB7-RILP.

Late endosomal tethering by RILP and HOPS is required for Ebola virus infectivity

RILP couples late endosomal minus-end transport by the dynein motor complex and tethering by the HOPS complex. Overexpression of RILP induces late endosomal clustering at the MTOC and this clustering is a consequence of p150^{Glued}-dynein motor recruitment (driving minus-end transport) (Jordens et al., 2001) and HOPS complex recruitment (for vesicle tethering) (Fig 1-4). To study the relative contribution of RILP-HOPS interactions in late endosomal dynamics, we defined RILP mutants that allowed interactions with p150^{Glued} but not with the HOPS complex. To define critical position in RILP to uncouple both processes, we first determined charged amino acids (these are likely exposed to the protein surface) in the N-terminus of RILP and conserved between a series of species. We reversed the charge (for example, R to E or E to R) and tested for recruitment of p150^{Glued} or HOPS subunits (Fig S4A-H). Most mutations that affected RILP interactions with HOPS subunits also affected p150^{Glued} recruitment, suggesting that HOPS stabilizes p150^{Glued} binding to RILP and confirming data from our SPR experiments (Fig 4). Only one mutant, RILPD125RE126R, markedly affected recruitment of most HOPS subunits with negligible effects on p150^{Glued} recruitment (Fig S4A-H, quantified in Fig 5A).

To visualize the contribution of HOPS recruitment to late endosomal tethering, we co-expressed RILP mutants and p50^{dynamitin} (to disrupt the dynein motor (Vallee et al., 2012)). Under these conditions wild-type RILP is still capable of clustering vesicles (Fig 1). Expression of RILP mutants that fail to recruit the HOPS complex– RILPD125RE126R and RILP E93RE94R – are less potent in clustering LE and in combination with p50^{dynamitin} overexpression yielded cells with many small clusters and single endosomes (Fig. 5B). The experiment was repeated by silencing the DHC subunit of the dynein motor (Fig S4I). Again, RILP mutants unable to recruit HOPS yielded cells with mainly small RILP mutant containing vesicular clusters, indicating that recruitment of HOPS by RILP is required for late endosomal tethering.

► + sem are shown for indicated HOPS subunits. Representative images are shown in Fig. S2B. * indicates p<0,05, ** indicates p<0,01 and *** indicates p<0,001 when tested to WT RILP. n >20 for each condition. (**C**) Interaction of RILP Δ50, Δ100, Δ150 and Δ199 RILP truncation mutants with VPS18. Lysates of MelJuso expressing Flag-tagged VPS18 and HA-RILP truncation mutants were immunoprecipitated (IP) with anti-HA before separation by SDS-PAGE and WB probed with anti-HA and anti-Flag. Bottom panel: input, Top panel: isolated RILP mutant with co-isolated FLAG-VPS18. (**D**) Map showing the regions of RILP recruiting different HOPS complex subunits and p150^{Glued}, as deduced from Figure 3B/3C/S2B/S2C.

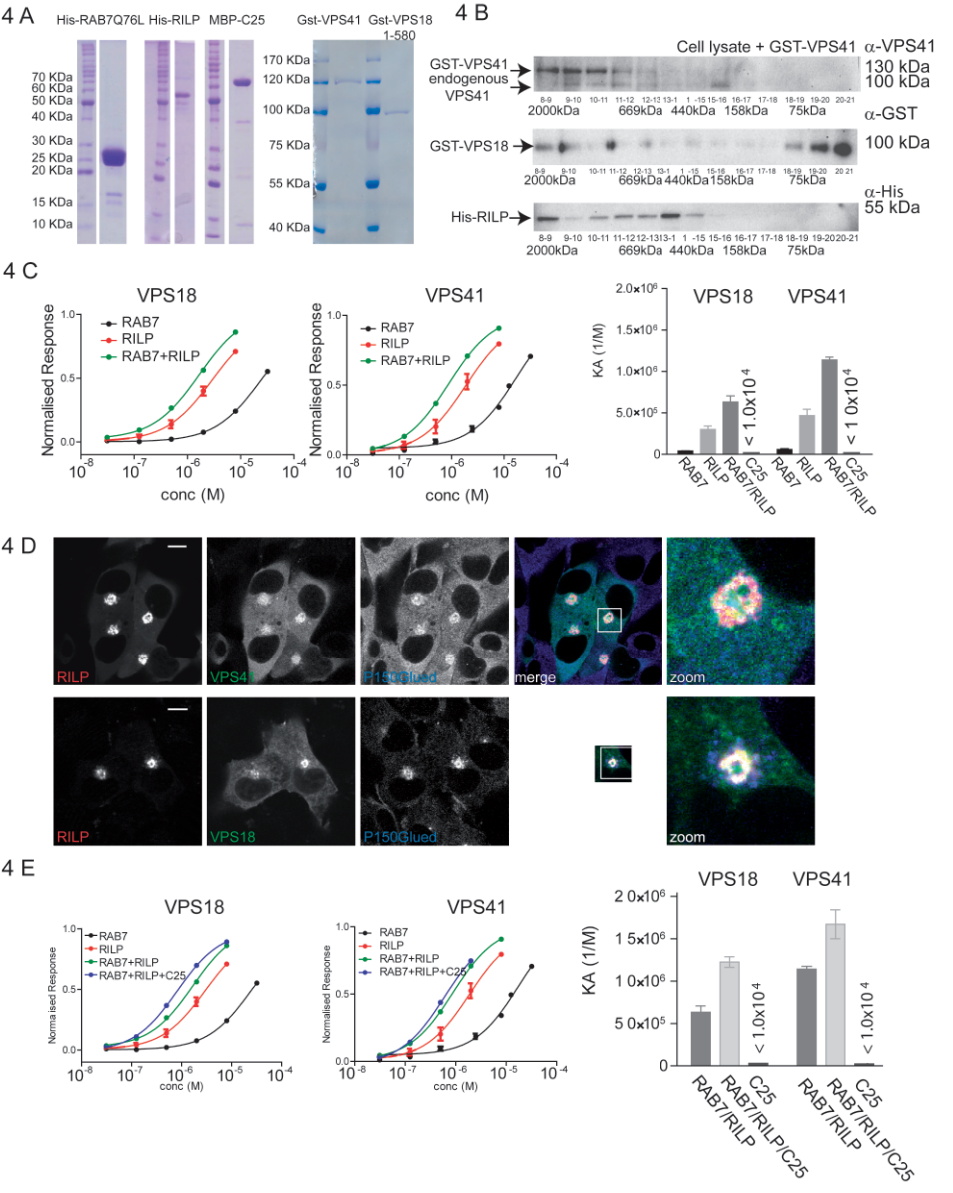


Figure 4. Simultaneous binding of HOPS subunits and p150^{Glued} to RILP. (**A**) Coomassie-stained SDS-PAGE gels with the recombinant proteins used for the SPR-experiments, as indicated. Position marker proteins is shown. (**B**) Recombinant proteins used in SPR-studies are incorporated into higher molecular weight complexes. Recombinant GST-VPS41, GST-VPS18[1-512] or His-RILP were incubated with lysates of MelJuSo cells and lysates were subsequently size separated using gel filtration. Fractions were subjected to SDS-PAGE and WB and probed for indicated antibodies to detect complexes containing the recombinant proteins. (**C**) GST-VPS18 (aa 1-580) or GST-VPS41 was immobilized to an SPR-chip and binding of RAB7Q76L, RILP, a RAB7Q76L-RILP complex and C25 in the presence of GTP-γS was determined. RAB7Q76L and RILP were pre-incubated with GTP-γS to assemble the complex. Shown are responses (corrected to GST-only) at different concentrations of RAB7, RILP or the RAB7-RILP complex. Right panel: From the SPR responses ►

A recent genetic screen identified 6 subunits of the HOPS complex as essential for successful cellular infection by Ebola virus (Carette et al., 2011). If RILP is the receptor for the HOPS complex, RILP mutants that fail to recruit the HOPS complex should also affect Ebola virus infection of cells. Cells expressing mRFP, mRFP-RILP, mRFP-RILPΔ199 or mRFP-RILPD125RE126R were infected with replication-competent Vesicular Stomatitis Virus bearing the Ebola virus glycoprotein (rVSV-GP-EboV)(Wong et al., 2010) that produces GFP upon replication in the cytosol of infected cells. rVSV-GP-EboV infectivity was reduced by half in cells expressing mRFP-RILP(D125RE126R) relative to control cells expressing either mRFP only or mRFP-tagged wild-type RILP when infection was assessed by microscopy (Fig 5C and 5D) or flow cytometry (Fig S4J). When late endosomal recruitment of both p150^{Glued} and HOPS was prevented with RILPΔ199, inhibition of infection of rVSV-GP-EboV remained attenuated to a level similar as inhibition of HOPS recruitment alone.

As the cholesterol sensor ORP1L acts as regulator of HOPS as well as dynein motor binding to RILP (Rocha et al., 2009, Fig 2D), we tested whether ORP1L also affected Ebola virus infection. Cells were transfected with mRFP, mRFP-ORP1L or mRFP-ORP1LΔORD (this mutant abolish RILP-HOPS and RILP–p150^{Glued} interactions) before infection with rVSV-GP-EboV (Fig 5E). A 50% reduction in rVSV-GP-EboV infectivity in cells expressing mRFP- ORP1LΔORD relative to control cells expressing either mRFP only or mRFP-tagged wild-type ORP1L was observed (Fig 5E). Collectively, our data suggest that RAB7-RILP is the late endosomal receptor for the HOPS complex and p150^{Glued} and that binding of these complexes to RILP is timed by the cholesterol sensor ORP1L to regulate endosomal maturation.

Discussion

The life of a vesicle can be described in a few general terms, including membrane transport and fusion. The small GTP-binding proteins of the Rab/Ypt family have been defined as key regulators of these processes (Stenmark, 2009). One member, RAB7 acts as the late endosome receptor for the dynein motor via its effector RILP (Jordens et al., 2001). In yeast, the RAB7 homologue Ypt7 recruits the HOPS complex to membranes to control correct interaction of late endosomes with vacuoles prior to fusion (Brocker et al., 2010). Homologues for all yeast HOPS subunits have been found in eukaryotic genomes, and two additional homologues VPS33b and SPE-39 (VPS16B/VIPAR) exist. Deletion or mutations of HOPS subunits *deep orange* (VPS18 homologue), *carnation* (VPS33a homologue) or *dvps16A* (VPS16 homologue) result in defective

► KA was calculated. Shown is KA of RAB7Q76L, RILP or RAB7Q76L-RILP binding *in vitro* to VPS18 (aa 1-580) or VPS41; all measured in the presence of GTP-γS). Shown is mean + sem. (**D**) MelJuSo cells expressing HA-RILP and GFP-VPS18 or GFP-VPS41 (as indicated) were fixed, immunolabelled with p150^{Glued} and HA-antibodies and imaged by CLSM. The zoom-in illustrates co-localization of RILP with p150^{Glued} and VPS18 or VPS41. Scale bar: 10μm, n>100. (**E**) *In vitro* binding of GST-VPS18 (aa 1-580) or GST-VPS41 immobilized on a SPR-chip to RAB7Q76L, RILP, the RAB7Q76L-RILP complex or the RAB7-RILP-C25 (the C-terminal domain of p150^{Glued}) complex (+sem). Binding was determined in the presence of GTP-γS and corrected for binding to GST only coupled to the SPR-chip. Right panel: From the SPR responses shown in Fig 4b, the KA was calculated. Shown is *in vitro* binding of the C-terminal p150^{Glued} fragment C25, the preformed complex of RAB7Q76L-RILP and RAB7Q67L-RILP-C25 to VPS18 (aa 1-580) and VPS41, all measured in the presence of GTP-γS (means + sem).

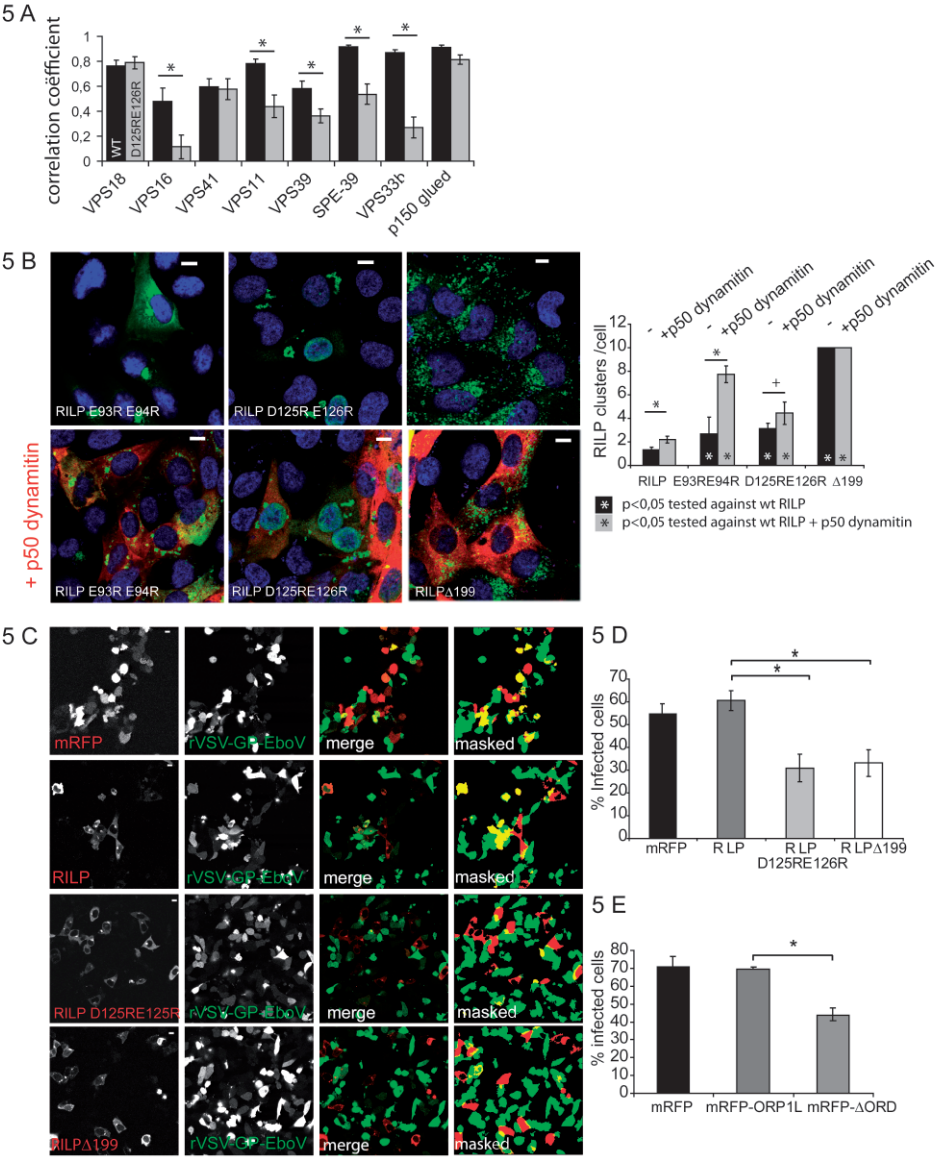


Figure 5. RILP induces late endosomal tethering. (**A**) Quantification of HOPS subunit recruitment to wtRILP and RILP D125RE125R. Mean correlation coefficients + sem are shown for indicated HOPS subunits. * indicates p<0,05. n >20 for each condition. (**B**) MelJuSo cells expressing HA-RILP, HA-RILPE93RE94R, HA-RILPD125RE126R either or not co-expressing mRFP-p50^{dynamitin} were fixed, immunolabelled with HA-antibodies (green) and DAPI (blue) and imaged by CLSM. Scale bar: 10µm, n>100. Quantification shows average number of individual clusters and/or vesicles per cell. Cells with >10 clusters were set at 10 (means + SD). * indicates p<0,05, + indicates p<0,1 (**C**) HAP-1 cells expressing mRFP, mRFP-RILP, mRFP-RILPΔ199 or mRFP-RILPD125RE126R were infected with rVSV-GP-EboV for 8 hours. The virus produces GFP in the host cytosol after successful infection which is detected and quantified. Right panel: cells were identified, masked and overlayed using Cell Profiler. Red: transfected cells, green: cells with successful infection of rVSV-GP-EboV, transfected and infected cells expressing the mRFP-labelled constructs are shown in ►

late endosomal and lysosomal biogenesis in *Drosophila melanogaster* (Pulipparacharuvil et al., 2005; Sevrioukov et al., 1999). Mutations in VPS41 can protect against α-synuclein-induced neurotoxicity in *C.elegans* and Parkinson's disease in mammalian model systems (Harrington et al., 2012; Ruan et al., 2010) and VPS41-deficient mouse embryos fail to develop beyond the gastrulation stage (Aoyama et al., 2012). In addition, the HOPS complex has been implicated in Ebola virus infection, EGFR trafficking, autophagolysosome formation and endosomal peptide loading of CD1d (Carette et al., 2011; Ganley et al., 2011; Chirivino et al., 2011; Garg et al., 2011). Mutations in the additional HOPS subunits VPS33b and SPE-39 cause complex multiorgan failures such as arthrogryposis-renal dysfunction-cholestasis (ARC) syndrome characterized by impairments in granule secretion and membrane fusion (Gissen et al., 2004; Cullinane et al., 2010). Although the HOPS complex is involved in all these processes, how the HOPS complex is regulated and recruited to late endosomal membranes in mammalian cells remains unclear.

Here we report that in mammals HOPS subunits are not recruited by RAB7 but by the RAB7 effector RILP. Using Surface Plasmon Resonance (SPR) experiments, we demonstrate that HOPS subunits (VPS18 and VPS41) exhibit low affinity for RAB7 alone, 10-15-fold higher affinity for RILP and even higher affinity for RILP associated to RAB7. In evolution, HOPS recruitment has apparently shifted from RAB7/YPT7 to its effector RILP. RILP also binds the p150^{glued} subunit of the dynein motor for minus-end directed microtubule transport (Jordens et al., 2001; Cantalupo et al., 2001). We have mapped recruitment of HOPS to the N-terminus RILP and revealed that there are multiple positions in RILP required for HOPS recruitment. These may reflect multiple non-overlapping RILP binding sites in the mammalian HOPS complex, as has been recently shown for Ytp7 and the yeast HOPS complex (Brocker et al., 2012). Mutations of RILP that abrogate HOPS complex recruitment also affect dynein motor recruitment and the C-terminus of p150^{Glued} increases the affinity of binding of Rab7-RILP in SPR studies with purified proteins. This suggests that HOPS is an integral part of the RAB7-RILP-p150^{Glued} complex (as the total has the highest affinity) and that minus-end transport and tethering for fusion are coupled processes. Such interplay between the dynein motor and HOPS complex could explain endosomal clustering near the MTOC observed upon over-expression of HOPS complex subunits (Caplan et al., 2001; Poupon et al., 2003; Pols et al., 2013). In these studies exogenous HOPS subunits were also observed on LE at steady state levels. We did not observe this, even when endogenous VPS11 was replaced by tagged-VPS11 expressed at endogenous levels (Fig. 1E), possibly indicating differences in the amount of recruitment machinery present between different cell lines. Recently, another GTPase, ARL8b, was shown to recruit HOPS subunit VPS41 to lysosomal membranes (Garg et al., 2011). Arl8 also binds the kinesin-1 linker SKIP, thereby regulating anterograde trafficking (Rosa-Ferreira and Munro, 2011). Whether these two processes are coupled, as in the case for RAB7-RILP, or

► yellow. Scale bar: 10μm. (**D**) Quantification of mRFP, mRFP-RILP, mRFP-RILPΔ199 or mRFP-RILPD125RE126R expressing cells successfully infected by rVSV-GP-EboV as measured by cytosolic GFP expression (means + sem). * p<0,05. (**E**) HAP-1 cells expressing mRFP, mRFP-ORP1L or mRFP-ORP1L ΔORD were infected with rVSV-GP-EboV for 8 hours. After successful infection, the virus produces GFP in the cytosol which is detected and quantified by flow cytometry. Shown is the quantification of the percentage of transfected (mRFP positive) and infected (GFP-positive) cells relative to transfected cells (mean + sem). * p<0,05.

mutually exclusive, remains to be established. ARL8b and RILP localise to different endosomes (our unpublished data), suggesting that they may act in different steps of endosomal trafficking as suggested before (Garg et al., 2011).

The timing of vesicle tethering has to be well coordinated in time and space to ensure for correct fusion. We observed that HOPS complex subunits under steady state conditions were predominantly localized in the cytosol. This might indicate that the association of HOPS complex with membranes is very transient and/or regulated by other factors such as phosphorylation or lipid conditions. Regulation of the HOPS complex by phosphorylation has been reported before (Ruan et al., 2010; Cabrera et al., 2010) and we have previously shown that the recruitment of the dynein motor to RAB7-RILP is regulated and timed by the late endosomal cholesterol sensor ORP1L (Rocha et al., 2009). At high cholesterol concentrations, ORP1L allows binding of the dynein motor to RAB7-RILP. ORP1L changes conformation at low cholesterol concentrations and exposes an FFAT motif to interact with the ER protein VAP-A. VAP-A removes the dynein motor from RAB7-RILP complexes and vesicles relocalize to the cell periphery. We now show that endosomal tethering via the HOPS complex is also controlled by cholesterol sensor ORP1L. ORP1L seems to act as a molecular switch, coordinating vesicle movement and tethering dependent on late endosomal content (cholesterol) (Fig 6).

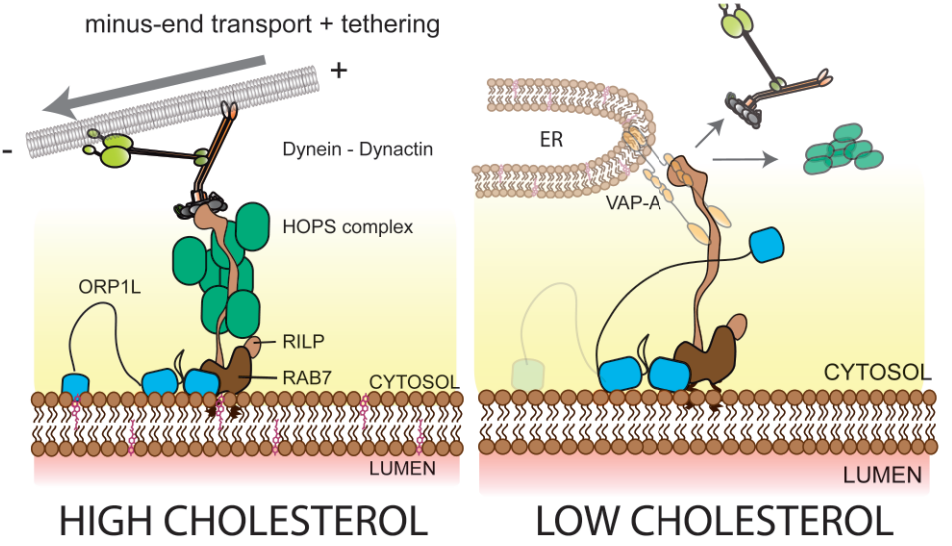


Figure 6. Model of ORP1L in control of binding of the HOPS complex and dynein-dynactin motor to RAB7-RILP. Late endosomes destined for fusion require close proximity (by minus-end transport) and tethering (by HOPS) for subsequent SNARE dependent fusion. Under high cholesterol conditions ORP1L (left panel) the dynein motor and the HOPS complex can both bind to RILP for efficient transport and fusion of lysosomes. Under low cholesterol conditions (right panel), the cholesterol binding domain of ORP1L is released from late endosomal membrane and exposes its FFAT domain for binding ER protein VAP-A. This terminates binding of the HOPS complex as well as $p150^{Glued}$ to RILP. This mechanism shows how late endosomal cholesterol controls transport and fusion mediated by the OPR1L-RAB7-RILP-dynein motor-HOPS complex.

As RILP coordinates vesicular tethering, it might modulate infectivity of pathogens entering the host via the endo-lysosomal pathway. For instance, *Salmonella* replicates in endosomes but avoids fusion with the degradative (phago)lysosome. Overexpression of RILP breaks this block and severely compromises intracellular bacterial infection (Guignot et al., 2004; Harrison et al., 2004; Marsman et al., 2004). Conversely, efficient delivery into late endosomes and lysosomes is essential for successful infection of Ebola virus by fusion and subsequent entry into the host cytosol. Here we show that RILP and ORP1L regulate fusion and infection by the Ebola virus. Various viruses including Dengue, influenza and HIV also have been reported to require late endosomal compartments for proper infectivity and propagation (van der Schaar et al., 2008; Caillet et al., 2011; Sieczkarski and Whittaker, 2003) and HIV propagation involves RILP as well (Lehmann et al., 2009; Levesque et al., 2006). Whether late endosomal transport and tethering by RILP-HOPS-dynein is indeed important for host cell infection with these viruses remains to be determined.

VPS33b and SPE-39 have previously been reported to interact with RAB11A (Cullinane et al., 2010), a RAB GTPase present on recycling endosomes. Recyling endosomes have been implicated in epithelial polarization, and defective endosomal recycling might cause the abnormalities observed in polarized kidney and liver cells of ARC syndrome patients (Cullinane et al., 2010). We show that VPS33b and SPE-39 can also be recruited by RILP and that a disease mutant of VPS33b (VPS33b L30P) that causes severe ARC phenotype fails to be recruited to RILP. Our data suggest that VPS33b and SPE-39 might also have a role later in the endosomal pathway of mammalian cells.

Many cellular transport steps rely on dynein motor activity for transport and on multi-subunit tethering complexes for initiation of fusion (Stenmark, 2009; Brocker et al., 2010) but the connection between these was unclear. We hypothesize that during evolution, organelles in higher eukaryotes may have required additional factors to recruit and time long-distance transport machineries, in addition to the tethering machinery. For late endosomes this is reflected by two additional RAB7 effectors not found in yeast; RILP and ORP1L. These additional effectors might have interfered with existing RAB7 – HOPS interactions and this, in addition with the loss of the membrane binding motif in VPS41, might have required new interactions for membrane recruitment of the HOPS complex. This problem may have been solved by involving the RAB7-effector RILP (or a shared surface of RAB7-RILP) in HOPS recruitment which, at the same time, also provides cells with an efficient way of coupling transport and tethering and allowing co-regulation by the cholesterol senor ORP1L. Whether transport and fusion processes are intricately coupled for other intracellular structures as well, remains to be determined.

Here, we have shown that the RAB7 effector RILP recruits protein complexes involved in two different but consecutive processes: the dynein-dynactin motor for minus-end transport of late endosomes and the HOPS complex for tethering for fusion of late endosomes and lysosomes. The cholesterol sensor ORP1L controls the timing of these processes, providing an additional layer of regulation (Fig 6). Coupling these processes efficiently prepares incoming maturing vesicles for subsequent tethering and fusion steps. This provides cells with an efficient way of cargo delivery, as exemplified here by Ebola glycoprotein containing viral entry into the host cytosol from late endosomal compartments.

Experimental procedures

Constructs and cloning

RAB7, RILP, ORP1L, p150^{Glued} and p50^{dynamitin} constructs have been described previously (Rocha et al., 2009; Jordens et al., 2001). GFP-VPS16 and GFP-VPS18 were gifts from Chengyu Liang (Liang et al., 2008) (Department of Molecular Microbiology and Immunology, University of Southern California, Los Angeles). Generation of other constructs is described below.

V5-VPS16 was generated by PCR using primerset1 (Supplementary information, Table 1) and inserted into the HINDIII – EcoR1 sites in pcDNA3.1. VPS18 was subcloned into the Xho1-EcoR1 sites of a 2FLAG-C1 vector. VPS33a was a gift of V. Faundez. VPS39 was a gift of J. Bonifacino (National Institutes of Health, Bethesda, MD) and was subcloned into a mRFP-C1 vector. Tag-VPS33b was generated by PCR (IMAGE CLONE 3449387) using primerset2 and was inserted into the EcoR1 sites of mGFP-C1, mCHERRY-C1 and 2MYC-C1 Image vectors. Tag-VPS41 was generated by PCR (IMAGE CLONE 4822048) using primerset3 and was inserted into the BamH1 sites of mGFP-C1, mCHERRY-C1 and 2HA-C1. VPS11 was generated by PCR (IMAGE CLONE 6144541) using primerset 4 and was inserted into the EcoR1 site of mGFP-C1 or mCherry-C1. Spe-39/C14orf133-Tag was generated by PCR (IMAGE CLONE 3920459) using primerset5 (fwd) and was inserted into the EcoR1 and BamH1 sites of mGFP-N1 or mCHERRY-N1. Spe-39-HA was generated by PCR using primerset6 and was inserted into the BamH1 and EcoR1 sites of a pcDNA3.1 vector.

Point mutants of RILP were generated by PCR using these respective primer sets

RILP E178R primerset7, RILP R159EH160E primerset8, RILP D125RE126R primerset9, RILP E93RE94R primerset 10, RILP E66R primerset11, RILP R60E primerset12, RILP E38R primerset13, RILP Y26A primerset14.

Reagents

Rabbit anti-GFP and Rabbit anti-mRFP antibodies were generated at home using purified His-mRFP or His-GFP recombinant proteins, respectively. Cross-reactivity has been excluded by Western blot analyses with various mRFP- or GFP-labeled fusion proteins. Other antibodies used were: mouse anti-CD63 (Vennegoor et al., 1985), mouse anti-γ-tubulin (Sigma) mouse anti-V5 and anti-V5-HRP (Invitrogen), anti-myc and anti-myc-HRP (Novus), anti-HA (Roche) and anti-HA-HRP (Abcam), anti-flag (M2) and anti-flag-HRP (Sigma) anti-VPS33A (C1C3) (GeneTex), anti-VPS33b (Proteintech), anti-VPS11 (Proteintech), anti-VPS41 (Proteintech), anti-VPS16 (Proteintech), anti-Dynein Intermediate Chain (Sigma, clone 70.1), anti-GAPDH (Sigma), Anti-SPE-39 was a gift of V. Faundez (Center for Translational Social Neuroscience, Emory University, Atlanta). Fluorescent and HRP-conjugated secondary antibodies were obtained from Invitrogen. GST-VPS18 (aa 1-580) and GST-VPS41 (full length) protein (produced in an *in vitro* wheat germ expression system) were purchased from Abnova. GTP-γS was purchased from Millipore.

Protein purification

His-RAB7Q76L, His-RILP and MBP-C25 were produced as previously described (Johansson et al., 2007; Rocha et al., 2009). Cells were lysed in 0.5% Triton X-100, 20mM Hepes, pH 7.5, 200mM NaCl,

8mM β-mercaptoethanol and complete EDTA-free protease inhibitor cocktail (Roche). The lysate was cleared by centrifugation and the supernatant was incubated with pre-equilibrated Talon Co^{2+} resin (Clontech Laboratories, Inc.) or MBP-beads (New England Biolabs) for 30 min. The resin was washed extensively with 20mM HEPES pH 7.5, 200mM NaCl and 8mM β-mercaptoethanol. Proteins were aliquoted and stored at −80°C until used for protein reconstitution experiments.

Surface Plasmon Resonance

Binding assays were performed using Biacore T200 (GE). A CM5 Chip was coated with goat α-GST antibodies, and subsequently GST-tagged VPS proteins were immobilized in separate flow cells whereas GST protein alone was immobilized in a reference flow cell. Increasing concentrations of the analyte proteins were sequentially injected over the Chip surface. Analysis of the data was done using Biacore T200 Evaluation Software (GE). Association constants were calculated using the equilibrium SPR response levels for each analyte concentration. Fitting of affinity constants and final figures applied Graphpad Prism (GraphPad Software, La Jolla California USA, www.graphpad.com).

Gel filtration

Transfected Meljuso cells were washed with ice-cold PBS and scraped into buffer (50mM Tris, 150mM NaCl, 5mM $MgCl_2$, pH 7.4) supplemented with complete EDTA-free Protease Inhibitor Cocktail. Cells were lysed using EMBL 8.020mm "cell cracker" homogenizer (ball sizes 8.010, 15 times) followed by a centrifugation for clearing membranes and nuclei. In experiments with recombinant proteins, untransfected MelJuso cells were used and indicated recombinant proteins were mixed with the lysate for 30 min at 4°C. All supernatants were loaded onto a Superose 6 10/300 column connected to an Åkta purifier system (GE Healthcare). The column was equilibrated with running buffer (25 mM Tris-HCl pH 7.5, 150 mM NaCl) and the flow-rate of the column was set at 0.2 - 0.3 ml/minute. Fractions (1 ml) were collected and analysed by SDS-PAGE and WB with indicated antibodies. Protein (complex) molecular weights were calculated by comparison of the respective elution volumes with protein markers with molecular weights ranging from 75 to 2,000 kDa.

Melting curves

His-RAB7 and His-RILP were co-incubated in the presence of 100μM GTP-γS and melting curves were determined using SYPRO® Orange dye in MyiQ Real time PCR detection system (Biorad).

Transfection

Expression constructs were transfected using Effectene reagents (Qiagen) according to manufacturer's instructions. For silencing, cells were transfected with Dharmafect1 (Thermo Fisher Scientific) with siRNA's (ON-TARGETplus SMARTpool) against VPS16, VPS33b, VPS33a, VPS11, Dynein Heavy Chain or control siRNA (Thermo Fisher Scientific).

Cell culture and microscopy

MelJuSo cells were cultured in Iscove's modified Dulbecco's medium (IMDM; Invitrogen) supplemented with 8% FCS in a 5% CO_2 humidified culture hood at 37°C. All specimens were analyzed by confocal laser-scanning microscopes (TCS-SP1, TCS-SP2, or AOBS; Leica) equipped

with HCX Plan-Apochromat 63× NA 1.32 and HCX Plan-Apochromat lbd.bl 63× NA 1.4 oil-corrected objective lenses (Leica). The acquisition software used was LCS (Leica). For electron microscopy a CM10 electron microscope (FEI, Eindhoven, the Netherlands) was used.

Protein immunoprecipitation

MelJuSo cells were washed with ice-cold PBS and scraped into cell lysis buffer (50mM Tris-HCl, 150mM NaCl, 5mM $MgCl_2$, 1% NP40, 10% glycerol, pH 7.4) supplemented with complete EDTA-free Protease Inhibitor Cocktail. Cell lysates were obtained by incubation on ice for 10 min followed by centrifugation for clearing. The supernatants were incubated for 2h with respective antibodies followed by capture with protein G-Sepharose 4 FF resin and washed extensively with wash-buffer (50mM Tris, 150mM NaCl, 5mM $MgCl_2$, 10% glycerol, pH 7.4). For GFP-tagged pull-down, GFP-TRAP beads were used (Chromotek).

Microscopy sample preparation

Transfected cells were fixed 24h post-transfection with ice-cold methanol (Fig 1A and 1B) or 4% formaldehyde (all other figures) in PBS for 30 min and formaldehyde-fixed samples were permeabilized for 5 min with 0.05% Triton X-100 in PBS at room temperature. Non-specific binding of antibodies was blocked by 0.5%BSA in PBS for 40 min, after which cells were incubated with primary antibodies in 0.5%BSA in PBS for 1h at room temperature. Bound primary antibodies were visualized with Alexa-Fluor secondary antibody conjugates (Invitrogen). Cells were mounted in Vectashield mounting medium (Vector Laboratories).

VPS11 rescue experiment

Haploid Hap1 cells knockout for VPS11(Carette et al., 2011) were cultured in Iscove's modified Dulbecco's medium (IMDM; Invitrogen) supplemented with 8% FCS. Cells were electroporated with GFP-VPS11 and mRFP-VPS11 or mRFP-VPS11 in combination with GFP-RILP, or GFP-RILPΔ199 and, after 24 h, fixed with 4% formaldehyde in PBS for 30 min and mounted in Vectashield mounting medium (Vector Laboratories). The slides were analyzed by confocal laser-scanning microscopes.

Immuno-EM

Cells were fixed in 2% paraformaldehyde + 0,2% glutaraldehyde in 0.1 M PHEM buffer (60 mM Pipes, 25mM Hepes, 2mM $MgCl_2$, and 10mM EGTA, pH 6.9) and then processed for ultrathin cryosectioning. 50nm-thick cryosections were cut at −120°C using diamond knives in a cryo-ultramicrotome (Leica, Vienna) and transferred with a mixture of sucrose and methylcellulose onto formvar-coated copper grids. The grids were placed on 35-mm 2% gelatin plates at 37°C. The grids were incubated with the various antibodies at room temperature and then incubated with 10nm protein A–conjugated colloidal gold (Cell microscopy Center, UMC utrecht). After immunolabeling, the sections were embedded in a mixture of methylcellulose and 0.6% uranylacetate and examined by a CM10 electron microscope (FEI, Eindhoven,the Netherlands)(Calafat et al., 1997).

Epon embedding

Cultured cells were fixed in Karnovsky fixative. To increase contrast, a post-fixation step with 1% Osmiumtetroxide in 0,1 M cacodylatebuffer was performed. After washing, the pellets were

stained *en bloc* with Ultrastain 1 (Leica, Vienna, Austria) followed by an ethanol dehydration series. Finally, the cells were embedded in a mixture of DDSA/NMA/Embed-812 (EMS, Hatfield, U.S.A), sectioned and stained with Ultrastain 1 and Ultrastain 2 (Leica, Vienna, Austria) before analysis by a CM10 electron microscope.

Ebola-VSV infection

Haploid wildtype Hap1 cells(Carette et al., 2011) were cultured in Iscove's modified Dulbecco's medium (IMDM; Invitrogen) supplemented with 8% FCS. Cells were electroporated with mRFP, mRFP-RILP or mRFP-RILP D125RE125R expression constructs. 24 hours post-transfection, the cells were exposed to rVSV-GP-EboV at MOI ~100 for 8 hours. 8 hours post-infection, cells were fixed with 4% formaldehyde and prepared for analysis by confocal microscopy or flow cytometry. 8 hours post-infection, cells were fixed with 4% formaldehyde in PBS for 30 min and mounted in Vectashield mounting medium (Vector Laboratories), as described above. The specimens were analyzed by confocal laser-scanning microscopes equipped with HCX Plan-Apochromat 63× NA 1.32 and HCX Plan-Apochromat lbd.bl 63× NA 1.4 oil-corrected objective lenses (Leica). The acquisition software used was LCS (Leica). All images were taken with identical settings. For quantification, we selected transfected (marked by mRFP) cells and determined infection by rVSV-GP-EboV (marked by GFP expressed by the virus).

In order to visualize and quantify single and double fluorescent cells in our Ebola-VSV infection experiment (masked overlays), we used CellProfiler (www.cellprofiler.org) to detect and mask cells in the red and the green channel, which were subsequently overlaid to create the masked merged images. For flow cytometry analysis, the transfection and infection protocol was identical. Cells were harvested by trypsinization and fixed with 4% formaldehyde in PBS for 30 min. Cells were analyzed on a BD LSR II flow cytometer (BD Biosciences) using FACSDiva software(BD Biosciences) using appropriate settings to detect GFP and RFP.

Statistical analysis

For calculation of correlation coefficients the signal intensity over a vector was plotted using the plot profile tool in ImageJ (http://imagej.nih.gov/ij/index.html) in both the green and red channel. Correlation coefficients for the two plots were calculated in Excel using the function.

For Figure 3B statistics were performed in GraphPad Prism using one-way ANOVA followed by Bonferroni's post-hoc comparisons tests. All other statistics were performed in Microsoft Excel using a two sided Student's t-test.

Acknowledgements

We thank C. Liang, J. Bonifacino, V. Faundez, S. Zlatic and J. Hoogenraad for providing reagents and our colleagues at the 2012 Gordon Conference on Lysosomes for discussions, M. Garstka for primer design, R.Spaapen for FACS and statistical analyses, N.Ong for processing electron micrographs, P. Celie and M. Stadnik-Spiewak for protein production and gel filtration and I.Zondervan, W.Wong, A.Jaramillo and R. Ligthart for helping with experiments and I.Berlin for reading the manuscript. This work is supported by an ERC Advanced Grant and a TOP grant of NWO-CW.

Author contributions

R.vd.K designed and performed experiments, analysed data and wrote the paper; A.F. performed SPR-experiments, L.J, S.K and N.N assisted experiments, H.J. performed electron microscopy, T.B. and J.C. performed Ebola-VSV experiments, N.R. designed and performed experiments, J.N. designed experiments and wrote the paper.

Reference List

1. Aoyama,M., Sun-Wada,G.H., Yamamoto,A., Yamamoto,M., Hamada,H., and Wada,Y. (2012). Spatial restriction of bone morphogenetic protein signaling in mouse gastrula through the mVam2-dependent endocytic pathway. Dev. Cell *22*, 1163-1175.
2. Basuray,S., Mukherjee,S., Romero,E.G., Seaman,M.N., and Wandinger-Ness,A. (2013). Rab7 mutants associated with charcot-marie-tooth disease cause delayed growth factor receptor transport and altered endosomal and nuclear signaling. J. Biol. Chem. *288*, 1135-1149.
3. Brocker,C., Engelbrecht-Vandre,S., and Ungermann,C. (2010). Multisubunit tethering complexes and their role in membrane fusion. Curr. Biol. *20*, R943-R952.
4. Brocker,C., Kuhlee,A., Gatsogiannis,C., Kleine Balderhaar,H.J., Honscher,C., Engelbrecht-Vandre,S., Ungermann,C., and Raunser,S. (2012). Molecular architecture of the multisubunit homotypic fusion and vacuole protein sorting (HOPS) tethering complex. Proc. Natl. Acad. Sci. U S A.
5. Cabrera,M., Langemeyer,L., Mari,M., Rethmeier,R., Orban,I., Perz,A., Brocker,C., Griffith,J., Klose,D., Steinhoff,H.J., Reggiori,F., Engelbrecht-Vandre,S., and Ungermann,C. (2010). Phosphorylation of a membrane curvature-sensing motif switches function of the HOPS subunit Vps41 in membrane tethering. J. Cell Biol. *191*, 845-859.
6. Cabrera,M., Ostrowicz,C.W., Mari,M., LaGrassa,T.J., Reggiori,F., and Ungermann,C. (2009). Vps41 phosphorylation and the Rab Ypt7 control the targeting of the HOPS complex to endosome-vacuole fusion sites. Mol. Biol. Cell *20*, 1937-1948.
7. Caillet,M., Janvier,K., Pelchen-Matthews,A., Delcroix-Genete,D., Camus,G., Marsh,M., and Berlioz-Torrent,C. (2011). Rab7A is required for efficient production of infectious HIV-1. PLoS Pathog. *7*, e1002347.
8. Calafat,J., Janssen,H., Knol,E.F., Weller,P.F., and Egesten,A. (1997). Ultrastructural localization of Charcot-Leyden crystal protein in human eosinophils and basophils. Eur. J. Haematol. *58*, 56-66.
9. Cantalupo,G., Alifano,P., Roberti,V., Bruni,C.B., and Bucci,C. (2001). Rab-interacting lysosomal protein (RILP): the Rab7 effector required for transport to lysosomes. EMBO J. *20*, 683-693.
10. Caplan,S., Hartnell,L.M., Aguilar,R.C., Naslavsky,N., and Bonifacino,J.S. (2001). Human Vam6p promotes lysosome clustering and fusion in vivo. J. Cell Biol. *154*, 109-122.
11. Carette,J.E., Raaben,M., Wong,A.C., Herbert,A.S , Obernosterer,G., Mulherkar,N., Kuehne,A.I , Kranzusch,P.J., Griffin,A.M., Ruthel,G., Dal Cin,P., Dye,J.M., Whelan,S.P., Chandran,K., and Brummelkamp,T.R. (2011). Ebola virus entry requires the cholesterol transporter Niemann-Pick C1. Nature *477*, 340-343.
12. Chirivino,D., Del Maestro,L., Formstecher,E., Hupe,P., Raposo,G., Louvard,D., and Arpin,M. (2011). The ERM proteins interact with the HOPS complex to regulate the maturation of endosomes. Mol. Biol. Cell *22*, 375-385.
13. Christoforidis,S., McBride,H.M., Burgoyne,R.D., and Zerial,M. (1999). The Rab5 effector EEA1 is a core component of endosome docking. Nature *397*, 621-625.
14. Cullinane,A.R., Straatman-Iwanowska,A., Zaucker,A., Wakabayashi,Y., Bruce,C.K., Luo,G., Rahman,F., Gurakan,F., Utine,E., Ozkan,T.B., Denecke,J., Vukovic,J., Di Rocco,M., Mandel,H., Cangul,H., Matthews,R.P., Thomas,S.G., Rappoport,J.Z., Arias,I.M., Wolburg,H., Knisely,A.S., Kelly,D.A., Muller,F., Maher,E.R., and Gissen,P. (2010). Mutations in VIPAR cause an arthrogryposis, renal dysfunction and cholestasis syndrome phenotype with defects in epithelial polarization. Nat. Genet. *42*, 303-312.
15. Daniele,T., Hackmann,Y., Ritter,A.T., Wenham,M , Booth,S., Bossi,G., Schintler,M., Auer-Grumbach,M., and Griffiths,G.M. (2011). A role for Rab7 in the movement of secretory granules in cytotoxic T lymphocytes. Traffic *12*, 902-911.
16. Ganley,I.G., Wong,P.M., Gammoh,N., and Jiang,X. (2011). Distinct autophagosomal-

lysosomal fusion mechanism revealed by thapsigargin-induced autophagy arrest. Mol. Cell *42*, 731-743.

17. Garg,S., Sharma,M., Ung,C., Tuli,A., Barral,D.C., Hava,D.L., Veerapen,N., Besra,G.S., Hacohen,N., and Brenner,M.B. (2011). Lysosomal trafficking, antigen presentation, and microbial killing are controlled by the Arf-like GTPase Arl8b. Immunity *35*, 182-193.
18. Gissen,P., Johnson,C.A., Gentle,D., Hurst,L.D., Doherty,A.J., O'Kane,C.J., Kelly,D.A., and Maher,E.R. (2005). Comparative evolutionary analysis of VPS33 homologues: genetic and functional insights. Hum. Mol. Genet. *14*, 1261-1270.
19. Gissen,P., Johnson,C.A., Morgan,N.V., Stapelbroek,J.M., Forshew,T., Cooper,W.N., McKiernan,P.J., Klomp,L.W., Morris,A.A., Wraith,J.E., McClean,P., Lynch,S.A., Thompson,R.J., Lo,B., Quarrell,O.W., Di Rocco,M., Trembath,R.C., Mandel,H., Wali,S., Karet,F.E., Knisely,A.S., Houwen,R.H., Kelly,D.A., and Maher,E.R. (2004). Mutations in VPS33B, encoding a regulator of SNARE-dependent membrane fusion, cause arthrogryposis-renal dysfunction-cholestasis (ARC) syndrome. Nat. Genet. *36*, 400-404.
20. Guignot,J., Caron,E., Beuzon,C., Bucci,C., Kagan,J., Roy,C., and Holden,D.W. (2004). Microtubule motors control membrane dynamics of Salmonella-containing vacuoles. J. Cell Sci. *117*, 1033-1045.
21. Harrington,A.J., Yacoubian,T.A., Slone,S.R., Caldwell,K.A., and Caldwell,G.A. (2012). Functional Analysis of VPS41-Mediated Neuroprotection in Caenorhabditis elegans and Mammalian Models of Parkinson's Disease. J. Neurosci. *32*, 2142-2153.
22. Harrison,R.E., Brumell,J.H., Khandani,A., Bucci,C., Scott,C.C., Jiang,X., Finlay,B.B., and Grinstein,S. (2004). Salmonella impairs RILP recruitment to Rab7 during maturation of invasion vacuoles. Mol. Biol. Cell *15*, 3146-3154.
23. Hoepfner,S., Severin,F., Cabezas,A., Habermann,B., Runge,A., Gillooly,D., Stenmark,H., and Zerial,M. (2005). Modulation of receptor recycling and degradation by the endosomal kinesin KIF16B. Cell *121*, 437-450.
24. Huizing,M., Didier,A., Walenta,J., Anikster,Y., Gahl,W.A., and Kramer,H. (2001). Molecular cloning and characterization of human VPS18, VPS 11, VPS16, and VPS33. Gene *264*, 241-247.
25. Johansson,M., Rocha,N., Zwart,W., Jordens,I., Janssen,L., Kuijl,C., Olkkonen,V.M., and Neefjes,J. (2007). Activation of endosomal dynein motors by stepwise assembly of Rab7-RILP-p150Glued, ORP1L, and the receptor betalll spectrin. J. Cell Biol. *176*, 459-471.
26. Jordens,I., Fernandez-Borja,M., Marsman,M , Dusseljee,S., Janssen,L., Calafat,J., Janssen,H , Wubbolts,R., and Neefjes,J. (2001). The Rab7 effector protein RILP controls lysosomal transport by inducing the recruitment of dynein-dynactin motors. Curr. Biol. *11*, 1680-1685.
27. Jordens,I., Westbroek,W., Marsman,M., Rocha,N., Mommaas,M., Huizing,M., Lambert,J , Naeyaert,J.M., and Neefjes,J. (2006). Rab7 and Rab27a control two motor protein activities involved in melanosomal transport. Pigment Cell Res. *19*, 412-423.
28. Kuijl,C., Savage,N.D., Marsman,M., Tuin,A.W., Janssen,L., Egan,D.A., Ketema,M., van den Nieuwendijk,R., van den Eeden,S.J., Geluk,A., Poot,A., van der Marel,G., Beijersbergen,R.L., Overkleeft,H., Ottenhoff,T.H., and Neefjes,J. (2007). Intracellular bacterial growth is controlled by a kinase network around PKB/AKT1. Nature *450*, 725-730.
29. Lehmann,M., Milev,M.P., Abrahamyan,L., Yao,X.J , Pante,N., and Mouland,A.J. (2009). Intracellular transport of human immunodeficiency virus type 1 genomic RNA and viral production are dependent on dynein motor function and late endosome positioning. J. Biol. Chem. *284*, 14572-14585.
30. Levesque,K., Halvorsen,M., Abrahamyan,L., Chatel-Chaix,L., Poupon,V., Gordon,H., DesGroseillers,L., Gatignol,A., and Mouland,A.J. (2006). Trafficking of HIV-1 RNA is mediated by heterogeneous nuclear ribonucleoprotein A2 expression and impacts on viral assembly. Traffic *7*, 1177-1193.
31. Liang,C., Lee,J.S., Inn,K.S., Gack,M.U., Li,Q., Roberts,E.A., Vergne,I., Deretic,V., Feng,P., Akazawa,C., and Jung,J.U. (2008). Beclin1-binding UVRAG targets the class C Vps complex to coordinate autophagosome maturation and endocytic trafficking. Nat. Cell Biol. *10*, 776-787.
32. Marsman,M., Jordens,I., Kuijl,C., Janssen,L., and Neefjes,J. (2004). Dynein-mediated vesicle transport controls intracellular Salmonella replication. Mol. Biol. Cell *15*, 2954-2964.
33. Ostrowicz,C.W., Brocker,C., Ahnert,F., Nordmann,M., Lachmann,J., Peplowska,K., Perz,A., Auffarth,K., Engelbrecht-Vandre,S., and Ungermann,C. (2010). Defined subunit arrangement and rab interactions are required for functionality of the HOPS tethering complex. Traffic *11*, 1334-1346.
34. Paul,P., van den Hoorn,T., Jongsma,M.L., Bakker,M.J., Hengeveld,R., Janssen,L., Cresswell,P., Egan,D.A., van Ham,M., Ten Brinke,A., Ovaa,H., Beijersbergen,R.L.,

Kuijl,C., and Neefjes,J. (2011). A Genome-wide multidimensional RNAi screen reveals pathways controlling MHC class II antigen presentation. Cell *145*, 268-283.

35. Pols,M.S., ten Brink,C., Gosavi,P., Oorschot,V., and Klumperman,J. (2013). The HOPS proteins hVps41 and hVps39 are required for homotypic and heterotypic late endosome fusion. Traffic *14*, 219-232.
36. Poupon,V., Stewart,A., Gray,S.R., Piper,R.C., and Luzio,J.P. (2003). The role of mVps18p in clustering, fusion, and intracellular localization of late endocytic organelles. Mol. Biol. Cell *14*, 4015-4027.
37. Pulipparacharuvil,S., Akbar,M.A., Ray,S., Sevrioukov,E.A., Haberman,A.S., Rohrer,J., and Kramer,H. (2005). Drosophila Vps16A is required for trafficking to lysosomes and biogenesis of pigment granules. J. Cell Sci. *118*, 3663-3673.
38. Raaijmakers,J.A., van Heesbeen,R.G., Meaders,J.L., Geers,E.F., Fernandez-Garcia,B., Medema,R.H., and Tanenbaum,M.E. (2012). Nuclear envelope-associated dynein drives prophase centrosome separation and enables Eg5-independent bipolar spindle formation. EMBO J. *31*, 4179-4190.
39. Rocha,N., Kuijl,C., van der Kant,R., Janssen,L., Houben,D., Janssen,H., Zwart,W., and Neefjes,J. (2009). Cholesterol sensor ORP1L contacts the ER protein VAP to control Rab7-RILP-p150 Glued and late endosome positioning. J. Cell Biol. *185*, 1209-1225.
40. Rosa-Ferreira,C. and Munro,S. (2011). Arl8 and SKIP act together to link lysosomes to kinesin-1. Dev. Cell *21*, 1171-1178.
41. Ruan,Q., Harrington,A.J., Caldwell,K.A., Caldwell,G.A., and Standaert,D.G. (2010). VPS41, a protein involved in lysosomal trafficking, is protective in Caenorhabditis elegans and mammalian cellular models of Parkinson's disease. Neurobiol. Dis. *37*, 330-338.
42. Sevrioukov,E.A., He,J.P., Moghrabi,N., Sunio,A., and Kramer,H. (1999). A role for the deep orange and carnation eye color genes in lysosomal delivery in Drosophila. Mol. Cell *4*, 479-486.
43. Sieczkarski,S.B. and Whittaker,G.R. (2003). Differential requirements of Rab5 and Rab7 for endocytosis of influenza and other enveloped viruses. Traffic *4*, 333-343.
44. Sobo,K., Le Blanc,I., Luyet,P.P., Fivaz,M., Ferguson,C., Parton,R.G., Gruenberg,J., and van der Goot,F.G. (2007). Late endosomal cholesterol accumulation leads to impaired intra-endosomal trafficking. PLoS One *2*, e851.
45. Spinosa,M.R., Progida,C., De Luca,A., Colucci,A.M., Alifano,P., and Bucci,C. (2008). Functional characterization of Rab7 mutant proteins associated with Charcot-Marie-Tooth type 2B disease. J. Neurosci. *28*, 1640-1648.
46. Stenmark,H. (2009). Rab GTPases as coordinators of vesicle traffic. Nat. Rev. Mol. Cell Biol. *10*, 513-525.
47. Uusi-Rauva,K., Kyttala,A., van der Kant,R., Vesa,J , Tanhuanpaa,K., Neefjes,J., Olkkonen,V.M., and Jalanko,A. (2012). Neuronal ceroid lipofuscinosis protein CLN3 interacts with motor proteins and modifies location of late endosomal compartments. Cell Mol. Life Sci. *69*, 2075-2089.
48. Vallee,R.B., McKenney,R.J., and Ori-McKenney,K.M. (2012). Multiple modes of cytoplasmic dynein regulation. Nat. Cell Biol. *14*, 224-230.
49. van der Schaar,H.M., Rust,M.J., Chen,C., Ende-Metselaar,H., Wilschut,J., Zhuang,X., and Smit,J.M. (2008). Dissecting the cell entry pathway of dengue virus by single-particle tracking in living cells. PLoS Pathog. *4*, e1000244.
50. Vennegoor,C., Calafat,J., Hageman,P., van Buitenen,F., Janssen,H., Kolk,A., and Rumke,P. (1985). Biochemical characterization and cellular localization of a formalin-resistant melanoma-associated antigen reacting with monoclonal antibody NKI/C-3. Int J. Cancer *35*, 287-295.
51. Vihervaara,T., Uronen,R.L., Wohlfahrt,G., Bjorkhem,I., Ikonen,E., and Olkkonen,V.M. (2011). Sterol binding by OSBP-related protein 1L regulates late endosome motility and function. Cell Mol. Life Sci. *68*, 537-551.
52. Wickner,W. (2010). Membrane fusion: five lipids, four SNAREs, three chaperones, two nucleotides, and a Rab, all dancing in a ring on yeast vacuoles. Annu. Rev. Cell Dev. Biol. *26*, 115-136.
53. Wong,A.C., Sandesara,R.G., Mulherkar,N., Whelan,S.P., and Chandran,K. (2010). A forward genetic strategy reveals destabilizing mutations in the Ebolavirus glycoprotein that alter its protease dependence during cell entry. J. Virol. *84*, 163-175.
54. Wu,X., Wang,F., Rao,K., Sellers,J.R., and Hammer,J.A., III (2002). Rab27a is an essential component of melanosome receptor for myosin Va. Mol. Biol. Cell *13*, 1735-1749.
55. Zhu,G.D., Salazar,G., Zlatic,S.A., Fiza,B., Doucette,M.M., Heilman,C.J., Levey,A.I., Faundez,V., and L'hernault,S.W. (2009). SPE-39 family proteins interact with the HOPS complex and function in lysosomal delivery. Mol. Biol. Cell *20*, 1223-1240.

Supplementary material

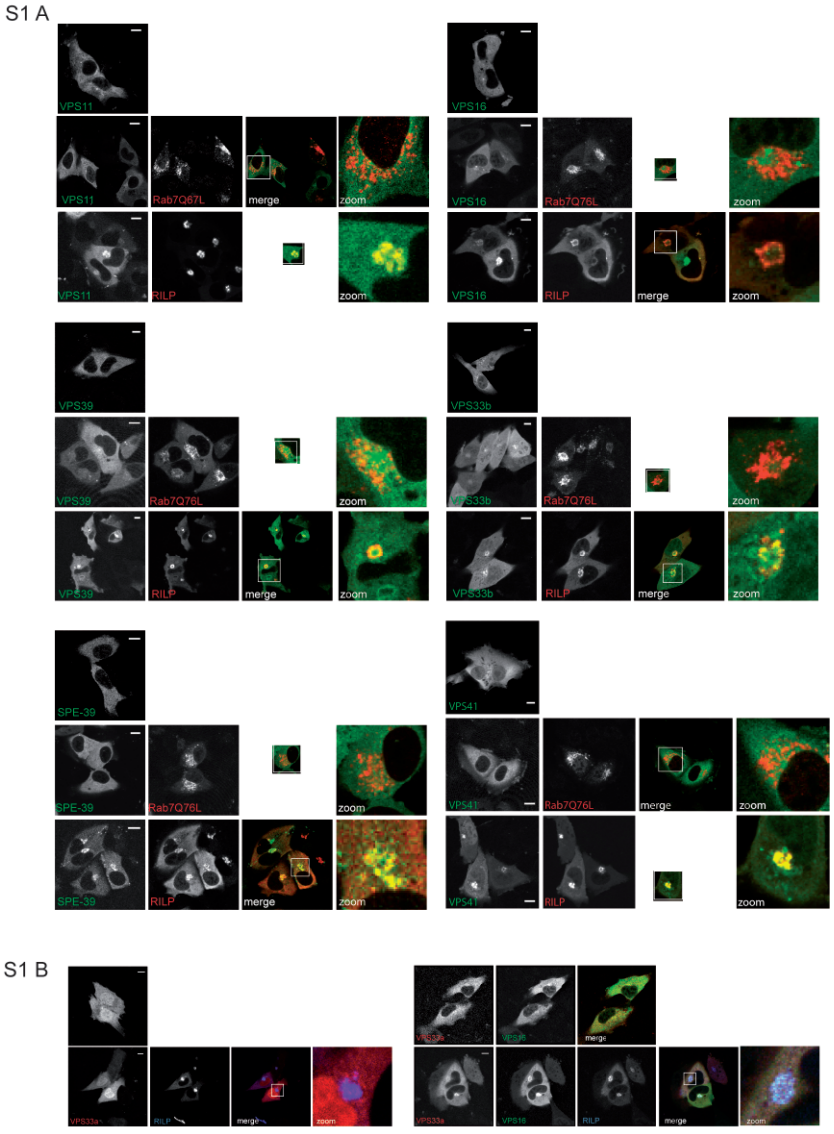
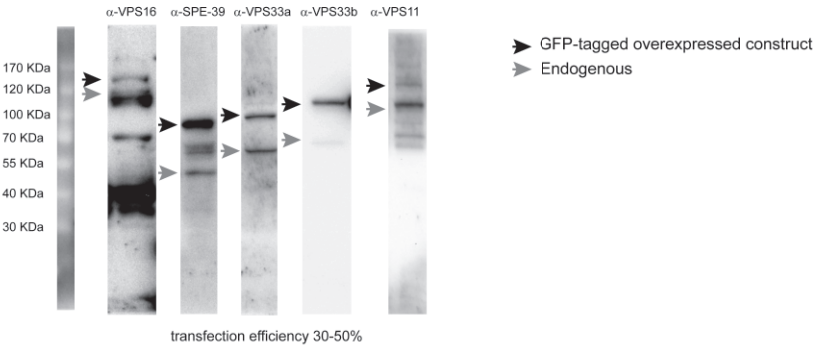


Figure S1. RILP recruits VPS11, VPS41, VPS39, VPS16, VPS33b and SPE-39 to late endosomes. (**A**) Localization and membrane recruitment of HOPS complex subunits. MelJuSo cells expressing the GFP constructs indicated in combination with myc-RAB7Q67L or HA-RILP (as indicated) were fixed, immunolabelled with myc- or HA-antibodies and imaged by confocal fluorescence microscopy. Zoom-in indicated. Scale bar: 10µm. n>100 (**B**) Localization and endosomal membrane recruitment of VPS33a. MelJuSo cells expressing mRFP-VPS33a in the presence or absence of HA-RILP, GFP-VPS16 or combinations (as indicated) were fixed, immunolabelled with myc- or HA-antibodies and imaged by confocal fluorescence microscopy. Box indicate zoom-in area. Scale bar: 10µm. n>100.

S1 C



S1 D

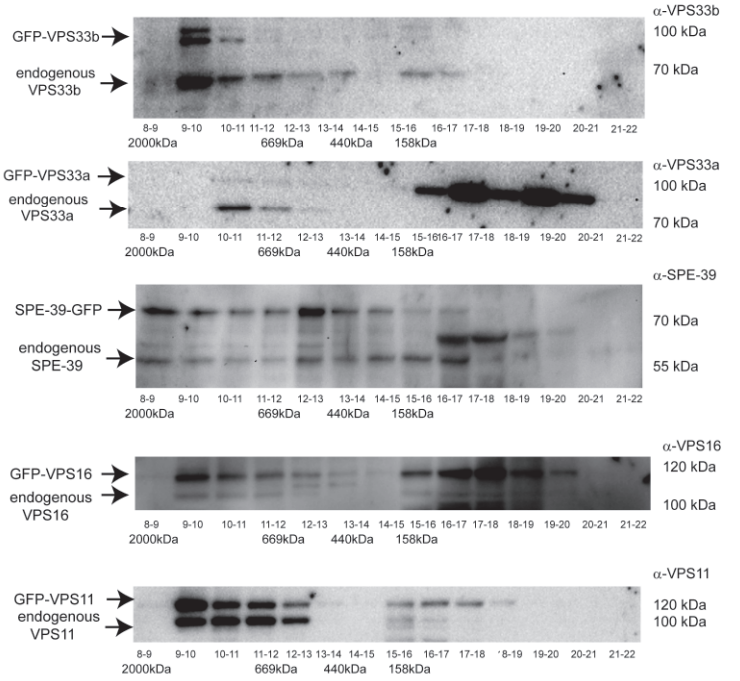


Figure S1. Continued. (**C**) Relative expression levels of GFP-tagged VPS proteins compared to their endogenous levels. MelJuSo cells were transfected with the constructs indicated and proteins were separated by SDS-PAGE and WB with antibodies indicated. Dark arrow shows position of GFP-tagged constructs, gray arrow the position of endogenous protein. Position of marker proteins indicated. (**D**) Tagged VPS proteins are incorporated into high molecular weight complexes. Lysates of MelJuSo cells expressing GFP-tagged VPS16, VPS11, VPS33b, VPS33a or SPE-39 were size separated by gel filtration. The elution of control proteins (and their mass) is indicated. Fractions of different sizes were separated by SDS-PAGE and WB and probed with antibodies indicated to detect complexes containing the GFP-tagged overexpressed proteins and their endogenous counterparts. For GFP-VPS33a only a very small fraction of total overexpressed protein was incorporated into higher molecular weight complexes, while other GFP tagged-HOPS subunits migrated similar as their untagged endogenous counterparts. MelJuSo cells expressing individual tagged-HOPS subunits (SPE39, VPS11, VPS18, VPS39, VPS41, VPS16, VPS33b) and HA-RILP were co-transfected with

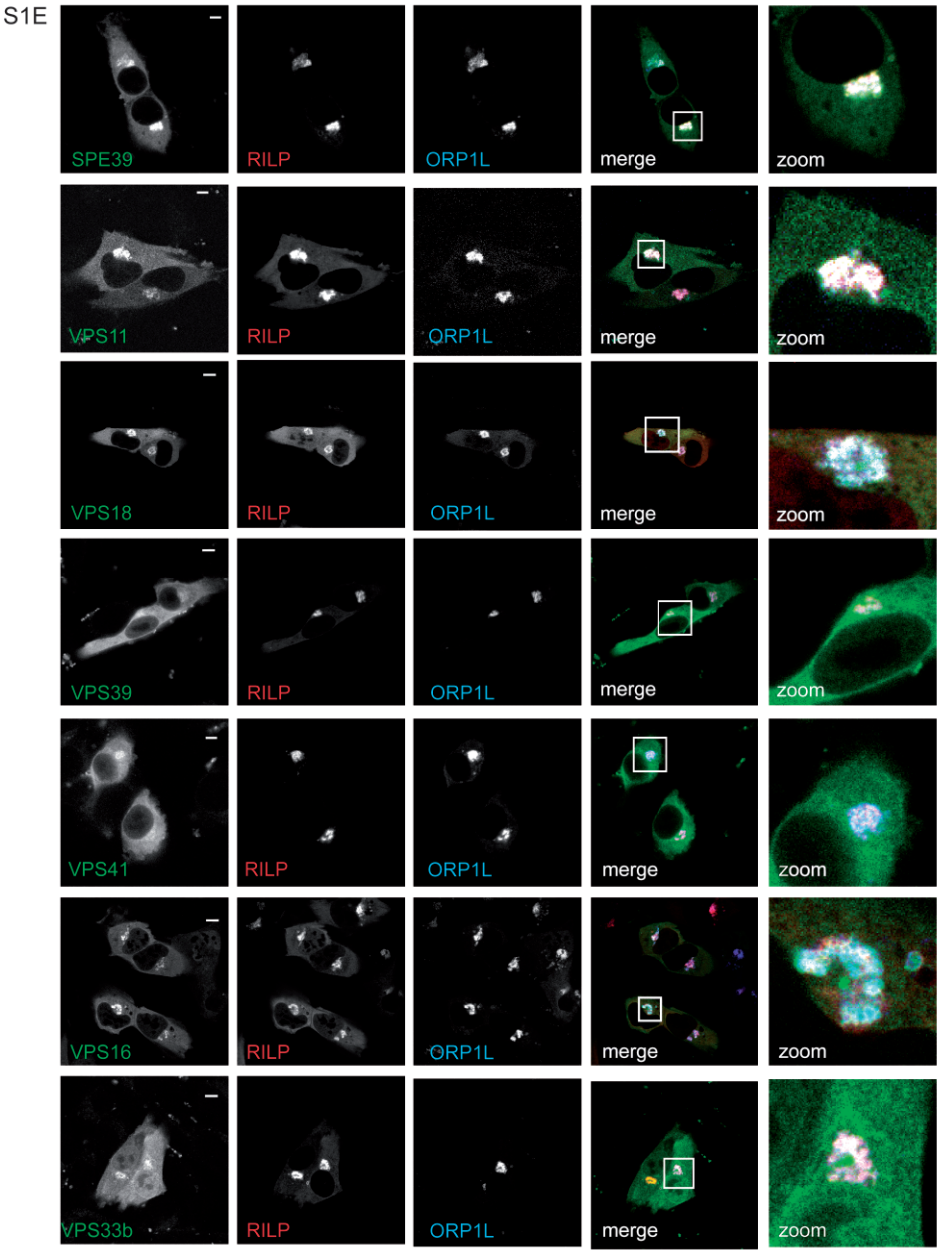


Figure S1. Continued. (E) mRFP-ORP1L

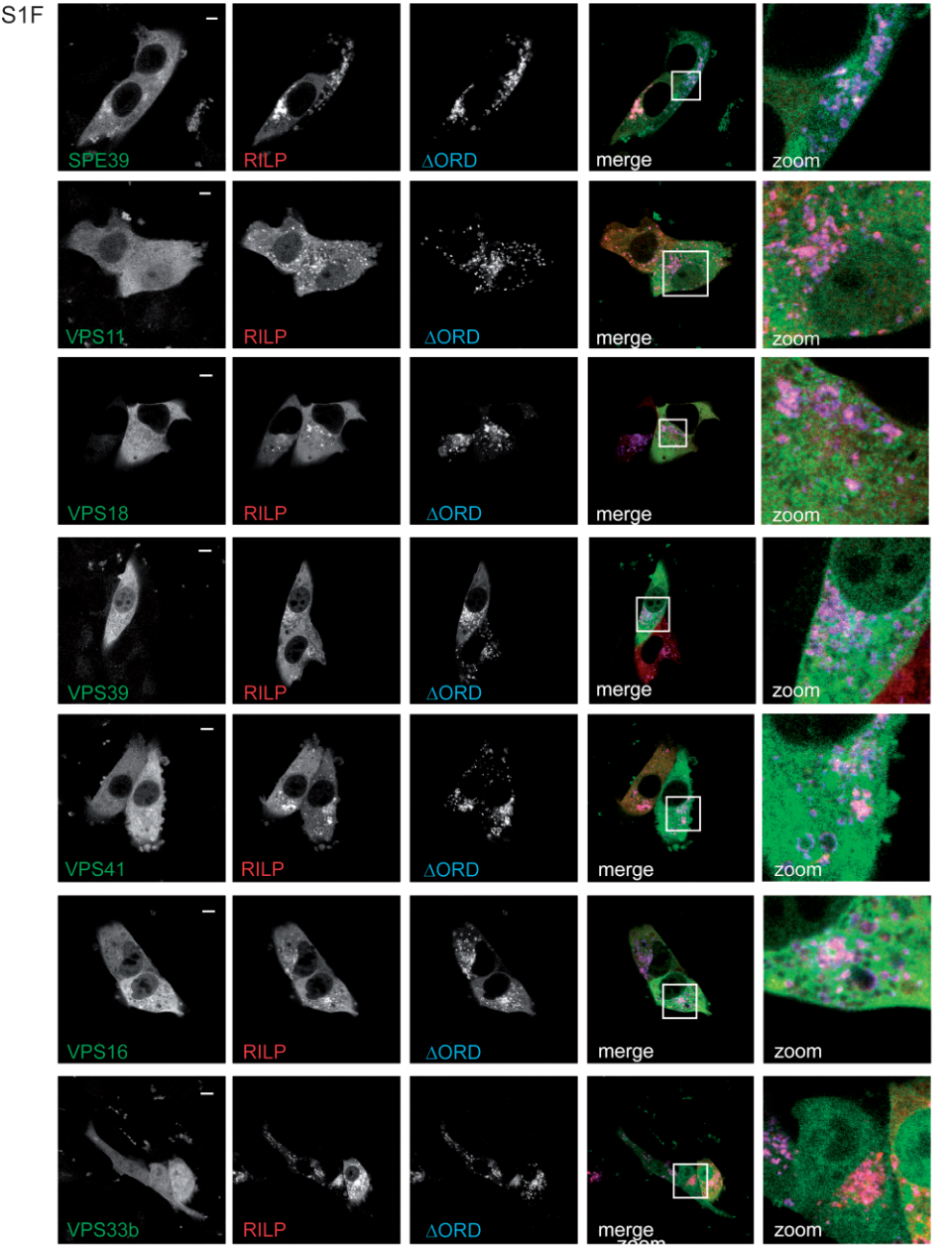


Figure S1. Continued. (F) mRFP-ORP1LΔORD

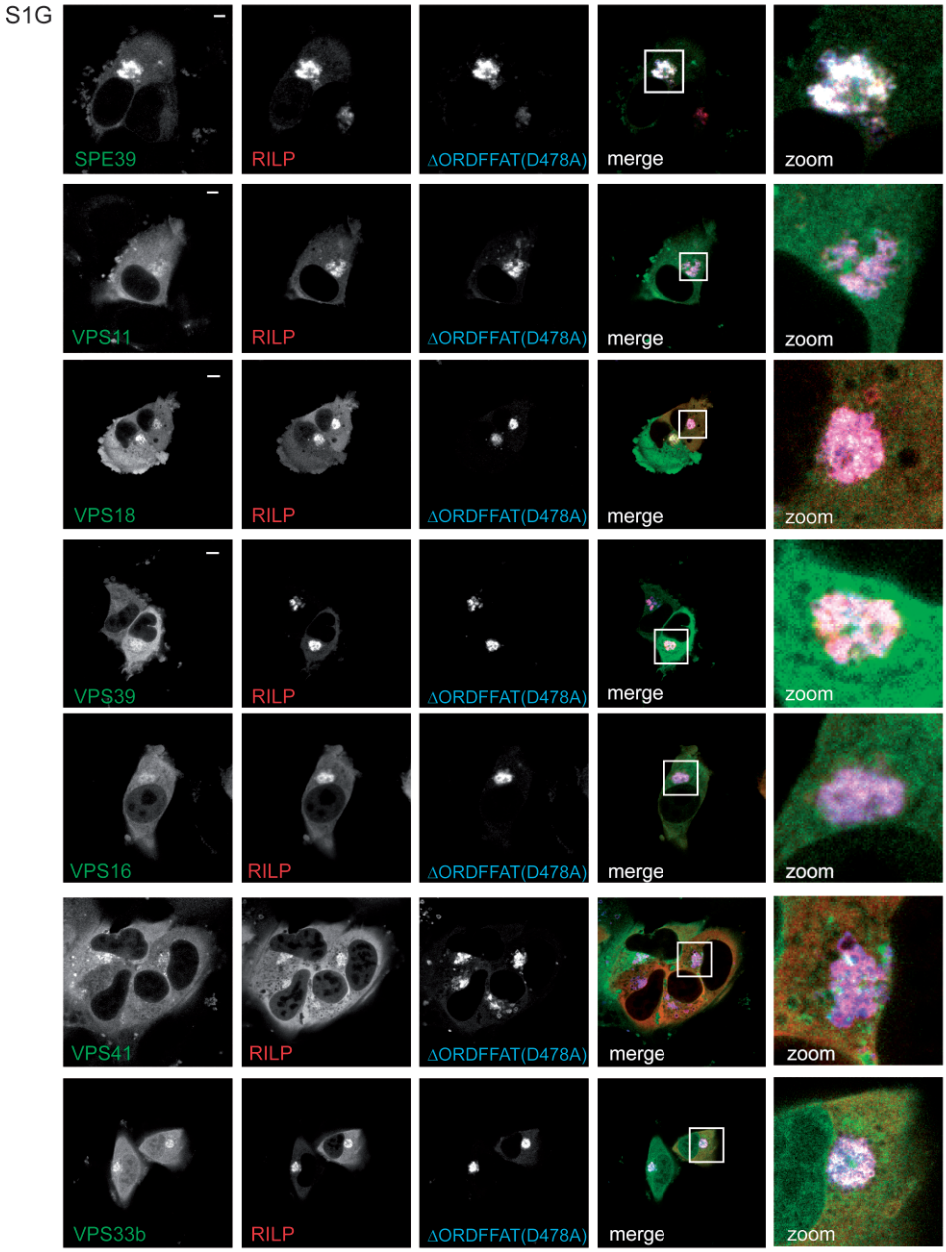


Figure S1. Continued. (**G**) mRFP-ORP1LΔORDFFAT(D478A). Cells were fixed and immunolabeled with HA-antibodies before imaging by confocal fluorescence microscopy. Boxed area shows the zoom-in. Scale bar: 10μm. Representative images for n>100.

S2 A

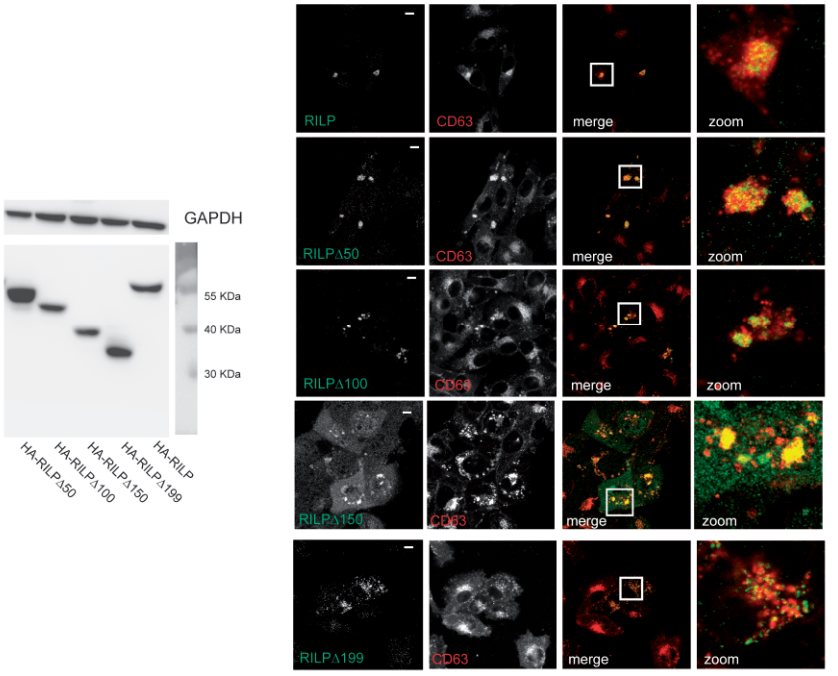


Figure S2. Binding of HOPS complex subunits to RILP. (**A**) Expression and localization of RILP truncation mutants. Left panel: HA-tagged RILP truncation mutants were expressed in MelJuSo cells. Lysates were separated by SDS-PAGE and WB and detected by anti-HA antibody. Expression of GAPDH is shown as a loading control. Marker proteins indicated. Right panel: MelJuSo cells expressing HA-tagged RILP truncation mutants were fixed, immuno-labeled with anti-HA and anti-CD63 antibodies and imaged by confocal microscopy. Box shows the zoomed-in area. Scale bar: 10µm. n>100

S2 B

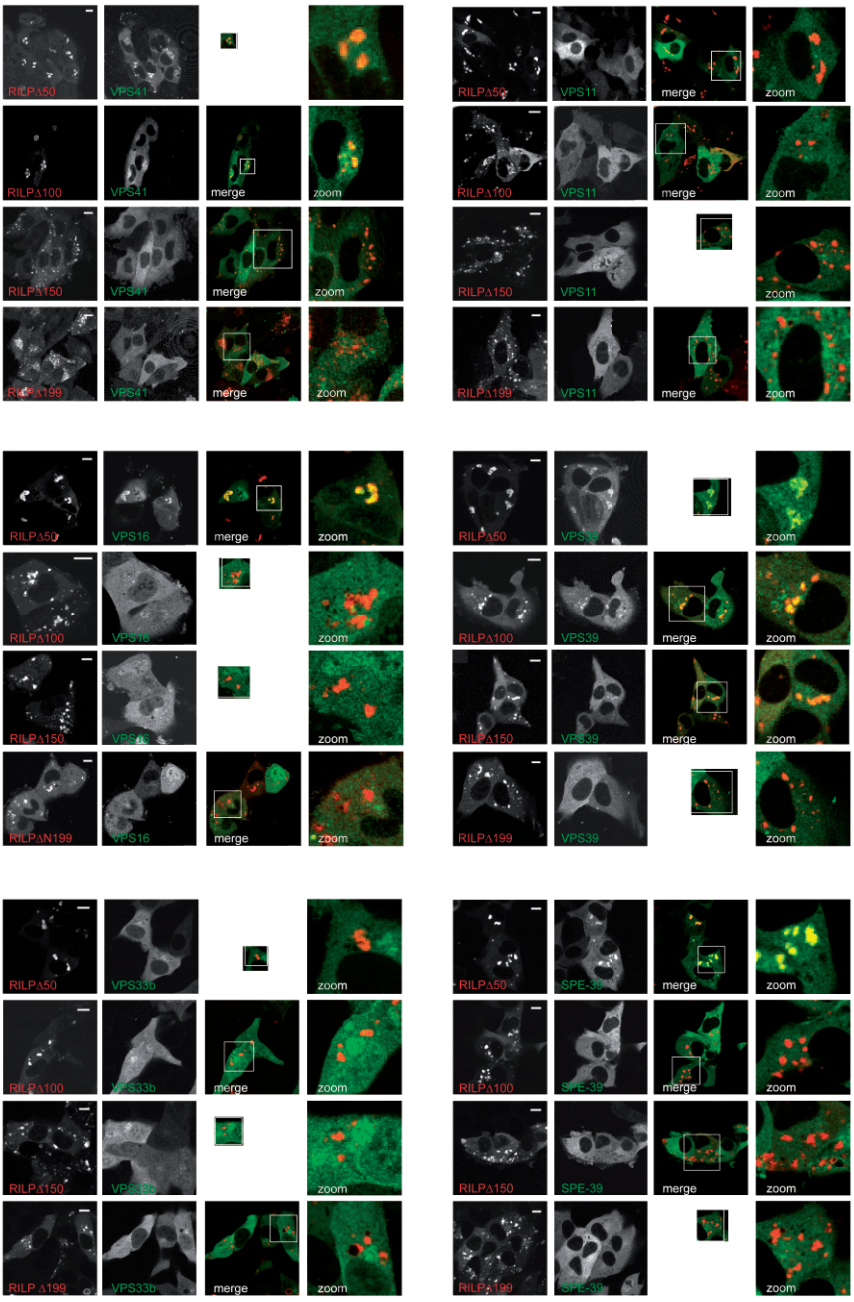
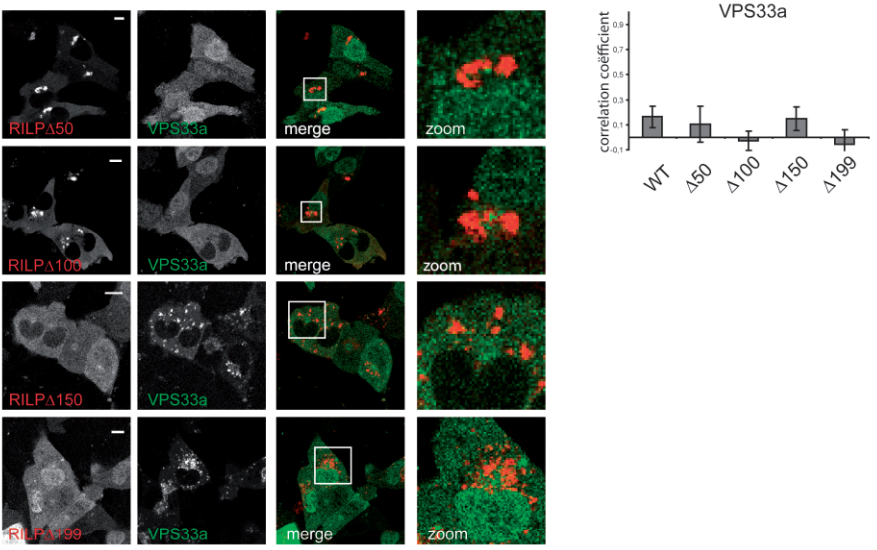


Figure S2. Continued. (**B**) Recruitment of VPS11, VPS39, VPS16, VPS33b and SPE-39 to N-terminal truncation mutants of RILP. MelJuSo cells expressing GFP-labelled HOPS subunits as indicated and HA-tagged truncation mutants of RILP (Δ50, Δ100, Δ150 and Δ199 respectively) were fixed, immunolabelled with HA-antibodies and imaged by confocal fluorescence microscopy. Box shows zoomed-in area. Scale bar: 10µm. n>100.

S2 C



S2 D

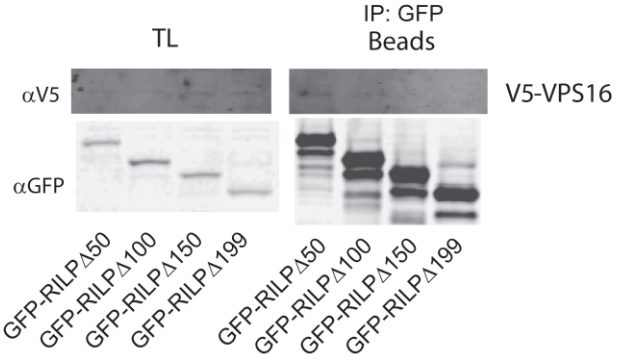


Figure S2. Continued. (**C**) MelJuSo cells expressing GFP-VPS33a and HA-tagged truncation mutants of RILP (Δ50, Δ100, Δ150 and Δ199 respectively) were fixed, immunolabelled with HA-antibodies and imaged by confocal fluorescence microscopy. Box shows zoomed-in area. Scale bar: 10μm. n>100. Right panel: Quantification of VPS33a recruited to RILP mutants. Mean correlation coefficients + sem are shown. n >10 for each condition. (**D**) Interaction of RILP truncation mutants with V5-VPS16. Lysates of Meljuso expressing V5-tagged VPS16 and GFP-RILP truncation mutants were immunoprecipitated (IP) with anti-GFP, then probed by anti-V5 and anti-GFP. TL: total lysate; IP: immunoprecipation.

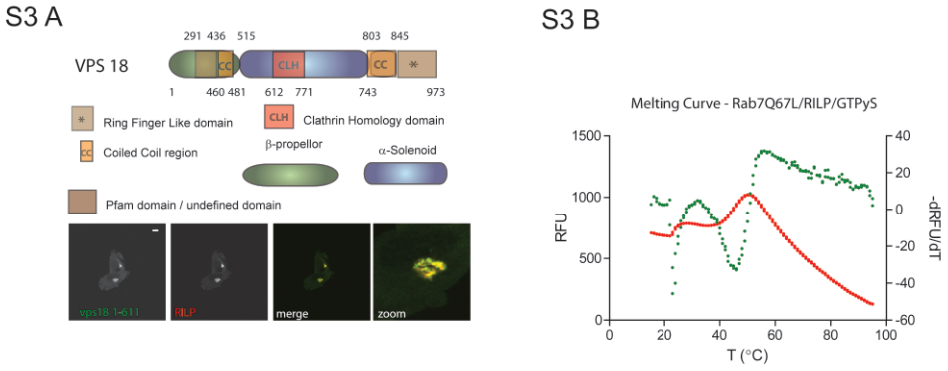


Figure S3. Proteins used in SPR-experiments. (**A**) The N-terminus of VPS18 is sufficient for RILP recruitment. Upper panel: schematical map of VPS18 domains. Lower panel: MelJuSo cells expressing GFP-VPS18 [1-611] and RILP-HA were fixed, stained with anti-HA antibodies and imaged by confocal microscopy. The N-terminus of VPS18, as used for SPR experiments is recruited to RILP positive endosomes. Bar: 10 μm (**B**) The Rab7Q67L/RILP complex is a stable complex. A Rab7Q67L complex with RILP was generated in the presence of GTP-γS and the temperature stability of the complex was measured. Red line is the melting curve in relative fluorescence units (RFU). The green line is first derivative of melting curve that shows Tm of 55°C (peak).

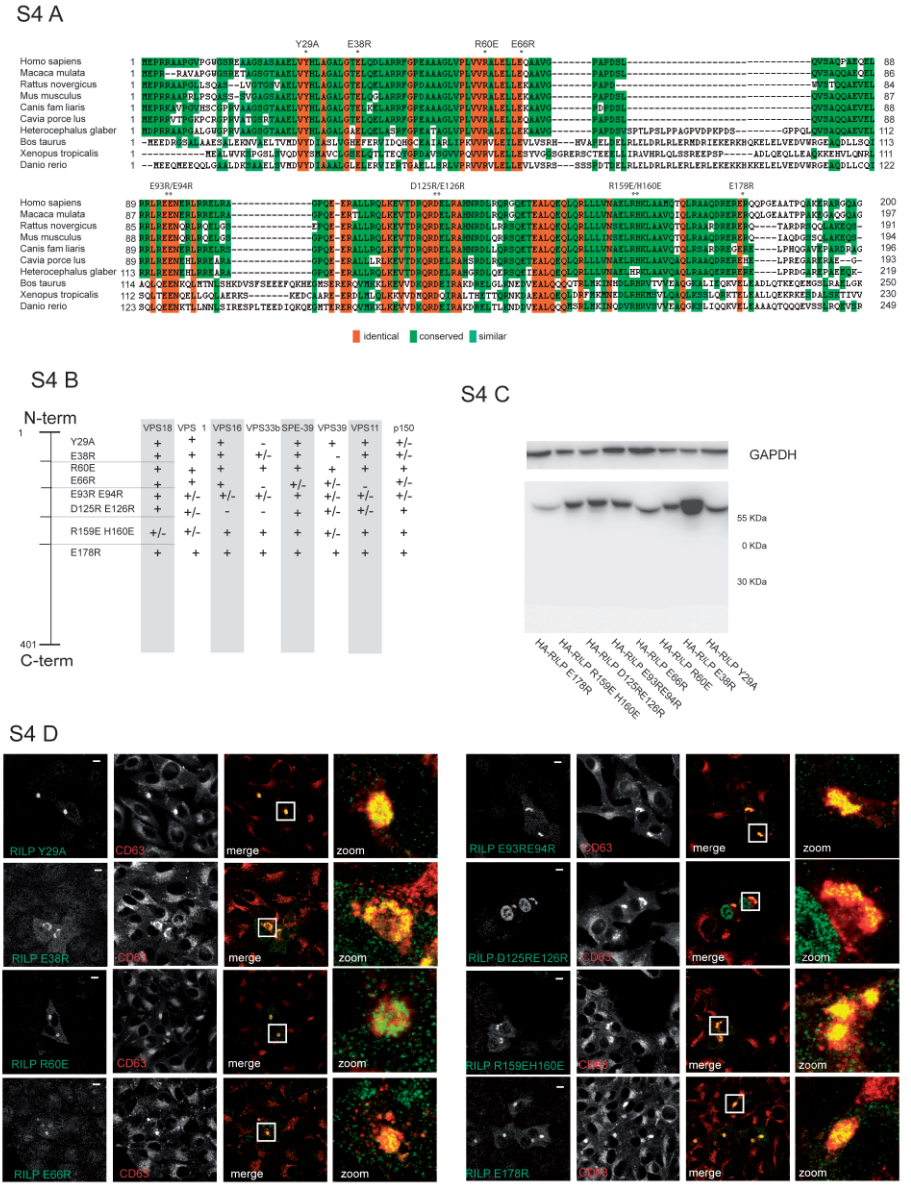


Figure S4. RILP point mutants and the binding of HOPS subunits. Sequence alignment of the RILP N-terminus (*Homo sapiens* AA 1-200) and nine other species. Red: identical amino acids, dark green: conserved amino-acids, light green: similar amino acids. Asterisks indicate charged amino acids mutated in the opposite charge in our study. (**B**) Semi-quantitative representation of p150^{Glued} and HOPS subunit recruitment to RILP mutants (see Fig 4A, S4E-H). Levels of recruitment are depicted as '+' (strong recruitment) to '–' (no recruitment). (**C**) Expression levels of RILP point mutants expressed in MelJuSo cells. Cell lysates were separated by SDS-PAGE and WB probed with an anti-HA antibody. GAPDH is shown as a loading control. Marker proteins indicated. (**D**) MelJuSo cells expressing HA-tagged RILP point mutants were fixed, immuno-labeled with anti-HA and anti-CD63 antibodies and imaged by confocal microscopy. Boxed area zoomed-in. Scale bar: 10µm. Shown is representative cell of n>100.

S4 E

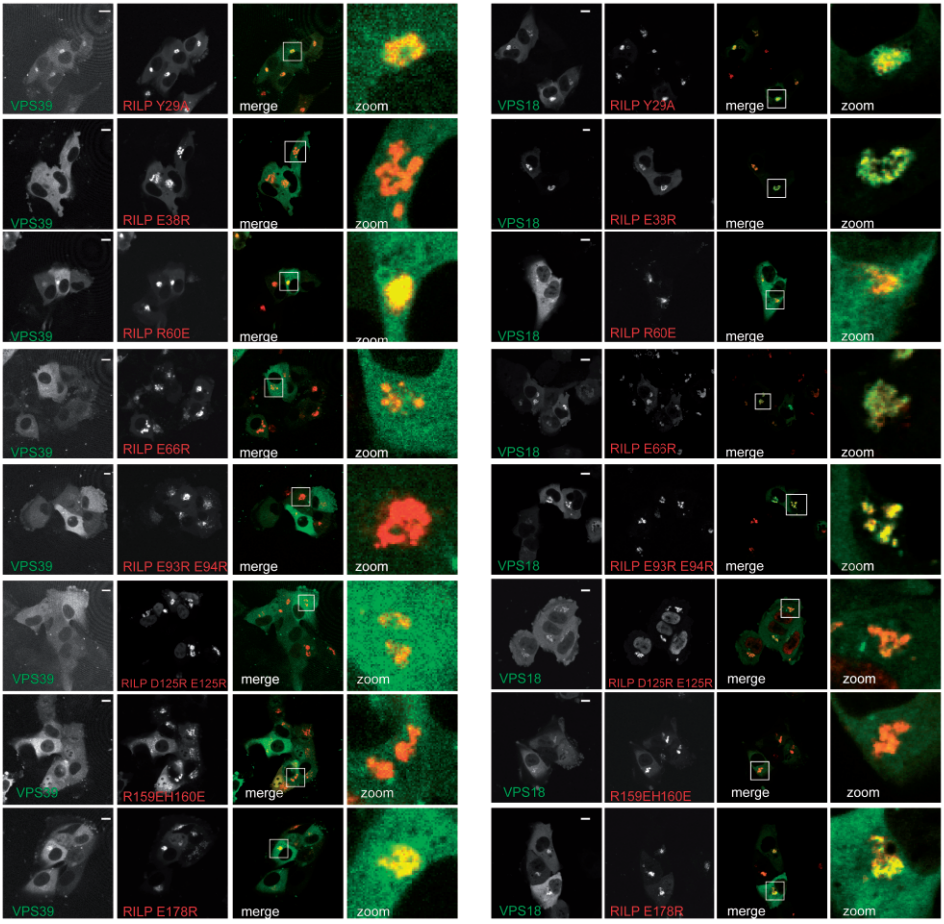


Figure S4. Continued. (**E**) RILP mutants and VPS39 and VPS18. MelJuSo cells expressing HA-RILP mutants (as indicated) and MYC-mRFP-VPS39 (left) or GFP-VPS18 (right) were fixed and immunolabeled with HA-antibodies and imaged by confocal fluorescence microscopy. Scale bar: 10µm. Representative of n>100

S4 F

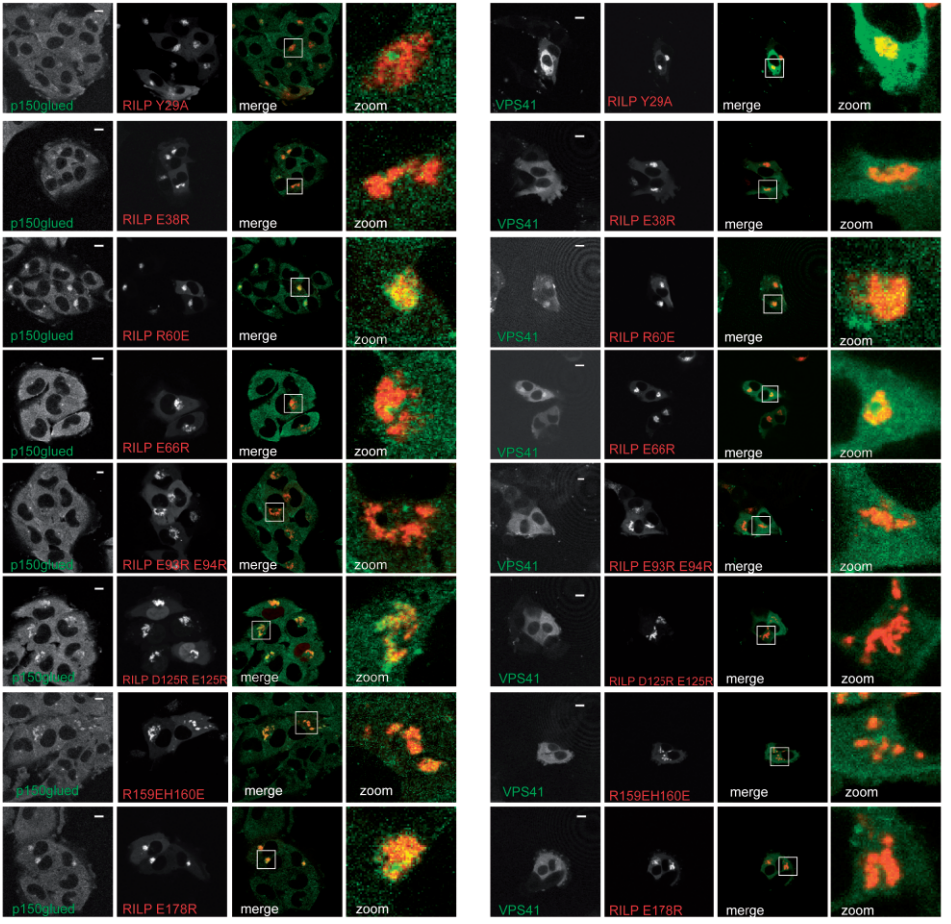


Figure S4. Continued. (**F**) RILP mutants and p150^{Glued} and VPS41. MelJuSo cells expressing GFP-RILP mutants (as indicated) were fixed and immunolabelled with p150^{Glued}-antibodies (left). MelJuSo cells expressing HA-RILP mutants and GFP-VPS41 were fixed and immunolabeled with HA-antibodies and imaged by confocal fluorescence microscopy (right). Scale bar: 10µm. n>100

S4 G

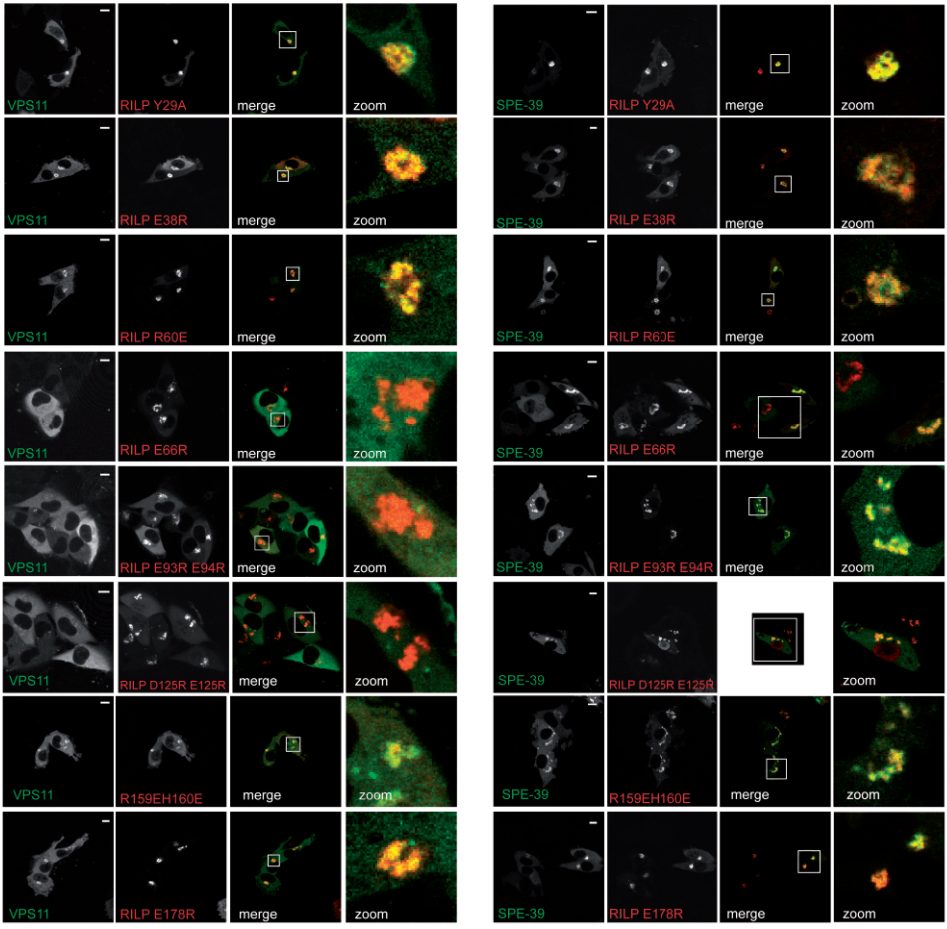


Figure S4. Continued. (**G**) RILP mutants, VPS11 and SPE-39. MelJuSo cells expressing HA-RILP mutants and GFP-VPS11 (left) or SPE-39-GFP (right) were fixed, immunolabeled with HA-antibodies and imaged by confocal fluorescence microscopy. Scale bar: 10µm. n>100

S4 H

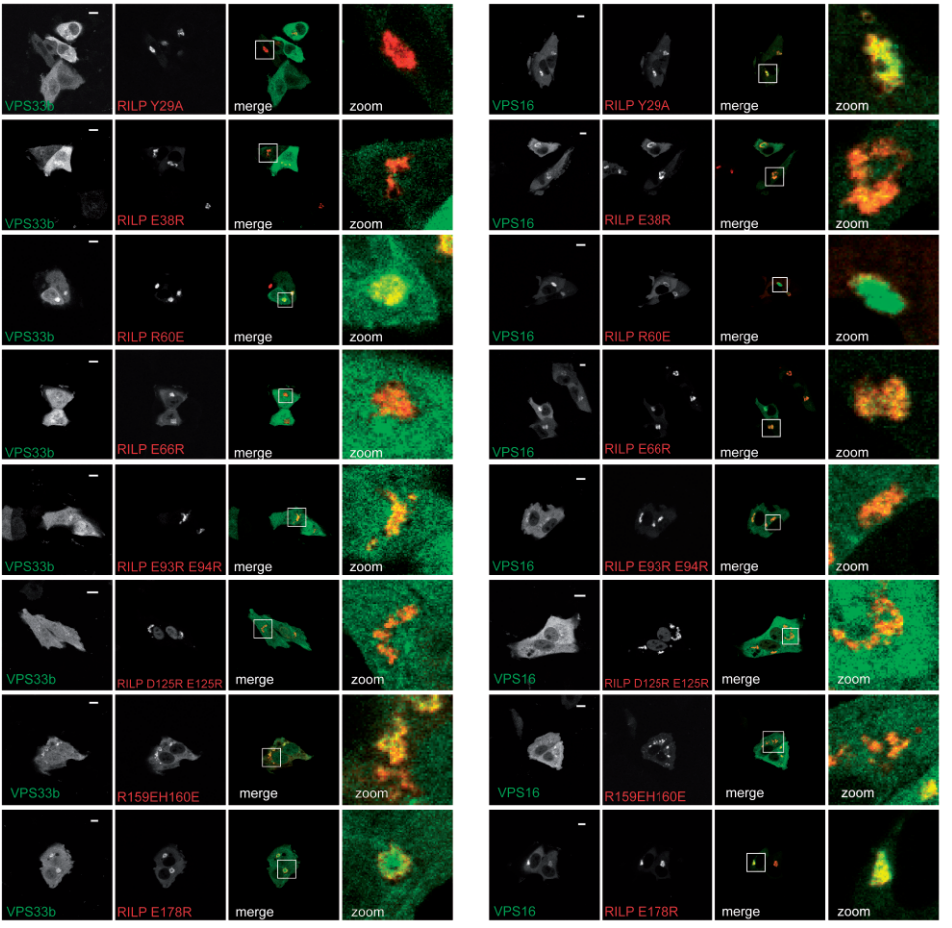
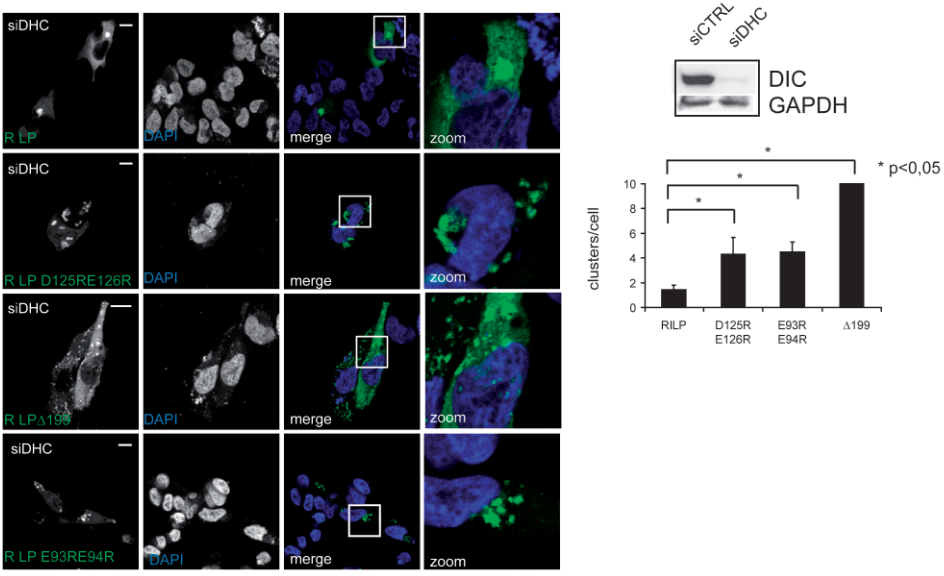


Figure S4. Continued. (**H**) RILP mutants, VPS33b and VPS16. MelJuSo cells expressing HA-RILP mutants and GFP-VPS33b (left) or GFP-VPS16 (right) were fixed, immunolabeled with HA-antibodies and imaged by confocal fluorescence microscopy. Scale bar: 10µm. n>100.

S4I



S4 J

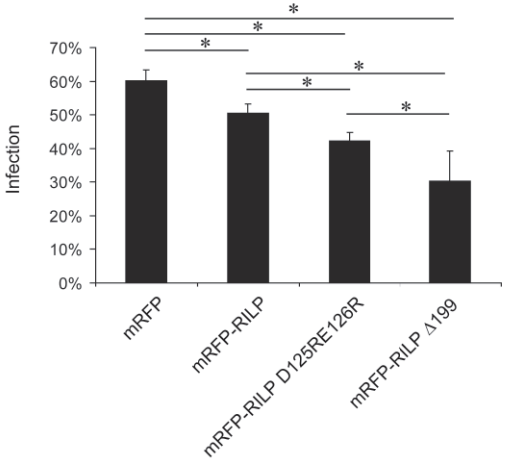


Figure S4. Continued. (I) MelJuSo cells silenced for Dynein heavy chain and expressing HA-RILP, HA-RILPΔ199, HA-RILP D125RE126R or HA-RILP E93RE94R were fixed, immunolabelled with HA-antibodies and DAPI and imaged by CLSM. Scale bar: 10µm, representative of n>100. Right bottom panel: Quantification shows average number of individual vesicle clusters and/or free vesicles per cell. Cells with >10 clusters were set at 10 (means + SD; n>100). Right top panel: Western blot shows silencing for Dynein heavy chain by staining for co-depleted Dynein intermediate chain (Raaijmakers et al., 2012). (J) HAP-1 cells expressing mRFP, mRFP-RILP, mRFP-RILPD125RE126R or mRFP-RILPΔ199 were infected with rVSV-GP-EboV for 8 hours. After successful infection, the virus produces GFP in the host cell's cytosol which is detected and quantified by flow cytometry. Shown is the percentage virus infection (by GFP) in mRFP-RILP or mRFP-RILP mutant expressing cells (mean + sem). * p<0,05.

Supplemental table 1

	fwd	
primerset 1	CCCAAAGCTTGCCACCATGGGTAAGCCTATCCCTAACCCT CTCCTCGGTCTCGATTCTACGATGGACTGCTACACGGCGA	vps16
primerset 2	CCCAGAATTCCATGGCTTTTCCCCATCG	vps33b
primerset 3	CCCAGGATCCATGGCGGAAGCAGAGGAGCA	vps41
primerset 4	ATGGCGGCCTACCTGCAGTG	vps11
primerset 5	CCCAGAATTCACCACCATGAATCGGACAAAGGGTGA	spe39
primerset 6	CCCAGGATCCATGAATCGGACAAAGGGTGA	spe39
primerset 7	agaggAGGcgccagcagcctggcgaag	RILP E178R
primerset 8	gctgGAGGAGaagctggcggccatgcagac	RILP R159EH160E
primerset 9	gcggCGCCGActccgggcgcacaaccgc	RILP D125RE126R
primerset 10	gcggAGGAGGaacgagcgcctccgcagg	RILP E93RE94R
primerset 11	tcttgAGAcaggctgccgtggggccc	RILP E66R
primerset 12	tggtgGAGgcgctggagctcttggaaca	RILP R60E
primerset 13	agcgcCTCcaccactagcggcaccagc	RILP E38R
primerset 14	cttgtgGCCcatctagccggggccctgg	RILP Y26A
	rev	
primerset 1	cccagaattcTCACTTCTTCTGGGCTTGTG	vps16
primerset 2	CCCAGAATTCTCAGGCTTTCACCTCACTCA	vps33b
primerset 3	CCCAGGATCCCTATTTTTTCATCTCCAA	vps41
primerset 4	CCCAGAATTCTTAAGTGCCCC-TCCTGGAGT	vps11
primerset 5	CCCAGGATCCAAATTCTTCCATCGAATTTGC	spe39
primerset 6	CCCAGAATTCTCAAGCGTAATCAGGAACGT	spe39
primerset 7	tggcgCCTcctctcgcggtcctgcgc	RILP E178R
primerset 8	ggagTCGGCGccgctgtcggtccgtgacc	RILP R159EH160E
primerset 9	ggagTCGGCGccgctgtcggtccgtgacc	RILP D125RE126R
primerset 10	cgttCCTCCTccgcagccgccgcagctcc	RILP E93RE94R
primerset 11	gcctgTCTcaagagctccagcgcccgc	RILP E66R
primerset 12	agcgcCTCcaccactagcggcaccagc	RILP R60E
primerset 13	tgcagCCTagtgcccagggccccggc	RILP E38R
primerset 14	tagatgGGCcacaagctccgcggccgat	RILP Y26A

chapter **FIVE**

Identification and characterization of the mammalian CORVET and HOPS tethering complexes and a VPS33b-SPE-39 complex mutated in ARC syndrome

Rik van der Kant[1]
Lennert Janssen[1]
Jacques Neefjes[*]

[1]Division of Cell Biology, the Netherlands Cancer Institute, Plesmanlaan 121, 1066CX Amsterdam NL

[*]Correspondence; j.neefjes@nki.nl – Tel; +31-20-5122017 Fax; +31-20-5122029

In preparation

Abstract

Membrane dynamics within the eukaryotic endomembrane system are specified by Rab GTPases that define organelle identity and recruit transport and fusion machinery. To initiate membrane fusion, Rab GTPases recruit multisubunit complexes that tether vesicles to prepare them for subsequent SNARE-mediate fusion. Endo-lysosomal biogenesis is well studied in yeast were the CORVET complex is required for endosome-endosome fusion and the HOPS complex for subsequent lysosomal fusion. The yeast CORVET and HOPS complex are composed of 4 class C proteins (Vps11, Vps16, Vps18, Vps33) that associate with the Rab binding modules Vps8-Vps3 (CORVET) and Vps41-Vps39 (HOPS). A number of mammalian proteins with high sequence identity to all these proteins have been identified. Several of these putative mammalian CORVET and HOPS complex members function in endosomal maturation, bacterial and viral infection, autophagosome clearance, membrane receptor signalling and embryonic development. Mutations in human VPS33b (vps33 homologue) and SPE-39 (vps16 homologue) cause arthrogryposis, renal dysfunction, and cholestasis (ARC) syndrome. However, it is not known if and how these putative subunits assemble into complexes or in which step of endosomal maturation these complexes function. Here we map the mammalian CORVET and HOPS complexes and identify a third complex (SPE-39/VPS33b) that is mutated in ARC syndrome. Using detailed molecular mapping of the complexes we indentified interactions among subunits under normal- and disease-conditions. Our data suggest that there are at least 3 mammalian endosomal tethering complexes that function at different stages of endosomal maturation. These findings offer important new insights in our understanding of mammalian endo-lyosomal biogenesis and lysosomal disease.

Keywords: transport, fusion, tethering, HOPS, CORVET, RAB7, RILP, late endosomes, lysosomes, endosomal maturation, ARC syndrome.

Abbreviations

CORVET complex, class C core vacuole/endosome tethering complex; HOPS complex, Homotypic fusion and vacuole Protein Sorting complex; ARC syndrome, arthrogryposis, renal dysfunction, and cholestasis syndrome

Introduction

The endocytic pathway is a dynamic system in which vesicles are continuously fusing, moving and budding in order to deliver their cargo to the correct compartment. Cargo destined for degradation such as internalized nutrients, activated growth receptors and endocytosed pathogens are targeted to the late endosome/lysosome (LE) where the acidic environment and resident proteases allow for degradation. Proteins of the RAB and ARF GTPase family in conjunction with motor proteins and sorting- and tethering complexes control the dynamics of endosomal compartments (Stenmark, 2009). Endosomal biogenesis is dependent on two RAB GTPases, RAB5 and RAB7, that subsequently function at the early endosomal and late endosomal stage (Huotari and Helenius, 2011). Maturation and fusion between these different compartments requires tethering complexes that tether two vesicles in close proximity and subsequently recruit SNARE for fusion (Nickerson et al., 2009). These processes are well understood in yeast where the 6-subunit class C core vacuole/endosome tethering complex (CORVET) complex is a Vps21 (yeast Rab5 ortholog) acceptor that controls endosome-endosome tethering (Markgraf et al., 2009;Peplowska et al., 2007;Balderhaar and Ungermann, 2013;Balderhaar et al., 2013). Subsequent cargo entry into the vacuole (the yeast lysosome) requires the HOmotypic fusion and vacuole Protein Sorting (HOPS) complex that controls tethering for fusion of late endosomes and Golgi-derived AP-3 vesicles with the vacuole (Seals et al., 2000;LaGrassa and Ungermann, 2005;Starai et al., 2008;Rehling et al., 1999).

The yeast CORVET complex is composed of six vacuolar protein-sorting (Vps) proteins: Vps18, Vps11, Vps16, Vps33a, Vps8 and Vps3, whereas the yeast HOPS complex is composed of Vps18, Vps11, Vps16, Vps41, Vps39 and Vps33a (Wickner, 2010;Sato et al., 2000;Wurmser et al., 2000;Nakamura et al., 1997;Peplowska et al., 2007). The interactions between these proteins, and the domains involved, have been carefully mapped (Plemel et al., 2011;Ostrowicz et al., 2010;Brocker et al., 2012) and recently the structure of the HOPS complex was resolved by electron microscopy (Brocker et al., 2012). HOPS appears a flexible, 28- to 35-nm-long seahorse-like structure with Vps39 and Vps41 at two opposite ends (head and tail) that bind Ypt7 (the yeast RAB7 ortholog) for membrane recruitment (Brocker et al., 2012). In addition, Vps41 also binds to lipids via its ALPS (amphipathic lipid packaging) motif. The head part of the yeast HOPS complex consists of Vps33/Vps16/Vps41 and Vps18 that interact with a tail of Vps39/Vps11 (Brocker et al., 2012). After tethering the HOPS complex recruits SNARE proteins to drive actual fusion (Starai et al., 2008;Lobingier and Merz, 2012). Although the structure of the CORVET complex has not been resolved it is assumed that it is similar to HOPS, but Vps41 is replaced by Vps8 and Vps3 replaces Vps39 (Balderhaar and Ungermann, 2013). Both Vps8 and Vps3 can bind Vps21 (yeast RAB5) for membrane recruitment (Ostrowicz et al., 2010;Brocker et al., 2012).

All 8 subunits of the yeast HOPS and CORVET complex seem conserved in mammals with two additional homologue proteins; VPS33b (VPS33 homologue) and SPE-39 (VPS16 homologue, also called VIPAR or VPS16b) (Gissen et al., 2005;Caplan et al., 2001;Huizing et al., 2001;Solinger and Spang, 2013;Zhu et al., 2009;Zlatic et al., 2011). It is unclear what are the mammalian orthologs of yeast Vps3 and Vps39. Both mammalian VPS39 and transforming growth factor-beta receptor-associated protein 1 (TGFBRAP1) share sequence homology with yeast Vps39 and

Vps3 (Plemel et al., 2011;Balderhaar and Ungermann, 2013;Wurthner et al., 2001;Messler et al., 2011). TGBFRAP1 is a modulator of TGB-β signalling and essential for embryonic development (Messler et al., 2011;Wurthner et al., 2001). More major differences between species exist as some domains in HOPS subunits are lost and the mammalian HOPS complex is not recruited to LE by RAB7 but by it's effector RILP (van der Kant et al., 2013).

Studies and their interpretation regarding the human CORVET and HOPS complexes has been hampered by a lack of knowledge on the assembly of these complexes in human. A role for HOPS in endosomal- and phagosomal maturation has been assigned by the study of single subunits that might be shared with the CORVET complex. These include studies that have implicated subunits of HOPS or CORVET in EGFR routing (Chirivino et al., 2011) and autophagosome maturation (Liang et al., 2008). Putative HOPS is also critical for efficient cytosolic entry of Ebola virus from NPC-1 containing late endosomes (Carette et al., 2011). The small GTPase ARL8b controls lipid loading of CD1 molecules in lysosomes through interactions with some subunits of a putative HOPS complex (Garg et al., 2011). VPS39 and VPS41 are required for homotypic and heterotypic late endosomal fusion (Pols et al., 2013a) and VPS41 functions in direct Trans-Golgi-Network to late endosomal transport of lysosomal proteins (Pols et al., 2013b) Mutations in SPE-39 and VPS33b are reported to cause arthrogryposis, renal dysfunction, and cholestasis (ARC) a multisystem disorder associated with abnormalities in polarized liver and kidney cells and recurrent infections (Cullinane et al., 2010;Gissen et al., 2004). SPE-39 and VPS33b are both essential for megakaryocyte and platelet α-granule biogenesis, a process requiring TGN to LE transport and LE maturation (Lo et al., 2005). Without a good understanding of complex assembly and composition it is impossible to understand the roles of these complexes in endosomal biogenesis and human disease.

Here we have studied the assembly and function of the mammalian HOPS and CORVET subunits homologues. We find three complexes; CORVET, HOPS and an additional complex of VPS33b-SPE-39. We identify TGFBRAP1 as the mammalian Vps3 ortholog. TGFBRAP1 is recruited to early endosomes and is incorporated into a complex containing VPS16-VPS11-VPS8-VPS33a and VPS18. The mammalian HOPS complex consists of VPS39-VPS11-VPS18-VPS41-VPS16-VPS33a and our detailed molecular mapping indicates that the architecture of the complex is similar to yeast HOPS. We show that mutations in ARC syndrome patients either selectively affect VPS33b-SPE-39 assembly or protein recruitment to RILP. HOPS and VPS33b-SPE-39 are both recruited to RAB7 via RILP but function in different processes related to late endosomal transport and fusion. This suggests that various processes controlling transport and fusion coalescent on RAB7 and suggest higher order regulation to control late endosomal transport and fusion in time and space.

Results and discussion

VPS33b and SPE-39 assemble in a complex distinct from CORVET and HOPS

To map the interactions between the 10 homologues of the putative mammalian HOPS and CORVET complex (Fig 1A), we performed endogenous immunoprecipitation against different

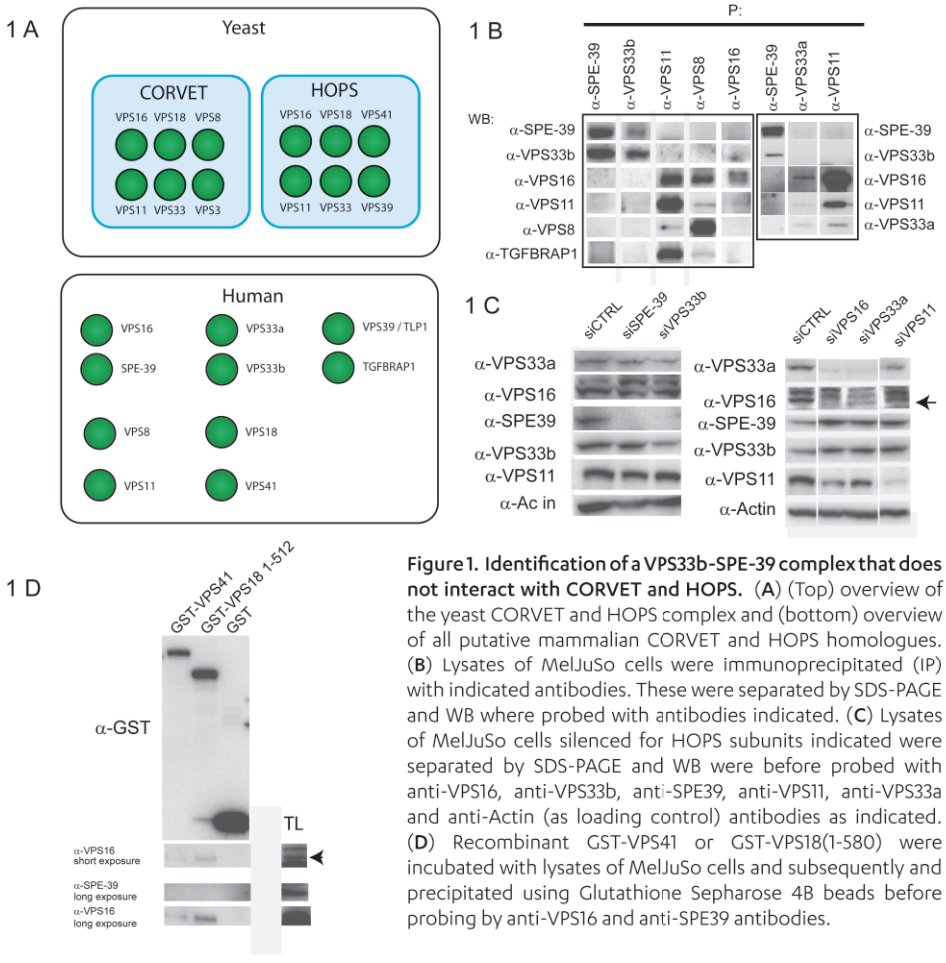


Figure 1. Identification of a VPS33b-SPE-39 complex that does not interact with CORVET and HOPS. (**A**) (Top) overview of the yeast CORVET and HOPS complex and (bottom) overview of all putative mammalian CORVET and HOPS homologues. (**B**) Lysates of MelJuSo cells were immunoprecipitated (IP) with indicated antibodies. These were separated by SDS-PAGE and WB where probed with antibodies indicated. (**C**) Lysates of MelJuSo cells silenced for HOPS subunits indicated were separated by SDS-PAGE and WB were before probed with anti-VPS16, anti-VPS33b, anti-SPE39, anti-VPS11, anti-VPS33a and anti-Actin (as loading control) antibodies as indicated. (**D**) Recombinant GST-VPS41 or GST-VPS18(1-580) were incubated with lysates of MelJuSo cells and subsequently and precipitated using Glutathione Sepharose 4B beads before probing by anti-VPS16 and anti-SPE39 antibodies.

subunits for which we could acquire antibodies and visualized the associated proteins of the different subunits by western blot (WB) (Fig 1B). As previously reported (Cullinane et al., 2010;Zhu et al., 2009) we observed a strong interaction between SPE-39 and VPS33b. We also detected interactions between VPS11/VPS8/TGFBRAP1/VPS16/VPS11 and VPS33a. However no interactions were observed between SPE-39 and VPS33b and any other of the HOPS/CORVET subunits, indicating that VPS33b-SPE39 assembles in a distinct complex unrelated to HOPS or CORVET.

Stability of proteins within a complex is usually higher than that of the free subunits of the complex. We used this to further examine the interaction between the putative HOPS/CORVET subunits. We depleted several subunits by siRNA silencing and assessed the effects on their endogenous interaction partners by WB. Silencing of VPS16 significantly decreased VPS33a and VPS11 protein levels, while VPS33b and SPE-39 levels remained unaffected (Fig. 1C). Similarly, silencing of VPS33b compromised SPE-39 levels without affecting cellular abundance of VPS16, VPS33a or VPS11 (Fig. 1C) indicating that VPS33b and SPE-39 assemble in a complex that is distinct from HOPS and

CORVET. In line with this data, a pull-down of MelJuSo lysates with purified GST-VPS41 and GST-VPS18 indicates that these proteins interacted with VPS16 but not SPE-39 (Fig 1D).

Our findings of VPS33b and SPE-39 assembly in a distinct complexes disagree with a previous finding (Zhu et al., 2009) where human SPE-39 was reported to interact with both VPS33a and VPS33b. We do not detect interactions of SPE-39 with VPS33a and this interaction was also not detected in genetic Drosophila screens. In these assays Drosophila dVps16A (human VPS16) interacts with Carnation (human VPS33a) but not with dVps33b, and dVps16B (human SPE-39) interacted with dVps33b but not with Carnation (human VPS33a) (Pulipparacharuvil et al., 2005). Deep orange (human VPS18) interacted with both Vps16 homologues (Pulipparacharuvil et al., 2005). Our data as well as the genetic Drosophila data, supports the existence of distinct complexes. This in line with functional data where the putative HOPS subunits, but not VPS33b and SPE-39, are required for Ebola virus infection (Carette et al., 2011).

Characterization of the mammalian CORVET and HOPS complexes

Yeast HOPS and CORVET share four common subunits; vps16, vps18, vps11 and vps33 (Fig. 1A). These proteins are complemented by vps8 and vps3 for CORVET and vps39 and vps41 for HOPS. Our endogenous pull-downs indicate that mammalian VPS8 interacts with TGFBRAP1 (vps3 ortholog), VPS16 and VPS11 indicative for a CORVET complex (Fig 1B). Yeast CORVET acts at the early endosome and is a vps21 (RAB5 ortholog) effector. To test localization of VPS8 and TGFBRAP1 we expressed tagged-constructs in MelJuSo cells and stained these cells with an antibody against the RAB5 effector EEA1. While the localization of VPS8 was predominantly cytosolic (data not shown) strong early endosomal localization was observed for TGFBRAP1 (Fig 2A). Together these data indicate that TGFBRAP1 is the mammalian vps3 ortholog and that mammalian CORVET is composed of TGFBRAP1/VPS8/VPS16/VPS18/VPS11 and VPS33a. As VPS11 can also assemble in a CORVET complex we tested whether TGFBRAP1 would suffice to recruit VPS11 to early endosomal membranes. At steady state levels VPS11 has a cytosolic localization (van der Kant et al., 2013) (Fig 2B), but can be recruited to late endosomes by RILP (van der Kant et al., 2013). Upon co-expression of TGBFRAP1 and VPS11, VPS11 was recruited to early endosomes indicating TGFBRAP1 targets other subunits of the CORVET complex to early endosomes (Fig. 2B). VPS33b, SPE-39, VPS39 and VPS41 were not recruited to early endosomes by TGFBRAP1 (Fig S1), again indicating these are not part of the CORVET complex.

Although we were able to map interactions between shared subunits of HOPS/CORVET with CORVET complex specific subunits, no antibodies were available for HOPS specific VPS39 and VPS41.To place these subunits we ectopically co-expressed all 6 differently tagged putative HOPS proteins + VPS33b and SPE-39, and assessed their interactions by co-immunoprecipitation and WB (Fig. 2C). Again interactions were observed between VPS33b and SPE-39, but not with other subunits. As in yeast, mammalian VPS16 was found to interact with VPS41, VPS18 and VPS33a, while VPS11 bound VPS39. Unlike in the endogenous co-IP (Fig. 1A), no interactions between exogenous VPS16/41/18/33a and VPS11/39 subunits were detectable, which may reflect a limitation of the over-expression system or interference by the tags. Together our data suggest that the putative mammalian HOPS and CORVET subunits assemble into three distinct complexes; a CORVET complex (VPS33a/VPS16/VPS18/VPS3/VPS8/TGFBRAP1), a HOPS complex

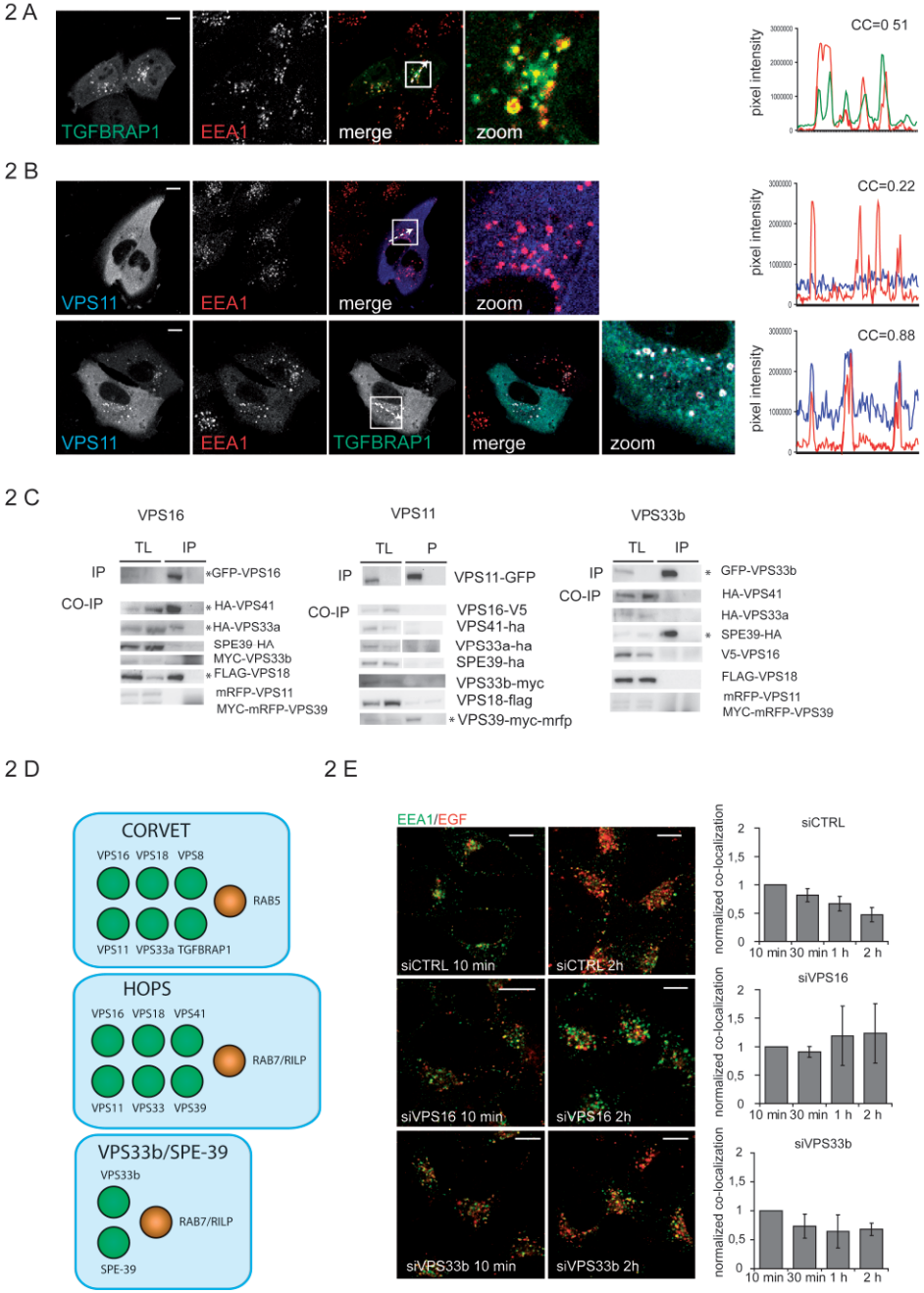


Figure 2. Identification of CORVET and HOPS complexes and subunit organization. (**A**) MelJuSo cells expressing GFP-TGFBRAP1 were fixed and stained with EEA1-antibodies before imaging by confocal microscopy. Scale bar: 10µm. n>100. Right panel: Plot profile for cell indicated in left panels depicted with white arrow. In Red: mRFP intensity (EEA1) and in Green: GFP intensity (TGFBRAP1) over line indicated in left panel. CC = correlation coefficient. (**B**) MelJuSo cells expressing mRFP-VPS11 or co-expressing GFP- ▶

► TGFBRAP1 and mRFP-VPS11 were fixed and stained with EEA1-antibodies before imaging by confocal microscopy. Scale bar: 10μm. n>100. Right panel: Plot profile for cell indicated in left panels depicted with white arrow. In Red: mRFP intensity (EEA1 and in Blue: mRFP intensity (VPS11) over lines indicated in left panel. CC = correlation coefficient (**C**) Lysates of MelJuSo cells co-expressing tagged-VPS constructs as indicated were immunoprecipitated (IP) with anti-GFP before separation by SDS-PAGE and WB, and WB filters were probed with anti-HA, anti-Flag, anti-MYC, anti-V5, anti-mRFP and anti-GFP antibodies (**D**) Schematic overview of mammalian CORVET, HOPS and VPS33b-SPE39 complexes and their target RAB GTPase. (**E**) Hela cells silenced for indicated subunits were serum-starved for 1 hour before incubation with alexa-fluor555-conjugated EGF for indicated time points. Scale bar: 10μm. n>100. Right; Quantification of the percentage of EGF that is in early endosomes at indicated time points, normalized to 10 minutes. n=1.

of VPS33a/VPS16/VPS18/VPS41/VPS39/VPS11 and an alternative complex of VPS33b and SPE-39 (Fig. 2D). In line with a role of VPS16 in the CORVET and HOPS complex, exit of cargo (EGF) from early endosomes is delayed when VPS16 is silenced (Fig. 2E). VPS33b silencing did not affect exit of cargo from early endosomes, indicative of a role outside CORVET.

Molecular architecture of the mammalian HOPS complex

Interactions within the yeast HOPS complex have been extensively mapped using biochemical (Ostrowicz et al., 2010;Plemel et al., 2011) and structural (Brocker et al., 2012) approaches. To study the architecture of the mammalian HOPS complex we expressed the various HOPS subunits and their sub-domains to map interactions between subunits. Domain organization of the mammalian HOPS and CORVET complex subunits (Plemel et al., 2011) are depicted in figure 3A. To study the interactions within the proposed head (VPS16/VPS33a/VPS18/VPS11 in yeast) of the HOPS complex, we expressed tagged-truncation mutants of one protein and assessed interactions with the remaining three other proteins by co-immunoprecipitation and WB (Fig 3B). We observed that VPS16 is a central protein in the head, with its C-terminus binding VPS33a and its N-terminus VPS41 and VPS18. This confirms previous interactions between VPS16 and VPS33a (in the C-terminus of VPS16) in yeast and drosophila (Plemel et al., 2011;Pulipparacharuvil et al., 2005). Interactions between VPS41 and VPS18 have been observed before in yeast (Ostrowicz et al., 2010) and are apparent from the yeast HOPS complex structure (Brocker et al., 2012). Our domain studies suggest that the RING-like domain of VPS18 and the RING domain of VPS41 interact with VPS16 possibly acting in a tripartite-interaction with the N-terminus of VPS16 (Fig 3C).

VPS39 in the proposed tail of the mammalian HOPS complex is the least conserved of all HOPS components. The human VPS39 ortholog is much shorter (886 versus 1029 AA in yeast) and previous reports (Plemel et al., 2011) and our own alignments indicate that whereas the C-terminus of VPS39 resembles yeast vps39, the vps39 N-terminal region resembles better the N-terminal region of yeast vps3 (part of the CORVET complex (Plemel et al., 2011;Peplowska et al., 2007;Solinger and Spang, 2013). As in yeast, the C-terminus of VPS39 binds VPS11 (Fig 3B) (Plemel et al., 2011). We did not observe interactions between VPS41 and VPS39 as observed in yeast (Plemel et al., 2011;Ostrowicz et al., 2010). This may be due to the loss of conservation of the N-terminus of vps39 between yeast and humans, as the yeast vps39 N-terminus interacts with vps41 (Plemel et al., 2011). Our fine mapping (summarized in Fig. 3C) indicates that canonical HOPS has a similar architecture as yeast HOPS (Brocker et al., 2012).

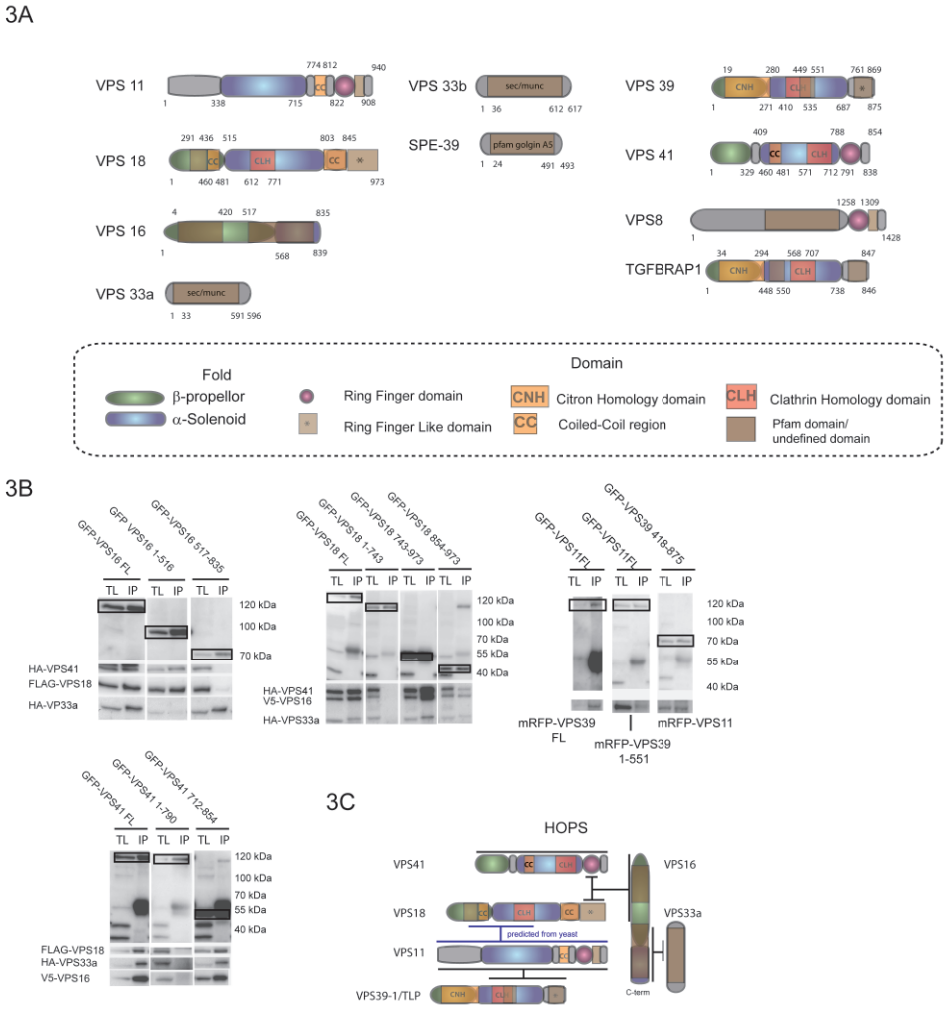


Figure 3. Molecular architecture of the mammalian HOPS complex. (**A**) Domain organization of the mammalian HOPS and CORVET subunit homologues. (**B**) Lysates of MelJuSo cells co-expressing tagged-VPS constructs as indicated were immunoprecipitated (IP) with anti-GFP antibodies before SDS-PAGE. WB filters were probed with anti-HA, anti-Flag, anti-MYC, anti-V5 and anti-GFP antibodies as indicated. (**C**) Summary of interactions within the mammalian HOPS complex. The observed interaction between VPS11 and VPS18 could not be mapped in our study and is predicted from yeast data.

Mapping membrane recruitment domains in the HOPS complex

A major difference between yeast HOPS and human HOPS is their mode of membrane recruitment. Two subunits of yeast HOPS, vps39 and vps41, bind Ypt7 (the yeast RAB7 ortholog), whereas mammalian VPS41 and VPS18 and possibly other human HOPS subunits directly bind the RAB7 effector RILP (van der Kant et al., 2013). We mapped the minimal domains for membrane recruitment in mammalian HOPS complex subunits by expressing tagged truncations mutants together with

RILP (Fig. 4A-E) and assessed their recruitment to RILP containing late endosomes by microscopy. The first 420 amino-acids of the β-propeller region in VPS16 (that are not involved in the interaction between VPS18 and VPS41, but is required for VPS33a binding) sufficed to localize VPS16 to RILP containing vesicles (Fig 4A). An N-terminal domain of VPS18 (AA 1-611) is also recruited to vesicles by RILP whereas two individual VPS18 mutants (AA 1-500 and AA 500-612) remained cytosolic even when RILP was expressed (Fig 4B). Possibly RILP interacts with a surface between the β-propeller and α-solenoid of VPS18. VPS41 recruitment to RILP required the full-length protein (Fig. 4C). We previously observed (van der Kant et al., 2013) that purified VPS41 has low affinity for RAB7 binding but that constitutive active RAB7 failed to recruit VPS41 to membranes. Binding affinity to RILP was about 10-fold higher, whereas even higher affinity was determined for the RAB7/RILP complex (this thesis) and here we could not specify a domain of VPS41 binding to RILP. A small coiled-coil region in VPS11 (AA 774-812) sufficed for recruitment to RILP (Fig. 4D). We identified two C-terminal domains (AA 511-761 and AA 761-875) in VPS39 for recruitment to membranes by RILP (Fig 4E).

Together this may indicate that multiple positions within VPS41 are required for binding to a shared interface between RAB7 and RILP. The CORVET member TGFBRAP1 is not recruited to RILP (Fig. 4F). In conclusion, at least three (VPS16, VPS18 and VPS41) yet possibly more (VPS39 and VPS11) subunits in the mammalian HOPS complex are involved in RILP binding for recruitment to RAB7-containing late endosomes and lysosomes (Fig. 4G). This data might also explain how recruitment of the CORVET complex to RAB7/RILP is prevented. In the absence of VPS41 and VPS39 only three protein domains capable of binding RILP remain; the C-terminal of VPS16, the coiled-coil domain in VPS11 and the N-terminal domain in VPS18. These are also the domains that in yeast bind VPS8 and TGFBRAP1 (yeast vps3 ortholog) (Plemel et al., 2011). This indicates that VPS8 and TGFBRAP1 might compete with RILP for binding shared subunits of the HOPS and CORVET complex. In this way a CORVET complex can not be assembled on RAB-RILP, and this might explain the target-organelle specificity of the CORVET and HOPS complex to prevent erroneous fusion events.

Interactions in the VPS33b-SPE39 complex and ARC syndrome mutants

VPS33b and SPE-39 do not exist in yeast and patient mutations in these proteins result in ARC syndrome (Gissen et al., 2004;Cullinane et al., 2010). Both VPS33b (sec-munc1 domain) and SPE-39 (GolginA5 domain) are single domain proteins. We mapped the effect of the ARC syndrome associated mutations in VPS33b-SPE-39 interactions and their interactions with RILP. Co-expression of the disease-associated truncation mutant of VPS33b (1-437) prevents it's interaction with SPE-39 (Fig. 5A). However, VPS33b 1-437 was recruited to RILP, indicating that VPS33b can bind RILP independent of SPE-39 (Fig. 5B). Another ARC mutation in VPS33b, L30P, has a different effect. Although VPS33b L30P still interacted with SPE-39 (Fig. 5A), it was no longer recruited to RILP (Fig. 5B). The mutations in ARC patients affect either the assembly or recruitment of the VPS33b-SPE39 complex to late endosomes which may explain some of the resulting phenotypes as observed in patients with ARC syndrome.

In summary we identified and characterized the mammalian CORVET and HOPS complex and a third complex VPS33b-SPE-39. The CORVET complex (TGFBRAP1-VPS8-VPS16-VPS11-VPS18-VPS33a) functions at the early endosome, while both the HOPS complex (VPS39-VPS41-VPS16-VPS11-

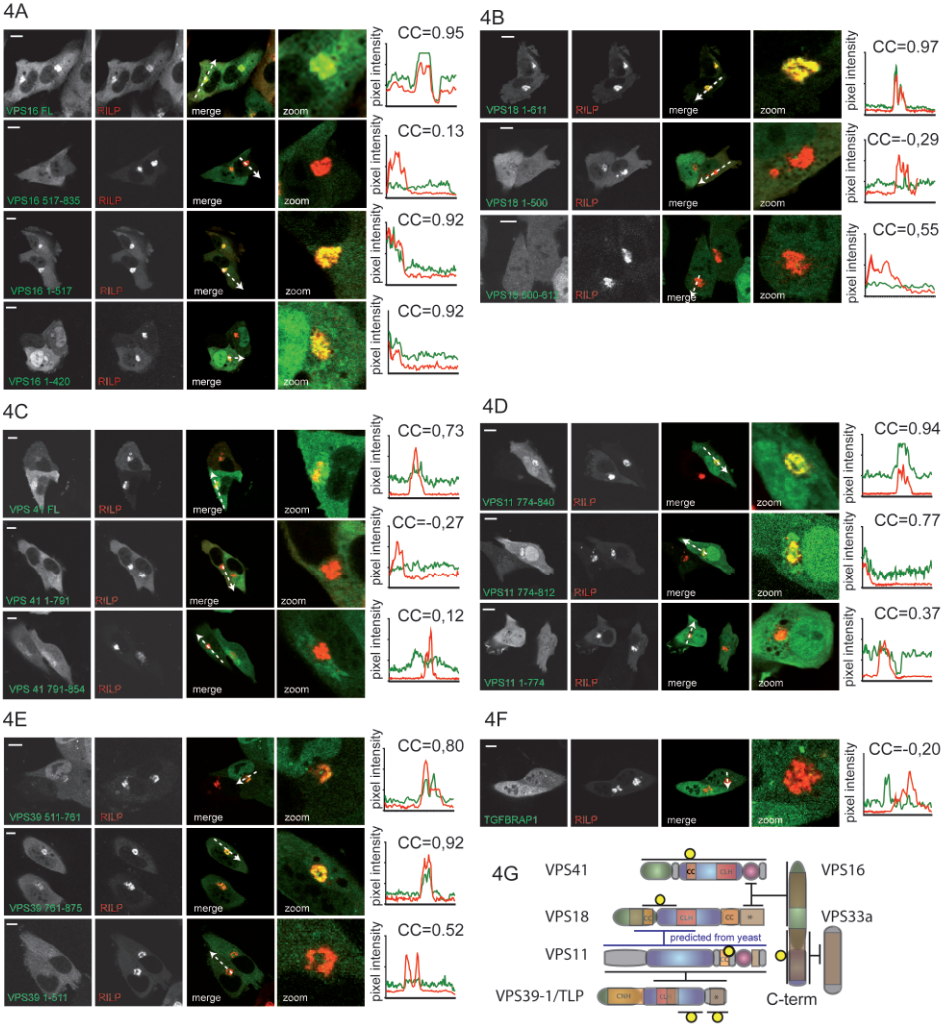


Figure 4. Identification of membrane targeting domains in HOPS subunits. (**A-E**) Left panel: MelJuSo cells expressing HA-RILP and GFP-tagged truncation mutants of indicated HOPS subunits were fixed and stained with HA-antibodies before imaging by confocal microscopy. Scale bar: 10µm. n>100. Right panel: Plot profiles for cells indicated in left panels depicted with white arrow. In Red: mRFP intensity (RILP) and in Green: GFP intensity (VPS mutants) over lines indicated in left panel. CC = correlation coefficient. (**F**) Left panel: MelJuSo cells expressing HA-RILP and GFP-TGFBRAP1 were fixed and stained with HA-antibodies before imaging by confocal microscopy. Scale bar: 10µm. n>100. Right panel: Plot profile for cell indicated in left panels depicted with white arrow. In Red: mRFP intensity (RILP) and in Green: GFP intensity (TGFBRAP1) over line indicated in left panel. CC = correlation coefficient. (**G**) Overview of interactions in the HOPS complex and with RILP. Yellow dots represent RILP binding domains required for membrane recruitment.

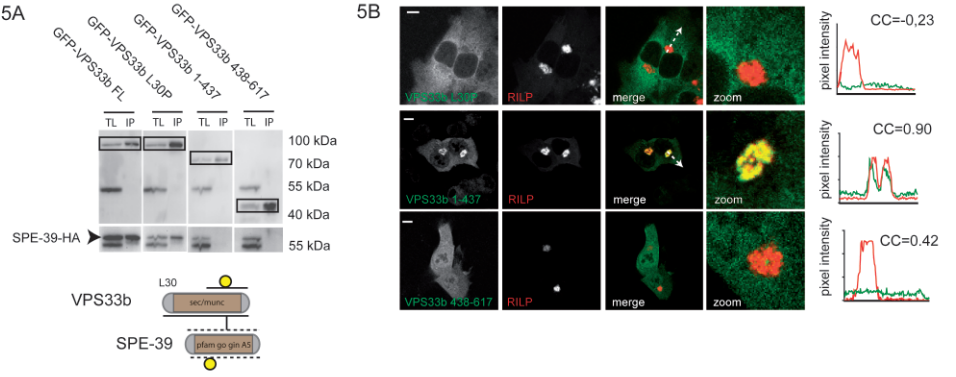


Figure 5. Interactions within the VPS33b-SPE-39 complex and the ARC syndrome. (**A**) Lysates of MelJuSo cells co-expressing tagged-VPS33b truncation constructs as indicated were immunoprecipitated (IP) with anti-GFP before SDS-PAGE and WB filters were probed with anti-HA and anti-GFP antibodies as indicated. (**B**) Left panel: MelJuSo cells expressing HA-RILP and GFP-VPS33b tagged truncation mutants as indicated were fixed and stained with HA-antibodies before imaging by confocal microscopy. Scale bar: 10µm. n>100. Right panel: Plot profiles for cells indicated in left panels depicted with white arrow. In Red: mRFP intensity (RILP) and in Green: GFP intensity (VPS33b mutants) over lines indicated in left panel. CC = correlation coefficient

VPS18-VPS33a) and the VPS33b-SPE-39 complex are recruited by RILP to LE. The two complexes have different functions in cell biology. SPE-39 and VPS33b assemble in a distinct complex and only disease variant of VPS33b and SPE-39 are found in ARC syndrome patients. Ebola virus infection requires the HOPS complex components but not SPE-39-VPS33b (Carette et al., 2011)

We mapped ARC mutations and show how they either affect VPS33b-SPE-39 assembly or interaction with the RAB7 effector RILP. Our data offers important insights in the architecture and organization of the mammalian endosomal tethering complexes and provides a basis to study the role of tethering complexes in the endocytic system.

Materials and methods

Reagents

Rabbit anti-GFP and Rabbit anti-mRFP antibodies were generated using purified His-mRFP or His-GFP recombinant proteins, respectively. Cross-reactivity has been excluded by Western blot analyses with various mRFP- or GFP-labeled fusion proteins. Other antibodies used were: mouse anti-CD63 (Vennegoor et al., 1985), mouse anti-V5 and anti-V5-HRP (Invitrogen), anti-myc and anti-myc-HRP (Novus), anti-HA (Roche) and anti-HA-HRP (Abcam), anti-flag (M2) and anti-flag-HRP (Sigma) anti-VPS33a (C1C3) (GeneTex), anti-EEA1 (Abcam), anti-VPS33b (Proteintech), anti-VPS11 (Proteintech), anti-VPS41 (Proteintech), anti-VPS16 (Proteintech), anti-TGFBRAP1 (sigma) and anti-SPE-39 was a gift of V. Faundez (Center for Translational Social Neuroscience, Emory University, Atlanta). Fluorescent and HRP-conjugated secondary antibodies were obtained from Invitrogen. GST-VPS18 (aa 1-580) and GST-VPS41 (full length) (produced in a *in vitro* wheat germ expression system) were purchased from Abnova.

Constructs and cloning

RAB7, RILP, VPS41, VPS33b constructs have been described previously (Rocha et al., 2009;Jordens et al., 2001;van der Kant et al., 2013). GFP-VPS16 and GFP-VPS18 were gifts from Chengyu Liang (Department of Molecular Microbiology and Immunology, University of Southern California, Los Angeles), VPS33a was a gift of V. Faundez, VPS39 was a gift of J. Bonifacino (National Institutes of Health, Bethesda, MD). VPS8 was a gift from J. Klumperman (Cell Microscopy Center, UMC Utrecht). TGFBRAP1 was generated from IMAGE CLONE :4420120 using forward primer CCCAAGATCTATGATGAGCATCAAAGCCTT and reverse primer CCCAGGTACCTCAAGTCCGAGTGCCAGGAC and was inserted into the BGLII and ASP718I sites in GFP-C1. Generation of mutants is described in Supplemental table 1.

Cell culture and microscopy

MelJuSo cells were cultured in Iscove's modified Dulbecco's medium (IMDM; Invitrogen) supplemented with 8% FCS in a 5% CO_2 humidified culture hood at 37°C. Hela cells were cultured in Dulbecco's modified eagle medium (DMDM; Invitrogen) supplemented with 8% FCS in a 5% CO_2 humidified culture hood at 37°C. All specimens were analyzed by confocal laser-scanning microscopes (TCS-SP1, TCS-SP2, or AOBS; Leica) equipped with HCX Plan-Apochromat 63× NA 1.32 and HCX Plan-Apochromat lbd.bl 63× NA 1.4 oil-corrected objective lenses (Leica). The acquisition software used was LCS (Leica).

Transfection

Expression constructs were transfected using Effectene reagents (Qiagen) according to manufacturer's instructions. For silencing, cells were transfected with Dharmafect1 (Thermo Fisher Scientific) with siRNA's (ON-TARGETplus SMARTpool) against VPS16, VPS33b, VPS33a, SPE-39 or control siRNA (Thermo Fisher Scientific).

Microscopy sample preparation

Transfected cells were fixed 24h post-transfection with 4% formaldehyde in PBS for 15 min and permeabilized for 10 min with 0.05% Triton X-100 in PBS at room temperature. Non-specific binding of antibodies was blocked by 0.5%BSA in PBS for 40 min, after which cells were incubated with primary antibodies in 0.5%BSA in PBS for 1h at room temperature. After washing three times with PBS, primary antibodies were visualized with Alexa-Fluor secondary antibody conjugates antibodies in 0.5%BSA in PBS for 30min at room temperature (Invitrogen). After three washes with PBS, samples were mounted in Vectashield mounting medium (Vector Laboratories).

Protein immunoprecipitation

MelJuSo cells were washed with ice-cold PBS and scraped into cell lysis buffer (50mM Tris-HCl, 150mM NaCl, 5mM $MgCl_2$, 1% NP40, 10% glycerol, pH 7.4) supplemented with complete EDTA-free Protease Inhibitor Cocktail. Cell lysates were obtained by incubation on ice for 10 min followed by centrifugation for clearing. The supernatants were incubated for 2h with respective antibodies followed by capture with protein G-Sepharose 4 FF resin and washed extensively with wash-buffer

(50mM Tris, 150mM NaCl, 5mM $MgCl_2$, 10% glycerol, pH 7.4). For GFP-tagged pulldown, GFP-TRAP beads were used (Chromotek). For GST-pulldown, Glutathione Agarose beads (Pierce) were used.

EGF exit from early endosomes

After silencing for 72 hours, Hela cells were placed on serum-free medium for 1 hour and subsequently incubated with Alexa Fluor 555-conjugated EGF (25ng/ml) (Molecular Probes) for indicated time points. Cells were then fixed, stained for EEA1 and imaged by confocal microscopy at identical settings. The Manders M1 (the percentage of channel A (EGF) that co-localizes with channel B (EEA1)) was calculated using the JaCoP plugin in ImageJ. Results are normalized to the 10 minute time-point.

Correlation Coefficients

For calculation of correlation coefficients the signal intensity over a vector was plotted using the plot profile tool in ImageJ (http://imagej.nih.gov/ij/index.html) in both the green and red channel. Correlation coefficients for the two plots were calculated in Excel using the function.

Acknowledgements

We thank J. Bonifacino, V. Faundez, S. Zlatic, and J. Klumperman for reagents. This work is supported by an ERC Advanced Grant and a TOP grant of NWO-CW.

References

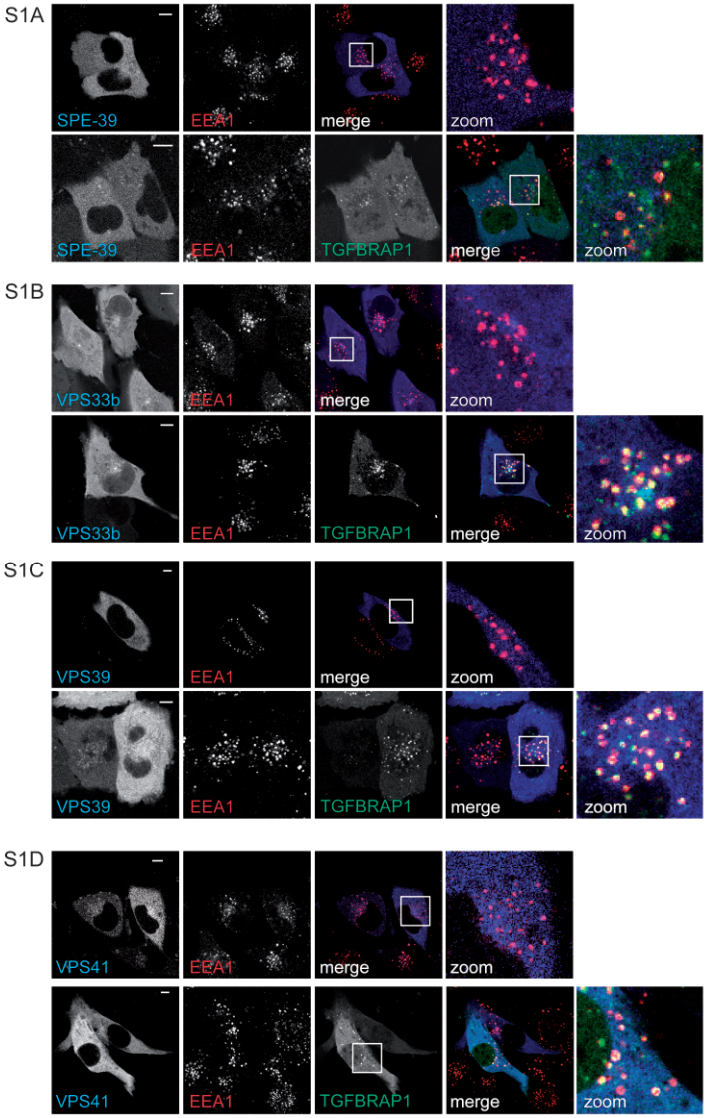
1. Balderhaar, H.J., J.Lachmann, E.Yavavli, C.Brocker, A.Lurick, and C.Ungermann. 2013. The CORVET complex promotes tethering and fusion of Rab5/Vps21-positive membranes. *Proc. Natl. Acad. Sci. U S A* 110:3823-3828.
2. Balderhaar, H.J. and C.Ungermann. 2013. CORVET and HOPS tethering complexes - coordinators of endosome and lysosome fusion. *J. Cell Sci.* 126:1307-1316.
3. Brocker, C., A.Kuhlee, C.Gatsogiannis, H.J.Balderhaar, C.Honscher, S.Engelbrecht-Vandre, C.Ungermann, and S.Raunser. 2012. Molecular architecture of the multisubunit homotypic fusion and vacuole protein sorting (HOPS) tethering complex. *Proc. Natl. Acad. Sci. U S A* 109:1991-1996.
4. Caplan, S., L.M.Hartnell, R.C.Aguilar, N.Naslavsky, and J.S.Bonifacino. 2001. Human Vam6p promotes lysosome clustering and fusion in vivo. *J. Cell Biol.* 154:109-122.
5. Carette, J.E., M.Raaben, A.C.Wong, A.S.Herbert, G.Obernosterer, N.Mulherkar, A.I.Kuehne, P.J.Kranzusch, A.M.Griffin, G.Ruthel, P.Dal Cin, J.M.Dye, S.P.Whelan, K.Chandran, and T.R.Brummelkamp. 2011. Ebola virus entry requires the cholesterol transporter Niemann-Pick C1. *Nature* 477:340-343.
6. Chirivino, D., L.Del Maestro, E.Formstecher, P.Hupe, G.Raposo, D.Louvard, and M.Arpin. 2011. The ERM proteins interact with the HOPS complex to regulate the maturation of endosomes. *Mol. Biol. Cell* 22:375-385.
7. Cullinane, A.R., A.Straatman-Iwanowska, A.Zaucker, Y.Wakabayashi, C.K.Bruce, G.Luo, F.Rahman, F.Gurakan, E.Utine, T.B.Ozkan, J.Denecke, J.Vukovic, M.Di Rocco, H.Mandel, H.Cangul, R.P.Matthews, S.G.Thomas, J.Z.Rappoport, I.M.Arias, H.Wolburg, A.S.Knisely, D.A.Kelly, F.Muller, E.R.Maher, and P.Gissen. 2010. Mutations in VIPAR cause an arthrogryposis, renal dysfunction and cholestasis syndrome phenotype with defects in epithelial polarization. *Nat. Genet.* 42:303-312.
8. Garg, S., M.Sharma, C.Ung, A.Tuli, D.C.Barral, D.L.Hava, N.Veerapen, G.S.Besra, N.Hacohen, and M.B.Brenner. 2011. Lysosomal trafficking, antigen presentation, and microbial killing are controlled by the Arf-like GTPase Arl8b. *Immunity* 35:182-193.
9. Gissen, P., C.A.Johnson, D.Gentle, L.D.Hurst, A.J.Doherty, C.J.O'Kane, D.A.Kelly, and E.R.Maher. 2005. Comparative evolutionary analysis of VPS33 homologues: genetic and functional insights. *Hum. Mol. Genet.* 14:1261-1270.

10. Gissen, P., C.A.Johnson, N.V.Morgan, J.M.Stapelbroek, T.Forshew, W.N.Cooper, P.J.McKiernan, L.W.Klomp, A.A.Morris, J.E.Wraith, P.McClean, S.A.Lynch, R.J.Thompson, B.Lo, O.W.Quarrell, M.Di Rocco, R.C.Trembath, H.Mandel, S.Wali, F.E.Karet, A.S.Knisely, R.H.Houwen, D.A.Kelly, and E.R.Maher. 2004. Mutations in VPS33B, encoding a regulator of SNARE-dependent membrane fusion, cause arthrogryposis-renal dysfunction-cholestasis (ARC) syndrome. *Nat. Genet.* 36:400-404.
11. Huizing, M., A.Didier, J.Walenta, Y.Anikster, W.A.Gahl, and H.Kramer. 2001. Molecular cloning and characterization of human VPS18, VPS 11, VPS16, and VPS33. *Gene* 264:241-247.
12. Huotari, J. and A.Helenius. 2011. Endosome maturation. *EMBO J.* 30:3481-3500.
13. Jordens, I., M.Fernandez-Borja, M.Marsman, S.Dusseljee, L.Janssen, J.Calafat, H.Janssen, R.Wubbolts, and J.Neefjes. 2001. The Rab7 effector protein RILP controls lysosomal transport by inducing the recruitment of dynein-dynactin motors. *Curr. Biol.* 11:1680-1685.
14. LaGrassa, T.J. and C.Ungermann. 2005. The vacuolar kinase Yck3 maintains organelle fragmentation by regulating the HOPS tethering complex. *J. Cell Biol.* 168:401-414.
15. Liang, C., J.S.Lee, K.S.Inn, M.U.Gack, Q.Li, E.A.Roberts, I.Vergne, V.Deretic, P.Feng, C.Akazawa, and J.U.Jung. 2008. Beclin1-binding UVRAG targets the class C Vps complex to coordinate autophagosome maturation and endocytic trafficking. *Nat. Cell Biol.* 10:776-787.
16. Lo, B., L.Li, P.Gissen, H.Christensen, P.J.McKiernan, C.Ye, M.Abdelhaleem, J.A.Hayes, M.D.Williams, D.Chitayat, and W.H.Kahr. 2005. Requirement of VPS33B, a member of the Sec1/Munc18 protein family, in megakaryocyte and platelet alpha-granule biogenesis. *Blood* 106:4159-4166.
17. Lobingier, B.T. and A.J.Merz. 2012. Sec1/Munc18 protein Vps33 binds to SNARE domains and the quaternary SNARE complex. *Mol. Biol. Cell* 23:4611-4622.
18. Markgraf, D.F., F.Ahnert, H.Arlt, M.Mari, K.Peplowska, N.Epp, J.Griffith, F.Reggiori, and C.Ungermann. 2009. The CORVET subunit Vps8 cooperates with the Rab5 homolog Vps21 to induce clustering of late endosomal compartments. *Mol. Biol. Cell* 20:5276-5289.
19. Messler, S., S.Kropp, V.Episkopou, A.Felici, J.Wurthner, R.Lemke, M.Jerabek-Willemsen, R.Willecke, S.Scheu, K.Pfeffer, and J.U.Wurthner. 2011. The TGF-beta signaling modulators TRAP1/TGFBRAP1 and VPS39/Vam6/TLP are essential for early embryonic development. *Immunobiology* 216:343-350.
20. Nakamura, N., A.Hirata, Y.Ohsumi, and Y.Wada. 1997. Vam2/Vps41p and Vam6/Vps39p are components of a protein complex on the vacuolar membranes and involved in the vacuolar assembly in the yeast Saccharomyces cerevisiae. *J. Biol. Chem.* 272:11344-11349.
21. Nickerson, D.P., C.L.Brett, and A.J.Merz. 2009. Vps-C complexes: gatekeepers of endolysosomal traffic. *Curr. Opin. Cell Biol.* 21:543-551.
22. Ostrowicz, C.W., C.Brocker, F.Ahnert, M.Nordmann, J.Lachmann, K.Peplowska, A.Perz, K.Auffarth, S.Engelbrecht-Vandre, and C.Ungermann. 2010. Defined subunit arrangement and rab interactions are required for functionality of the HOPS tethering complex. *Traffic* 11:1334-1346.
23. Peplowska, K., D.F.Markgraf, C.W.Ostrowicz, G.Bange, and C.Ungermann. 2007. The CORVET tethering complex interacts with the yeast Rab5 homolog Vps21 and is involved in endo-lysosomal biogenesis. *Dev. Cell* 12:739-750.
24. Plemel, R.L., B.T.Lobingier, C.L.Brett, C.G.Angers, D.P.Nickerson, A.Paulsel, D.Sprague, and A.J.Merz. 2011. Subunit organization and Rab interactions of Vps-C protein complexes that control endolysosomal membrane traffic. *Mol. Biol. Cell* 22:1353-1363.
25. Pols, M.S., C.Ten Brink, P.Gosavi, V.Oorschot, and J.Klumperman. 2013a. The HOPS proteins hVps41 and hVps39 are required for homotypic and heterotypic late endosome fusion. *Traffic* 14:219-232.
26. Pols, M.S., E.van Meel, V.Oorschot, C.Ten Brink, M.Fukuda, M.G.Swetha, S.Mayor, and J.Klumperman. 2013b. hVps41 and VAMP7 function in direct TGN to late endosome transport of lysosomal membrane proteins. *Nat. Commun.* 4:1361.
27. Pulipparacharuvil, S., M.A.Akbar, S.Ray, E.A.Sevrioukov, A.S.Haberman, J.Rohrer, and H.Kramer. 2005. Drosophila Vps16A is required for trafficking to lysosomes and biogenesis of pigment granules. *J. Cell Sci.* 118:3663-3673.
28. Rehling, P., T.Darsow, D.J.Katzmann, and S.D.Emr. 1999. Formation of AP-3 transport intermediates requires Vps41 function. *Nat. Cell Biol.* 1:346-353.
29. Rocha, N., C.Kuijl, R.van der Kant, L.Janssen, D.Houben, H.Janssen, W.Zwart, and J.Neefjes. 2009. Cholesterol sensor ORP1L contacts the ER protein VAP to control Rab7-RILP-p150 Glued and late endosome positioning. *J. Cell Biol.* 185:1209-1225.
30. Sato, T.K., P.Rehling, M.R.Peterson, and S.D.Emr. 2000. Class C Vps protein complex regulates

vacuolar SNARE pairing and is required for vesicle docking/fusion. *Mol. Cell* 6:661-671.

31. Seals, D.F., G.Eitzen, N.Margolis, W.T.Wickner, and A.Price. 2000. A Ypt/Rab effector complex containing the Sec1 homolog Vps33p is required for homotypic vacuole fusion. *Proc. Natl. Acad. Sci. U S A* 97:9402-9407.
32. Solinger, J.A. and A.Spang. 2013. Tethering complexes in the endocytic pathway: CORVET and HOPS. *FEBS J.*
33. Starai, V.J., C.M.Hickey, and W.Wickner. 2008. HOPS proofreads the trans-SNARE complex for yeast vacuole fusion. *Mol. Biol. Cell* 19:2500-2508.
34. Stenmark, H. 2009. Rab GTPases as coordinators of vesicle traffic. *Nat. Rev. Mol. Cell Biol.* 10:513-525.
35. van der Kant, R., A.Fish, L.Janssen, H.Janssen, S.Krom, N.Ho, T.Brummelkamp, J.Carette, N.Rocha, and J.Neefjes. 2013. Late endosomal transport and tethering are coupled processes controlled by RILP and the cholesterol sensor ORP1L. *J. Cell Sci.*
36. Vennegoor, C., J.Calafat, P.Hageman, F.van Buitenen, H.Janssen, A.Kolk, and P.Rumke. 1985. Biochemical characterization and cellular localization of a formalin-resistant melanoma-associated antigen reacting with monoclonal antibody NKI/C-3. *Int J. Cancer* 35:287-295.
37. Wickner, W. 2010. Membrane fusion: five lipids, four SNAREs, three chaperones, two nucleotides, and a Rab, all dancing in a ring on yeast vacuoles. *Annu. Rev. Cell Dev. Biol.* 26:115-136.
38. Wurmser, A.E., T.K.Sato, and S.D.Emr. 2000. New component of the vacuolar class C-Vps complex couples nucleotide exchange on the Ypt7 GTPase to SNARE-dependent docking and fusion. *J. Cell Biol.* 151:551-562.
39. Wurthner, J.U., D.B.Frank, A.Felici, H.M.Green, Z.Cao, M.D.Schneider, J.G.McNally, R.J.Lechleider, and A.B.Roberts. 2001. Transforming growth factor-beta receptor-associated protein 1 is a Smad4 chaperone. *J. Biol. Chem.* 276:19495-19502.
40. Zhu, G.D., G.Salazar, S.A.Zlatic, B.Fiza, M.M.Doucette, C.J.Heilman, A.I.Levey, V.Faundez, and S.W.L'hernault. 2009. SPE-39 family proteins interact with the HOPS complex and function in lysosomal delivery. *Mol. Biol. Cell* 20:1223-1240.
41. Zlatic, S.A., K.Tornieri, S.W.L'hernault, and V.Faundez. 2011. Metazoan cell biology of the HOPS tethering complex. *Cell Logist.* 1:111-117.

Supplementary material



Supplemental Figure 1. TGFBRAP1 does not recruit SPE-39, VPS33b, VPS39 and VPS41 to early endosomes. (**A**) MelJuSo cells expressing mRFP-SPE-39 or co-expressing GFP-TGFBRAP1 and mRFP-SPE-39 were fixed and stained with EEA1-antibodies before imaging by confocal microscopy. Scale bar: 10µm. n>100. (**B**) MelJuSo cells expressing mRFP-VPS33b or co-expressing GFP-TGFBRAP1 and mRFP-VPS33b were fixed and stained with EEA1-antibodies before imaging by confocal microscopy. Scale bar: 10µm. n>100. (**C**) MelJuSo cells expressing mRFP-VPS39 or co-expressing GFP-TGFBRAP1 and mRFP-VPS39 were fixed and stained with EEA1-antibodies before imaging by confocal microscopy. Scale bar: 10µm. n>100. (**D**) MelJuSo cells expressing mRFP-VPS41 or co-expressing GFP-TGFBRAP1 and mRFP-VPS41 were fixed and stained with EEA1-antibodies before imaging by confocal microscopy. Scale bar: 10µm. n>100.

chapter SIX

Cholesterol binding molecules MLN64 and ORP1L mark distinct late endosomes with transporters ABCA3 and NPC1

Rik van der Kant[1]
Ilse Zondervan[1]
Lennert Janssen[1]
Jacques Neefjes*

[1]Division of Cell Biology, the Netherlands Cancer Institute, Plesmanlaan 121, 1066CX Amsterdam NL

*Correspondence: j.neefjes@nki.nl, tel. +31-20-5122017, fax +31-20-5122029

Journal of Lipid Research, Volume 54, No.7. August 2013

Abstract

Cholesterol is an essential lipid in eukaryotic cells and is present in membranes of all intracellular compartments. A major source for cellular cholesterol are internalized lipoprotein particles that are transported toward acidic late endosomes and lysosomes (LE). Here the lipoprotein particles are hydrolysed and free cholesterol is redistributed to other organelles. The LE can contain over half of the cellular cholesterol and as a major sorting station contain many cholesterol binding proteins from the ABCA, STARD and ORP families. Here we show that MLN64 (STARD3) and ORP1L define two sub-populations of LE. MLN64 is present on a LE containing the cholesterol transporter ABCA3, whereas ORP1L localizes to another population of LE containing NPC1, a cholesterol exporter. Endocytosed cargo passes through MLN64/ABCA3 positive compartments before it reaches ORP1L/NPC1 positive LE. The MLN64/ABCA3 compartments cycle between LE and plasma-membrane and frequently contact "later" ORP1L/NPC1 containing LE. We propose two stages of cholesterol handling in late endosomal compartments; cholesterol first enters MLN64/ABCA3 positive compartments from where it can be recycled to the plasma membrane, and later, cholesterol enters ORP1L/NPC1 endosomes that mediate cholesterol export to the ER.

Keywords: Cholesterol, late endosome, lysosome, MLN64, STARD3, ORP1L, ABCA3, NPC1

Abbreviations

LE, late endosomal compartment; MLN64, Metastatic Lymph Node 64; NPC1,Niemann Pick disease type C1; ORP1L, Oxysterol binding protein Related Protein 1L; RILP, RAB7-interacting lysosomal protein;

Introduction

Cholesterol is a key component of cellular membranes and is essential for the regulation of membrane rigidity, cellular compartmentalization, enzyme function and the production of steroid hormones (1). A major source of cellular cholesterol is the endocytosis of lipoproteins from the cell surface and subsequent processing of these particles in late endosomal and lysosomal (LE) compartments. At the plasma membrane of cells low density lipoprotein receptors (LDLR) internalize lipoprotein particles by clathrin-coated endocytosis. These lipoprotein particles including VLDL and LDL are a major source of cholesterol in most cells. After initial endocytosis the lipoproteins are transported towards acid LE compartments where cholesteryl esters are hydrolised by acid lipases to generate free unesterified cholesterol (1). This free cholesterol can subsequently be transferred to other compartments such as recycling endosomes, the endoplasmic reticulum (ER), the plasma membrane (PM) and mitochondria (1-4). Late (multivesicular) endosomes can contain over half of the total cellular cholesterol content (5) and many cholesterol-binding proteins localize to these compartments to control the flow of intercellular cholesterol. How the function of these proteins relates to each other, and how they communicate to distribute the LE cholesterol to other compartments is unclear. Metastatic lymph node 64 (MLN64), also known as STARD3, is a lipid binding protein from the steroidogenic acute regulatory protein (StAR)-related lipid transfer domain (START) protein family with two functional domains; a C-terminal domain containing the START domain that projects into the cytoplasm and an N-terminal 4-transmembrane domain (6). MLN64 is reported to be involved in the egress of cholesterol from LE to mitochondria (4;7) and regulates late endosomal tethering and fusion dynamics involving actin (8). Another cholesterol binding protein that controls LE dynamics is the Oxysterol binding protein Related Protein 1L (ORP1L). ORP1L is recruited to LE membranes by binding to the small GTPase RAB7, and is part of a tripartite complex of RAB7-RILP-ORP1L that regulates recruitment of the dynein motor and the HOmotypic fusion and vacuole Protein Sorting (HOPS) complex to late endosomes and thereby minus-end transport and tethering (9-12). Although ORP1L is probably not directly involved in shuttling cholesterol out of the LE, it is able to sense the amount of cholesterol on the cytosolic face of the LE limiting membrane and induces contact sites between LE and the ER to control binding of the dynein motor and the HOPS complex to RAB7-RILP (10, 12). Cholesterol levels thus control positioning and tethering of LE. Another protein associating with the RAB7-RILP complex that controls late endosomal transport is Neuronal ceroid lipofuscinosis protein CLN3. When mutated this proteins causes classical juvenile onset neuronal ceroid lipofuscinosis, a fatal inherited neurodegenerative lysosomal storage disorder where lipopigments accumulate in lysosomes (13). Proteins of the ATP binding cassette class A (ABCA) proteins have also recently been shown to be present in LE compartments due to a conserved targeting motif (14). ABCA proteins are transporters that use ATP to drive translocation of various substrates, including lipids, across membranes. ABCA3 probably functions as lipid pump for the translocation of phospholipids and cholesterol into lysosomal-like organelles (lamellar bodies) (14).The different cholesterol-binding proteins on late endosomes are likely involved in different steps of cholesterol transport and handling, and different diseases are associated to these molecules. Mutations in ABCA3 causes fatal respiratory distress syndrome in newborns probably due to a defect in lamellar

body biogenesis where exocytosis is required for the formation of lipid surface lining layer of the alveolar epithelium of lungs (15). Cholesterol egress from the LE into the ER requires proteins such as Niemann Pick type C proteins 1 (NPC1) and NPC2, that transfer cholesterol from the lumen of the LE into the LE limiting membrane (16;17). Mutations in the Niemann Pick Type C proteins cause a fatal, neurodegenerative disorder where cholesterol accumulates in LE and disturbs transport when the altered cholesterol content is sensed by ORP1L (10).

How cholesterol is transferred from the LE to the ER is debated. Cholesterol could be directly transferred from the LE to the ER (18) possibly mediated by an ER-resident protein of the oxysterol-binding protein family (ORP5) (19). However only approximately 30% LE cholesterol is directly transported from LE to the ER whereas 70% passes through the plasma membrane prior to esterification in the ER (2). LE cholesterol is rapidly moved toward the plasma membrane while re-esterification in the ER shows a 0,5-1h lag arguing against direct LE to ER movement of cholesterol (3). MLN64 has been shown to egress cholesterol from LE to mitochondria even in the absence of functional Niemann-Pick Type C1 proteins (4;7).

Apart from these findings little is known about the exact localization and cross-talk between the different cholesterol sensing and transferring proteins on the LE. Here we addressed the location of MLN64 in relation to ORP1L. We show that MLN64 and ORP1L define two distinct late endosomal compartments. Whereas MLN64 is present in "early" ABCA3 positive late endosomal compartments, ORP1L defines a population of "late" late endosomes labelled by the cholesterol transporter NPC1. The subcompartements possibly reflect sites where LE cholesterol is handled differently in order to ensure proper cellular homeostasis of this essential and complex hydrophobic molecule.

Experimental procedures

Reagents

Rabbit anti-GFP and Rabbit anti-mRFP antibodies were generated in house using purified His-mRFP or His-GFP recombinant proteins, respectively. The rabbit-anti MLN64 serum was generated in house using purified His-START domain of human MLN64. Other antibodies used: anti-NPC1 (Novus Biologicals), rabbit anti-ORP1L (gift from V. Olkkonen [National Public Health Institute, Helsinki, Finland], mouse anti-CD63 (20) , mouse monoclonal anti-EEA1 (BD biosciences), Other antibodies used: anti-HA (Roche), anti-EEA1 (BD biosciences), anti-M6PR (Affinity Bioregeants) and anti-NPC1 (BD biosciences).

Cell culture

MelJuSo cells were cultured in Iscove's modified Dulbecco's medium (IMDM; Invitrogen) supplemented with 8% FCS, SKBR3 cells were cultured in Dulbeco's Modified Eagle Medium (DMEM) supplemented with 8% FCS in a 5% CO_2 humidified culture hood at 37°C.

Microscopy

Transfected cells were fixed 24h post-transfection with 4% formaldehyde in PBS for 30 min and permeabilized for 5 min with 0.05% Triton X-100 in PBS at room temperature. Non-specific

binding of antibodies was blocked by 0.5%BSA in PBS for 40 min, after which cells were incubated with primary antibodies in 0.5%BSA in PBS for 1h at room temperature. Bound primary antibodies were visualized with Alexa-Fluor secondary antibody conjugates (Invitrogen). Cells were mounted in Vectashield mounting medium (Vector Laboratories). For methanol fixation, cells were fixed for 5 minutes in ice-cold methanol subsequently blocked by 0.5%BSA in PBS for 40 min and treated similar to the formaldehyde-fixed samples. All specimens were analyzed by confocal laser-scanning microscopes (TCS-SP1, TCS-SP2, or AOBS; Leica) equipped with HCX Plan-Apochromat 63× NA 1.32 and HCX Plan-Apochromat lbd.bl 63× NA 1.4 oil-corrected objective lenses (Leica). The acquisition software used was LCS (Leica).

Constructs and cloning

RILP and ORP1L constructs have been described previously (9;10;21). YFP-MLN-64 was a kind gift from Dr Alpy (Département de Pahtologie Moléculaire, Insitut de Genetique et de Biologie Moleculaire et Cellulaire, Communauté Urbaine de Strasbourg, France). YFP-MLN64 M307R, N311D was generated using site-directed mutagenesis and sequence verified.

Ovalbumin and LDL uptake and transport

Cells transfected with ORP1L, ΔORD, ΔORDPHDPHD and MLN64, or combinations of these were incubated at 37°C with Alexa647-conjugated ovalbumin (Molecular Probes) or Dil-LDL (Molecular probes, final concentration 20μg/ml) in serum-free medium for 20 minutes. After washing, cells were cultured and fixed after various times of culture and analyzed as described.

Image quantification

Figure 2: a region of interest (vector) was drawn over cells and a histogram showing the intensity over the vector was generated in ImageJ. For the other figures the Manders M1 and M2 coefficients (the percentage of channel A that co-localizes with channel B and reverse) were calculated using the JaCoP plugin in ImageJ.

Results

Localization of endogenous MLN64 on late endosomal compartments and the plasma membrane

To study the endogenous localization of MLN64, we generated a rabbit anti-serum antibody against the C-terminal START-domain of human MLN64. This anti-serum recognized MLN64 by WB (Fig 1A); human MLN64 has a predicted molecular weight of 49kDa. Expression levels of MLN64 are reported to be similar in most tissues with the exception of higher expression in lung and blood cells (8;22). We were unable to detect significant endogenous MLN64 in Hela and MelJuSo cells, but could detect endogenous MLN64 in the breast cancer cell line SKBR3 in which MLN64 is amplified. To study the localization of MLN64 we fixed untransfected and MLN64-YFP transfected SKBR3 cells with paraformaldehyde (PFA), permeabilized cells with Triton-X100 and stained for MLN64 using our antibody. Our antibody recognized high levels of MLN64 in MLN64-YFP transfected cells (Fig 1B). In untransfected cells, endogenous MLN64

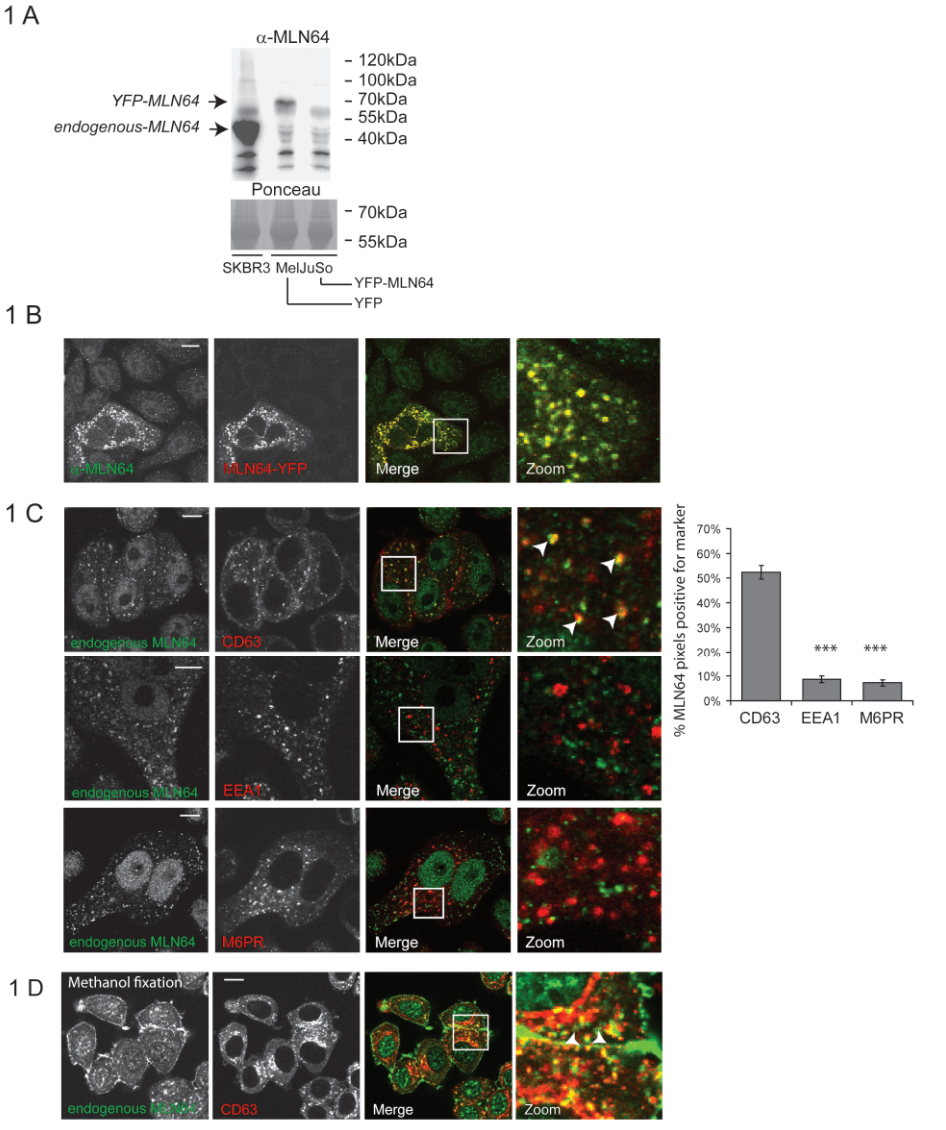


Figure 1. Endogenous MLN64 on late endosomal compartments and the plasma membrane. (**A**) Lysates of SKBR3 and MelJuSo cells transfected with YFP-MLN64 or YFP were analyzed by SDS-PAGE and WB before probing with anti-MLN64 antibodies, position of marker proteins as indicated (**B**) SKBR3 cells un-transfected (upper cells) or transfected with MLN64-YFP (lower left) were paraformaldehyde (PFA) fixed, permeabilized and immunolabelled by anti-MLN64 antibodies before imaging by confocal microscopy. Zoom-ins of merged pictures indicated. Scale bar: 10μm. n>100. (**C**) SKBR3 cells were PFA fixed, permeabilized and stained by anti-MLN64 antibodies (green) and anti-CD63, anti-EEA1 or anti-M6PR antibodies (red) before imaging by confocal microscopy. Zoom-ins of merged pictures indicated. White arrow heads indicate co-localization Scale bar: 10μm. Right panel: quantification of colocalization using Manders coefficient. Plotted is the percentage of MLN64 signal also positive for the indicated markers. n>25, *** indicates p<0,001 (**D**) SKBR3 cells were fixed by methanol and stained by anti-MLN64 antibodies (green) and anti-CD63 antibodies (red) and imaged by confocal microscopy. Zoom-ins of merged pictures indicated. Scale bar: 10μm. n>100. White arrow heads indicate plasma membrane location.

showed a vesicular staining pattern in addition to a nuclear background staining. Vesicular staining was not observed when cells were stained with pre-immune serum (Fig S1). Previous studies employing tagged-MLN64 revealed that MLN64 is a late endosomal protein (4;6-8).We could confirm the localization of endogenous MLN64 at CD63 marked late endosomes (Fig 1C). MLN64 was absent from early endosomes (EEA1 labeled) or Mannose-6-Phosphate-receptor (M6PR)-positive vesicles (Fig 1C). Fixation and permeabilization can affect epitope accessibility (23). As an alternative for PFA/Triton-X100 fixation methanol can also be used. Under these conditions we again observed a vesicular staining of MLN64 that colocalized with CD63. In addition we detected staining for MLN64 at the plasma membrane (PM) (Fig 1D). Our data suggest that endogenous MLN64 is present at the plasma membrane and in late endosomes.

MLN64 cycles to the plasma membrane

Although lysosomes are the supposedly end-stage for most cargo internalized from the plasma membrane, many lysosomal proteins are found at the plasma membrane as the result of late endosomal-plasma membrane fusion. These include LE markers such as CD63 and CD83 that are usually rapidly recycled back to late endosomes by targeting signals in their cytoplasmic tail (24;25). When we expressed YFP-tagged MLN64 at high levels, we could observe a small fraction at the plasma membrane (Fig. 2A). To further test that MLN64 cycles between the plasma membrane and LE, we blocked endocytosis by expression of dominant negative dynamin (DN-dynamin) (26). MLN64 accumulated at the plasma membrane when endocytosis was blocked (Fig 2B).

ORP1L and MLN64 localize to distinct late endosomal sub-populations

MLN64 is proposed to regulate late endosomal dynamics and silencing of MLN64 results in dispersion of late endosomes and a delay in degradation of endosomal cargo (8). Another cholesterol-binding protein that controls late endosomal dynamics is ORP1L. ORP1L regulates late endosomal transport by recruiting the ER protein VAP-A that removes dynein from LE (10). ORP1L also regulates multi-vesicular body formation (27). As both ORP1L and MLN64 localize to late endosomes, we hypothesized that these could act in assembly to control cholesterol dependent processes at LE. However, we observed that only a minor fraction of ORP1L and MLN64 co-localized on the same vesicles, whereas the majority of ORP1L and MLN64 localized to different compartments (Fig 3A). ORP1L was located on (and clustered) small CD63-positive LE whereas MLN64 was localized on other enlarged late endosomal compartments also containing the LE marker CD63. In fact, these cholesterol-sensing proteins subdivided the late endosomes. MLN64- and ORP1L-vesicles were located adjacent to each other, while colocalization was observed on only a few vesicles. To further study the dynamics of the ORP1L and MLN64 vesicles, we performed live-cell imaging on cells overexpressing ORP1L and MLN64 (Movie M1, Fig 3B). Again, we observed mutual exclusion of ORP1L and MLN64 on vesicles that closely localized. Vesicles with ORP1L moved together with vesicles containing MLN64 over long distances in the periphery of cells, indicating some sort of interaction or tethering between these vesicles. To further verify these findings we expressed ORP1L in cells and stained for endogenous MLN64 or expressed MLN64 while staining for ORP1L (Fig S2). Again a predominant mutual-exclusion of closely adjacent vesicles of both types was observed.

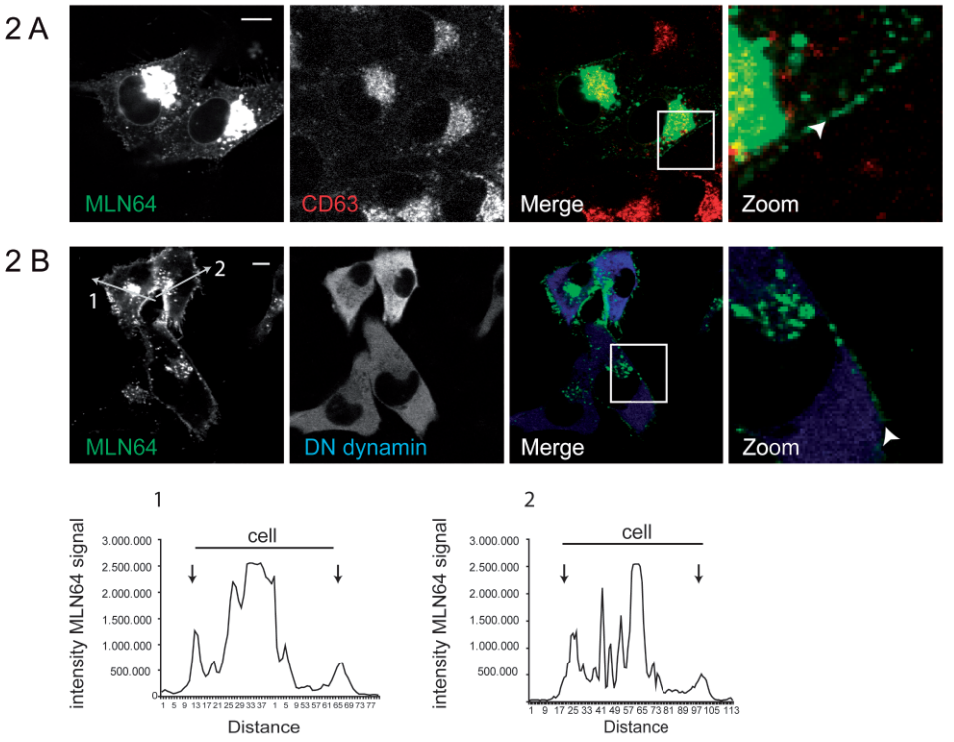


Figure 2. MLN64 cycles to the plasma membrane. (**A**) MelJuSo cells over-expressing high levels of MLN64-YFP (indicated MLN64) were immunolabelled by anti-CD63 antibodies and imaged by confocal microscopy. Zoom-ins of merged pictures indicated. Scale bar: 10µm. n>100. White arrow heads indicate plasma membrane staining. (**B**) MelJuSo cells expressing MLN64-YFP in combination with dominant-negative dynamin were PFA fixed permeabilized and immunolabelled with anti-dynamin antibodies before imaging by confocal microscopy. Zoom-ins of merged pictures indicated. Scale bar: 10µm. n>100. White arrow heads indicate plasma membrane location. Intensity histograms over indicated lines for the MLN64 channel are shown. Black arrows indicate peaks originating from plasma membrane staining at the edge of cells.

ORP1L is part of a tripartite complex of RAB7-RILP-ORP1L. As ORP1L and MLN64 are on different vesicles, we wondered whether RILP and MLN64 are also mutually exclusive. Indeed whereas ORP1L and RILP localize to same vesicles (Fig 3C, upper panel), RILP and MLN64 localized to different late endosomal sub-populations (Fig 3C, lower panel). Together, our data suggest that MLN64 and RAB7-RILP-ORP1L localize to distinct late endosomal sub-populations.

Cholesterol binding ORD domain of ORP1L is involved in spatial separation of ORP1L and MLN64 within late endosomes

ORP1L and MLN64 both contain a cholesterol sensing domain that can bind cholesterol at the cytosolic site of the late endosomal limiting membrane. To test whether these domains are important for the mutual exclusion of MLN64 and ORP1L within the late endosomal compartment, we expressed proteins with mutations in these domains. The START domain of MLN64 requires two amino-acids (M307 and N311) for cholesterol binding, and a MLN64 M307R,

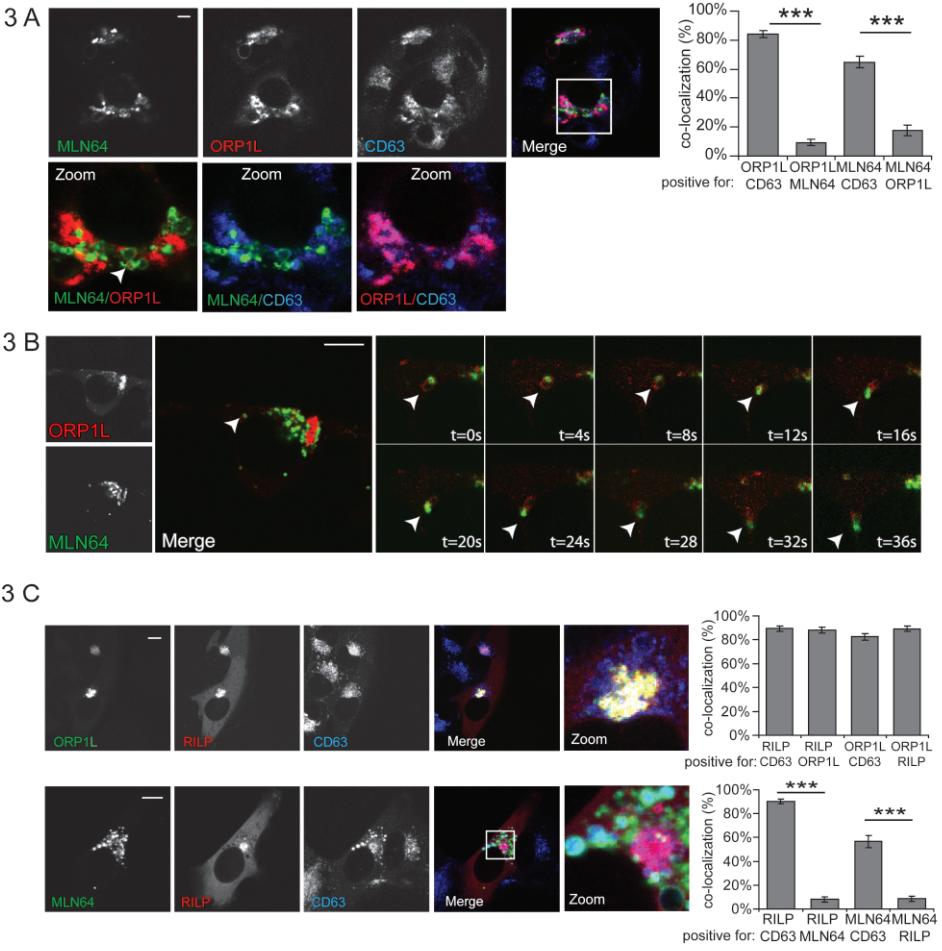


Figure 3. ORP1L and MLN64 localize to late endosomal sub-populations. (**A**) MelJuSo cells expressing MLN64-YFP (green) and mRFP-ORP1L (red) were PFA fixed, permeabilized and immunolabelled with anti-CD63 antibodies (blue) before imaging by confocal microscopy. Zoom-ins of merged pictures indicated. Scale bar: 10µm. n>100. White arrow head indicates a vesicle positive for both MLN64 and ORP1L. Right panel: quantification of colocalization using Manders coefficient. Plotted is the percentage of signal A that is also positive for signal B for the indicated combinations. n>25, *** indicates p<0,001. (**B**) MelJuSo cells expressing MLN64-YFP (green) and ORP1L-mRFP (red) were imaged by time-lapse confocal microscopy and merged zoomed snapshots at different time points are shown (right panel). White arrow heads indicate MLN64-positive and ORP1L positive-vesicles interacting over prolonged times. Images correspond to Movie M1. (**C**) MelJuSo cells expressing ORP1L-GFP and mRFP-RILP (upper panel) or expressing MLN64-YFP (green) and mRFP-RILP (red) (lower panel) were PFA fixed, permeabilized and immunolabelled with anti-CD63 antibodies (blue) before imaging by confocal microscopy. Zoom-ins of merged pictures indicated. Scale bar: 10µm. Right panel: quantification of colocalization using Manders coefficient. Plotted is the percentage of signal A that is also positive for signal B for the indicated combinations. n>25, *** indicates p<0,001.

N311D mutation has been reported to be deficient in cholesterol binding (8). We verified the late endosomal location of a MLN64(M307R, N311D)-YFP construct (Fig 4A). Expression of this construct with ORP1L again yielded mutual exclusion of both proteins within late endosomes (Fig 4B, upper panel) suggesting that cholesterol binding by the MLN64 START domain in not essential for spatial segregation of MLN64 and ORP1L. We then tested whether the cholesterol binding ORD domain of ORP1L is involved by co-expressing a truncation mutant of ORP1L missing the ORD domain (ORP1L-ΔORD) and MLN64. Again a predominant exclusion of both proteins within LE could be observed (Fig 4B, middle panel). However, In about 20% of cells we observed enlarged vesicles in the periphery of cells that were positive for both MLN64 and ORP1L-ΔORD. In addition, under these conditions of ORP1L-ΔORD expression the MLN64 positive LE clustered (Fig 4B and S3). ORP1L has two conformations on the late endosomal membrane, the ORP1L-ΔORD mutant reflects a cholesterol-unbound conformation whereas ORP1L-ΔORDPHDPHD reflects a membrane-bound conformation of the ORD domain which occurs when LE cholesterol is high (10). Upon co-expression of this ORP1L mutant with MLN64, MLN64 vesicles did not label for ORP1L-ΔORDPHDPHD. However, most ORP1L-ΔORDPHDPHD endosomes now acquired low levels of MLN64 suggesting fusion and retention of the two proteins in a fused compartment (Fig 4B, lower panel). We validated our observations by expressing tagged-ORP1L-ΔORDPHDPHD in SKBR3 cells and staining for endogenous MLN64 (Fig 4C). Again, MLN64 localized to ORP1L-ΔORDPHDPHD positive vesicles. Correct expression at expected molecular weight of all ORP1L and MLN64 mutants was verified by western blotting (Fig S4). Our data indicate that the mutual exclusion of ORP1L and MLN64 within the LE compartment involves the cholesterol binding domain of ORP1L, but not cholesterol binding by the START domain of MLN64.

MLN64 defines an early late endosomal compartment preceding ORP1L-containing late endosomes

If MLN64 and ORP1L define two LE subcompartments, how are these related? We expressed MLN64 and ORP1L in cells before feeding cells with fluorescent-LDL to study the trafficking of LDL through these compartments (Fig 5A). At early time-points (20 minutes pulse followed by 30 and 60 minutes chase) MLN64 positive vesicles acquired the fluorescent LDL (Fig 5A). At later time points (3h and 5h after the original pulse) the LDL accumulated in ORP1L vesicles while the signal decreased in MLN64 vesicles. We repeated these experiments using fluorescent-ovalbumin as a fluid-phase endocytosis marker (Fig 5B). Again at early time-points (20 minutes pulse followed by 30 and 60 minutes chase) MLN64 positive vesicles acquired the fluorescent ovalbumin (Fig. 5A, 5B) while at later time points (3h and 5h after the original pulse), the ovalbumin had left the MLN64 positive vesicles and entered ORP1L positive vesicles. These data suggest that internalized cargo first enters MLN64 containing late endosomal compartments and subsequently enters ORP1L containing compartments. During live-imaging, we again observed extensive co-trafficking of MLN64 and ORP1L positive vesicles in the cell periphery after 3 hours of pulse with fluorescent-ovalbumin (Fig. 5C, Movie M2 and M3). These data also suggest that endocytosed cargo reaches “early” (MLN64 positive) late endosomal compartments that transfer cargo to “later” (ORP1L positive) late endosomes.

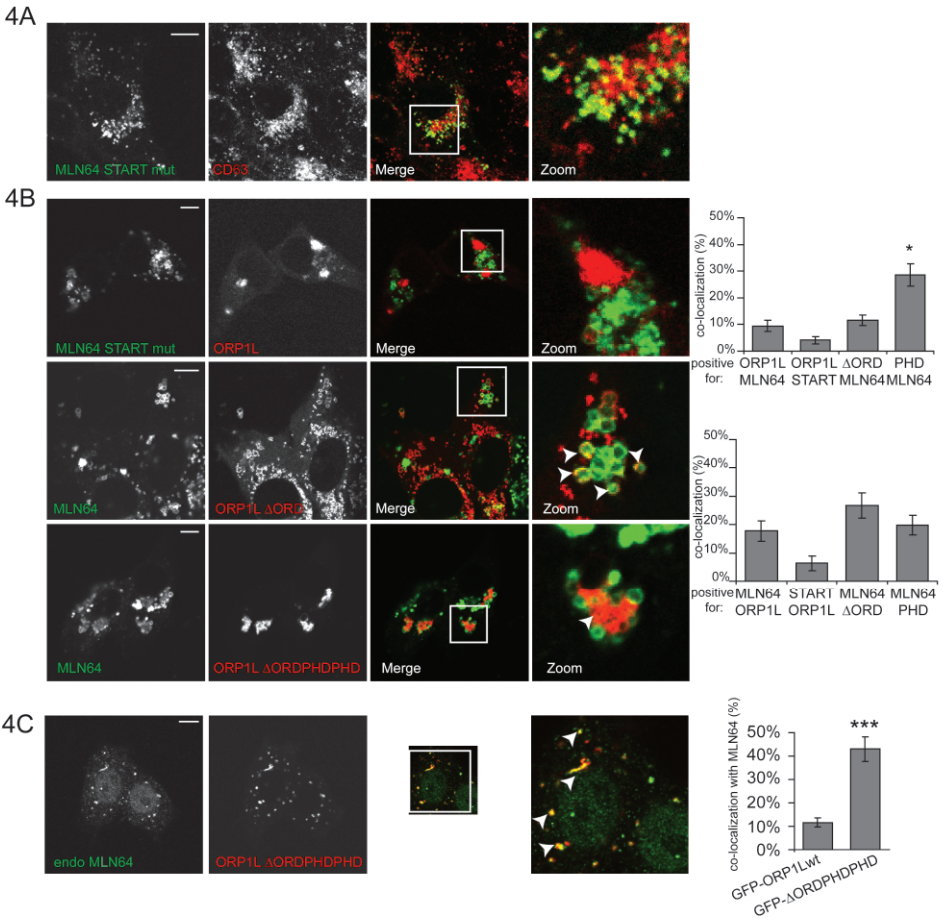


Figure 4. The role of the cholesterol-binding domain of ORP1L and MLN64 on localization. (**A**) Upper panel: MelJuSo cells expressing MLN64(M307R, N311D)-YFP were PFA fixed, permeabilized and immunolabelled with anti-CD63 antibodies (red) before imaging by confocal microscopy. Zoom-ins of merged pictures indicated. Scale bar: 10µm. n>100. (**B**) MelJuSo cells expressing MLN64(M307R, N311D)-YFP (green) and mRFP-ORP1L (red) (upper panel) or expressing YFP-MLN64 (green) together with mRFP-ORP1LΔORD (red) (middle panel) or mRFP-ORP1LΔORDPDHPHD (red) (lower panel) were PFA fixed and imaged by confocal microscopy. Zoom-ins of merged pictures indicated. Scale bar: 10µm. Right panel: quantification of colocalization using Manders coefficient. Plotted is the percentage of signal A that is also positive for signal B for the indicated combinations. n>25. * indicates p<0,05. Abbreviations used: START; MLN64(M307R, N311D), ΔORD; ORP1LΔORD, PHD; ORP1LΔORDPHDPHD. (**C**) SKBR3 cells expressing mRFP-ORP1LΔORDPHDPHD (red) were PFA fixed, permeabilized with Triton-X100, stained with an MLN64-antibody and imaged by confocal microscopy. Zoom-ins of merged pictures indicated. Scale bar: 10µm. White arrow heads indicate vesicle positive for both endogenous MLN64 and mRFP-ORP1LΔORDPHDPHD. Right panel: quantification of colocalization using Manders coefficient. Plotted is the percentage of signal of ORP1Lwt or ORP1LΔORDPHDPHD that is also positive for endogenous MLN64. n>25, *** indicates p<0,001.

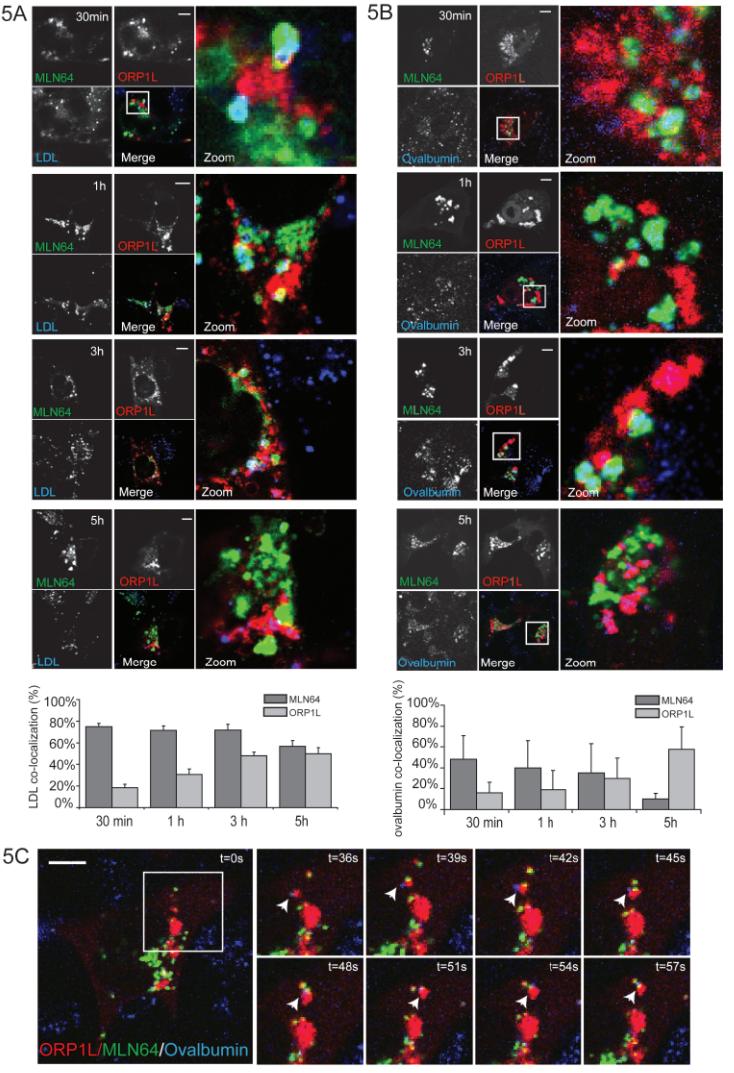


Figure 5. Endocytic cargo passes from a MLN64 positive compartment to an ORP1L positive compartment. (**A**) MelJuSo cells expressing MLN64-HA (green) and GFP-ORP1L (red) were incubated with Dil-LDL (blue) for 20 minutes (pulse) followed by a chase for indicated time points. Cell were then PFA fixed, permeabilized and immunolabelled with anti-HA antibodies (green). Zoom-ins of merged pictures indicated. Scale bar: 10µm. Lower panel; Localization of Dil-LDL in HA-MLN64 or GFP-ORP1L vesicles was quantified using Manders coefficient (the percentage of blue pixels (LDL) overlapping with green (MLN64) or red (ORP1L) pixels). n>25. (**B**) MelJuSo cells expressing MLN64-YFP (green) and mRFP-ORP1L (red) were incubated with Cy5-ovalbumin (blue) for 20 minutes (pulse) followed by a chase for indicated time points. Zoom-ins of merged pictures indicated. Scale bar: 10µm. n>100. Lower panel; Localization of Cy5-Ovalbumin in YFP-MLN64 or mRFP-ORP1L vesicles was quantified using Manders coefficient (the percentage of blue pixels (Ovalbumin) overlapping with green (MLN64) or red (ORP1L) pixels). n>15. (**C**) MelJuSo cells expressing MLN64-YFP (green) and ORP1L-mRFP (red) incubated with Cy5-ovalbumin (blue) for 20 minutes (pulse) followed by a chase for 3 hours were imaged by time-lapse confocal microscopy and merged zoomed snapshots at different time points are shown (right panel). White arrow head indicates MLN64-positive, ORP1L-positive and Ovalbumin-positive vesicles interacting over prolonged times. Images correspond to Movie M2.

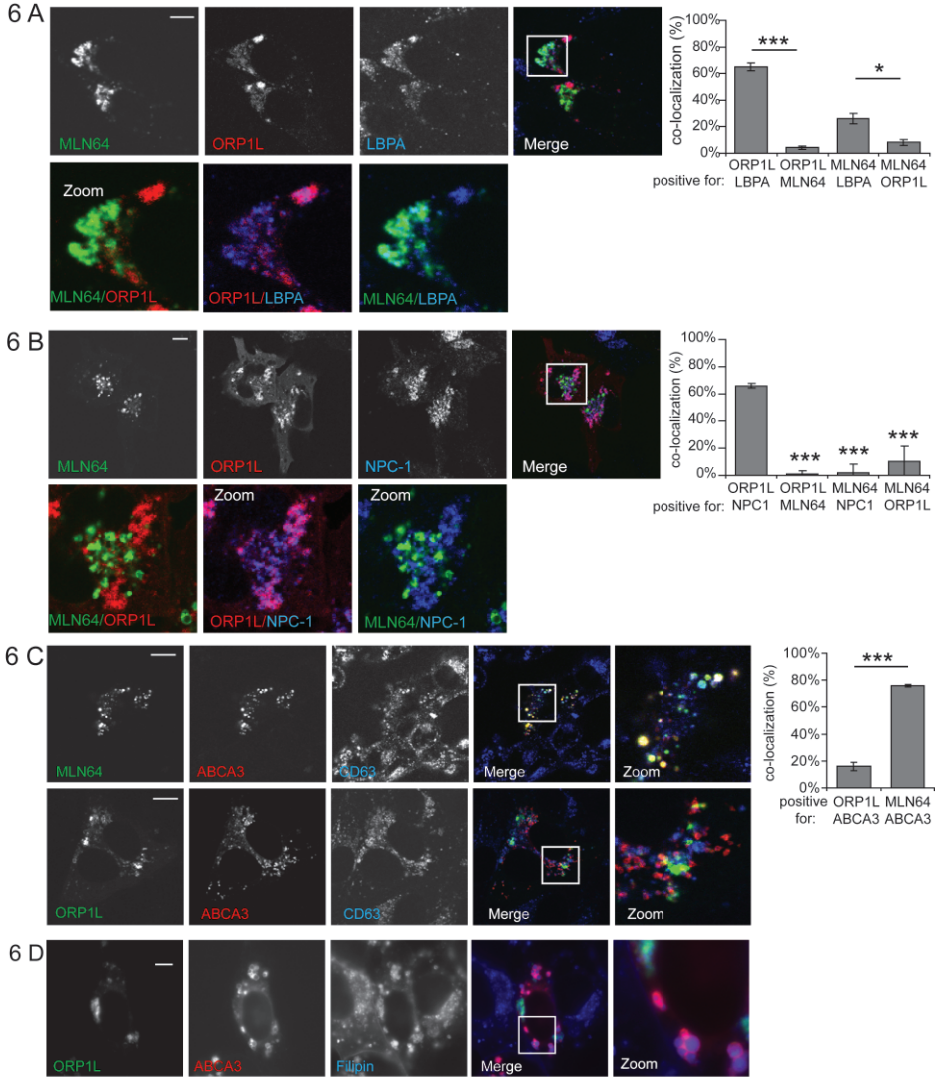


Figure 6. Defining localization of late endosomal cholesterol handling proteins. MelJuSo cells expressing MLN64-YFP (green) and m-RFP-ORP1L (red) were PFA fixed, permeabilized and immunolabelled with anti-LBPA antibodies. (**A**) or anti-NPC1 antibodies (**B**) and imaged by confocal microscopy. Zoom-ins of merged pictures indicated. Scale bar: 10µm. Right panel: quantification of colocalization using Manders coefficient. Plotted is the percentage of signal A that is also positive for signal B for the indicated combinations. n>25, * indicates p<0,05, *** indicates p<0,001. (**C**) Upper panel: MelJuSo cells expressing MLN64-mRFP (green) and GFP-ABCA3 (red) were PFA fixed, permeabilized and immunolabelled with anti-CD63 antibodies. Lower panel: MelJuSo cells expressing mRFP-ORP1L (green) and GFP-ABCA3 (red) were PFA fixed, permeabilized and immunolabelled with anti-CD63 antibodies. Right panel: quantification of colocalization using Manders coefficient. Plotted is the percentage of signal A that is also positive for signal B for the indicated combinations. n>25. (**D**) MelJuSo cells expressing MLN64-mRFP (green) and GFP-ABCA3 (red) were PFA fixed, permeabilized and immunolabelled with Filipin for cholesterol staining followed by analysis by wide-field microscopy.

MLN64 and ORP1L localize with different late endosomal cholesterol pumps ABCA3 and NPC1

Cholesterol metabolism in late endosomes is regulated by a number of cholesterol binding and transporting proteins. Regulators also include lipids such as lysobisphosphatidic acid (LBPA) that have been suggested to regulate cholesterol levels in LE (28). LBPA is exclusively found in late endosomes, and we wondered whether it would localize to MLN64 positive, ORP1L positive or both LE compartments. We stained ORP1L and MLN64 expressing cells with an antibody against LBPA (Fig 6A). A fraction of both compartments labelled for LBPA. Cholesterol egresses from LE by the action of the Niemann Pick 1 protein (NPC1) (16;18) and acts upstream from ORP1L (10). We labelled cells for NPC1 and observed that NPC1 almost exclusively localized to ORP1L positive vesicles while being absent from MLN64 positive late endosomes (Fig 6B). Members of the ABCA family can pump cholesterol across membranes and localize to late endosomes and the PM (14;29). Similar to MLN64, ABCA3 levels are high in lung (15). MLN64 and ABCA3 co-localized on CD63 positive LE (Fig 6C). Unlike NPC1, ABCA3 did not localize to ORP1L-positive LE (Fig 6C). ORP1L vesicles represent cholesterol-rich endosomes (10) and overexpression of MLN64 also accumulates cholesterol in enlarged MLN64-positive compartments (4;6-8) data not shown). We wondered whether ABCA3 would also label vesicles accumulating cholesterol, like MLN64. We stained cells transfected with ORP1L and ABCA3 with filipin to detect free cholesterol and observed that also the enlarged ABCA3-positive vesicles were loaded with cholesterol (Fig 6D). In assembly our data indicate that MLN64 and ABCA3 are cholesterol binding proteins on cholesterol-rich late endosomal compartments preceding later late endosomes in which NPC1 and ORP1L act together to coordinate cholesterol-egress and late endosomal transport.

Discussion

Egress of cholesterol from late endosomes requires the coordinated action of multiple cholesterol binding and transporting molecules present on location. Here we studied two proteins with cholesterol sensing capabilities at the cytosolic leaflet of LE that regulate late endosomal dynamics, MLN64 and ORP1L. We show that these proteins locate to two late endosomal subpopulations. MLN64 is a membrane integrated protein and we show that it cycles with vesicles between LE and the PM and accumulates at the PM when endocytosis is blocked. This is similar to other late endosomal protein such as CD63, CD83 and HLA-DM (24;25;30;31;32). LDL and fluid phase cargo first enters MLN64-positive LE before transport into ORP1L-positive LE, defining MLN64-positive LE are “early” late endosomes and ORP1L-positive LE as “late” late endosomes. ORP1L is recruited to LE endosomes by the small GTPase RAB7 which also recruits the RAB7 interacting lysosomal protein (RILP) to membranes. RILP recruits the dynein motor for minus-end transport to late endosomes, and overexpression of RILP induces strong clustering of LE vesicles near the microtubule organizing centre (20). Conversely silencing of RILP or a dominant negative mutant of RILP (20) results in the scattering of endosomes such as has been observed for MLN64 depletion indicating that these may be representing similar processes. Yet we find that RILP and MLN64 are not on the same vesicles. This supports a observation by

Holtta-Vuori and colleagues showing that RILP expression was unable to rescue the scattering of DiL-LDL labelled endosomes in MLN64 depleted cells (8). In assembly, our data indicates that the CD63 containing LE can be subdivided into a subpopulation of MLN64-positive LE and a later subpopulation of late endosomes marked by RAB7-RILP-ORP1L.

The ORP1L- and MLN64-positive sub-populations displayed frequent contacts over longer periods of time (Fig 3B, supplemental movies). We also observed a small fraction of LE containing both MLN64 and ORP1L. This can be expected when cargo is transferred from MLN64- to ORP1L-positive late endosomes by kiss-and-run events or alternatively by fusion of MLN64 containing LE with ORP1L positive vesicles and fast sorting away from membrane embedded MLN64. We have no evidence that MLN64 actively dissociates ORP1L from membranes. MLN64 has been proposed to promote endosomal tethering between endosomes via actin (8) and this might explain the interactions between ORP1L and MLN64 endosomes over long periods of time in living cells. If ORP1L and MLN64 positive vesicles are able to (partially) fuse to exchange cargo, how is their spatial separation then achieved? A possible explanation might be fast tubulation and fission events that separates MLN64 and ORP1L vesicles quickly after they have formed a hybrid-organelle. Tubulation and fission depend on the coordinated action of dynein and kinesin motors (32;33) and ORP1L controls the recruitment of dynein motors to LE (10). ORP1L allows binding of the dynein motor under high LE cholesterol conditions, but changes conformation when cholesterol is low in order to remove the dynein-motor and allow for plus-end transport of LE by the kinesin motor (10). We observed that expression of an ORP1L mutant (ORP1LΔORDPHDPHD) that stabilizes dynein motor binding to LE induced co-localization of MLN64 on ORP1L ΔORDPHDPHD positive late endosomes. This might indicate that MLN64 and ORP1L vesicles are normally separated by the fission opposing actions of kinesin and dynein motor activities, a process controlled by functional ORP1L. Similarly this might explain why the expression of ORP1L ΔORD, that prevents dynein motor recruitment and therefore might disturb fission events, induces enlarged vesicles also positive for MLN64.

What is the role for the different sub-populations of late endosomes? If LE are separated in two sub-populations that precede each other and associate with different cholesterol sensing proteins, they possibly have different roles in cholesterol trafficking, transfer and distribution. ORP1L and the cholesterol transporter NPC1 localize on a subset of LE while MLN64 and the cholesterol transporter ABCA3 localize to another LE subpopulation. The ORP1L/NPC1 vesicles might reflect a final stage in the internalization of LDL and transport of cholesterol from LE to the ER for further cellular distribution (10;17;19). Based on our observations and previous literature we propose that the MLN64/ABCA3-positive late endosomes reflect an earlier stage in late endosomal maturation where LDL is first hydrolysed and where free cholesterol can still be recycled back to the PM and/or cholesterol can be effluxed from the cell via apolipoproteins. The exact function of ABCA3, which supposedly pumps lipids back into the lysosome (34), is unknown. ABCA3 might import cholesterol or other lipids required from laminar-body biogenesis from other donor organelles into the LE (Fig. 7) or ABCA3 might be involved in the recycling of lipids from organelles such as mitochondria into LE where these then become available for redistribution to other compartments by NPC1-ORP5 (19) or Hrs

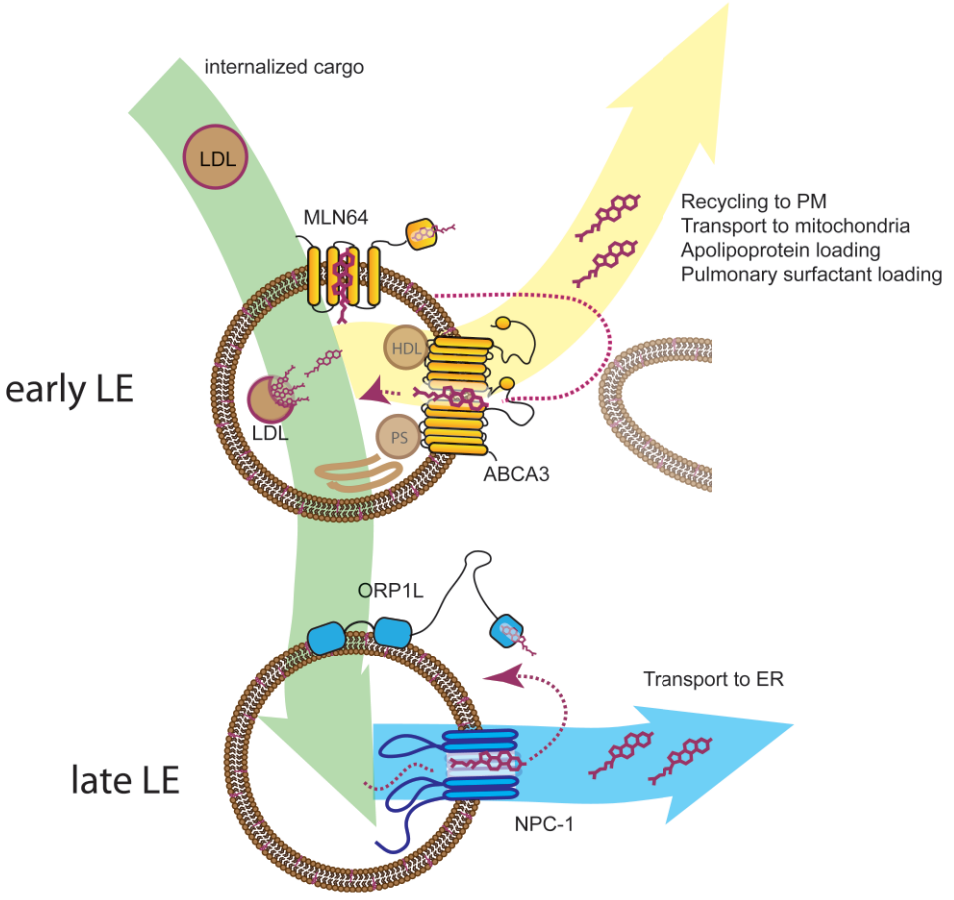


Figure 7. Model of cholesterol dynamics in MLN64/ABCA3 and ORP1L/NPC1 vesicles. LDL particles derived from internalization enter via early endosomes into a MLN64/ABCA3 positive "early" late endosome where LDL can be hydrolysed and cholesterol released. From here cholesterol can be recycled to the plasma membrane by the action of MLN64/ABCA3 vesicles. Alternatively cholesterol is further transported to ORP1L/NPC1 positive "late" LE that can contact the ER to export cholesterol from the LE to the ER for further distribution throughout the cell.

(35). Alternatively ABCA3 might be involved in the loading of free LE cholesterol or other lipids onto HDL or pulmonary surfactant lipoprotein particles thereby decreasing LE lipid load. ABCA3 has been shown to be involved in early steps of late endosomal biogenesis before (15) and both MLN64 and ABCA3 have higher expression in lung where ABCA3 has been shown to be important for the secretion of late endosomal lipids at the PM. Cholesterol destined for the mitochondria passes through the PM (36), MLN64 is involved in the egress of cholesterol from LE to mitochondria (4) and this process is independent of NPC1 (7). Indicating that MLN64 may be involved in the trafficking of cholesterol upstream of NPC1- and ORP1L-containing late endosomes as an additional step for LE cholesterol export. The existence of two consecutive

late endosomal compartments, each different in cholesterol handling to donor compartments, might explain earlier observations that one pool of LE cholesterol is quickly transported to the plasma membrane whereas another pool of cholesterol exist LE to reach the ER slower (2;3;18) and that NPC2 can function in cholesterol delivery to mitochondria independent of NPC1 (37).

Increased levels of MLN64 such as observed in breast cancer and prostate cancer (38-41) might stimulate the transfer of cholesterol from LE to mitochondria where steroidgenesis occurs to produce hormones such as progesterone, estrogen and testosterone required for tumor growth. Conversely this would result in a decrease of cholesterol traffic towards "later" late endosomes and the ER. Indeed over-expression of MLN64 in macrophages increases cholesterol efflux and prevents increases in ER cholesterol esterification in response to acetylated LDL inducing an anti-artherogenic lipid phenotype (42).

In summary, MLN64 and ORP1L define two-subpopulations of late endosomes that precede each other in maturation stages. The cholesterol influx pump ABCA3 is present on MLN64-positive "early" late endosome and the cholesterol effluxer NPC1 is present on ORP1L-positive later late endosomes (Fig. 7). MLN64/ABCA3 vesicles can cycle to the plasma-membrane whereas ORP1L/NPC1 vesicles reflect a later stage in endocytosis. Together our findings indicate that these late endosomal sub-populations define different states of cholesterol handling.

Acknowledgements

We thank V. Olkkonen and F Alpy for providing reagents. This work was supported by grants from NWO-TOP and the ERC.

Reference List

1. Ikonen E. Cellular cholesterol trafficking and compartmentalization. Nat Rev Mol Cell Biol 2008; 9(2):125-138.
2. Neufeld EB, Cooney AM, Pitha J et al. Intracellular trafficking of cholesterol monitored with a cyclodextrin. J Biol Chem 1996; 271(35):21604-21613.
3. Lange Y, Ye J, Chin J. The fate of cholesterol exiting lysosomes. J Biol Chem 1997; 272(27):17018-17022.
4. Zhang M, Liu P, Dwyer NK et al. MLN64 mediates mobilization of lysosomal cholesterol to steroidogenic mitochondria. J Biol Chem 2002; 277(36):33300-33310.
5. Mobius W, van Donselaar E, Ohno-Iwashita Y et al. Recycling compartments and the internal vesicles of multivesicular bodies harbor most of the cholesterol found in the endocytic pathway. Traffic 2003; 4(4):222-231.
6. Alpy F, Stoeckel ME, Dierich A et al. The steroidogenic acute regulatory protein homolog MLN64, a late endosomal cholesterol-binding protein. J Biol Chem 2001; 276(6):4261-4269.
7. Charman M, Kennedy BE, Osborne N, Karten B. MLN64 mediates egress of cholesterol from endosomes to mitochondria in the absence of functional Niemann-Pick Type C1 protein. J Lipid Res 2010; 51(5):1023-1034.
8. Holtta-Vuori M, Alpy F, Tanhuanpaa K, Jokitalo E, Mutka AL, Ikonen E. MLN64 is involved in actin-mediated dynamics of late endocytic organelles. Mol Biol Cell 2005; 16(8):3873-3886.
9. Johansson M, Rocha N, Zwart W et al. Activation of endosomal dynein motors by stepwise assembly of Rab7-RILP-p150Glued, ORP1L, and the receptor betalll spectrin. J Cell Biol 2007; 176(4):459-471.
10. Rocha N, Kuijl C, van der Kant R et al. Cholesterol sensor ORP1L contacts the ER protein VAP to control Rab7-RILP-p150 Glued and late endosome positioning. J Cell Biol 2009; 185(7):1209-1225.
11. Johansson M, Lehto M, Tanhuanpaa K, Cover TL, Olkkonen VM. The oxysterol-binding protein homologue ORP1L interacts with Rab7 and alters functional properties of late

endocytic compartments. Mol Biol Cell 2005; 16(12):5480-5492.

12. van der Kant R, Fish A, Janssen L, Janssen H et al. Late endosomal transport and tethering are coupled processes controlled by RILP and the cholesterol sensor ORP1L. J Cell Science; in press
13. Uusi-Rauva K, Kyttala A, van der Kant R et al. Neuronal ceroid lipofuscinosis protein CLN3 interacts with motor proteins and modifies location of late endosomal compartments. Cell Mol Life Sci 2012; 69(12):2075-2089.
14. Beers MF, Hawkins A, Shuman H et al. A novel conserved targeting motif found in ABCA transporters mediates trafficking to early post-Golgi compartments. J Lipid Res 2011; 52(8):1471-1482.
15. Cheong N, Zhang H, Madesh M et al. ABCA3 is critical for lamellar body biogenesis in vivo. J Biol Chem 2007; 282(33):23811-23817.
16. Naureckiene S, Sleat DE, Lackland H et al. Identification of HE1 as the second gene of Niemann-Pick C disease. Science 2000; 290(5500):2298-2301.
17. Mukherjee S, Maxfield FR. Lipid and cholesterol trafficking in NPC. Biochim Biophys Acta 2004; 1685(1-3):28-37.
18. Underwood KW, Andemariam B, McWilliams GL, Liscum L. Quantitative analysis of hydrophobic amine inhibition of intracellular cholesterol transport. J Lipid Res 1996; 37(7):1556-1568.
19. Du X, Kumar J, Ferguson C et al. A role for oxysterol-binding protein-related protein 5 in endosomal cholesterol trafficking. J Cell Biol 2011; 192(1):121-135.
20. Vennegoor C, Rumke P. Circulating melanoma-associated antigen detected by monoclonal antibody NKI/C-3. Cancer Immunol Immunother 1986; 23(2):93-100.
21. Jordens I, Fernandez-Borja M, Marsman M et al. The Rab7 effector protein RILP controls lysosomal transport by inducing the recruitment of dynein-dynactin motors. Curr Biol 2001; 11(21):1680-1685.
22. Wu C, Orozco C, Boyer J et al. BioGPS: an extensible and customizable portal for querying and organizing gene annotation resources. Genome Biol 2009; 10(11):R130.
23. Schnell U, Dijk F, Sjollema KA, Giepmans BN. Immunolabeling artifacts and the need for live-cell imaging. Nat Methods 2012; 9(2):152-158.
24. Pols MS, Klumperman J. Trafficking and function of the tetraspanin CD63. Exp Cell Res 2009; 315(9):1584-1592.
25. Klein E, Koch S, Borm B et al. CD83 localization in a recycling compartment of immature human monocyte-derived dendritic cells. Int Immunol 2005; 17(4):477-487.
26. Lee A, Frank DW, Marks MS, Lemmon MA. Dominant-negative inhibition of receptor-mediated endocytosis by a dynamin-1 mutant with a defective pleckstrin homology domain. Curr Biol 1999; 9(5):261-264.
27. Kobuna H, Inoue T, Shibata M et al. Multivesicular body formation requires OSBP-related proteins and cholesterol. PLoS Genet 2010; 6(8).
28. Matsuo H, Chevallier J, Mayran N et al. Role of LBPA and Alix in multivesicular liposome formation and endosome organization. Science 2004; 303(5657):531-534.
29. Schaller-Bals S, Bates SR, Notarfrancesco K, Tao JQ, Fisher AB, Shuman H. Surface-expressed lamellar body membrane is recycled to lamellar bodies. Am J Physiol Lung Cell Mol Physiol 2000; 279(4):L631-L640.
30. Hoorn T, Paul P, Janssen L, Janssen H, Neefjes J. Dynamics within tetraspanin pairs affect MHC class II expression. J Cell Sci 2012; 125(Pt 2):328-339.
31. Copier J, Kleijmeer MJ, Ponnambalam S et al. Targeting signal and subcellular compartments involved in the intracellular trafficking of HLA-DMB. J Immunol 1996; 157(3):1017-1027.
32. Mrakovic A, Kay JG, Furuya W, Brumell JH, Botelho RJ. Rab7 and Arl8 GTPases are Necessary for Lysosome Tubulation in Macrophages. Traffic 2012.
33. Soppina V, Rai AK, Ramaiya AJ, Barak P, Mallik R. Tug-of-war between dissimilar teams of microtubule motors regulates transport and fission of endosomes. Proc Natl Acad Sci U S A 2009; 106(46):19381-19386.
34. van Meer G, Halter D, Sprong H, Somerharju P, Egmond MR. ABC lipid transporters: extruders, flippases, or flopless activators? FEBS Lett 2006; 580(4):1171-1177.
35. Du X, Kazim AS, Brown AJ, Yang H. An essential role of Hrs/Vps27 in endosomal cholesterol trafficking. Cell Rep 2012; 1(1):29-35.
36. Lange Y, Steck TL, Ye J, Lanier MH, Molugu V, Ory D. Regulation of fibroblast mitochondrial 27-hydroxycholesterol production by active plasma membrane cholesterol. J Lipid Res 2009; 50(9):1881-1888.
37. Kennedy BE, Charman M, Karten B. Niemann-Pick Type C2 protein contributes to the transport of endosomal cholesterol to mitochondria without interacting with NPC1. J Lipid Res 2012; 53(12):2632-2642.
38. Kauraniemi P, Barlund M, Monni O, Kallioniemi A. New amplified and highly expressed genes

discovered in the ERBB2 amplicon in breast cancer by cDNA microarrays. Cancer Res 2001; 61(22):8235-8240.

39. Moog-Lutz C, Tomasetto C, Regnier CH et al. MLN64 exhibits homology with the steroidogenic acute regulatory protein (STAR) and is over-expressed in human breast carcinomas. Int J Cancer 1997; 71(2):183-191.

40. Alpy F, Boulay A, Moog-Lutz C et al. Metastatic lymph node 64 (MLN64), a gene overexpressed in breast cancers, is regulated by Sp/KLF transcription factors. Oncogene 2003; 22(24):3770-3780.

41. Vinatzer U, Dampier B, Streubel B et al. Expression of HER2 and the coamplified genes GRB7 and MLN64 in human breast cancer: quantitative real-time reverse transcription-PCR as a diagnostic alternative to immunohistochemistry and fluorescence in situ hybridization. Clin Cancer Res 2005; 11(23):8348-8357.

42. Borthwick F, Allen AM, Taylor JM, Graham A. Overexpression of STARD3 in human monocyte/macrophages induces an anti-atherogenic lipid phenotype. Clin Sci (Lond) 2010; 119(7):265-272.

Supplementary material

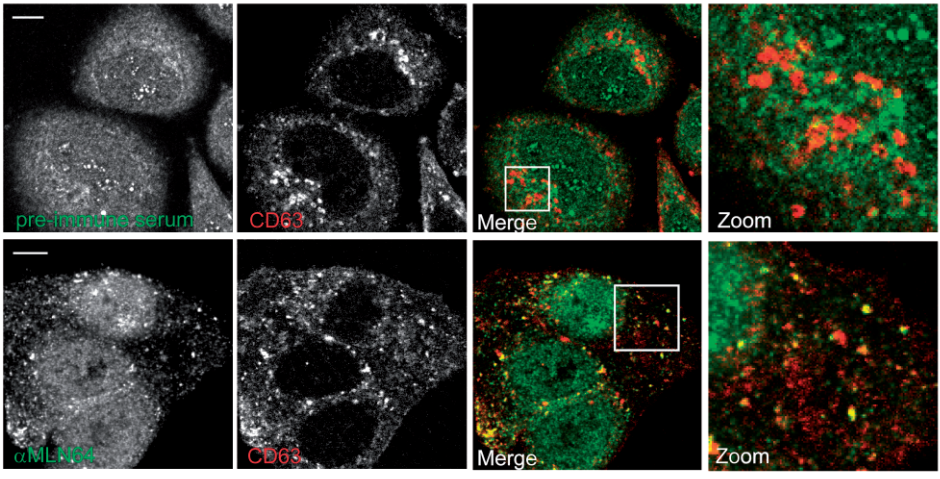


Figure S1. SKBR3 cells un-transfected were paraformaldehyde (PFA) fixed, permeabilized and immunolabelled by pre-immune serum (upper panel) or anti-MLN64 (lower panel) antibodies before imaging by confocal microscopy. Zoom-ins of merged pictures indicated. Scale bar: 10µm. n>100.

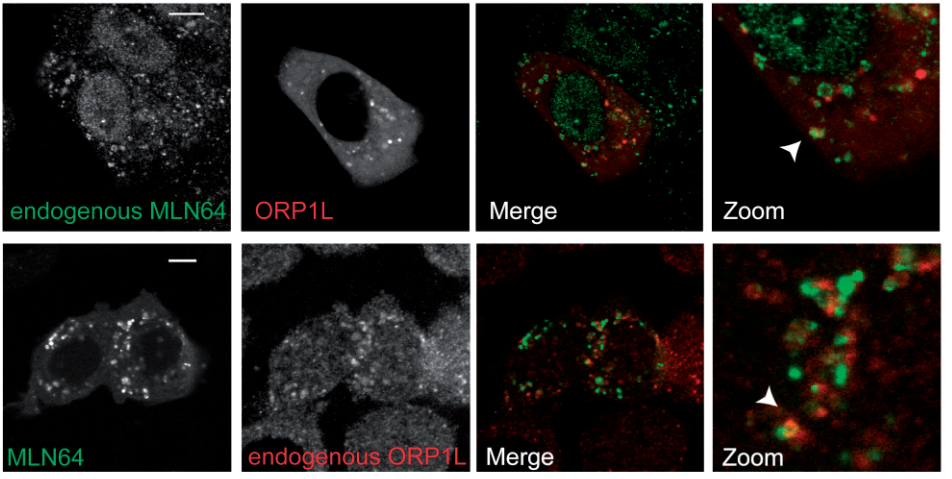


Figure S2. Upper panel; SKBR3 cells expressing mRFP-ORP1L (red) were PFA fixed, permeabilized and immunolabelled by anti-MLN64 antibodies (green) before imaging by confocal microscopy. Lower panel; SKBR3 cells expressing MLN64-YFP (green) were PFA fixed, permeabilized and immunolabelled with anti-ORP1L antibodies (red) before imaging by confocal microscopy. Zoom-ins of merged pictures indicated. Scale bar: 10µm. n>100. White arrow indicates vesicle positive for both MLN64 and ORP1L. Right panel: Scatter plots of pixel intensities for respective channels of entire image.

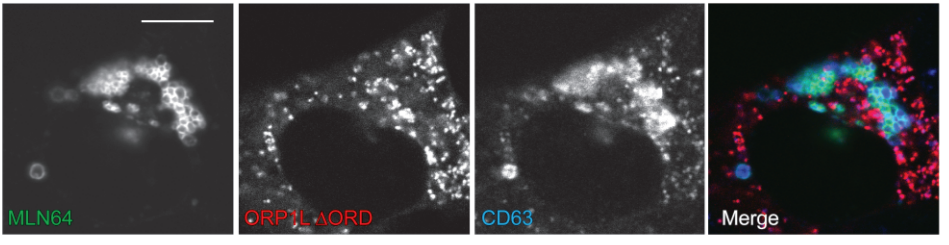
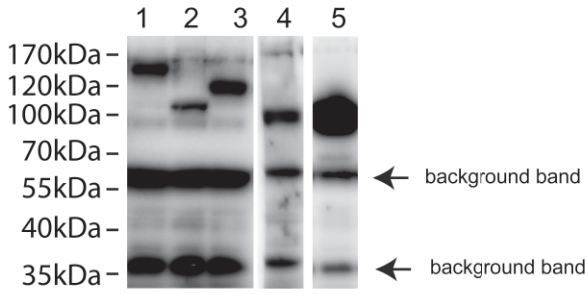


Figure S3. MelJuSo cells expressing MLN64-YFP (green) and mRFP-ORP1LΔORD (red) were PFA fixed and imaged by confocal microscopy. Zoom-ins of merged pictures indicated. Scale bar: 10µm. n>100. Scale bar: 10µm. n>100.



1. GFP-ORP1L
2. GFP-ORP1L ΔORDPHDPHD
3. GFP-ORP1L ΔORD
4. YFP-MLN64
5. GFP-MLN64 START mut

Figure S4. Lysates of MelJuSo cells expressing indicated constructs were analyzed by SDS-PAGE and WB before probing with the anti-GFP antibodies (GFP-antibodies also recognizing YFP-epitope). Position of protein marker as indicated.

Legend Movie M1. Time laps movie of cells expressing YFP-MLN64 (green) and mRFP-ORP1L (red). Movie is recorded at 3 seconds intervals between frames, total recording time is 60 seconds.

Legend Movie M2. Time laps movie of cells expressing YFP-MLN64 (green) and mRFP-ORP1L (red) after 3 hours of Cy5-ovalbumin internalization (blue). Movie is recorded at 3 seconds intervals between frames, total recording time is 60 seconds.

Legend Movie M3. Zoom in of time laps movie of cells expressing YFP-MLN64 (green) and mRFP-ORP1L (red) after 3 hours of Cy5-ovalbumin internalization (blue) indicating the co-trafficking of the green, red and blue channel.

chapter SEVEN

Summary and discussion
Nederlandse samenvatting

Late endosomal (LE) compartments (late endosomes and lysosomes) contribute to cellular homeostasis in a variety of ways. A major role for these organelles in all cells is the digestion of nutrients and the redistribution of the digestion products (such as amino-acids and lipids) to other parts of the cell, where they can be used for proliferation and growth (Luzio et al., 2007b). The LE also offers a platform for signal transduction, which can be used to convey growth factor receptor signalling over the long distances covered by late endosomes (Palfy et al., 2012). Signal termination is also regulated by the LE, which can send signalling proteins into intra-lumenal vesicles for subsequent degradation (Luzio et al., 2007b). Due to its acidic environment, the LE can also eliminate pathogens that enter our body while other pathogens (such as influenza virus and Ebola virus) have co-evolved to use the acidic LE environment to their benefit (Fairn and Grinstein, 2012). To complete these complicated tasks, LE dynamics (transport and fusion events) are tightly regulated in time and space via cross-talk between numerous LE associated proteins and inter-compartmental contacts with other organelles. Not surprisingly, mutations in LE proteins lead to very severe developmental- and neurodegenerative diseases often lethal early in life. However other LE proteins (and polymorphisms) have before been implicated in late-onset neurodegenerative and neurological diseases such as Alzheimer's, Parkinson's and Schizofrenia (reviewed in chapter 1). The role and regulation of LE proteins that cause these diseases are relatively understudied, yet could explain disease phenotypes at the cellular and molecular level for which currently no satisfactory explanation exists. The studies described in this thesis aim at a better understanding of the molecular regulation of late endosomal and lysosomal dynamics. We have studied how LE transport and fusion events are regulated by complex multi-subunit protein complexes and the role of cholesterol in this regulation.

One example of a rare but devastative neurodegenerative disease is Niemann-Pick disease type C. In this disease the proteins NPC1 or NPC2 are mutated, causing the accumulation of cholesterol in LE and subsequent trafficking defects by an unknown mechanism (Chang et al., 2005). We have identified (chapter 3) the oxysterol-binding protein related protein 1L (ORP1L) as a sensor of LE cholesterol levels and a regulator of LE transport. ORP1L senses cholesterol in the LE membrane and controls the recruitment of the microtubule minus-end dynein motor to RAB7 interacting lysosomal protein (RILP). When cholesterol is low, ORP1L changes conformation it exposes a small domain (FFAT domain) that interacts with a resident ER protein (VAP-A) that can remove the dynein motor from vesicles. This results in the outward movement of LE by action of the kinesin motor. In the case when cholesterol is high, as in the case of NPC type C disease patients, the ORP1L conformation prevents contacts between the ER and the LE and the dynein motor get "stuck" on the LE resulting in minus-end clustering of these LE. LE cholesterol levels also control late endosomal tethering by the HOPS complex (chapter 5). From these results it is apparent that defects in late endosomal cholesterol levels (such as in NPC type-C disease) have huge impact on vesicular trafficking, and our findings may explain some of the phenotypes observed in NPC type C disease. Even more, we were able to partly restore the NPC-1 phenotype in cells lacking NPC-1 using ORP1L mutants, indicating that ORP1L or other cholesterol binding molecules might offer interesting new therapeutic targets. Although NPC type C disease is rare, it partly pheno-copies Alzheimer's disease where the Aβ plaques accumulate (Nixon, 2004).

Alzheimer's disease is the most common form of dementia predicted to affect 1 in 85 people in 2050 (Brookmeyer et al., 2007) and cholesterol metabolism and lysosomal deficits have often been associated with this disease (Di Paolo and Kim, 2011; Leduc et al., 2010; Cataldo et al., 1996; Cataldo et al., 1991; Nixon and Cataldo, 2006; Coen et al., 2012) indicating a possible contribution of late endosomal dynamics controlled by cholesterol in this disease as well.

By concomitantly recruiting the dynein motor (chapter 4) and the 6-subunit canonical HOPS complex (chapter 5) into one multi-protein complex, RILP efficiently combines LE transport and fusion events and puts these under the control of cholesterol, ORP1L and the ER. The Ebola virus requires HOPS mediated fusion by the HOPS complex for escape into the cytosol and replication (Carette et al., 2011). We find that RILP and ORP1L are also host factors for Ebola virus (chapter 5). As also other viruses (such as Dengue, influenzea and HIV) require late endosomal compartments for infectivity (van der Schaar et al., 2008; Caillet et al., 2011; Sieczkarski and Whittaker, 2003), these findings might apply to a broader spectrum of viruses.

Although many lysosomal diseases result in neuro-degenerative defects (reviewed in the Introduction), examples of mutations in endosomal proteins can also result in developmental disorders such as arthrogryposis, renal dysfunction, and cholestasis (ARC) a multisystem disorder associated with abnormalities in polarized liver and kidney cells and recurrent infections. SPE-39 and VPS33b are HOPS subunit homologues and mutations in these proteins result in ARC syndrome. We show that these can also be recruited to LE membranes by RILP (chapter 4) and that disease mutants of these HOPS proteins specifically fail to interact with RILP or with their partner proteins (chapter 4 and 5) indicating a lysosomal component in ARC syndrome. In addition, we show that SPE-39 and VPS33b assemble in an "alternative" complex that is different from the canonical HOPS es complex and CORVET (chapter 5).

Cholesterol is a major regulator of late endosomal dynamics as it controls transport and fusion of LE. The LE on the other hand are major regulators of cholesterol metabolism; they can contain over 50% of total cellular cholesterol and are a major sorting station for the distribution of cholesterol to other compartments such as the ER, lipid droplets, the plasma membrane and mitochondria (Ikonen, 2008). ORP1L is not the only cholesterol-sensing molecule on late endosomes; MLN64 (STARD3) is a transmembrane LE molecule that also contains a sterol sensing domain of the START family. In chapter 6 we describe the interplay between MLN64 and ORP1L. Although both are present on late endosomes, they are not present on the same endosomes. In fact these two proteins divide the late endosomes into two sub-populations that seem to have diverse roles in cholesterol handling. MLN64 is present on a LE compartment containing the lipid pump ABCA3 and precede a LE compartment positive for ORP1L and the cholesterol efflux pump NPC-1. These findings might explain how MLN64 and NPC-1 function independently of each other, and how MLN64 is involved in the egress of cholesterol to the plasma membrane and mitochondria whilst NPC1 and ORP1L control transport of cholesterol to the ER and further to other cellular compartments. Trafficking of cholesterol to mitochondria is required for the production of hormones and interestingly MLN64 is often-overexpressed and a marker for bad prognosis in hormone-dependent cancers such as breast- and prostate cancer (Vinatzer et al., 2005; Alpy et al., 2003; Moog-Lutz et al., 1997). Our findings might

explain how on the cellular level higher MLN64 levels increases entry of the most essential building block to mitochondria for hormone production, and why MLN64 is a bad prognostic factor for hormone-sensitive tumors.

Why cholesterol?

This thesis describes that cholesterol is a major regulator of LE dynamics. This is not the first example of a lipid as a regulator of the dynamics of an organelle. Especially phosphoinositides are more commonly known as regulators of membrane trafficking (van Meer et al., 2008; Jean and Kiger, 2012). Many species of phosphoinositides exist which are easily inter-converted making them ideal signalling molecules. Although phosphoinositides do regulate LE dynamics, especially LE maturation, we find that cholesterol is also a major controller of LE transport and fusion events. But why cholesterol? An interesting hypothesis may lie in the fact that LE are major determinants of cholesterol metabolism and cholesterol levels might serve as an LE maturation signal. Cholesterol-rich LDL particles are transported to LE where the cholesterol is hydrolysed and released from the LDL particles. It is expected from this that dissociation starts in "early" late endosomes that contain much LDL but little free cholesterol, while during maturation of LE more free cholesterol accumulates in the limiting membranes of the LE. Cholesterol might therefore serve as an indicator for the maturity of LE. Only when cholesterol levels are high enough, the LE are further transported towards lysosomes (by the dynein motor) for fusion (by the HOPS complex). The transport and fusion of immature LE (with low cholesterol levels) is inhibited by ORP1L such that these early LE do not pre-maturely fuse with lysosomes. This might be a mechanism to allow for sufficient time for the recycling of proteins and lipids away from early LE and prevent the pre-mature degradation of these components in lysosomes.

Although this might explain why cholesterol levels regulate LE dynamics, this does not explain why ER-LE contacts are initiated under low cholesterol levels. This might strictly be for the regulation of LE dynamics, yet as the ER and LE have an intrinsic relationship in cholesterol handling, the transfer of cholesterol or other lipids is likely also regulated at these contacts. Cholesterol is transferred from LE to the ER by an interaction between NPC-1 and the ER protein ORP5 (Du et al., 2011). It would be expected that LE-ER contacts are initiated when LE cholesterol levels are high so that transfer of cholesterol from the LE to the ER can occur. Yet we observe that these contacts are initiated when LE cholesterol is low. One explanation for this could be the presence of micro-domains on the LE membrane. NPC-1 and other cholesterol binding transmembrane proteins might bind cholesterol and sequester it away from ORP1L. This would allow the "loading" of NPC-1 molecules with cholesterol. As ORP1L can not sense the cholesterol in these micro-domains it initiates contacts with the ER which then allow the NPC1 associated cholesterol to be shuttled from the LE to the ER. Alternatively, oxysterols in a role of signalling sterols might also be sensed by ORP1L and control ER contact site formation and cholesterol transport (Ikonen, 2008). Another explanation for ER-LE contacts might be the transfer of calcium from the calcium rich ER to LE that need calcium to regulate fusion and fission events (Lloyd-Evans and Platt, 2011; Pryor et al., 2000; Luzio et al., 2007a). Interestingly, defects in LE

calcium have been reported in NPC patients and other lysosomal storage diseases (Lloyd-Evans and Platt, 2011). If and how the transfer of cholesterol and calcium are co-regulated and/or coupled for LE-ER transfer remains to be investigated.

Cross-compartmental control by the ER

A major finding in this thesis is the observation that late endosomal transport and fusion are controlled by the ER. In recent years the control of dynamics of other organelles such as mitochondria, lipid droplets, the plasma-membrane and early endosomes has also been shown to be regulated by the ER. This poses the intriguing possibility that the ER can act as a central organelle organizer (chapter 2). By contacting and regulating the functioning of other organelles across the entire cellular space the ER might act as a cellular nervous system integrating and conducting inter-organellar signalling. This has major implications for disease processes; defects in proteins functioning in calcium signalling in the mitochondria might indirectly regulate remote processes such as calcium flow between ER and late endosome or the ER and the plasma membrane. This might partly explain how mutations in single proteins can give rises to seemingly multiple defects over a range of organelles. This is especially apparent in neurodegenerative diseases such as Parkinson's and Alzheimer's for which the molecular mechanisms have not been resolved and phenotypes have been attributed to defects in a range of organelles from autophagosomal accumulation, lysosomal fusion defects to mitochondrial dysfunction and ER-stress. Our and other studies implicate that organelles can not be viewed as isolated entities but that their functioning is regulated at an integrated level and that communication between organelles is essential for proper cellular homeostasis. These finding might offer important insights in our understanding of organellar biology, their cross-connectivity and role in human disease.

Reference List

1. Alpy,F., Boulay,A., Moog-Lutz,C., Andarawewa,K.L., Degot,S., Stoll,I., Rio,M.C., and Tomasetto,C. (2003). Metastatic lymph node 64 (MLN64), a gene overexpressed in breast cancers, is regulated by Sp/KLF transcription factors. Oncogene *22*, 3770-3780.
2. Brookmeyer,R., Johnson,E., Ziegler-Graham,K , and Arrighi,H.M. (2007). Forecasting the global burden of Alzheimer's disease. Alzheimers. Dement *3*, 186-191.
3. Caillet,M., Janvier,K., Pelchen-Matthews,A., Delcroix-Genete,D., Camus,G., Marsh,M., and Berlioz-Torrent,C. (2011). Rab7A is required for efficient production of infectious HIV-1. PLoS Pathog. *7*, e1002347.
4. Carette,J.E., Raaben,M., Wong,A.C., Herbert,A.S , Obernosterer,G., Mulherkar,N., Kuehne,A.I , Kranzusch,P.J., Griffin,A.M., Ruthel,G., Dal Cin,P., Dye,J.M., Whelan,S.P., Chandran,K., and Brummelkamp,T.R. (2011). Ebola virus entry requires the cholesterol transporter Niemann-Pick C1. Nature *477*, 340-343.
5. Cataldo,A.M., Hamilton,D.J., Barnett,J.L., Paskevich,P.A., and Nixon,R.A. (1996). Abnormalities of the endosomal-lysosomal system in Alzheimer's disease: relationship to disease pathogenesis. Adv. Exp. Med. Biol. *389*, 271-280.
6. Cataldo,A.M., Paskevich,P.A., Kominami,E., and Nixon,R.A. (1991). Lysosomal hydrolases of different classes are abnormally distributed in brains of patients with Alzheimer disease. Proc. Natl. Acad. Sci. U S A *88*, 10998-11002.
7. Chang,T.Y., Reid,P.C., Sugii,S., Ohgami,N., Cruz,J.C., and Chang,C.C. (2005). Niemann-Pick type C disease and intracellular cholesterol trafficking. J. Biol. Chem. *280*, 20917-20920.
8. Coen,K., Flannagan,R.S., Baron,S., Carraro-Lacroix,L.R., Wang,D., Vermeire,W., Michiels,C., Munck,S., Baert,V., Sugita,S., Wuytack,F.,

Hiesinger,P.R., Grinstein,S., and Annaert,W. (2012). Lysosomal calcium homeostasis defects, not proton pump defects, cause endo-lysosomal dysfunction in PSEN-deficient cells. J. Cell Biol. *198*, 23-35.

9. Di Paolo,G. and Kim,T.W. (2011). Linking lipids to Alzheimer's disease: cholesterol and beyond. Nat. Rev. Neurosci. *12*, 284-296.
10. Du,X., Kumar,J., Ferguson,C., Schulz,T.A., Ong,Y.S., Hong,W., Prinz,W.A., Parton,R.G., Brown,A.J., and Yang,H. (2011). A role for oxysterol-binding protein-related protein 5 in endosomal cholesterol trafficking. J. Cell Biol. *192*, 121-135.
11. Fairn,G.D. and Grinstein,S. (2012). How nascent phagosomes mature to become phagolysosomes. Trends Immunol. *33*, 397-405.
12. Ikonen,E. (2008). Cellular cholesterol trafficking and compartmentalization. Nat. Rev. Mol. Cell Biol. *9*, 125-138.
13. Jean,S. and Kiger,A.A. (2012). Coordination between RAB GTPase and phosphoinositide regulation and functions. Nat. Rev. Mol. Cell Biol. *13*, 463-470.
14. Leduc,V., Jasmin-Belanger,S., and Poirier,J. (2010). APOE and cholesterol homeostasis in Alzheimer's disease. Trends Mol. Med. *16*, 469-477.
15. Lloyd-Evans,E. and Platt,F.M. (2011). Lysosomal Ca(2+) homeostasis: role in pathogenesis of lysosomal storage diseases. Cell Calcium *50*, 200-205.
16. Luzio,J.P., Bright,N.A., and Pryor,P.R. (2007a). The role of calcium and other ions in sorting and delivery in the late endocytic pathway. Biochem. Soc. Trans *35*, 1088-1091.
17. Luzio,J.P., Pryor,P.R., and Bright,N.A. (2007b). Lysosomes: fusion and function. Nat. Rev. Mol. Cell Biol. *8*, 622-632.
18. Moog-Lutz,C., Tomasetto,C., Regnier,C.H., Wendling,C., Lutz,Y., Muller,D., Chenard,M.P., Basset,P., and Rio,M.C. (1997). MLN64 exhibits homology with the steroidogenic acute regulatory protein (STAR) and is over-expressed in human breast carcinomas. Int J. Cancer *71*, 183-191.
19. Nixon,R.A. (2004). Niemann-Pick Type C disease and Alzheimer's disease: the APP-endosome connection fattens up. Am. J. Pathol. *164*, 757-761.
20. Nixon,R.A. and Cataldo,A.M. (2006). Lysosomal system pathways: genes to neurodegeneration in Alzheimer's disease. J. Alzheimers. Dis. *9*, 277-289.
21. Palfy,M., Remenyi,A., and Korcsmaros,T. (2012). Endosomal crosstalk: meeting points for signaling pathways. Trends Cell Biol. *22*, 447-456.
22. Pryor,P.R., Mullock,B.M., Bright,N.A., Gray,S.R., and Luzio,J.P. (2000). The role of intraorganellar Ca(2+) in late endosome-lysosome heterotypic fusion and in the reformation of lysosomes from hybrid organelles. J. Cell Biol. *149*, 1053-1062.
23. Sieczkarski,S.B. and Whittaker,G.R. (2003). Differential requirements of Rab5 and Rab7 for endocytosis of influenza and other enveloped viruses. Traffic *4*, 333-343.
24. van der Schaar,H.M., Rust,M.J., Chen,C., Ende-Metselaar,H., Wilschut,J., Zhuang,X., and Smit,J.M. (2008). Dissecting the cell entry pathway of dengue virus by single-particle tracking in living cells. PLoS Pathog. *4*, e1000244.
25. van Meer,G., Voelker,D.R., and Feigenson,G.W. (2008). Membrane lipids: where they are and how they behave. Nat. Rev. Mol. Cell Biol. *9*, 112-124.
26. Vinatzer,U., Dampier,B., Streubel,B., Pacher,M., Seewald,M.J., Stratowa,C., Kaserer,K., and Schreiber,M. (2005). Expression of HER2 and the coamplified genes GRB7 and MLN64 in human breast cancer: quantitative real-time reverse transcription-PCR as a diagnostic alternative to immunohistochemistry and fluorescence in situ hybridization. Clin. Cancer Res. *11*, 8348-8357.

Nederlandse samenvatting

Het menselijke lichaam bestaat uit organen met verschillende functies: het opnemen van voedingstoffen, het rondpompen van zuurstof en het aansturen van onze bewegingen en gedachten. Deze organen worden gevormd door miljoenen cellen die samenwerken om deze taken goed uit te voeren. Iedere cel is een wereld op zichzelf, en nog belangrijker, bijna iedere cel is zelfvoorzienend. Zoals op de voorkant van dit boekje te zien is, kan een cel vergeleken worden met een stad. Er is een centrum (de nucleus) waar besloten wordt wat er gebeurt in de stad, er zijn energieplantages (mitochondriëen) om energie op te wekken en fabrieken (endoplasmatisch reticulum) om nieuw producten te maken. Ook is er een uitgebreid transportsysteem (het endocytische systeem) dat zorgt voor de aanvoer van bouw- en voedingstoffen.

In vele ziektes lijkt dit cellulaire transportsysteem verstoort. Hierdoor ontstaan er files in de cel en kunnen bouwstoffen niet meer op de juiste plek worden afgeleverd. Op den duur zorgt dit ervoor dat de cellen dood gaan en organen zoals de hersenen, lever en anderen niet meer goed functioneren. Helaas weten we nog niet genoeg van het transportsysteem van de cel om ziektes helemaal te kunnen verklaren. We weten nog veel te weinig om deze ziektes daadwerkelijk te genezen. Het werk in dit proefschrift is uitgevoerd om de transportprocessen in de cel op moleculair niveau te begrijpen. Dit proefschrift beschrijft hoe cholesterol en grote eiwitcomplexen het cellulaire transportsysteem sturen en hoe deze processen verstoord zijn in twee erfelijke ziektes; de ziekte van Niemann-Pick en het ARC syndroom. Beide zijn ernstige erfelijke aandoeningen, kinderen met Niemann-Pick ziekte worden zelden ouder dan 10-20 jaar en de meerderheid van kinderen met het ARC syndroom sterven voor hun eerste levensjaar.

Hoe ziet het transportsysteem in cellen eruit, en wat hebben wij hierover ontdekt?

Zoals gezegd kan iedere cel zelfvoorzienend zijn. Dit betekent dat iedere cel zelf in staat is om voedsel op te nemen, zijn energieverbruik te regelen en te reageren op stimuli uit zijn omgeving. Het transportsysteem dat voedingstoffen opneemt heet het “endocytotische systeem”. Dit systeem bestaat uit kleine blaasjes – endosomen – die voedingstoffen van buiten de cel kunnen opnemen en verteren. Endosomen zijn er in verschillende vormen; zure en niet zure. De niet-zure endosomen nemen voedingstoffen van buiten op, maar alleen de zure endosomen (lysosomen genoemd) kunnen deze voedingstoffen afbreken (zoals de maag). Vervolgens leveren ze deze afgebroken voedingstoffen, zoals vetten en koolhydraten, af op de gewenste plek in de cel. Hiervoor moeten deze endosomen door de cel heen getransporteerd worden; dit is geen makkelijke opgave. Hoewel cellen erg klein zijn, zijn endosomen nog vele malen kleiner. In relatief lange cellen zoals Purkinje cellen (hersencel) die 4 millimeter lang kunnen worden kan het wel 4,5 dag duren voordat een endosoom van de ene- naar de andere kant getransporteerd is. In motorneuronen (hersencellen die de spieren aansturen) kan een endosoom er zelfs 125 dagen over doen om de extreme afstand van 1 meter af te leggen. Om deze afstanden af te leggen heeft de cel speciale motoreiwitten die de endosomen voorttrekken.

Endosomen kunnen gezien worden als kleine gemotoriseerde vrachtwagens die voedingstoffen transporteren van de periferie van de stad, naar het centrum van de stad. Ze

halen goederen op en zorgen er ook voor dat deze op de goede plek worden afgeleverd. Naast deze functie worden de vrachtwagens ook gebruikt om signalen van buiten de cel (post) door te geven naar het regelcentrum (de nucleus) van de cel. Groeihormoon bijvoorbeeld, wordt door deze vrachtwagens van buiten opgehaald. Vervolgens wordt deze getransporteerd en geeft bij de nucleus het signaal door dat de cel moet delen. Je kunt je voorstellen dat problemen met dit transportsysteem dan ook leiden tot ernstige ziektes.

Net zoals iedere chauffeur moet een endosoom ook weten welke kant hij op moet. Het is echter niet bekend hoe een endosoom weet waar hij is in de cel en hoe hij bepaalt welke kant hij op moet. **Hoofdstuk 3** beschrijft ons onderzoek hiernaar. We hebben gevonden dat de hoeveelheid cholesterol in een endosoom, bepaalt welke kant een endosoom op gaat. Cholesterol is één van de voedingstoffen die door endosomen opgehaald wordt aan de buitenkant van de cel. De endosomen die vol zitten met cholesterol moeten vervolgens naar het centrum van de cel worden getransporteerd. Daar zitten namelijk de lysosomen (zure endosomen) die de cholesteroldeeltjes kunnen verteren.

Wij hebben gevonden dat een eiwit, ORP1L, op endosomen zit en meet hoeveel cholesterol in de endosomen zit. Wanneer de endosoom vol zit met cholesterol, stuurt ORP1L de endosoom naar het binnenste van de cel. Als er weinig cholesterol in de endosoom zit, ontkoppelt ORP1L de motor zodat de endosoom niet naar binnen gaat.

In de ziekte van Niemann-Pick Type-C is er een genetische fout in het cholesterolmetabolisme. De eiwitten NPC-1 of NPC-2, die normaal cholesterol uit de endosoom wegpompen, werken niet. Hierdoor accumuleert er cholesterol in de endosomen en lysosomen. Hierdoor raakt ORP1L van slag, en wordt de regulering van endosomaal transport verstoord. Hierdoor ontstaan er als het ware files van endosomen en worden voedingstoffen en signalen niet meer goed afgeleverd. Dit levert enorme problemen op, voornamelijk in cellen die rijk zijn aan cholesterol zoals levercellen en in lange hersencellen. Kinderen met Niemann-Pick ziekte ontwikkelen hierdoor leverfalen en dementie (Niemann-Pick wordt ook wel jeugd-Alzheimer genoemd). Uiteindelijk leidt dit tot verlamming en stopt de ademhaling. Onze bevindingen helpen bij het beter begrijpen van deze ziekte en kunnen in de toekomst helpen bij de zoektocht naar medicijnen.

Hoewel we oorspronkelijk dachten dat alleen het transport van endosomen verstoord was in Niemann-Pick ziekte, kregen we tijdens dit onderzoek het vermoeden dat ook “fusie” van endosomen verstoord is in deze ziekte. Dit onderzoek is beschreven in **Hoofdstuk 4**. Wanneer endosomen in het binnenste van de cel aankomen, moeten ze hun vracht doorgeven aan lysosomen. Zoals gezegd zijn endosomen en lysosomen blaasjes. Als deze blaasjes zich openen komt de hele inhoud van deze blaasjes vrij, ook de zuren die in de blaasjes zitten. De endosomen en lysosomen kunnen niet zomaar openen in de cel; de maagsappen zouden het binnenste van de cel kapot maken. Om vracht door te geven gebruiken endosomen daarom fusie. Wanneer een endosoom en een lysosoom elkaar tegenkomen plakken ze aan elkaar (vergelijkbaar met twee zeepbellen uit een bellenblaas). De buitenkanten van de blaasjes fuseren daarna met elkaar, zodat er één nieuw blaasje wordt gemaakt (twee zeepbellen die één worden). Op die manier kunnen voedingstoffen veilig worden doorgeven van de niet zure endosomen naar de

zure lysosomen. Het was echter niet bekend hoe de niet-zure endosomen de zure endosomen herkennen en wij hebben uitgezocht hoe dit werkt. We hebben gevonden dat er een eiwit-complex bestaat (het HOPS complex) dat speciaal is uitgerust voor deze klus. Dit eiwit-complex wordt aan endosomen vastgemaakt door het eiwit RILP dat als soort van trekhaak dient. Het HOPS complex bestaat uit verschillende eiwitten en is gespecialiseerd in het herkennen van lysosomen. Als het HOPS complex een lysosoom ziet, zorgt hij ervoor dat de endosoom hieraan vast plakt. Hierdoor kan er fusie plaatsvinden tussen het endosoom en het lysosoom. Net zoals het transport proces, wordt ook het fusieproces gestuurd door cholesterol en ook de fusie van endosomen is verstoord in de ziekte van Niemann-Pick.

Hoewel we wisten dat het HOPS complex een rol speelt bij fusie, was het destijds onbekend welke componenten er precies in dit complex zitten. In tegenstelling tot andere modelsystemen, zoals bakkersgist, is het in mensen niet bekend hoe het HOPS complex eruitziet. In bakkersgist bestaat het HOPS complex uit 6 eiwitten. Ook bestaat er nog een ander complex (CORVET) dat niet de fusie van lysosomen met endosomen reguleert, maar de fusie van endosomen onderling. Het vermoeden bestond dat deze complexen ook aanwezig zijn in menselijke cellen, maar dat was niet zeker. In **Hoofdstuk 5** laten wij eerste keer zien dat beide complexen inderdaad ook bestaan in de mens, en hoe ze er precies uitzien. Bovendien ontdekten we dat er nog een derde complex bestaat, dat in bakkersgist niet voorkomt.

Genetische foutjes in dit derde complex veroorzaken het ARC syndroom, een ernstige ontwikkelingsziekte waarbij kinderen vaak niet ouder dan 1 jaar worden.

Hoewel het op dit moment nog niet precies duidelijk is hoe deze foutjes leiden tot deze ziekte, wijst onze data erop dat dit complex is bij de fusie van het lysosoom (de zure variant van de endosoom).

Het zou kunnen dat de lysosomen van ARC patiënten niet goed voeding kunnen verteren, en dat de cellen en organen daardoor niet functioneren. Hierdoor ontwikkelen de organen van deze kinderen zich niet goed.

Het is ook belangrijk dat het nu bekend is hoe het HOPS- en CORVET complex eruitzien in mensen. Verschillende componenten van deze complexen spelen een rol bij virale (Ebola) en bacteriële (salmonella) infecties en de complexen zijn ook belangrijk voor het doorgeven van groeihormonen en de embryonale ontwikkeling. Veranderingen in de complexen kunnen leiden tot de ziekte van Parkinson. Met de kennis die wij vergaart hebben kunnen deze processen nu beter begrepen worden.

Hoofdstuk 6 beschrijft de identificatie van twee verschillende populaties van lysosomen, die beide een andere eindbestemming hebben binnen de cel. Op de ene populatie zit het eiwit ORP1L achter het stuur, bij de andere het eiwit MLN64. Beide endosomen vervoeren cholesterol maar brengen dit cholesterol naar andere locaties: ORP1L endosomen brengen het cholesterol naar de opslag (endoplasmatisch reticulum), de MLN64 endosomen brengen dit cholesterol naar fabrieken (mitochondrieën). In deze fabrieken worden er hormonen gemaakt van het cholesterol. Het blijkt dat sommige vormen van borst- en prostaattumoren erg veel

MLN64 maken. Het zou kunnen dat ze dit doen om meer cholesterol naar de mitochondrieën te brengen en zo meer hormoon te maken. Dit hormoon stimuleert vervolgens de tumor om verder te groeien. Onze bevindingen kunnen verklaren hoe MLN64 ervoor zorgt dat er meer hormoon geproduceerd wordt en hoe hormoongevoelige tumoren hiervan profiteren.
Samengevat hebben we uitgezocht hoe het transport en de fusie van endosomen gereguleerd wordt door cholesterol en eiwitcomplexen (**Protein complexes and cholesterol in the control of late endosomal dynamics)**. Dit onderzoek heeft ons erg veel geleerd over de dynamiek en regulatie van endosomen en over ziektes waarin deze processen niet goed gereguleerd wordt. Deze kennis kan de basis vormen naar verder onderzoek naar (zeldzame) genetische ziektes.

Ook is er in de afgelopen jaren gebleken dat endosomaal transport is verstoord in veelvoorkomende ziektes zoals Alzheimer en Parkinson. Hoe en wat daar het probleem is, is nog grotendeels onbekend.

Onze ontdekkingen ten aanzien van de zeldzame genetische ziektes kunnen als model dienen en helpen bij ontdekkingen voor deze veelvoorkomende ziektes.

Appendices

Curriculum vitae
List of publications
Acknowledgements

Curriculum Vitae

Rik van der Kant werd geboren op 12 augustus 1984 te Deurne. In 2002 behaalde hij zijn VWO diploma op het Peelland College te Deurne. In datzelfde jaar startte hij zijn studie Biologie aan de Radboud Universiteit te Nijmegen. Gedurende zijn master-studie werden er een drietal stages gedaan. In zijn eerste stage werkte hij aan een gedeeld project tussen het lab van Bart Ellenbroek op de afdeling Pscychoneuropharmacology (Nijmegen) en het lab van Marco Riva op de afdeling Farmacologie (Milaan). Het onderzoek richtte zich op de rol van D1 dopamine receptoren in drugsverslaving en werd begeleid door Joselien Oliviers. Tijdens een tweede korte stage nam hij deel aan een veldonderzoek op Aruba. Hierbij onderzocht hij het belang van verschillende marine-habitats voor de rifvis het roodbekje. Dit onderzoek werd uigevoerd onder begeleiding van Monique Grol in het lab van Ivan Nagelkerken.

Rik van der Kant voerde zijn afstudeerstage uit in de groep van Prof. Dr. J. Jacques Neefjes, Cel biologie II in het Nederlands Kanker Instituut te Amsterdam. Hier voerde hij onder begeleiding van Nuno Rocha onderzoek uit naar de rol van het eiwit MLN64 in het functioneren van late endosomen. Na het behalen van zijn Master of Science diploma, begon hij oktober 2007 aan zijn promotie onderzoek in de groep van Prof. Dr. J. Jacques Neefjes, wat geresulteerd heeft in dit proefschrift. Per oktober 2013 zal hij beginnen als post-doctoraal onderzoeker in het lab van Prof. Dr. L.S. Goldstein op het Sanford Consortium for Regenerative Medicine, UCSD, San Diego, VS, waar hij op zoek gaat naar de oorzaken voor de ziekte van Alzheimer.

Publications

van der Kant, R., R.Galmes, R., C.T.H.Jonker, L.Janssen, J.Klumperman and J.Neefjes. Identification and characterization of the mammalian CORVET and HOPS tethering complexes and a VPS33b-SPE-39 complex mutated in ARC syndrome. *Manuscript in preparation*.

Van der Kant, R. and J.Neefjes. Small regulators, major consequences: Ca^{2+} and cholesterol at the late endosomal - ER interface. *Review in preparation for Journal of Cell Science*.

Van der Kant, R. and J.Neefjes. Stuck in traffic; an emerging theme in diseases of the nervous system. *Review in preparation for Trends in Neurosciences*.

van der Kant, R., A.Fish, L.Janssen, H.Janssen, S.Krom, N.Ho, T.Brummelkamp, J.Carette, N.Rocha, and J.Neefjes. Late endosomal transport and tethering are coupled processes controlled by RILP and the cholesterol sensor ORP1L. *Journal of Cell Science, 2013 in press*.

van der Kant, R., I.Zondervan, L.Janssen, and J.Neefjes. Cholesterol binding molecules MLN64 and ORP1L mark distinct late endosomes with transporters ABCA3 and NPC1. *Journal of Lipid Research, Volume 54, No.7. August 2013*.

Uusi-Rauva, K., A.Kyttala, **R.van der Kant**, J.Vesa, K.Tanhuanpaa, J.Neefjes, V.M.Olkkonen, and A.Jalanko. 2012. Neuronal ceroid lipofuscinosis protein CLN3 interacts with motor proteins and modifies location of late endosomal compartments. *Cellular and Molecular Life Sciences*. 2012 69:2075-2089.

Verweij, F.J., M.A.van Eijndhoven, E.S.Hopmans, T.Vendrig, T.Wurdinger, E.Cahir-McFarland, E.Kieff, D.Geerts, **R.van der Kant**, J.Neefjes, J.M.Middeldorp, and D.M.Pegtel. LMP1 association with CD63 in endosomes and secretion via exosomes limits constitutive NF-kappaB activation. *EMBO Journal*. 2011 30:2115-2129.

Rocha, N., **R.van der Kant***, C.Kuijl*, L.Janssen, D.Houben, H.Janssen, W.Zwart, and J.Neefjes. Cholesterol sensor ORP1L contacts the ER protein VAP to control Rab7-RILP-p150 Glued and late endosome positioning. *Journal of Cell Biology*. 2009 185:1209-1225. *equal contributions.

Acknowledgements

I would like to thank everyone that contributed to this thesis.